Engineering small molecule-mediated communication between light-activatable synthetic cells and bacterial cells



Jefferson Smith

Lady Margaret Hall
University of Oxford

A thesis submitted for the degree of
Doctor of Philosophy

Hilary 2022

Abstract

Gene-expressing compartments are a minimal representation of living cells. By using DNA blueprints to inform an assembly line of biological machinery how to manufacture the proteins required for a particular function, these cell-like compartments, often referred to as synthetic cells, have been engineered to exhibit life-like behaviours, such as division and communication. Although, despite these advances, little emphasis has been placed on how their activities are regulated. For synthetic cells to become a mature and valuable technology, it is essential that we precisely control where and when their functions are executed. Should this be achieved, synthetic cells could be used for the controlled production of drugs or signalling molecules, and be interfaced with living cells/tissues to modulate their behaviours. This thesis delineates progress towards creating gene-expressing synthetic cells that are activated only in the presence of UV light and describes how light-activated synthetic cells could be interfaced with living cells.

Synthetic cells were constructed by functionalising giant unilamellar vesicles with a cell-free protein synthesis system and DNA template. The DNA template dictated which proteins were synthesised inside the vesicle and, therefore, the overall function of the compartment. Photo-sensitive blocking groups were subsequently installed into the promoter regions of the DNA templates to regulate *in situ* gene expression; transcription, and in turn, translation, was prevented until the promoter was uncaged with UV light. This

method of regulation enabled the resulting light-activated synthetic cells to be controlled remotely and in a spatiotemporally-controlled manner. To demonstrate the versatility of this platform, light-activated synthetic cells that participated in one-way communication with living cells were constructed. These compartments expressed an N-acyl homoserine lactone synthase in response to UV light, which synthesised an N-acyl homoserine lactone that was released and detected by engineered *E. coli* cells.

Acknowledgements

I would like to sincerely thank everyone that has supported me during my DPhil and made these last four years a very rewarding experience. Firstly, Dr Michael Booth for his unwavering support throughout my entire PhD and for granting me the opportunity and freedom to explore exciting research. You have made me the scientist I am today. Second, to Prof. Hagan Bayley, for making me feel included within the extended Bayley group, especially during the early years of my PhD. Also to all Booth and Bayley group members, past and present, for their advice and for making the CRL an amazing place to work. Special mentions go out to Matthew Cornall, Giacomo Mazzotti, Pablo Martin-Baniandres, Khoa Chung, Dr Boon Lim, and Jack Holland for all the pub trips and brightening long days when science did not behave itself. To Razia Chowdhry, alongside whom I am lucky to have spent my entire DPhil journey, for being a thoughtful friend and sharing my love (and loathing) of vesicles. To Assala Al Samad, for being a best office neighbour and buying the tastiest snacks, and to Denis Hartmann, for synthesising the isovaleryl homoserine lactone used in this work. Finally, I would like to thank my family, who have always supported me in every way imaginable, and to Sophia Carlarne, for putting up with me, the late nights, missed weekends and being my absolute angel. I also want to express my gratitude to the Synthetic Biology CDT and the Engineering and Physical Sciences Research Council for giving me the opportunity to undertake this research.

Abbreviations

3OC6-HSL = N-(3-oxohexanoyl)-L-homoserine lactone

3OC12-HSL = N-(3-oxododecanoyl)-L-homoserine lactone

αHL = α-hemolysin

AβC = Artificial beta cell

ACP = Acyl carrier protein

AI-2 = Auto-inducer 2

AHSL = N-acyl homoserine lactone

AnExILs = Antigen-expressing immunostimulatory liposomes

araC = Arabinose-sensitive repressor

ATP = Adenosine triphosphate

Bac2A = Bactenecin

BDNF = Brain-derived neurotrophic factor

BSA = Bovine serum albumin

C4-HSL = N-butyryl-L-homoserine lactone

C6-HSL = N-hexanoyl-L-homoserine lactone

C8-HSL = N-octanoyl-L-homoserine lactone

cDice = Continuous droplet interface crossing encapsulation

CFPS = Cell-free protein synthesis

CoA = Coenzyme A

CTP = Cytosine triphosphate

Dox = Doxycycline

epPCR = Error-prone polymerase chain reaction

GFP = Green fluorescent protein

GOI = Gene of interest

GTP = Guanosine triphosphate

GUV = Giant unilamellar vesicle

IPTG = Isopropyl β-D-1-thiogalactopyranoside

IV-CoA = Isovaleryl coenzyme A

IV-HSL = N-isovaleryl-L-homoserine lactone

IVTT = *In vitro* transcription translation

LA-DNA = Light-activated DNA

LacI = Lac repressor

LacZ = β-galactosidase

MLV = Multi-lamellar vesicle

mNG = mNeonGreen

mSA = Monovalent streptavidin

NT = Nucleotide

NTPs = Ribonucleotide triphosphates

ORF = Open reading frame

PC = Phosphatidyl choline

PCB = Photocleavable biotin group

PCR = Polymerase chain reaction

PEG = Poly(ethylene) glycol

PFO = Perfringolysin O

PURE = Protein synthesis using recombinant elements

QS = Quorum sensing

RBS = Ribosome binding site

RNAP = RNA polymerase

SAM = S-adenosyl methionine

SC = Synthetic cell

SCRaMbLE = Synthetic chromosome recombination and modification by LoxP-mediated evolution

SELEX = Systematic evolution of ligands by exponential enrichment

sfGFP = Super folder green fluorescent protein

SUV = Small unilamellar vesicles

TetR = Tetracycline repressor

TF = Transcription factor

TR = Texas Red

UTR = Untranslated region

UV = Ultraviolet

WCF = Watson-Crick-Franklin

W/O = Water/Oil

Contents

1 Introduction **1**

1.1 Rengineering biology 1

1.1.1 Top-down synthetic cells 3

1.1.2 Bottom-up synthetic cells 8

1.2 Designing gene-expressing synthetic cells cells from the bottom-up 9

1.2.1 Compartmentalisation 10

1.2.1.1 Liposomes 10

1.2.1.2 Polymersomes 12

1.2.1.3 Proteinosomes 13

1.2.2 Cell-free protein synthesis 13

1.2.2.1 Cell-free lysates 15

1.2.2.2 Protein synthesis Using Recombinant Elements 16

1.3 Gene-expressing synthetic cells 18

1.3.1 Regulating gene expression in synthetic cells with small molecules 18

1.3.2 Regulating gene expression with light 22

1.4 Synthetic cell communication 26

1.4.1 Cellular communication in natural systems 27

1.4.2 Quorum sensing 28

1.4.3 Communication in gene-expressing synthetic cells 31

1.4.3.1 *In situ* release of membrane impermeable messengers . . 31

1.4.3.2 *In situ* synthesis of membrane permeable messengers . . 33

1.5 Therapeutic applications of synthetic cells 35

1.6 Summary of thesis work 38

2 Gene expressing liposomes as programmable synthetic cells 40

2.1 Introduction 40

2.1.1 Formation of giant unilamellar vesicles 40

2.1.1.1 Spontaneous swelling of lipid films 41

2.1.1.2 Electroformation 42

2.1.1.3 Freeze dried liposome hydration 42

2.1.1.4 Emulsion droplet transfer 43

2.1.1.5 Continuous droplet interface crossing encapsulation . . . 45

2.1.1.6 Microfluidics 45

2.1.2 Chapter overview 46

2.2 Assembly of gene expressing giant unilamellar vesicles 47

2.3 *In vitro* gene expression 47

2.4 Preparation of GUVs 49

2.4.1 Lipid in oil 50

2.4.2 Emulsification 51

2.4.3 Outer solution 52

2.4.4 Centrifugation 53

2.4.5 Wash steps 54

2.4.6 Imaging 54

2.5 *In situ* gene expression inside GUVs 55

3 Light-activated gene expression in GUVs 64

3.1 Introduction 64

3.1.1 Maximising gene expression in cell-free systems 64

3.1.2 Chapter overview 66

3.2 Preparing and testing light-activated DNA 66

3.3 Maximising protein synthesis with LA-DNA templates 71

3.4 Light-activated gene expression inside GUVs 76

3.5 Spatial control of light-activated synthetic cells 80

4 Communication between synthetic cells and bacteria 86

4.1 Introduction 86

4.1.1 Quorum sensing for synthetic cell communication 86

4.1.2 Directed evolution 89

4.1.3 Directed evolution of transcription factors involved in quorum sensing 93

4.1.4 Chapter overview 94

4.2 Charactering BjaR receiver cells 95

4.3 Directed evolution of BjaR 97

4.4 BjaR mutant characterisation 101

4.5 Assembly of IV-HSL producing synthetic cells 105

4.6 Synthetic cell to living cell communication 113

5 Dual input activation of synthetic cells 117

5.1 Introduction 117

5.1.1 Riboswitches in synthetic cells 117

5.1.2 Chapter overview 119

5.2 Controlling CFPS with translational riboswitches 119

5.3 Controlling CFPS with light and histamine 123

6 Conclusion and future directions 126

7 Methods 131

7.1 Materials 131

7.2 General methods 132

7.2.1 Homologous recombination 132

7.2.2 Preparation of linear DNA templates 133

7.2.3 Ethanol precipitation 133

7.2.4 DNA quantification 134

7.3 Chapter 2 methods 134

7.3.1 Plasmid construction 134
7.3.2 Linear DNA templates 135
7.3.3 Cell-free protein synthesis 135
7.3.4 Formation of GUVs 135
7.3.5 Imaging chambers 137
7.3.6 Epifluorescence microscopy 138
7.3.7 Image processing 138
7.4 Chapter 3 methods 138
7.4.1 Plasmid construction 138
7.4.2 Linear DNA templates 142
7.4.3 Modification of amine DNA 142
7.4.4 HPLC 143
7.4.5 Formation of light-activated DNA 143
7.4.6 UV lamp irradiation 144
7.4.7 Gel electrophoresis 144
7.4.8 Cell-free protein synthesis 144
7.4.9 Assembling LA-SCs 145
7.5 Chapter 4 methods 145
7.5.1 Media 145
7.5.2 BjaI gene synthesis 146
7.5.3 Plasmid construction 146
7.5.4 Directed evolution 152
7.5.5 Measuring BjaR reporter performance 153
7.5.6 Preparation of linear DNA templates 153
7.5.7 Preparing LA-BjaI DNA templates 154
7.5.8 CFPS of BjaI 154
7.5.9 Preparing a OnePot PURE system 154
7.5.10 Preparation of synthetic cells 154
7.5.11 Preparing agarose pads 155

7.6 Chapter 5 methods 155
7.6.1 Plasmid construction 155
7.6.2 Preparation of linear DNA templates 157
7.6.3 Preparation of LA-DNA templates 158
7.6.4 Cell-free protein synthesis 158
7.6.5 GUV assembly 158
7.7 Primer sequences 159

1

Introduction

1.1 Rengineering biology

A major aspiration of synthetic biology is to re-engineer living systems to perform new functions outside their natural capabilities and apply them in an industrial or commercial setting. To reach this goal, a significant amount of time and resources have been invested into developing new tools to manipulate DNA [1–4] and in learning the design rules necessary to programme cells with biological gene circuits [5]. Still, it remains challenging to design gene circuits that perform as intended from first principles alone, as natural sys-

tems are incredibly complex and intrinsically variable. For example, when heterologous genes are introduced into a host, even into model organisms such as *Escherichia coli* or *Saccharomyces cerevisiae*, the integrated parts are not immediately interchangeable and often do not perform as expected. This could be for a number of reasons. The heterologous proteins may be expressed at a different level than anticipated, or in some cases, not at all. Alternatively, the new parts may not function correctly under their new biological context as heterologous pathways can compete for resources with host pathways, disrupting cellular homeostasis. Also, introducing a designed gene circuit could impose a significant burden on the host, reducing its fitness and making the circuit unstable [6].

Consequently, new cellular functions have to be engineered iteratively through multiple design-build-test cycles that gradually improve gene circuit performance and cellular fitness. In this way, gene circuits that encode the machinery capable of performing the desired function are designed in silico, then built according to these blueprints and introduced into the host cell. The performance of the resulting cells is then scrutinised against the design specifications, and these insights are used to infer the design of the next generation of gene circuits. Each laborious cycle can often take weeks or months without automated high throughput workflows; hence, simpler and more tractable alternatives for creating designer cells, for particular applications, are sought. The concept of using synthetic cells (SCs) which have a well-defined biological background has been proposed as a solution to this problem. These can either be constructed from the top-down or the bottom-up, and offer the potential to design cells that function as intended (Figure 1.1).

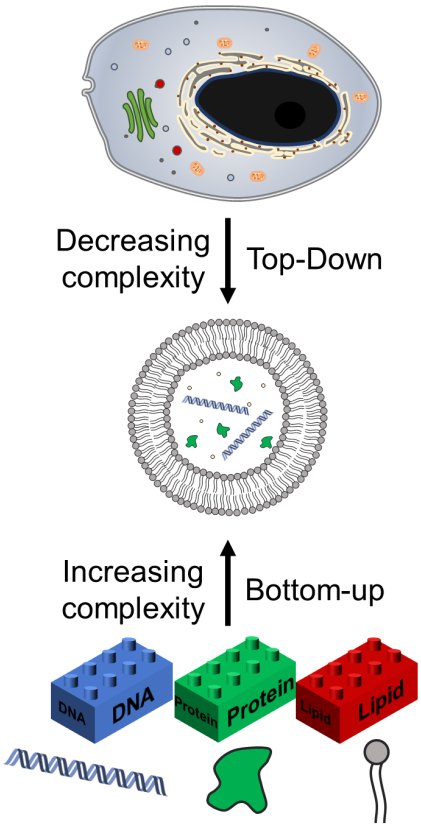


Figure 1.1: Top-down vs bottom-up synthetic cell
Top-down SCs are assembled by reducing the complexity of natural cells, whereas bottom-up SCs are modular entities built from only the building blocks necessary for the desired function.

1.1.1 Top-down synthetic cells

Top-down SC research revolves around manipulating the genetic makeup of living cells - either removing, adding, or mutating genes - to create new cells capable of the desired, novel function. While multiple avenues are being explored to reach this goal, one particularly ambitious route focuses on creating minimal SCs programmed by designer genomes. Using the *Mycoplasma mycoides* genome sequence, one of the smallest known to exist in nature, as a starting point, researchers were able to assemble a synthetic version of the bacterial genome from short oligonucleotides [7]. When this synthetic genome was transplanted into a closely related *Mycoplasma capricolum* recipient cell that had been stripped of its own genome, the naturally-derived cellular hardware successfully accommo-

dated the chemically-derived genetic software yielding viable SCs (denoted JVCI-syn1.0) (Figure 1.2) [8]. JVCI-syn1.0 cells were morphologically distinct from the *M. capcicolum* host, and had a different growth rate and total protein profile. Instead, they reflected the *M. mycoides* phenotype encoded by the synthetic genome, and exhibited the additional hallmarks that were introduced during assembly of the synthetic genome to distinguish it from the wild-type genome; namely, genetic watermark sequences and expression of a heterologous reporter gene (lacZ). Collectively, this work outlined the tools necessary to assemble a new class of SCs and confirmed that novel genetic material introduced during genome assembly process was tolerated, laying the foundations for creating living cells programmed by designer genomes.

Consequently, in pursuit of a truly minimal genome in which novel functions could be built, JVCI-syn1.0 cells were subsequently subjected to global transposon mutagenesis to elucidate whether each gene in the synthetic genome was dispensable or essential for life [9]. During this process each gene was knocked out, individually and at random, in the hope to better characterise the fundamental biochemical processes that underpin cell biology and make cell engineering a more predictable endeavour. A minimised synthetic genome assembled from only 473 of the initial 985 genes, those deemed essential for cell viability, was sufficient to generate living cells (denoted JVCI-syn3.0) [9], but this minimal cell could only grow and divide robustly after seven additional genes deemed non-essential during mutagenesis were reintroduced in the synthetic genome [10]. Five of these seven genes and around 17% of the minimal genome were functionally undefined, representing how much more we still need to understand before we can construct autonomous, robust cells from scratch. Consequently, the initial optimism toward creating tailor-made cells from de novo designed genomes has yet to be translated into meaningful progress.

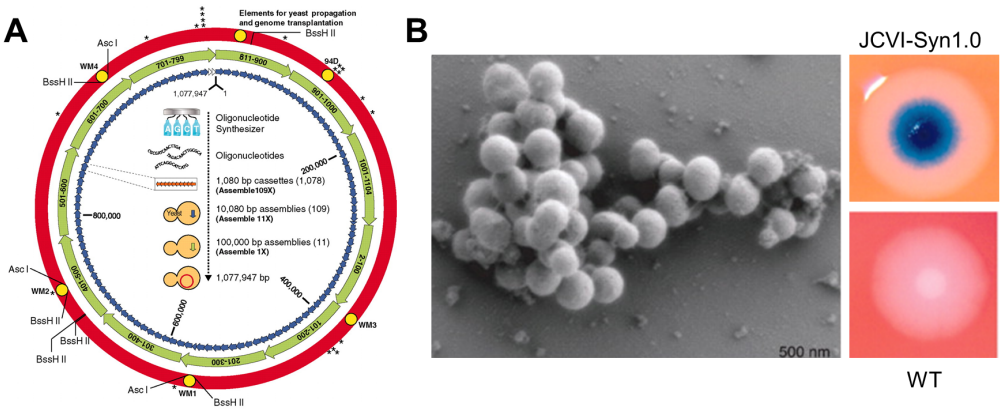


Figure 1.2: Top-down synthetic cells
A) Design of the synthetic genome via the hierarchical assembly of smaller oligonucleotides. B) The resulting synthetic cell encoded from the transplanted synthetic genome. JVCI-Syn1.0 produced blue colonies on X-Gal plates due to LacZ expression. *M. mycoides* does contain lacZ and produced white colonies. (Figure adapted from [8] with permission from AAS).

Greater success has been achieved using synthetic, refactored yeast chromosomes [11]. The Sc2.0 project, an extensive collaborative effort involving 13 institutes across six different countries, has focused on chemically synthesising and customising each of the 16 chromosomes in *S. cerevisiae* [11]. These changes included the omission of troublesome genetic material, such as transposons, to improve the stability of the redesigned chromosomes, and inclusion of new sequence motifs to accommodate greater flexibility in the design and evolution of the engineered cells. By replacing all of the amber (UAG) stop codons with ochre (UAA) stop codons, the UAG codon was freed up and could be assigned to a novel tRNA synthetase that introduces user-defined non-native amino acids into polypeptides [12–14]. loxPsym sites were also inserted at the 3' end of non-essential genes and introns to establish an inducible recombinase-based evolution platform, termed Synthetic Chromosome Rearrangement and Modification by LoxP-mediated Evolution (SCRaMbLE) [15]. In this manner, upon addition of oestradiol, a Cre-recombinase fused to an oestrogen-binding domain was transiently expressed, recognised and cut at loxPsyn sites, catalysing recombination between the sequences with exposed ends. This process induced the random inversion, deletion, duplication, and translocation of non-essential

genes within the synthetic chromosomes, which consequently varied their expression either by placing them downstream of different promoters and ribosome binding sites (RBSs) or varying their copy number. Each of these changes represents an exciting route to re-engineer the cells and have already shown promise. For example, SCRaMbLE was deployed to increase the titres of deoxyviolacein and penicillin that were synthesised by yeast cells [16]. Yeast cells containing a SCRaMbLEd chromosome V produced up to 2.3-fold higher deoxyviolacein titres than the existing strain by deleting or inverting genes to increase plasmid copy number, changes which could not have been predicted by rational design. Despite the obvious benefits granted by improving the genetic background of engineered cells, the problem of truly designable function remains; gene circuits and *de novo* genomes do not always behave as we expect them to when introduced into cells.

A more radical top-down approach to generating SCs would be to remove the cell's genome altogether and repurpose the well-defined cellular hardware with only the genetic software necessary for the desired function. This type of platform has been approached in two ways; by budding genome-free miniature cellular compartments from a parent cell or by destroying the host genome with restriction enzymes (Figure 1.3). The first strategy exploits MinD mutant bacteria to initiate aberrant cell division. MinD, in conjunction with MinC and MinE, defines the midpoint of cells where FtsZ proteins assemble the cleavage furrow and split an elongated cell into two separate daughter cells [17]. Impairing the identification of the cell midpoint causes small <1 μm-sized cell-like structures to bud off the poles of a parent cell that contain the parental cytosolic material, including plasmids held within the parental cell, but lack the parental genome [18]. Alternatively, empty cell-sized compartments have been created by destroying the genome with a restriction enzyme, I-CeuI. I-CeuI recognises a 27 bp sequence found multiple times in many species of bacteria and thus can introduce several double-strand breaks into their genomes. Double-strand

breaks are incredibly toxic and are usually repaired immediately by the RecBCD-mediated homologous recombination; however, sustained cleavage by I-CeuI can create genome-less cellular compartments containing the complete complement of the host hardware [19]. In both cases, the resulting compartments referred to as mini-cells and sim-cells, respectively, retain the cellular machinery for transcription and translation, allowing the compartments to be repurposed with user-defined gene circuits. As the host genomes has been removed, these compartments are no longer autonomous living cells capable of growth and division, and represent an attractive chassis for applications where containment is an issue, for example, *in vivo* biosensing [20] and biological therapeutics. Although, it is currently difficult to establish homogeneous, pure mini-cell and sim-cell samples [21], and more work is necessary to establish the extent to which these compartments can be reprogrammed, including whether they can re-acquire DNA through horizontal gene transfer.

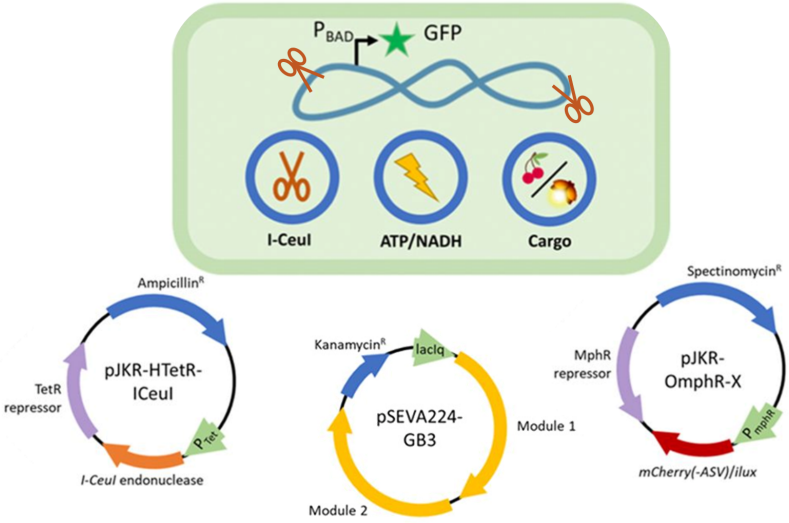


Figure 1.3: Genome-less cellular compartments as a chassis for synthetic biology
Plasmids encoding proteins for a desired function can be co-transformed with I-CeuI encoding plasmids to create chromosome-free compartments with a defined function. (Figure adapted from [19].)

1.1.2 Bottom-up synthetic cells

Unlike the traditional cell engineering approaches, bottom-up SCs offer a blank breadboard into which biological, chemical, or hybrid parts can be introduced. Despite adopting many different forms, SCs assembled from the bottom-up generally share similar design principles; they are self-contained systems defined by a physical boundary that use biological or biologically inspired parts to mimic cell-like processes. In nature, the boundary of a living cell is its plasma membrane, comprised of lipids, proteins, and carbohydrates. Similarly, SCs have also been assembly from lipid-based compartments known as liposomes or lipid vesicles [22], yet since SCs don't have to conform to natural design rules compartmentalisation has also been achieved with membranes made of polymers (polymersomes) [22], colloids (colloidosomes) [23], proteins (proteinosomes) [24], Janus dendrimers (dendrimersomes) [25], peptides [26], or with oppositely charged polymers that form membraneless-compartments by liquid-liquid phase separation (coacervates) [27]. These membranes restrict and regulate the transfer of material between the internal and external environments according to their intrinsic permeability [28] and whether membrane proteins are present [22, 29]. Consequently, the aqueous lumen inside each compartment can be filled with proteins, small molecules, or even complex mixtures of both proteins and small molecules that perform biochemical reactions such as those involved in gene expression [30, 31] or metabolic processes [32].

Many different varieties of SCs have been constructed, each with a different make-up based on the desired application. Some researchers use SCs containing purified proteins to study biological phenomena, including cell division [33–35] and transmembrane signalling [36], while others exploit chemically-derived SCs for their emergent, life-like properties [37]. To date, the most popular, generalisable SC model has been the assembly of li-

posomes that contain a cell-free protein synthesis (CFPS) system capable of performing both transcription and translation *in situ* [29, 31]. In this model system, DNA templates within the lumen are transcribed into the corresponding mRNA sequence and subsequently translated into the corresponding polypeptide sequence. By mirroring the central dogma of biology, the DNA template (genotype) dictates the protein made (phenotype), which dictates the function of these SCs. This versatile plug-and-play approach means the biological circuitry introduced operates under a completely neutral background, without crosstalk with other host processes or cellular burden, and new functions can be installed simply by changing the DNA template used. Manufacturing synthetic cells in this manner has multiple benefits. First, SC functions can be designed more predictably as the DNA operates in a neutral environment. If required, these new SC designs can also be rapidly screened for improved performance as the time it takes to complete each design-build-test cycle is on the order of hours to days, rather than the days to weeks required for the cloning, transformation, growth, and screening of living cells. In addition to this, SC are non-living, non-autonomous entities that do not mutate under a selection pressure. Consequently, they can be deployed in environments where living cells represent a biosecurity threat, for example, *in vivo* therapeutics. Finally, unlike living cells, SC are not limited to the toolbox of natural parts; they have a fully synthetic tool kit in addition to the biological parts and can therefore adopted behaviours unseen in the natural world.

1.2 Designing gene-expressing synthetic cells cells from the bottom-up

Gene-expressing SCs created from the bottom-up are incredibly versatile platform. Depending on the application and environment the SC is deployed in, different parts are

used. Thus, researchers face two major considerations when designing gene-expressing SCs. First, what properties does the membrane of the compartment need to fulfil its intended function, and what building blocks can be used to achieve this? Second, which type of CFPS system is most suited to achieve the desired outcome, and how can this in introduced inside the compartment? The following sections highlight the various building blocks used to assemble SCs.

1.2.1 Compartmentalisation

In nature, cell membranes are assembled from phospholipids, proteins, and carbohydrates, and play a fundamental role in cellular homeostasis beyond simply defining the cell boundary and entrapping genetic and cellular machinery. Membranes regulate the movement of molecules into and out of the cell in response to cellular requirements, and are essential for cell-cell signalling pathways. Although it is difficult to incorporate every one of these functions into model membranes, synthetic versions can be built using lipids and other alternative building blocks to mimic many of the properties found in natural cell membranes.

1.2.1.1 Liposomes

Liposomes are spherical compartments composed of phospholipids, amphipathic molecules that contain a hydrophilic head group linked to long hydrophobic acyl chains (Figure 1.4A). Owing to the disparate properties of either end of the phospholipid, lipids have interesting behaviours under aqueous conditions. Exposure of the hydrophobic tails to an aqueous solution is thermodynamically unfavourable as water molecules must be highly ordered to solvate the acyl chains, decreasing the system's entropy. In contrast, exposure of the polar head groups to water is thermodynamically favourable as the formation of hydro-

gen bonds between the head groups and water molecules contribute to increasing the system's entropy [38]. These phenomena are the driving forces behind the hydrophobic effect whereby the acyl chains are excluded from the aqueous solution and buried inside hydrophobic core, which is protected from the aqueous solution by the hydrophilic head groups. Hence, placing lipids in an aqueous environment triggers the spontaneous formation of spherical lipid clusters (micelles) or sealed compartments with an internal lumen separated from an external solution by a phospholipid bilayer (liposomes) (Figure 1.4B).

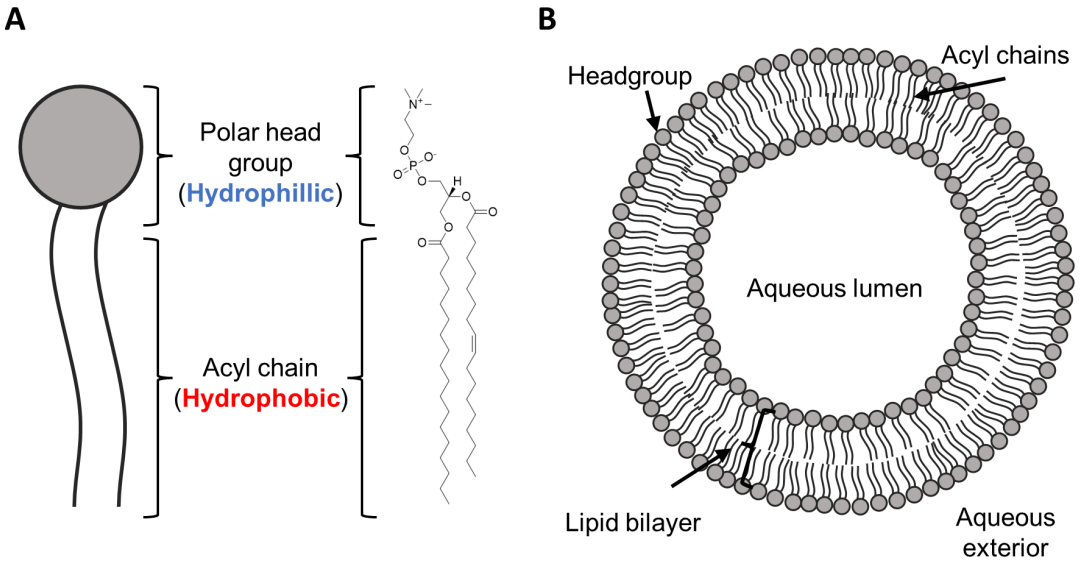


Figure 1.4: Lipids and liposomes
A) Schematic of lipids indicating the corresponding chemical composition. B) A liposome formed by the self-assembly of lipids into continuous spherical bilayers

Liposomes can be assembled using both natural and synthetic lipids, which themselves come in a variety of forms. Most lipids share a general structure but generally vary in the charge of their head group or length and saturation of their acyl chains. For example, 1,2-dioleoyl-sn-glycero-3-phospho-L-serine (DOPS), 1,2-dioleoyl-sn-glycero-3-phosphocholine (DOPC), and 1,2-dioleoyl-3-trimethylammonium-propane (DOTAP) have negatively, neutrally and positively charged headgroups, but the same chain length; 1,2-dimyristoyl-sn-glycero-3-phosphocholine (DMPC), 1,2-dipalmitoyl-sn-glycero-3-phosphocholine (DPPC), and distearoyl-sn-glycero-3-phosphocholine (DSPC) have the same headgroup but varying

acyl chain lengths; and DSPC, 1-stearoyl-2-oleoyl-sn-glycero-3-phosphocholine (SOPC), and DOPC have the same chain lengths but a different number of C=C bonds. All these properties represent opportunities to change the permeability, charge, fluidity and thickness of the lipid membrane and tailor them to different applications by forming membranes with different combinations of lipids.

1.2.1.2 Polymersomes

Polymersomes are similar structures to liposomes. They contain an internal lumen separated from the external environment by a membrane; however, the amphiphiles used in their assembly are block copolymers rather than lipids. As the name suggests, block copolymers are formed by connecting polymers with different properties into a single chain. Hydrophobic polymers, such as poly(butadiene), are flanked by hydrophilic polymers, such as poly(ethylene oxide), at one or both ends to mimic the acyl tails and head group regions of lipids, respectively [39]. Depending on the arrangement of the polymers used, polymersomes may have either a bilayer structure comprised of di-block or tri-block copolymers, or a monolayer structure comprised of horizontally aligned tri-block copolymers [39]. The hydrophobic interactions between the polymers are typically stronger than between lipids within bilayers, which combined with the improved chemical stability of polymers over lipids makes polymersomes more mechanically and chemically stable than liposomes - they can last on the order of months rather than hours or days [22, 40]. Their size is determined by the method used to prepare the vesicles, solvent composition, and polymer concentration used for polymersome formation, while the thickness of the membrane is tuned according to the molecular weight of the hydrophobic polymer [39]. Although polymersomes are typically impermeable to ions and small molecules, incorporating protein pores into the polymer membranes enables the exchange of material

between the lumen and external environment [41]. Like liposomes, CFPS systems can be encapsulated inside polymersomes to perform compartmentalised *in vitro* gene expression [42].

1.2.1.3 Proteinosomes

Proteinosomes are a class of compartments between liposomes and polymersomes that use both biological (proteins) and chemical (polymers) materials to assemble hybrid vesicles. Proteinosomes are formed by conjugating aliphatic polymers to a cationised protein of interest, establishing a large amphiphile with a protein-based head group. Polymers like poly(N-isopropylacrylamide) have been conjugated to globular proteins such as bovine serum albumin (BSA) and haemoglobin via exposed amines at the surface of the proteins [24], though other polymers and proteins, even enzymes, can be used to create catalytically active membranes. When Pickering emulsions are formed by placing water droplets containing the polymer-protein conjugates into an oil phase - protein-polymer vesicles self-assemble at the water/oil interface to stabilise the droplets. After the monomers are conjugated with one another, the resulting micron-sized compartments are sufficiently stable to be transferred back into the water phase while containing the droplet contents inside a water-filled lumen. Like a natural lipid membrane, the protein-polymer membranes are semi-permeable, even allowing the exchange of large biomolecules such as oligonucleotides across the membrane [43]. However, cargo such as CFPS systems can also be retained inside the compartment to perform *in vitro* gene-expression [24].

1.2.2 Cell-free protein synthesis

Protein synthesis proceeds in two steps, the conversion of a DNA sequence into an mRNA sequence (transcription), and subsequently, the conversion of the mRNA sequence into an

amino acid sequence (translation). During transcription, an RNA polymerase (RNAP) binds to a promoter sequence within a DNA template and synthesises an mRNA strand corresponding to the sense (coding) strand according to complementary Watson-Crick-Franklin (WCF) base pairing. In simple cases, this occurs constitutively and requires only the RNAP [44] or the pre-assembled holoenzyme [45] to polymerise free ribonucleotide triphosphates (NTPs) bound at the exposed nucleobases in the template strand. However, transcription in eukaryotes [46], and inducible gene expression systems require additional proteins known as transcription factors (TFs) to recruit the polymerase to the promoter [47]. Transcription of DNA occurs until the RNAP reaches a transcription terminator site or falls off the 3' ends of the DNA template.

During translation, a ribosome binds to a conserved RNA sequence towards the 5' end of an mRNA strand, the ribosome binding site (RBS), via WCF base-pairing between the mRNA and a complementary sequence located in the rRNA of the small ribosomal subunit. In prokaryotes, this occurs co-transcriptionally as soon as the RBS exits the RNAP, whereas in eukaryotes, translation follows the nuclear export of the mature-mRNA into the cytoplasm [48]. Initiation factors position the gene's start codon encoded in the mRNA, typically AUG, within the peptidyl site of the small ribosomal subunit via WCF base-pairing with the corresponding anti-codons in an initiating transfer RNA (tRNA). Upon binding the large ribosomal subunit, a stable initiation complex is formed, and ribosomes can sequentially add amino acids to the growing polypeptide chain according to codons in the mRNA until the ribosome reaches a stop codon and disassembles from the mRNA [48].

Transcription can be reduced down to a simple biochemical reaction involving only an RNAP in a physiological buffer solution containing NTPs, magnesium, and spermidine, and is frequently reconstituted *in vitro* to synthesise RNA [44]. On the other hand,

translation requires a complex ensemble of ribosomes, amino acids, tRNAs and up to 36 different proteins, including tRNA synthetases to load amino acids onto tRNAs, and enzymes involved in adenosine triphosphate (ATP) and guanosine triphosphate (GTP) regeneration, to synthesise proteins. By reconstituting the transcription and translation machinery *in vitro*, coupled cell-free transcription and translation can be achieved. The benefits of CFPS are multi-fold. 1) toxic proteins that would otherwise kill the host cell can be expressed at higher yields. 2) DNA constructs can be rapidly prototyped as they are added directly into the reaction mixture rather than transformed into cells and grown up in large cultures. 3) CFPSs are portable and can be deployed in the field as small aliquots or freeze-dried on paper. 4) New functional groups can easily be incorporated into the growing polypeptide chain by supplementing the reactions with non-native amino acids and tRNA synthetases [49]. CFPS can be performed with either cell lysates [50, 51] or recombinantly expressed and purified proteins, i.e. the Protein synthesis Using Recombinant Elements (PURE) system [52].

1.2.2.1 Cell-free lysates

Cell-free lysates are created by growing cells under controlled conditions, lysing them, and then separating lower molecular weight components (the enzymes and ribosomes) from the higher molecular weight components (the organelles and intact membranes) by centrifugation (Figure 1.5). Depending on the centrifugation speed used, 12,000 x g or 30,000 x g, different cellular components are removed, and lysates with different compositions are obtained, denoted S12 or S30 lysates respectively [53, 54]. To maximise the efficiency of CFPS, lysates are combined with an energy solution containing NTPs and amino acids, as well as small molecules involved in adenosine triphosphate (ATP) or guanosine triphosphate (GTP) regeneration (Creatine phosphates), and transcription

termination (spermidine). Cell lysates have been prepared from many different cell types depending on their requirements. *E. coli* lysates are most common and fulfill general protein synthesis requirements owing to the high level of gene expression and wealth of parts for controlling *E. coli* gene expression. Wheat-germ, rabbit reticulocyte or mammalian cell lysates are used to express more complex proteins that require post-translation modifications [55]. Lysates are closely aligned with natural systems; for example, they still contain glycolytic pathways [56], enzymes involved in fatty acid synthesis [57], and nucleases and proteases to turnover mRNA, DNA and proteins. Therefore, lysates still somewhat represent a black box and are difficult to fully define.

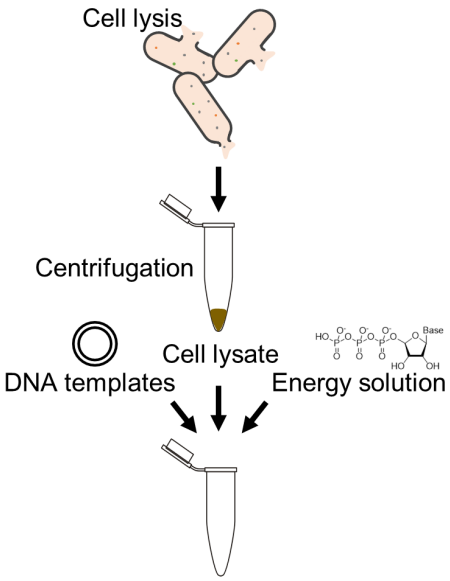


Figure 1.5: Preparation of cell lysates for cell-free protein synthesis
Cells are lysed, centrifuged, and the clarified lysate mixed with energy solution. Proteins are synthesised from DNA templates containing a gene of interest placed downstream of an *E. coli* host RNAP promoter.

1.2.2.2 Protein synthesis Using Recombinant Elements

The PURE system is essentially a stripped-down version of cell-lysates and represents the minimum requirements for robust CFPS. PURE is prepared by expressing each of the proteins necessary for transcription, translation, and ATP or GTP regeneration, sep-

arately, as N-terminally His-tagged fusion proteins in *E. coli*, purifying them from the host proteins and recombining them with ribosomes and an energy solution (Figure 1.6). However, unlike cell lysates, the host *E. coli* RNAP is replaced by the T7 bacteriophage RNAP to achieve higher rates of transcription from T7 promoter-containing DNA templates. These can either be plasmids or linear templates obtained by PCR as this system does not contain the host nucleases like cell lysates. Since all the components that make-up the PURE system are known, this system is a far more tractable CFPS system than cell-free lysates and less affected by batch-to-batch variation. Although, producing the PURE system in-house is a particularly labour-intensive process. To simplify and accelerate the process, engineered *E. coli* strains have been generated whereby His-tags were introduced into the genes encoding the PURE proteins within the *E. coli* genome [58] to aid purification. One-pot methods where all the enzymes are co-expressed and purified together [59–61] have also been used. Still, ready-made, commercially available PURE systems, such as PURExpress [62], are typically used for convenience.

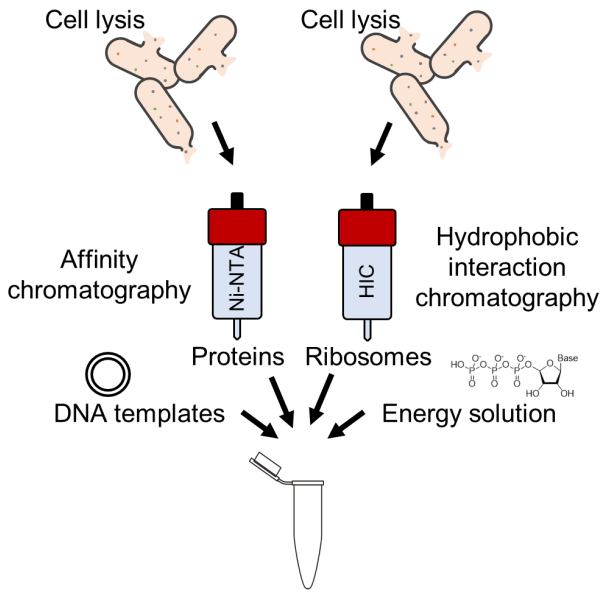


Figure 1.6: Preparation of the PURE system for cell-free protein synthesis
His-tagged proteins are expressed, individually, in *E. coli*. Proteins are purified from the lysate by affinity chromatography and combined with ribosome and energy solution. Proteins are synthesised from DNA templates containing a gene of interest placed downstream of a T7 RNAP promoter.

1.3 Gene-expressing synthetic cells

1.3.1 Regulating gene expression in synthetic cells with small molecules

Inspired by nature, gene expression inside SCs is regulated by targeting the transcription of DNA into mRNA or the translation of mRNA into protein. However, unlike living cells, SCs lack the membrane receptors, transmembrane transporters, and sophisticated signalling cascades responsible for relaying or importing the messengers that control transcription factor activity. Instead, membrane-permeable small molecules that can freely diffuse across lipid membranes (Figure 1.7 - left) or membrane-impermeable signals that are small enough diffuse through protein pores inserted in SC membranes (Figure 1.7 - right) interact directly with their cognate regulators to influence gene expression.

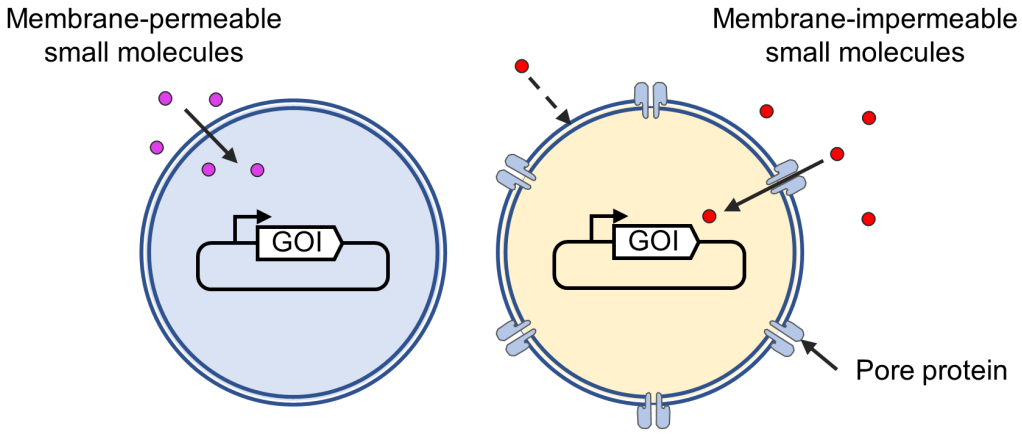


Figure 1.7: Entry of small molecules into synthetic cells
Membrane-permeable small molecules can diffuse across the lipid bilayer, but membrane-impermeable small molecules cannot and require protein pores in the membrane to access the lumen of the synthetic cell.

Most of the CFPS systems used to construct SCs are derived from bacteria; hence gene expression inside the SCs tends to be controlled with bacterial TFs. TFs including the lac repressor (LacI)[63], arabinose repressor (AraC) [64], and tetracycline repressor (TetR) [65] that are widely used in the expression of recombinant proteins were amongst

the first to be used in SCs [66]. LacI, AraC, and TetR inhibit transcription. In the absence of their cognate ligand, the proteins either bind to a promoter-proximal operator site(s) and sterically hinder the docking of an RNAP to a promoter or to operators downstream of a promoter to act as a transcription blockade for actively transcribing RNAPs. Upon binding to their corresponding ligand, the repressors are removed from the operator site, and an RNAP can interact with the promoter region to initiate transcription or continue to elongate the mRNA, respectively (Figure 1.8A). While arabinose is membrane permeable and able to diffuse across lipid bilayers unassisted, isopropyl β-D-1-thiogalactopyranoside (IPTG) and doxycycline, used to derepress LacI and TetR respectively, are membrane-impermeable and require protein pores such as αHL [66, 67] or the mechanosensitive channel of large conductance [68] to enter SCs.

More recently, TFs involved in quorum sensing (QS) have been deployed in SCs. LuxR, the archetypal QS receiver protein from *Vibrio fischeri* [69, 70], as well as EsaR, a LuxR-family protein from *Erwinia stewartii* [71], have been used to regulate transcription in SCs in response to membrane-permeable signalling molecules known as acyl-homoserine lactones (AHSLs) [57, 72–74]. While both EsaR and LuxR activate gene expression upon binding N-(3-oxo-hexanoyl)-L-homoserine lactone (3OC6-HSL), EsaR is a transcription repressor, and LuxR is a transcription activator. Activators perform the inverse function to repressors and facilitate RNAP binding rather than inhibiting it. LuxR interacts with the lux box, a conserved 20 bp inverted repeat located immediately upstream of the pLux promoter in the 3OC6-HSL bound state. Subsequently, RNAP is recruited to the promoter via protein-protein interactions, initiating transcription [70] (Figure 1.8B). In the absence of 3OC6-HSL, LuxR cannot bind the lux box and the RNAP alone is insufficient to recognise the pLux promoter, so no transcription occurs.

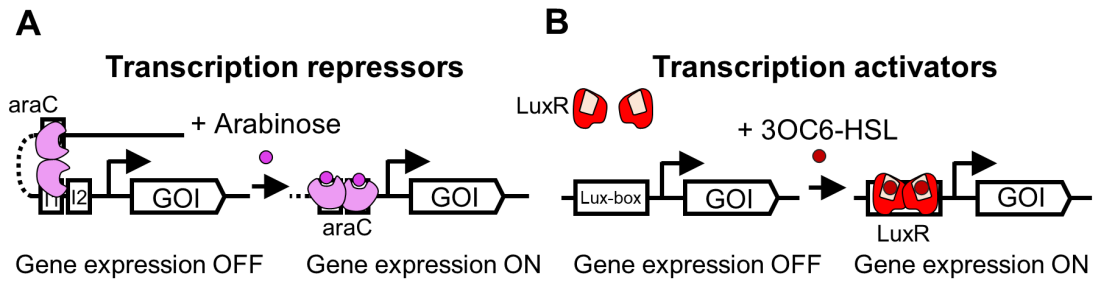


Figure 1.8: Controlling transcription in synthetic cells
Transcription can be activated by removing repressor proteins that block RNAP binding to promoters and relax looped DNA topologies (A) or recruiting RNAP to the promoters through protein-protein interactions with activator proteins bound adjacent to promoters (B).

Even after a gene of interest has been transcribed, its expression can still be regulated at the RNA level with translational riboswitches and toehold switches located in the 5' untranslated region (UTR) of an mRNA transcript. 5' UTRs are regions upstream of the start codon that were transcribed by an RNAP but are not translated by a ribosome. Riboswitches consist of an aptamer module followed by an expression platform. Aptamers are structural RNA motifs that recognise and bind to specific small molecules, while the expression platform contains the RBS necessary for translation initiation. Thus, by coupling the conformational changes that occur in the aptamer region to the sequestration or release of the RBS within the expression platform, translation initiation can be controlled with small molecules (Figure 1.9A). Theophylline riboswitches have been used to regulate the expression of genes inside SCs since theophylline is membrane permeable. However, a major caveat to this approach is the unpredictable performance of the riboswitches *in vitro*. The same theophylline riboswitch that strictly controlled gene expression in cells [75, 76] was incredibly leaky in cell-free systems [67], meaning the downstream gene is translated even in the absence of theophylline. Despite this, a promising technology that affords the potential to engineer better aptamers and, by extension, riboswitches is a method termed Sequential Evolution of Ligands by Exponential Enrichment (SELEX) [77, 78]. Through a process of rational design, to establish a baseline activity, followed by

mutagenesis and affinity selection to pull down and enrich the library with aptamers with high affinity to the molecule of interest, new riboswitches that respond to physiologically relevant small molecules including histamine [79] have been created.

Toehold switches function similarly to riboswitches, except the release of an RBS is mediated by the hybridisation of the toehold switch with a complementary ssDNA. Toehold switches are comprised of an RNA hairpin containing two stem-loops that sequester the RBS and start codon for a gene of interest, and a toehold, a region of exposed bases located immediately upstream of the hairpin. By designing a ssDNA trigger, half of which is complementary to the toehold, and half to the first stem of the hairpin, gene expression can be regulated according to base-pairing between the toehold switch and ssDNA trigger [80]. In the absence of the trigger, the RBS and start codon of the gene are sequestered in the hairpin, preventing translation initiation from occurring. Meanwhile, in the presence of the trigger, the ssDNA hybridises with the exposed bases and then unwinds the hairpin to form a double-stranded region of DNA paired to RNA. This displaces the complementary region of hairpin RNA, exposing the RBS and start codon, and enabling translation[80] (Figure 1.9B). Toehold switch-regulated gene expression is a versatile tool in biosensing applications, particularly for detecting viruses and bacteria [81], as the switch and trigger pair can be easily redesigned towards any desired target. However, they have yet to be successfully used to control SCs as attempts to regulate the switch were thwarted by the inability of ssDNA triggers to translocate through the mechanosensitive channel of large conductance (MscL) (diameter = ∼3 nm) [68]. Pores with diameters large enough to accommodate short ssDNAs such as FhuA (diameter = ∼4-5 nm) [82], or membranes that are permeable towards ssDNAs, such as those found in proteinosomes [43], are therefore necessary to successfully regulate SC activity with toehold switches.

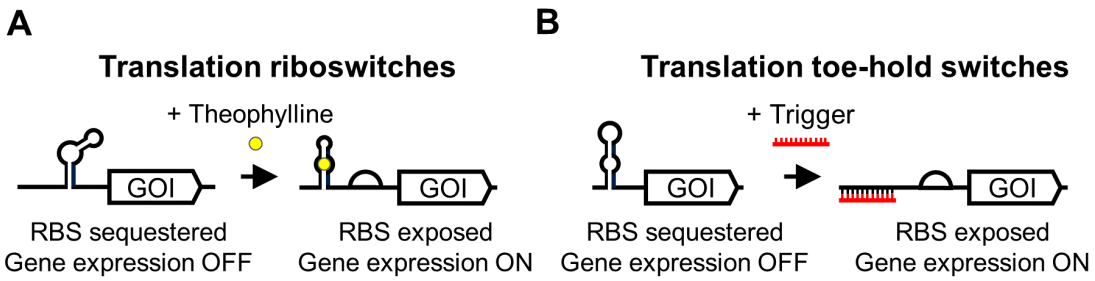


Figure 1.9: Controlling translation in synthetic cells
RBSs and start codons can be sequestered in RNA secondary structures and subsequently released by the binding small molecules with riboswitches (A) and ssDNAs with toehold switches (B).

1.3.2 Regulating gene expression with light

Using small molecules to regulate gene expression inside SCs has been helpful for proof-of-concept work, however, it is not without drawbacks. For example, inserting protein pores into SC membranes to enable the influx of membrane-impermeable molecules into the lumen simultaneously permits the efflux of small molecules residing inside the compartment, such as those required for CFPS. In addition, many of the membrane-permeable small molecules used previously are not physiologically useful or relevant, and the concentration of the small molecule in the lumen remains much lower than that of the external environment. Controlling gene expression with physical stimuli, such as light or temperature, could provide an alternative strategy that combats these limitations. Major benefits of using light rather than small molecules to activate gene expression inside SCs are multifold: light can be spatially controlled to activate specific SCs in a targeted manner, it is not diffusion limited, can be applied remotely, and tends to be biorthogonal.

Despite the abundance of protein-based optogenetic gene expression systems for mammalian, yeast, and bacterial cells [83], very few have been deployed in CFPS [84, 85] and only the YF1/FixJ two-component system has been implemented inside SCs [85]. Two-component systems are used ubiquitously in bacteria and couple a stimulus with a

genetic response using a stimuli-responsive kinase and downstream transcription factor. YF1 is an engineered light-responsive histidine kinase that regulates a transcription factor, FixJ. YF1 was constructed by replacing the Per-Arnt-Sim (PAS) motif-containing oxygen-sensing domain from a natural occurring kinase, FixL, with a comparable PAS motif-containing light-sensitive Light-Oxygen-Voltage (LOV) domain from a *Bacillus subtilis* protein, YvtA [86]. In response to blue light stimulation, rotation of the Jα alpha helix within the LOV domain causes a substantial conformational change in the kinase domain and reduces its activity 1000-fold. Consequently, in the presence of blue-light YF1 cannot phosphorylate FixJ and no gene expression occurs, whereas in the absence of light YF1 phosphorylates and activates FixJ, promoting gene expression. The opposite and arguably more useful switch has also been achieved by implementing a genetic inverter [87]. While YF1/FixJ showed up to a 70-fold difference in reporter gene expression in *E. coli* between light and no light conditions [87], only a 7-fold difference in gene expression was observed *in vitro* [85]. This marks one of the major obstacles hindering the development of cell-free systems: parts are not always conserved between cellular and cell-free systems.

A similar dynamic range was also achieved in another cell-free optogenetic switch, EL222, which has a different mode of action to YF1/FixJ. EL222 is a LOV domain-containing DNA-binding protein that dimerises and interacts with a conserved DNA sequence in response to blue light [88, 89]. In this sense, EL222 is mechanistically similar to LuxR. A blue-light responsive gene expression system has been developed by replacing the LuxR binding site from pLux promoters with the EL222 binding site [90]. This system achieved 5-fold activation of gene expression in *E. coli* cells, and >10-fold activation of cell-free gene expression [84], but has not been used in SCs.

As bottom-up SCs are non-living entities, they aren't restricted to using only biological light-sensitive machinery, and meaningful progress in this area has been made using

chemically modified light-activated DNA (LA-DNA) templates. LA-DNA is created by installing photosensitive small molecules at various positions within a DNA template. The first light-activated SCs were controlled using photocaged plasmids with up to two hundred and seventy 1-(4,5-dimethoxy-2-nitrophenyl)diazoethane (DMNPE) groups within the DNA backbone. In the absence of light, the DMPNE groups hindered transcription of the plasmid DNA into mRNA, but were removed from the DNA after exposure to UV light, which restored the ability of RNAP to transcribe the plasmid [91]. Upon irradiating DMNPE-caged plasmids encoding for GFP or luciferase with UV light, up to ∼5-fold activation of reporter gene expression was observed inside liposomes held both *in vitro* and inside mice [92]. This same system has also been used to initiate transcription inside vesicles that were endocytosed by platelets [93].

In our group, LA-DNA assembly was tackled using a different approach. Instead of conjugating a variable number of photocages at random positions within the plasmid backbone, photocleavable blockades were installed at seven pre-defined nucleotides within the T7 promoter of linear DNA templates. To achieve this, seven thymine bases within and immediately downstream of a T7 promoter were replaced with amino C6-thymine bases to install amine groups in the major groove, where T7 RNAP binds [94]. These amine groups were conjugated to a photocleavable module containing a nitrobenzyl group and terminal biotin group, to which monovalent streptavidin (mSA) was bound. Overall, the resulting LA-DNA had a T7 promoter that contained seven photo-labile blocking groups that collectively mimicked the behaviour of transcription repressor proteins; sterically hindered the T7 RNAP from binding to the T7 promoter and transcribing the downstream gene (Figure 1.10). In the absence of UV light, LA-DNA had an incredibly tight off-state, but this was completely restored after irradiation with 365 nm light affording a 100-fold activation of gene expression. These LA-DNA templates were used to drive the expression

of mVenus and αHL inside individual droplets of a 3D printed droplet interfaced bilayer (DIB) network in a spatiotemporally controlled manner [94, 95].

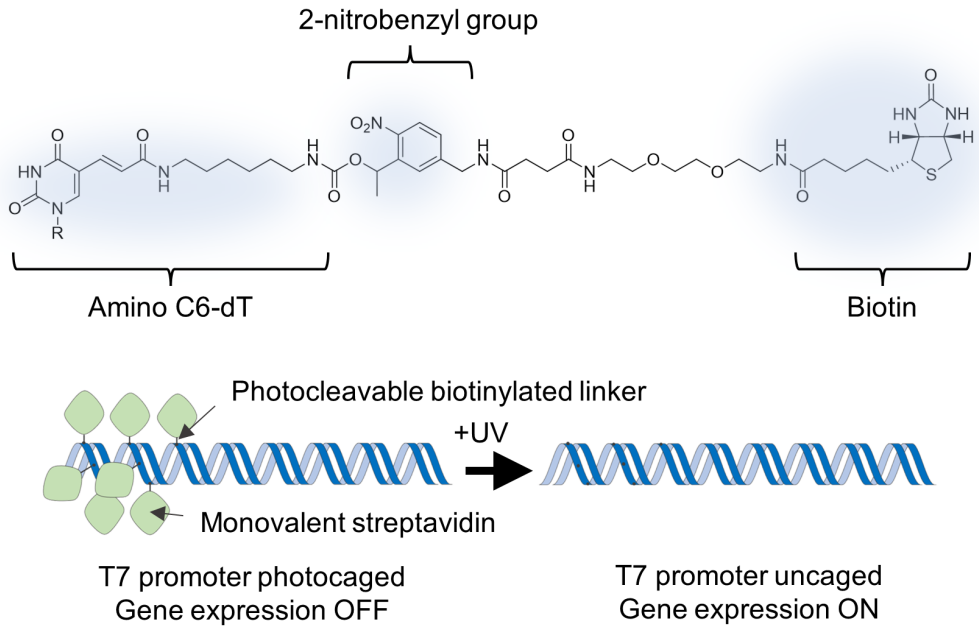


Figure 1.10: Controlling translation in synthetic cells
Photocleavable biotin groups are conjugated to amine-containing thymine nucleobases situated in a T7 promoter. Binding of mSA to the exposed biotin groups creates a steric block at the T7 promoter. In the absence of UV light, T7 RNA polymerase cannot bind to the photocaged promoter and transcription is repressed. After irradiation with 365 nm light, the 2-nitrobenzyl is cleaved and the T7 promoter containing only the amine modifications is restored. T7 RNA polymerase can bind to the uncaged T7 promoter and transcribe the downstream gene.

In addition to these one-way ON-switches whereby gene expression remains stably turned on once the photocages have been removed, two-way ON/OFF-switches that allow gene expression to be activated with one wavelength of light, then repressed in the absence of light have also been used to control CFPS. To this end, various azobenzene adducts that undergo trans-cis photoisomerisation in blue/UV light have been installed into the T7 promoters of DNA templates. In the absence of light, the trans isomer predominated and compromised the ability of the T7 RNAP to bind and unwind the T7 promoter. However, upon irradiation with 300 nm UV light (for azobenzene-4'-carboxlyic acid (Azo) and 2,6-dimethylazobenzene-4'-carboxylic acid (DM-Azo) containing DNA)

or 400 nm blue light (for 4-methylthioazobenzene-4'-carboxylic acid (S-Azo) and 2,6-dimethyl-4-(methylthio)azobenzene-4'-carboxylic acid (S-DM-Azo) containing DNA) the cis isomer predominated, triggering local deformations in the T7 promoter that allowed T7 RNAP to bind and transcribe the downstream gene [96]. Up to ∼12-fold activation of GFP expression was demonstrated on activation of SDM-Azo containing DNA with 400 nm light (when DNA was activated within in the CFPS reaction instead of before mixing), which is comparable with the light-activated plasmid [92], EL222 TF [84], and YF1/FixJ TCS [85], but much lower than LA-DNA with the photocaged T7 promoter [94]. Simpler strategies involving addition of azobenzene-based nucleic acid binders to CFPS systems, without attachment to the DNA, have also shown use in modulate gene expression with light [97, 98]. However, incorporating them into the DNA templates offers a greater level of control, and these molecules have been shown to rupture lipid bilayers [99], preventing their use in liposomes.

1.4 Synthetic cell communication

For compartments to be considered SCs, they must recapitulate some of the behaviours exhibited by natural living cells. Many different functions have been installed into the various compartmentalised systems such as metabolic processes [32], division [33, 35], motility [100], and communication with other SCs [66, 73, 101] or living cells [57, 67, 74, 102] by either installing the naturally occurring biological parts or engineering new ways of achieving the same outcome. Communication has received significant interest as it allows SCs to be interfaced with living cells via a common language they can both recognise. By extension, these communication systems could also be used to assemble interconnected communities of SCs, which could eventually be harnessed to achieve more complex functions as a collective.

1.4.1 Cellular communication in natural systems

Cellular communication is an essential trait that enabled the emergence of multicellularity and continues to fulfil cellular homeostasis in higher organisms by allowing different cell types to interact with one another. The same is even true for bacteria, which exist as individual planktonic cells and within interconnected microbial communities, such as those in the soil or the gut. Depending on the lifetime, distance, and complexity of the communication taking place, different classes of signalling molecule and modes of signal release are exploited by different cell types.

A primary mode of short-range signalling denoted paracrine signalling, is practised by both eukaryotic and prokaryotic cells. During paracrine signalling, small molecule messengers are released from one cell (the sender) towards an adjacent cell (the receiver) in the immediate vicinity, triggering a downstream response in that receiver cell [103]. Paracrine signalling is ubiquitous within the body and is observed during the propagation of chemical messengers across neuronal synapses, and tissue regeneration [104]. Likewise, bacteria simultaneously release auto-inducer peptides [105] or AHSLs [106] into their environment and detect the environmental concentration of these molecules to determine the number of related clonemates and synchronise the expression of gene operons such as those associated with biofilm formation [105, 106].

Instead of creating gradients of diffusible messengers in the environment, an alternative class of short-range cell-cell communication, denoted juxtacrine signalling, relies on direct contacts made between different cells or a cell with another cell's extracellular matrix. The exact nature of the communication is somewhat diverse and can involve either protein-protein interactions via receptors displayed on cell membranes with a ligand on the receiver cells or the direct transfer of molecules between the cytoplasms of separate

cells through gap junctions formed by connexins or innexins [107]. These are exemplified in Notch signalling in mammalian cells; the extracellular domain of the Notch receptor binds Delta, Jagged, or Serrate ligands on another cell [108], and are important in gap junction formation to synchronise the activity of cardiomyocyte activity [109]. Since the membranes of the separate cells are coupled, juxtacrine signalling is more controlled and targeted than paracrine signalling.

Finally, through endocrine signalling, longer-range cell-cell communication is accomplished in mammalian/higher organisms. Instead of creating a high, localised concentration of short-lived signalling molecules within the vicinity of the intended receiver cells, endocrine signalling uses long-lived messengers as it takes place over a much longer time frame and greater distances, using the endocrine system to reach every possible cell in the body [103]. Endocrine signalling is exemplified in blood sugar homeostasis; Beta cells within the pancreas release insulin into the blood to signal adipocytes to initiate glycogenesis and liver cells to stop gluconeogenesis [103].

1.4.2 Quorum sensing

QS is a type of prokaryotic paracrine signalling whereby bacteria communicate with one another through the release and detection of AHSLs (gram-negative bacteria) or autoinducer peptides (gram-positive bacteria) [105, 106]. The best-characterised QS system, LuxI/LuxR, was first identified in *V. fischeri*, a gram-negative marine symbiont found in the light organ of *Euprymna scolopes* [70]. LuxI is an AHSL-synthetase that synthesises 3OC6-HSL, a membrane permeable autoinducer that is released into the extracellular environment. LuxR is a 3OC6-HSL-sensitive transcription activator that regulates the expression of up to 13 genes located downstream of a pLux promoter [110]. One of these gene clusters, the so-called 'lux operon' encodes for LuxI, as well as proteins involved in

cellular bioluminescence, LuxCDABEG [69, 111]. Via the interplay between LuxI and LuxR, *V. fischeri* can sense the number of clonemates in their immediate environment, communicate with them, and coordinate the onset of bioluminescence at the population level.

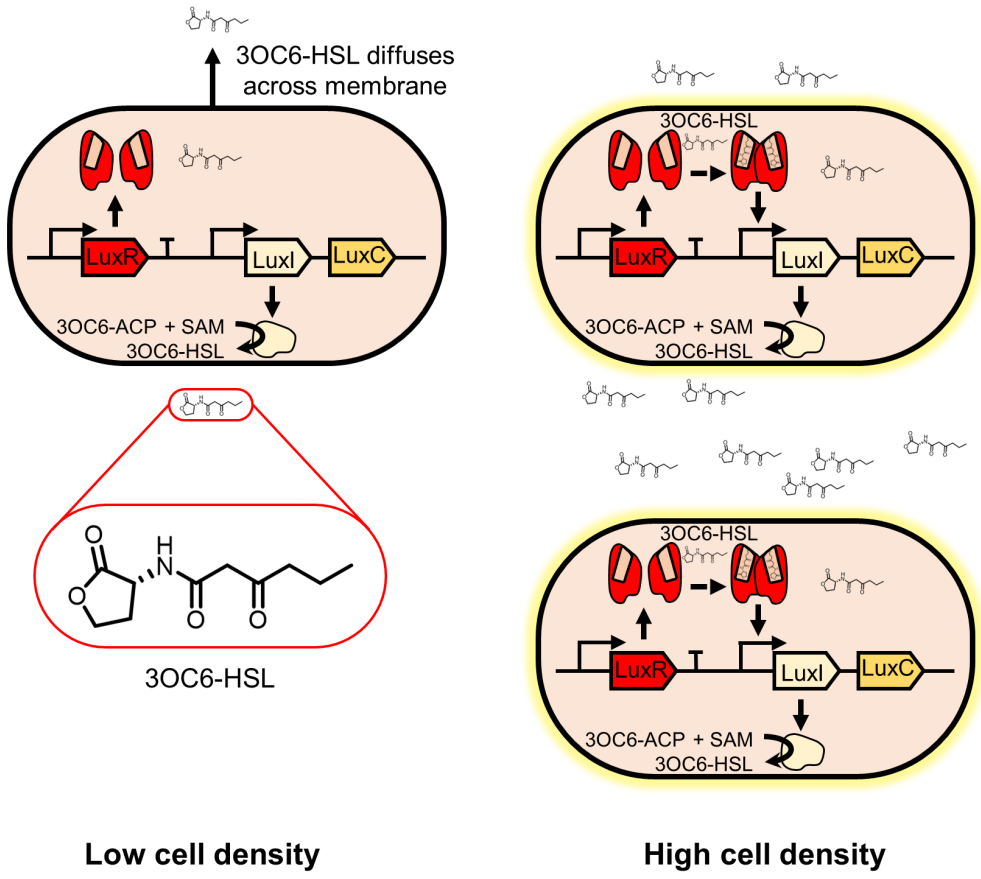


Figure 1.11: Quorum sensing in *V. fischeri*
A) At low cell densities, minimal activation of LuxR/leaky LuxR activity at the pLux promoter activate LuxI expression and the production of residual amounts of 3OC6-HSL. B) At high cell densities, LuxR is activated and enhances expression of the lux operon. Increase LuxI expression increases 3OC6-HSL synthesis and further increases lux operon expression, resulting in bioluminescence.

Under basal conditions *V. fischeri* express low amounts of LuxI, so little 3OC6-HSL is synthesised and released from the cell. Thus, at low *V. fischeri* cell densities, i.e. the free planktonic cells found in sea water, the environmental concentration of 3OC6-HSL is low, LuxR remains inactive, and the lux operon is not expressed (Figure 1.11 - Left). Conversely, at higher *V. fischeri* cell densities, i.e. the colonised light organ, the envi-

ronmental 3OC6-HSL concentration is elevated, and LuxR activates expression of LuxI and the Lux operon (Figure 1.11 - Right). This then acts as a positive autoinduction loop to amplify the signal: 3OC6-HSL activates LuxR, this triggers LuxI expression and increases 3OC6-HSL production, which further activates LuxI (and LuxCDABEG) expression. Once a critical 3OC6-HSL concentration is reached, LuxR is activated enough to simultaneously observe bioluminescence in all cells within the population [106].

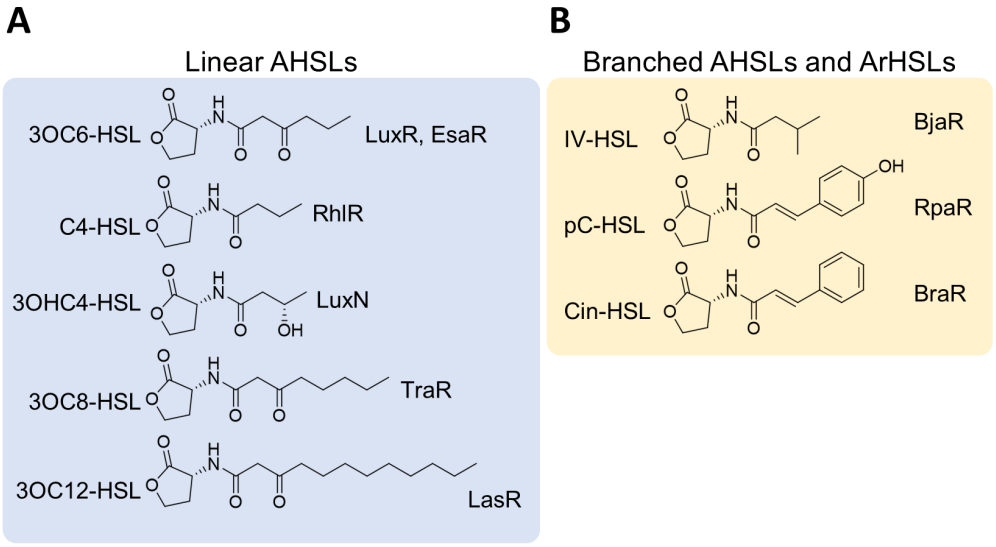


Figure 1.12: Variation in acyl homoserine lactones
The abbreviated names and structures of various AHSLs involved in QS, with the system from which they originate. Many QS systems recognise structurally similar, linear AHSLs (A), although more structurally diverse AHSLs (B) have also been discovered.

QS systems homologous to the LuxI/LuxR pair have since been discovered in a variety of gram-negative bacteria, including the LasI/LasR [112, 113] and RhlI/RhlR [114, 115] pathways from *Pseudomonas aeruginosa*, TraI/TraR pathway from *Agrobacterium tumefaciens* [116, 117] and EsaI/EsaR pathway from *E. stewartii* [71]. Despite the different hosts and protein partners used, these systems utilise structurally similar AHSLs that only tend to differ in the length of the acyl chain, number, or saturation of C-O groups within that chain, or saturation of C-C bonds [118](Figure 1.12A). Notable exceptions include the the RpaI/RpaR pathway from *Rhodopseudomonas palustris* [119], BraI/BraR pathway from *Bradyrhizobium* BTAi1 [120], and BjaI/BjaR pathway from *Bradyrhizobium*

japonicum [121], which utilise aromatic aryl homoserine lactones (ArHSLs), or branched AHSLs respectively (Figure 1.12B).

1.4.3 Communication in gene-expressing synthetic cells

While examples of juxtacrine signalling in SCs have been demonstrated [94, 122, 123], most SC communication mimics paracrine signalling in one of two ways: 1) Membrane-impermeable signalling molecules are encapsulated or produced inside SCs and released through protein pores inserted in the membrane. 2) Membrane-permeable signalling molecules are synthesised *in situ* from membrane-impermeable precursors and passively diffuse across the membrane. Both approaches have been used to create gene expressing SCs that can communicate with other SCs [66, 72] or living cells [57, 67, 72, 74, 102].

1.4.3.1 *In situ* release of membrane impermeable messengers

Communication between gene-expressing SCs and *E. coli* cells was first achieved through the release of a membrane-impermeable signalling molecule, IPTG. SCs were prepared by encapsulating IPTG along with PURExpress and a DNA template encoding the gene for αHL downstream of a theophylline riboswitch (Figure 1.13A). In the absence of theophylline, the RBS upstream of the αHL gene was sequestered by the riboswitch and no αHL was expressed. Upon adding theophylline into the external solution, theophylline diffused across the lipid bilayers into the SCs, bound to the aptamer region of the riboswitch and released the RBS. αHL was expressed inside the compartments, then inserted into the membrane and spontaneously heptamerised, forming a pore within the lipid bilayer, and releasing IPTG. IPTG released from SCs activated expression of luciferase in *E. coli* cells, incubated separately to the SCs [67]. Similarly, theophylline has also been used to regulate communication between two populations of SCs. In this case, theophylline-induced

expression of αHL was coupled to the release of doxycycline, which diffused into a second population of SCs through αHL, depressed a pTetR promoter, and activated luciferase expression [66]. The same workflow was also achieved using arabinose and IPTG, whereby arabinose diffused across the membranes of SCs, which derepressed a pBAD promoter to express αHL and subsequently release IPTG [66].

Communication via the controlled release of small molecules is a simplistic approach that mirrors the secretion of signalling molecules from living cells, such as those held within synaptic vesicles. However, the very nature of using encapsulated signalling molecules means that they can be released uncontrollably if the SC membrane is compromised by leaky expression of the αHL pores. In contrast, if the molecules are synthesised inside the compartment, they aren't released into the environment if the membrane ruptures prior to their production. Recent work has employed this strategy to interface SCs and mammalian cells. Rather than encapsulating or synthesizing small signalling molecules, a mammalian signalling protein, brain-derived neurotrophic factor (BDNF), was synthesised inside a liposome, then released on addition of 3OC6-HSL via the expression of perfringolysin O (PFO) from a pLux promoter (Figure 1.13B) [74]. PFO is a pore-forming protein that spontaneously oligomerizes and inserts into cholesterol-containing lipid membranes to form pores up to 25-30 nm in diameter [124]. Therefore, after constitutive expression of BDNF inside the SCs, 3OC6-HSL induced PFO expression created pores large enough to release BDNF and trigger differentiation of co-incubated neural stem cells or activate gene expression in HEK293 cells [74].

Pore dependent small molecule communication is a versatile tool in SC research, although this work is not without its drawbacks. For pore-dependent communication to have a tight off state, the lipid membrane of SCs needs to be both permeable to molecules that activate gene expression of the pore protein but impermeable to the signalling molecules

it entraps, which limits the lipid compositions that can be used to assemble SCs and potentially impairs pore insertion efficiency. In addition, the use of non-selective pores means that other small molecules present in the SC, such as ATP, nucleotides, and amino acids, are released in addition to the desired molecule, reducing protein synthesis capabilities. Also, when a high concentration of signalling molecule is required to activate the downstream process, an even higher concentration of that molecule must be encapsulated into SCs, which contributes significantly to the osmolarity and makes it challenging to balance SC osmolarity with known growth media or physiological conditions.

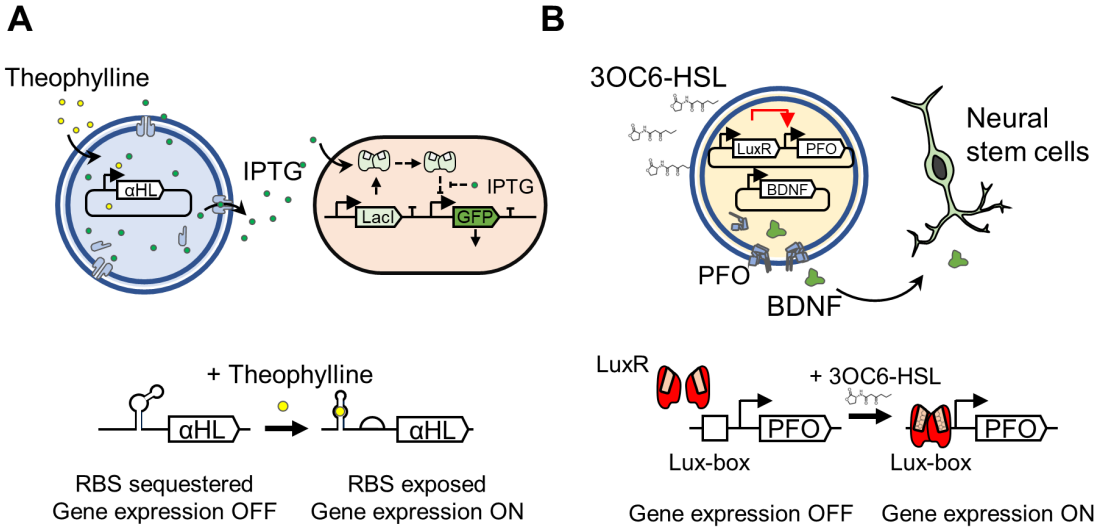


Figure 1.13: Release of signalling molecules by *in situ* pore expression
A) Theophylline diffused across the membrane of the synthetic cell, bound the theophylline riboswitch and exposed the RBS. Expression and insertion of αHL into the membrane released IPTG and activated GFP expression (Incubated separately) B) LuxR and BDNF were expressed inside SCs. Subsequent addition of 3OC6-HSL allowed PFO expression from the pLux promoter, and formation of large pores in the membrane. BDNF was diffused through these pores and trigger differentiation of neural stem cells (Co-incubated with SCs)

1.4.3.2 *In situ* synthesis of membrane permeable messengers

Early attempts at interfacing SCs with living cells diverged from natural systems and implemented an *in situ* autocatalytic formose reaction inside liposomes. From concentrated aldehyde feedstocks and an encapsulated $CaCO_3$ catalyst, furanosyl boronates that mim-

icked auto inducer-2 (AI-2) were synthesised inside the liposomes in response to an increase in pH. As a result, AI-2 analogues diffused across the lipid membrane and stimulated QS pathways in *Vibrio harveyi*, triggering bioluminescence [37]. More recently, molecules involved in QS have been synthesised enzymatically by AHSL synthetases expressed inside SCs. This approach has multiple benefits compared to communication via membrane pore expression. 1) It has an intrinsically tighter off state; the AHSL synthetase has to be translated, and the AHSL synthesised, so no molecule is released if the SC ruptures prior to this. 2) The QS receiver proteins often respond to lower cognate ligand concentrations than other small molecule TFs, e.g. nanomolar concentrations of 3OC6-HSL activate LuxR while LacI requires micromolar concentrations of IPTG. 3) The lack of a transmembrane pore means molecules involved in transcription and translation cannot escape, and SCs can sustain gene expression.

In their pioneering work, Lentini and Mansy *et al.* reconstituted the QS machinery from various proteobacteria to create SCs that recognised a signal produced by one species of bacteria and responded by producing the cognate AHSL for a different species. In their system, DNA encoding LuxR was expressed inside SCs containing S30 lysate, which subsequently regulated the expression of a second gene, LasI, placed downstream of a pLux promoter. Therefore, in the presence of 3OC6-HSL produced by LuxI-expressing sender cells, LasI was expressed inside the SC. Alongside the DNA templates, SAM and acetyl-CoA were encapsulated inside the SCs to enable the LasI-catalysed biosynthesis of N-(3-oxododecanoyl)-L-homoserine lactone (3OC12-HSL) into the environment. Enzymes involved in acyl transfer and oxidation of the C-3 carbon found in the S30 lysate to create the 3OC12-acyl carrier protein (ACP). Subsequently, 3OC12-HSL produced by the SCs activated GFP expression in LasR-expressing receiver cells (Figure 1.14). Although other were receivers tested in this system, including RhlR and LsrR, these did not work well

in vitro [57]. Similar systems have since been developed with different QS components. Rampioni and Stano *et al.* expressed RhlI inside SCs using the PURE system to synthesise N-(butyryl)-L-homoserine lactone (C4-HSL) from butyryl-CoA (C4-CoA) and SAM, and activate mCherry expression in *P. aeruginosa* cells [102]. Later, Ding and Tan *et al.* encapsulated EsaI inside SCs to synthesise 3OC6-HSL using substrates provided within an S12 lysate and activate GFP expression inside EsaR-expressing *E. coli* cells [72]. Cell-free detection of other AHSLs, such as 3OC12-HSL by LasR, has been shown using cell-free systems, but these have yet to be incorporated into SCs [125].

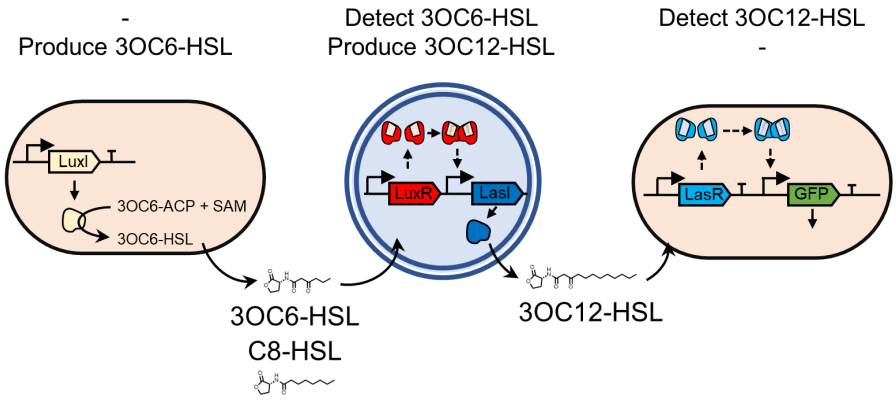


Figure 1.14: *In situ* synthesis of membrane permeable signalling molecules SCs sensed AHSLs produced by one population of bacteria (Sender cells) and responded by expressing an AHSL synthetase that synthesises a different AHSL. This second AHSLs was recognised by a separate population of bacteria (Receiver cells) triggering reporter gene expression

1.5 Therapeutic applications of synthetic cells

SCs have been applied in many different ways to satisfy various end goals. For example, lipid-based SCs containing purified proteins have been used to represent minimal cell-like systems in order to enhance our fundamental understanding of biological phenomena, such as integrin signalling [36] or cell division [33–35]. Alternatively, protocells assembled from prebiotic molecular building blocks thought to exist in a primitive Earth have been used to model the assembly of primordial life [126]. Yet another area of interest is the engineer-

ing SCs towards biotechnological or clinical applications, such as *in vivo* drug delivery, whereby cell-based alternatives have been difficult to implement due to cost, control, and bio-containment barriers. Biocompatible nanoscale vesicles (<200 nm) enclosed by lipids or polymers are already used to this end - multiple liposome-therapies already exist in the clinic as part of anti-cancer, anti-fungal, or pain relief therapies [127] and there are several ways in which these compartments have been re-engineered to improve delivery to target sites. These include decorating the surface with antibodies to target tumour sites [128], and implementing thermo-responsive lipids within the membrane to release the cargo under mild hyperthermia [129]. However, intelligent delivery devices with higher biosensing capabilities that detect physiologically relevant cues and respond by synthesizing the therapeutic agent only at the required time and location could offer further improvements to current therapeutics.

In this regard, SCs, particularly those capable of gene expression, are well situated to satisfy these goals: they are biocompatible, capable of detecting biomolecules, and can execute different functions simply by changing the DNA template used [130]. To date, gene-expressing SCs have been deployed as synthetic vaccines [131] or instilled with the ability to kill cancer cells [132] and bacteria [72]. Meanwhile, non gene-expressing SCs have been applied to treat diabetes [133] and phenylketonuria [134], inhibit quorum sensing in bacteria [135], and trigger vasodilation of blood vessels [136].

Amongst the earliest examples where SCs have been applied in a biomedical setting was the fabrication of antigen-expressing immunostimulatory liposomes (AnExILs). These $\sim$1.5 μm-sized compartments were created by either encapsulating a CFPS with DNA encoding for an antigen, β-galactosidase (LacZ), and expressed LacZ inside the lumen, or rehydrating lipid films using bulk-expressed His-tagged lacZ. In the latter case, LacZ was encapsulated inside the liposomes and decorated the outer leaflet of the membrane via

an interaction with Ni-NTA lipids. Anti-LacZ antibodies were generated by injecting the AnExILs into mice, and antibody titres were higher when AnExILs were injected than just liposomes containing purified LacZ. This suggests the CFPS provided an adjuvant quality to the compartments and a means to manufacture the desired antigen. In later studies, AnExILs were also shown to trigger T-cell and dendritic cell responses [137, 138]. Using a similar approach, Krinsky and Schroeder *et al.* created SCs that contained DNA encoding for a potent membrane-permeable toxin from *P. aeruginosa*, Exotoxin A. On injecting these SCs tumours of mice, Exotoxin A was expressed *in situ* and destroyed the neighbouring cancer cells upon its release (either by translocating through the lipid bilayer or on membrane rupture) [132].

These examples represent the versatility of gene-expressing SCs, but the proteins were synthesised constitutively rather than in response to physiological cues. SCs with 'sense then synthesise' circuits have, however, also been constructed. These compartments contained EsaR to sense their environnment for 3OC6-HSL, and regulate the expression of a bacterial toxin, Bactenecin 2A (Bac2A), from a pEsaR promoters In this way, Bac2A was only expressed in the presence of 3OC6-HSL-producing bacteria. Bac2A ruptured both the membranes of the SC and bacteria [72] (Figure 1.15A).

SCs have also been created to sense glucose concentration and release insulin, although CFPS was not used in this instance. These so-called artificial beta cells (AβCs) were assembled by entrapping small insulin-containing liposomes inside giant liposomes containing enzymes and membrane transporters to mediate fusion of the vesicles in a process akin to synaptic vesicle fusion. Glucose entered the AβC through glucose-specific membrane transporters in the membrane and was immediately consumed by a glucose oxidase/catalase reaction. Protons generated in this enzymatic reaction decreased the lumenal pH and caused the removal of PEG chains from the small internally held vesi-

cles. Displacement of these PEG groups exposed short membrane-embedded alpha helical peptides, which could now form a SNARE-like coiled-coil and fuse the inner leaflet of the GUV with the outer leaflet of the SUV and release insulin (Figure 1.15B).

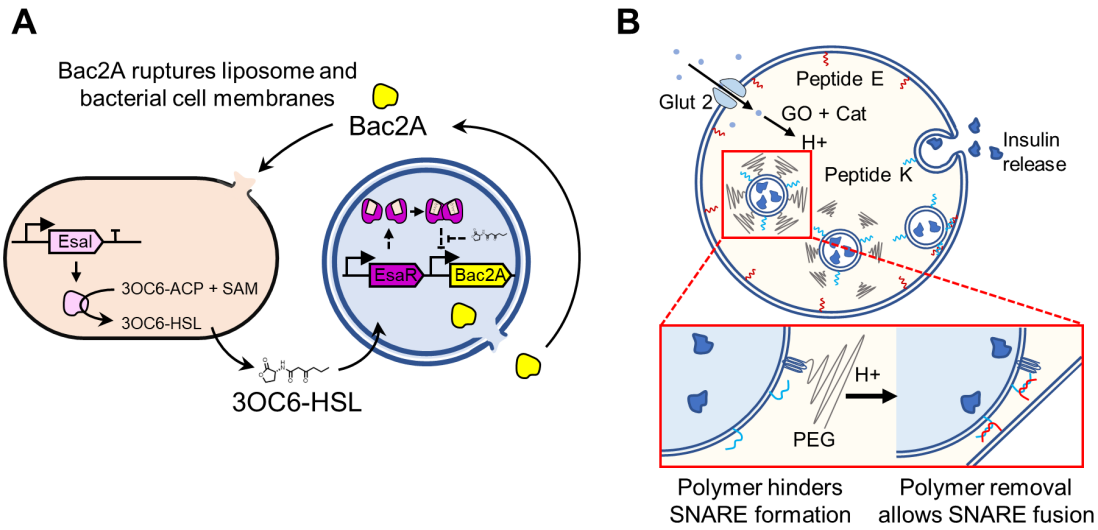


Figure 1.15: SCs as next generation therapeutics
A) SCs sensed an AHSL produced by bacteria and produced Bac2a in response. Bac2a ruptured both the GUV and bacterial membranes. B) SCs imported glucose and utilise it as a substrate in an enzymatic reaction to decrease the lumenal pH. This subsequently enabled fusion between the membranes of intracellular vesicles with the GUV membrane and the release of insulin.

1.6 Summary of thesis work

The overarching aim of this work was to create gene-expressing SCs from the bottom up that can be programmed with user-defined DNA templates and externally controlled using UV light. The end goal was to then apply these SCs in different ways to influence the behaviours of living cells. This work was partitioned into the following chapters:

Chapter 2 describes how a CFPS was encapsulated inside GUVs to create gene-expressing SCs. The steps necessary to obtain good yields of high-quality CFPS-containing GUVs are highlighted, and cell-free gene expression is characterised in bulk reactions and inside GUVs. This chapter also introduces an automated image processing workflow that

was created to extract simple metrics from microscopy images of GUVs.

Chapter 3 expands on this and introduces how light-activated DNA templates were constructed and used to control *in situ* gene expression inside the SCs. Patterned UV light methods were used to activate the SCs in a spatially-defined manner.

Chapter 4 describes how a quorum-sensing system from a marine proteobacterium was exploited to create a one-way communication system between SCs and living cells. SCs synthesised and released an acyl-homoserine lactone, which subsequently stimulated reporter gene expression in engineered *E. coli* cells.

Finally, **Chapter 5** highlights the progress that was made towards developing SCs that can be activated by multiple inputs as a step towards therapeutic applications. Light was used to regulate transcription, and histamine was used to regulate translation.

2

Gene expressing liposomes as programmable synthetic cells

2.1 Introduction

2.1.1 Formation of giant unilamellar vesicles

Over the last few decades, various methods have been developed to encapsulate molecules inside liposomes. Different methods are used depending on the desired size of the compartment, composition of the lipid membrane, and cargo to be encapsulated inside.

2.1.1.1 Spontaneous swelling of lipid films

First described in 1964 by Prof Alec Bangham [139], lipid film hydration is the most straightforward approach for assembling liposomes as it simply exploits the intrinsic amphipathic properties of phospholipids to self-assembly liposomes in an aqueous environment. In this method, phospholipids are dissolved in a volatile solvent, typically chloroform, then transferred to a glass surface and held under flowing nitrogen to evaporate the solvent and form thin lipid films. After hydrating these dried lipid films under a humid atmosphere, an aqueous solution is added, triggering the spontaneous budding of vesicle-like structures from the stacked layers of phospholipid; these eventually form free-standing spherical compartments containing the aqueous solution [140]. Due to the van der Waals interactions between the stacked lipid lamellae, multiple layers of phospholipids simultaneously swell and bud off from the planar lipid film, forming multilamellar vesicles enveloped by one or more lipid bilayers [141]. Although there are some instances where MLVs are desirable, unilamellar vesicles containing only a single bilayer are typically preferred as this more closely mimics the morphology of biological membranes.

Lipid hydration can be biased towards forming unilamellar vesicles by incorporating sugars [142] into the lipid films to increase the intra-lamellar spacing between the stacked layers of phospholipids, or including charged lipids into the films to establish repulsion between the layers [143]. In addition, swelling lipid films deposited on agarose [144], polyvinyl alcohol [145], or dextran–poly(ethylene glycol) [146] hydrogels also helps to form giant unilamellar vesicles (GUVs) and accelerates the tenuous lipid film hydration step.

In addition to heterogeneity in the lamellarity, vesicles prepared by the gentle hydration of lipid films are also heterogeneous in size; mixtures of large and giant MLVs

(1 μm) are generally observed. If compartments below 1 μm are required, heterogeneous populations of MLVs can be extruded through track etch membranes with a defined pore size to break down larger vesicles into smaller, more homogeneous vesicles [147].

These approaches are often an ideal starting point in liposome studies and have been used to encapsulate CFPS systems successfully and demonstrated *in vitro* gene expression [148, 149]. However, they typically require larger sample volumes than other methods, and solutions with physiological salt concentrations still have a low encapsulation efficiency [140].

2.1.1.2 Electroformation

Electroformation is a refinement of the lipid film hydration method that uses an alternating current to accelerate lipid swelling and reduce the lamellarity of the resulting vesicles [150]. Instead of forming lipid films on glass surfaces, lipids are deposited on tin-indium oxide coated glass or platinum electrodes positioned within a sealed chamber containing low volumes ($\sim$10 μL) of an aqueous solution. By applying a current through the chamber, GUVs containing the aqueous solution bud off from the hydrated lipid films. Vesicles formed in this way tend to have fewer lamellae than vesicles form via hydration alone; however, it is difficult to perform electroformation with solutions containing physiological salt concentrations or charged lipids [151], limiting this methods applicability in the encapsulation of CFPS systems.

2.1.1.3 Freeze dried liposome hydration

Another simple method shown to encapsulate CFPS systems inside liposomes successfully involves preparing empty liposomes by gentle hydration, lyophilising them, then rehydrat-

ing the pre-formed freeze-dried liposomes when required. Liposomes are first formed in water, extruded through track etch membranes to a uniform size, and then aliquoted out and lyophilised to form empty freeze-dried liposomes. Then, a CFPS can be added to re-hydrate the lipids in each aliquot and become encapsulated inside the reformed liposomes [31, 152]. This method has previously been used to express proteins inside liposomes; however, vesicles made using this method contain many defects (lipid aggregates, tubules), encapsulation efficiency is poor, and liposomes that form successfully vary significantly in size and lamellarity.

2.1.1.4 Emulsion droplet transfer

The inverted emulsion method, or emulsion droplet transfer method as it is otherwise known, circumvents the need to swell lipid films in aqueous solution. Instead, lipid bilayers are formed around aqueous droplets via the sequential deposition of 2 individual monolayers [153]. The first lipid monolayer is formed by adding an aqueous inner solution to a lipid-containing oil. Lipid molecules align at the interface between the droplet surface and oil by placing their polar headgroups in the aqueous phase and their hydrophobic tails in the oil phase (Figure 2.1A). Through mechanical agitation, typically vortexing, water droplets are then split into smaller droplets around 1-30 μm in diameter and stabilised by a monolayer of lipids. The second layer of lipids is acquired by passing these lipid-stabilised aqueous droplets through another monolayer of lipids that align at a second water/oil (W/O) interface. This monolayer is formed by placing a lipid-containing oil (or emulsion with an excess of lipid) on top of an isotonic aqueous solution. Again, due to the amphipathic nature of the lipids, they orient their polar headgroups towards the aqueous phase and hydrophobic tails towards the oil phase and stabilise (flatten) the W/O interface (Figure 2.1B). Lipid-stabilised emulsion droplets are then passed through the lipid

interface by centrifugation, aided by placing sucrose inside the droplets and equimolar glucose in the outer solution to establish a mass gradient (Figure 2.1C).

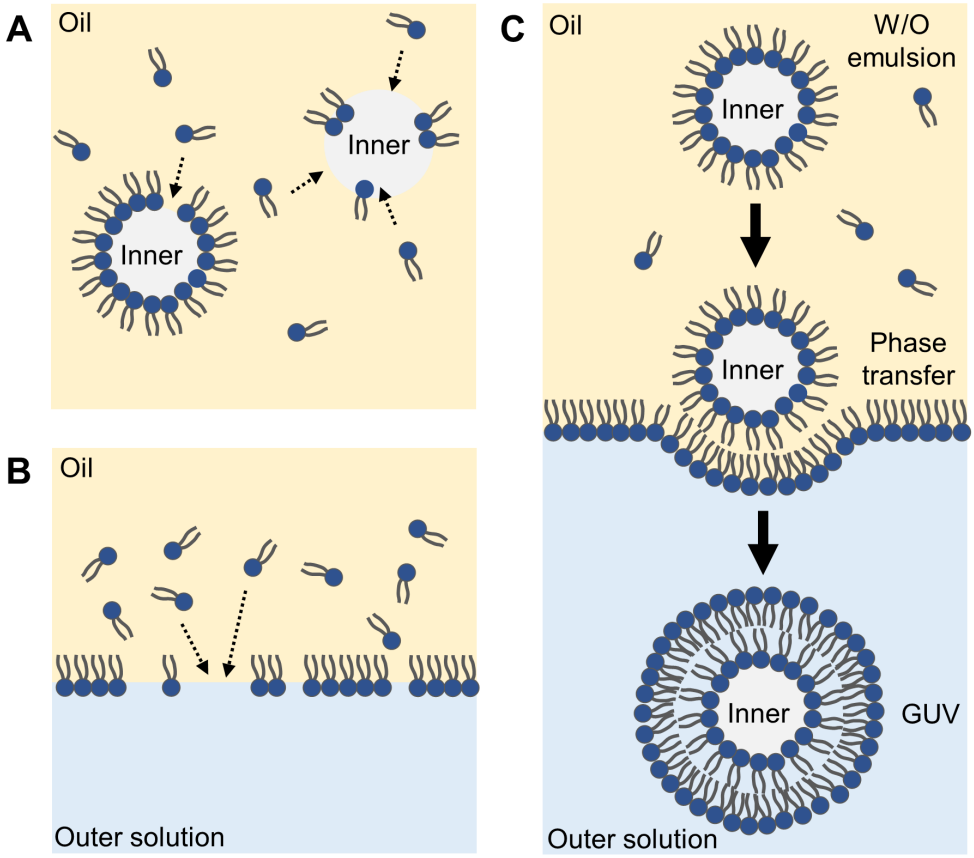


Figure 2.1: Formation of GUVs by emulsion droplet transfer
A) An aqueous sucrose-containing inner solution is emulsified in a lipid-containing oil to create droplets stabilised by a lipid monolayer. B) Lipid-containing oil is placed on top of an aqueous solution to form a second lipid monolayer at the W/O interface. C) Emulsion droplets are pulled through the second lipid monolayer into the outer solution by applying centrifugal force.

GUVs formed in this way are entirely unilamellar [154], can be obtained even with low volumes of inner solution (~2 μL) [153], and there are many examples whereby emulsion droplet transfer was used to generate GUVs capable of gene-expression [29, 74, 102, 155]. Unfortunately, the vesicles tend to be heterogeneous in size unless emulsification is controlled using microfluidics [156, 157], which translates into variable encapsulation of CFPS components and variable gene expression. Residual oil or solvent can also be retained in the lipid bilayer after passing through the W/O interface, which may influence the phase behaviour of the membrane.

2.1.1.5 Continuous droplet interface crossing encapsulation

Continuous droplet interface crossing encapsulation (cDICE) builds upon the two-phase approach described above to form vesicles with a tighter size distribution. The cDICE set-up comprises a spinning plate (4-100 x g) to which a cylindrical container is attached. An aqueous outer solution is added to the chamber, followed by a lipid-containing oil to create a lipid monolayer at the interface, perpendicular to the plane of rotation. Subsequently, an inner solution is introduced through a capillary, which drips into the oil phase and acquires its first layer of phospholipids, before passing through the second lipid monolayer at the W/O interface [158]. Lipid concentration and centrifugation speed are adjusted to allow enough time for a complete lipid monolayer to assembly around the aqueous droplet before it reaches the interface. Vesicle diameters are a product of the droplet size, and therefore the diameter of the capillary used to introduce inner solution and the centrifugation speed used to force this out of the capillary. While not completely necessary, tighter vesicle size distributions have been observed by first passing the inner solution through a low viscosity alkane phase. GUVs formed by cDICE are reported to have fewer membrane defects than those obtained by the emulsion droplet transfer method [159], and gene expression has been demonstrated inside vesicles prepared this way. However, fewer vesicles are formed, and the throughput is low unless multiple cDICE rigs are utilised.

2.1.1.6 Microfluidics

Microfluidics is typically the gold standard for the assembly of monodisperse GUVs. While many different chip designs and methods have been described [160–163], GUVs assembled by microfluidics are typically generated by flowing an aqueous inner solution through multiple W/O interfaces. An inner solution is flowed into a lipid/surfactant stabilised

oil phase at a junction to bud off droplets with a diameter defined by the flow rate of the aqueous and oil phases and the diameter of the aqueous solution inlet channel [164]. Vesicles are subsequently formed by passing lipid-stabilised droplets through another lipid stabilised w/o interface at a downstream inlet [165, 166], depositing lipids around droplets via a dewetting process driven by a difference in surface tension between two solvents [160, 161], or fusing SUVs held inside droplets with by interacting with charged polymers at the periphery of the droplet [162]. Many different cargos, including CFPS systems [160], have been encapsulated inside GUVs, which can be introduced at the encapsulation level, or after forming the droplets via picoinjection [162]. Gene expression inside GUVs prepared by microfluidics is less variable since all vesicles are large (50 μm – 100 μm) and encapsulate the same components. Although, it is not known if gene expression inside smaller vesicles ($\sim$10 μm - a similar size to GUVs prepared by droplet transfer) prepared by microfluidics, is still homogenous. Microfluidics offers a route to assembling uniform, unilamellar vesicles, yet drawbacks such as the specialised facilities and expertise necessary to manufacture the microfluidic chips, the expense associated with the experimental setup make this inaccessibly for many researchers.

2.1.2 Chapter overview

In this chapter, the *in vitro* expression of a reporter protein, mNeonGreen (mNG), was characterised using linear DNA templates and the PURExpress cell-free protein synthesis (CFPS) system. An emulsion droplet transfer protocol was optimised and used to encapsulate PURExpress inside GUVs. In situ mNG expression in GUVs was characterised qualitatively by fluorescence microscopy and quantitatively using an image analysis platform that measured the diameter and fluorescence of GUVs to obtain a deeper understanding of the system.

2.2 Assembly of gene expressing giant unilamellar vesicles

A prerequisite to forming DNA-programmable SCs with life-like functions is the encapsulation of a CFPS system into a compartment. In this work, PURExpress was chosen to execute the functions encoded on DNA templates as it has a well-defined makeup and is free from nucleases that could degrade linear DNA templates. PURExpress was encapsulated into GUVs by emulsion droplet transfer [153]. This method was preferred over the alternative options as it typically produces high yields of GUVs, and requires minimal equipment and low amounts of inner solution so multiple samples with different inner solution compositions can be prepared simultaneously. Furthermore, these compartments are versatile cell models as they are roughly cell-sized, their membrane permeability mimics biological membranes and their permeabilities can be tuned by altering the lipid composition. Methods to encapsulate complex biological material, including CFPS systems, inside the lumen of the vesicle by emulsion droplet transfer already exist in the literature – these were used as a starting point. To understand the basic requirements of CFPS and vesicle formation, the two processes were decoupled, characterised, and brought together to assembly GUVs capable of *in situ* gene expression.

2.3 *In vitro* gene expression

Linear DNA templates were selected to programme the behaviours of SCs as they would ultimately be modified to create the LA-DNA. The DNA templates fulfilled the minimum criteria for robust CFPS in PURExpress; they comprised of a T7 promoter, a strong RBS, a gene of interest (GOI) and a T7 terminator (Figure 2.2A)). In the first instance, a reporter gene encoding for the fluorescent protein, mNG, was used to monitor CFPS

as its expression could easily be quantified in bulk and inside vesicles using a fluorescent plate reader and epifluorescence microscope. mNG was successfully expressed from linear DNA templates in bulk PURExpress reactions (Figure 2.2B). mNG fluorescence increased rapidly during the first 2 hours of incubation at 37°C and then plateaued as substrates became limiting. Minimal increases in mNG fluorescence were observed after 4 hours of incubation (Data not shown).

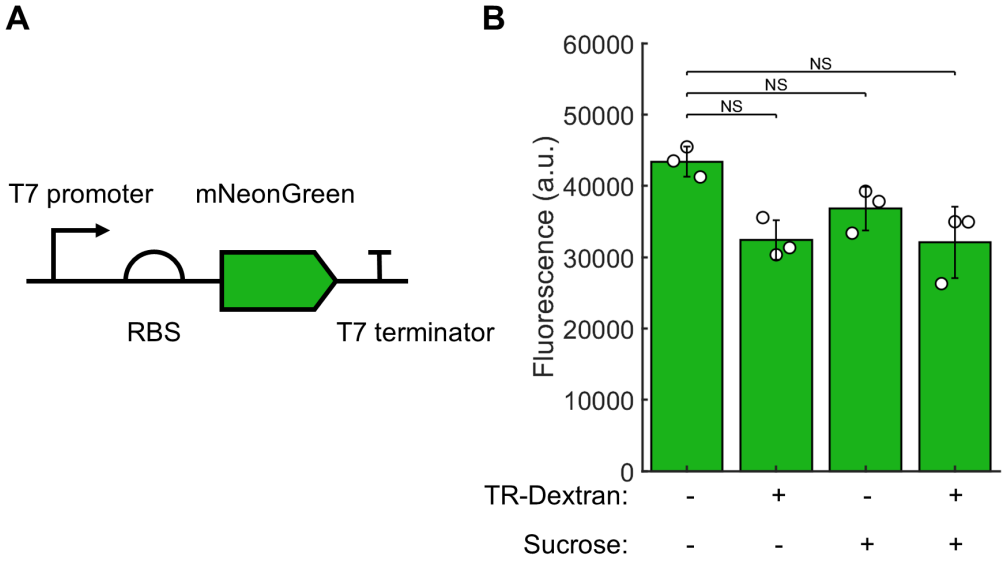


Figure 2.2: In vitro expression of mNeonGreen
A) Linear DNA templates used in this work. B) mNG was successfully expressed from linear DNA templates. Expression was slightly perturbed in the presence of 200 mM sucrose and 25 μM Texas-Red Dextran after 4 hours incubation at 37 °C, but was not statistically significant (Two-tailed, unpaired Student's t test). Error bars, s.d. of three independent experiments ($n = 3$).

During the assembly of GUVs, additional components such as sucrose or dyes are often added to the inner solution. These additives help to draw droplets through the W/O interface to acquire their second lipid monolayer and aid the visualisation of vesicles with an epifluorescence microscope, respectively. In addition to this, the reagents can also act as crowding agents, which have been shown to enhance *in vitro* transcription but perturb *in vitro* translation [167]. Thus, 200 mM sucrose and 25 μM Texas Red (TR) dextran (10 kDa) were added to the PURExpress reactions to determine if they impacted mNG expression. TR-Dextran and sucrose decreased mNG expression by 25%

and 16% respectively, and by 26% when added together (Figure 2.2B), however, this could potentially be limited in the future by reducing the concentration of sucrose and TR dextran added, or using a dextran-free fluorophore.

2.4 Preparation of GUVs

GUVs were prepared by emulsion droplet transfer in three stages. First, the solution to be encapsulated inside the vesicle (PURExpress) was emulsified in lipid-containing oil to form aqueous droplets stabilised by a lipid monolayer (Figure 2.1A). Next, a second lipid monolayer was assembled at a W/O interface by layering lipid-containing oil on top of a buffered isotonic solution (outer solution) (Figure 2.1B). Finally, the lipid stabilised emulsion droplets are forced through the W/O interface into the outer solution by centrifugation, becoming enveloped by the second monolayer of lipids in the process (Figure 2.1C). The resulting vesicles were comprised of an aqueous inner solution separated from an aqueous outer solution by a phospholipid bilayer. Although all emulsion transfer methods described in the literature share these same steps, these methods all differed in the preparation of the lipid-containing oil, inner solution composition, emulsification method, outer solution composition, and conditions used for droplet transfer. Many of these methods were not reproducible in our hands, so each step was studied in isolation to understand how they could be modified to aid PURExpress encapsulation. 10 mM 5,6-carboxyfluorescein was encapsulated along with the PURExpress system to help visualise the vesicle pellet and determine the stability of emulsion droplets and lipid monolayers. After this method had been iteratively refined, similar methods were published in the literature [74] indicating these measures were reproducible for encapsulation of CFPS systems inside GUVs.

2.4.1 Lipid in oil

Lipid-containing oil is typically prepared by dissolving dried lipid films in mineral or paraffin oil [29], or adding lipids dissolved in chloroform directly into the oil and heating to evaporate the chloroform and dissolve the lipids [155]. Elements from either approach were implemented in the hope a solvent-free lipid-containing oil that rapidly stabilised W/O interfaces could be attained. Lipids dissolved in chloroform were added to 2 mL glass vials and then held under nitrogen flow to evaporate the solvent and deposit the lipids as a thin film on the vial walls. The lipid films often appeared wet, especially when using cholesterol in the lipid mix, so these film containing vials were held under vacuum for a further 3 hours. After 3 hours, the films looked drier and hazy, indicating chloroform removal. Mineral oil was then added to the vials containing lipid films and heated, with the lids removed, at 80 °C for 10 minutes to help dissolve the lipids and remove any residual chloroform. At this point, lipid films were often still discernible on the base of the vial. To fully dissolve the lipid in the mineral oil, the vials were sonicated in a water bath at 50 °C for 1 hour and stored at room temperature overnight. Lipid-containing oil was prepared fresh the day before each experiment and sonicated for 10 minutes at room temperature immediately before use. Vesicles prepared with oil that was not freshly prepared could still form vesicles, but with a more variable yield.

Combinations of POPC and DOPC lipids with and without cholesterol were initially screened for their ability to form stable emulsions, however, at the high lipid concentrations used in the literature (∼10 mg/mL) [155], the emulsion droplets tended to aggregate and sediment. In contrast, Egg PC dissolved in mineral oil at a 2-5 mg/mL concentration formed stable emulsions, and the droplets did not cluster. When lipid-containing oil prepared with other methods was added on top of an aqueous solution, a domed interface

would initially form due to surface tension and then flatten on the formation of a lipid monolayer at the oil-water interface after incubation at room temperature for >10 minutes. Egg PC lipids dissolved in mineral oil prepared as described above immediately flatted the W/O interface on contacting the aqueous solution, indicating rapid recruitment of lipids and monolayer formation. This is important in replenishing lipids at the interface after emulsion droplets pass across the membrane.

2.4.2 Emulsification

The GUVs formed by the inverted emulsion method are templated by the emulsion droplets that cross the W/O interface. Therefore, the dimensions of the droplets dictate the dimensions of the GUVs. While uniform emulsion droplets can be prepared with microfluidics, this was outside the scope of this work. Initially, attempts were made to crudely template the size of the lipid-stabilised droplets by extruding the emulsions through a track etch membrane with a defined pore size (12 μm), however, the throughput was very low (multiple, slow passaged were necessary and the syringes had to be washed between samples) and the droplets were still polydisperse. Instead, bulk emulsification methods were used to enable multiple samples with different compositions to be prepared simultaneously. By dispersing the inner solution in the oil while aspirating it from a P10 pipette tip, small, somewhat uniform droplets formed, without coalescence, which could then be partitioned into smaller droplets by passing samples across a rumble strip. For droplets around 5-20 μm in diameter, the resulting emulsions appeared cloudy, but not milky and opaque – the latter was indicative of mostly smaller droplets around 1-5 μm in diameter. Forming the emulsions using a rumble strip created a more reproducible population of droplets than vortexing for a set speed and duration, since droplets tended to vary in size depending on their position in the vortex.

2.4.3 Outer solution

Most literature methods encapsulated material with a known composition, making it simple to match the osmolarity of the inner and outer solution and prevent vesicle from swelling or shrinking. However, PURExpress is a commercial CFPS, and its exact composition is unknown. Different outer solutions have been used previously to encapsulate PURExpress, yet these had different compositions and osmolarities [67, 149, 155, 168]. The osmolarity of PURExpress has previously been estimated ∼950-1100 mOsm [169, 170] and via freezing point depression, the osmolarity of PURExpress was found to be 1012 mOsm. Amongst these osmolytes, components such as glycerol can diffuse across lipid bilayers [28]. Based on previous experiments in droplet interfaced bilayer systems, [94], droplets containing 400-450 mOsm of NaCl were osmotically balanced with PURExpress containing droplets. Hence, the osmolarity of the non-membrane permeable components was assumed to be ∼800-900 mOsm. Outer solution was prepared with 50 mM HEPES (pH 7.6), 400 mM salt and 170-200 mM glucose (matched with internal sucrose concentration).

Buffers with various salts (potassium chloride, sodium chloride, and potassium glutamate) were tested for their ability to form GUVs, alongside other buffers used in the literature. Despite using the same emulsion in each case, vesicles prepared with sodium chloride and potassium chloride were much smaller than vesicles prepared with potassium glutamate and had oil/lipid aggregates on their membranes (Figure 2.3). This was attributed to the interaction of different salts with the lipid headgroups, influencing the membrane's fluidity and recruitment of lipids to the W/O interface, however, this was not explored further.

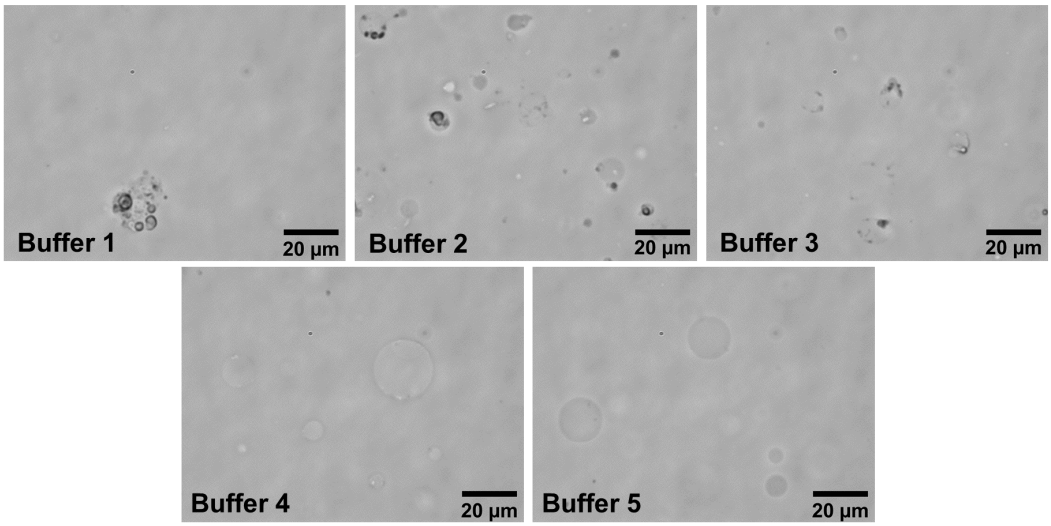


Figure 2.3: Vesicle formation with different outer solution compositions
Lipid/oil aggregates remained on GUV membranes after acquisition of the second lipid monolayer for buffers 1-3. These vesicles also tended to be smaller than vesicle prepared with buffers 4-6, which were relative free of lipid/oil aggregates. Buffer 1: 50 mM HEPES (pH 7.6), 200 mM glucose; Buffer 2: 50 mM HEPES (pH 7.6), 400 mM potassium chloride, 200 mM glucose; Buffer 3: 50 mM HEPES (pH 7.6), 400 mM sodium chloride, 200 mM glucose; Buffer 4: 50 mM HEPES (pH 7.6), 400 mM potassium glutamate, 200 mM glucose; Buffer 5: 100 mM HEPES (pH 7.6), 280 mM potassium glutamate, 24.5 mM magnesium acetate, 1.5 mM DTT, 200 mM glucose.

2.4.4 Centrifugation

Centrifugation speed is critical in the transfer of emulsion droplets through the lipid-stabilised W/O interface and the formation of phospholipid bilayers. Under room temperature conditions and with up to 25 μL inner solution, centrifugation speeds as low as 50 x g have been used to form GUVs [171]. Here, GUVs needed to be centrifuged at 4 °C to prevent the activation of gene expression inside the emulsion droplets. Thus, higher centrifugation speeds were used to account for the increased viscosity of the oil phase. The highest vesicle yields were obtained at 16,000 x g. Lower speeds meant emulsion droplets remained in the oil phase, while higher speeds risked rupturing or fusing the vesicles. Samples were centrifuged for 30 minutes as a significant proportion of the emulsion droplets remained inside the oil phase when shorter centrifugation steps were used.

2.4.5 Wash steps

To prevent GUVs from contacting the oil phase after centrifugation, vesicles are often removed through a pinhole in the bottom of the centrifuge tube [155]. More vesicles were recovered if the oil was aspirated from the aqueous solution and the pellet resuspended in a small amount of the remaining outer solution using a fresh pipette tip. By transferring this to a new tube containing 250 μL outer solution, dispersing the vesicles from the pellet by pipetting up and down gently and centrifuging again at 10,000 x g for 10 minutes, any oil carried through either adhered to the walls of the new tube or formed droplets on the surface of the aqueous solution. Removal of the outer solution, followed by resuspension of the pellets in 25 μL buffer and transfer to a new centrifuge tube, further removed the trace oil.

2.4.6 Imaging

Coverslips and slides often had particulates and dust adhered to their surface, introducing artefacts into microscopy images. To alleviate this, coverslips and glass slides were cleaned with 2% decon, isopropanol, sonicated in Milli-Q H_2O and then dried under N_2 flow before use. Initially, tunnel slides assembled with double-sided tape were used to image vesicles (Figure 2.4A), however, this allowed buffer to evaporate from either end of the channel meaning vesicles could not be incubated and imaged in real-time. Furthermore, GUVs often ruptured or wetted the glass coverslips of the tunnel slides. To resolve these issues, sealed imaging chambers were created, and plasma cleaned (hydrophilic) coverslips were coated with 0.1% (w/v) BSA to passivate the surface. The imaging chambers were made by sandwiching together passivated coverslips and microscope slides containing 1 mm holes together with a 25 μL gene frame (Figure 2.4B). Samples were added through inlet

holes, and then chambers were sealed with tape. Vesicles sedimented onto the BSA-coated coverslips without rupturing and could be incubated and imaged in the same chambers without evaporation of the buffer.

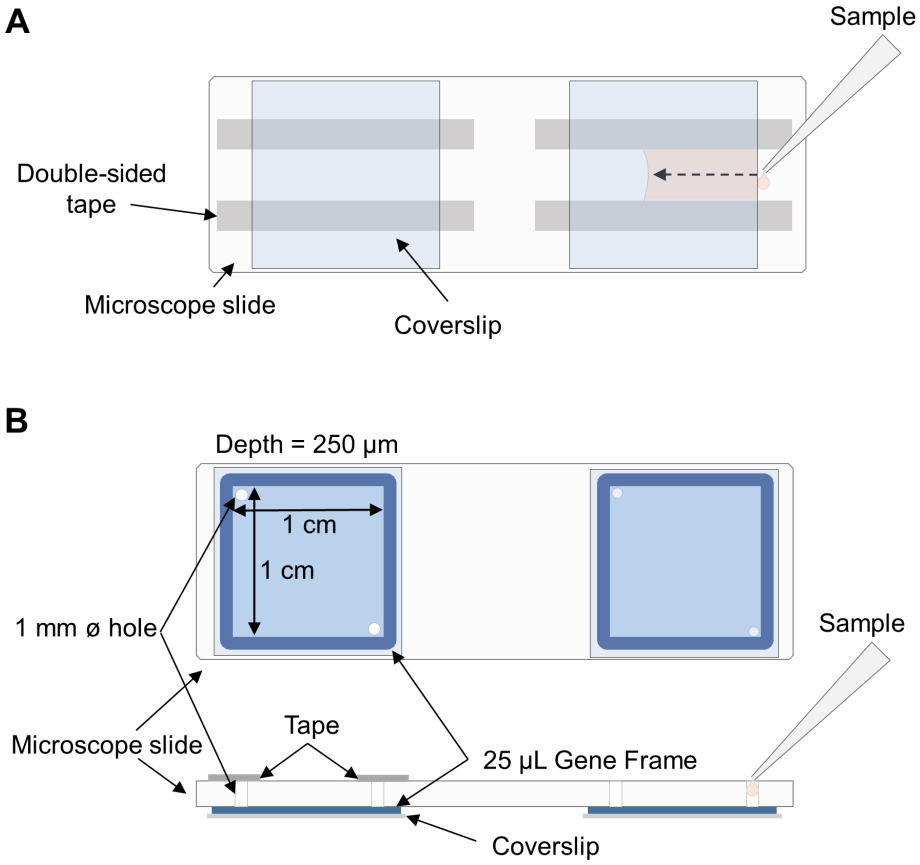


Figure 2.4: Imaging chambers used for vesicle incubation and visualisation A) Tunnel slides were prepared by attaching two pieces of double sided tape to a micrscopeslip parallel with one another, then adhering a coverslip on top. Samples were added at the open ends of the channel and moved cross the slide by capillary action. B) 1 mm holes were drilled through microscope slides corresponding with the corners of a 25 μL gene frame. A 25 μL gene frame was added and then a coverslip adhered to the other side of the gene frame. Samples were introduced through the 1 mm holes, which were sealed with tape.

2.5 *In situ* gene expression inside GUVs

In situ gene expression inside SCs was demonstrated by encapsulating PURExpress with linear DNA templates encoding mNG (Figure 2.5A). At t=0, DNA-containing SCs had no green fluorescent signature, but after 2 hours incubation at 37 °C green fluorescent

SCs were observed by fluorescence microscopy, confirming the successful transcription and translation of mNG inside the compartments (Figure 2.5B). Fluorescence generally increased with further incubation, however, vesicles that had depleted the substrates required for CFPS remained unchanged, and some SC still failed to express mNG even after 4 hours of incubation. SCs prepared without DNA did not increase in fluorescence, confirming that the DNA template dictated the protein synthesised inside the vesicles (Figure 2.5B). With prolonged incubation inside the imaging chambers, the SCs clustered together but the overall number of vesicles appeared relatively unchanged, confirming their stability over multiple hours of incubation.

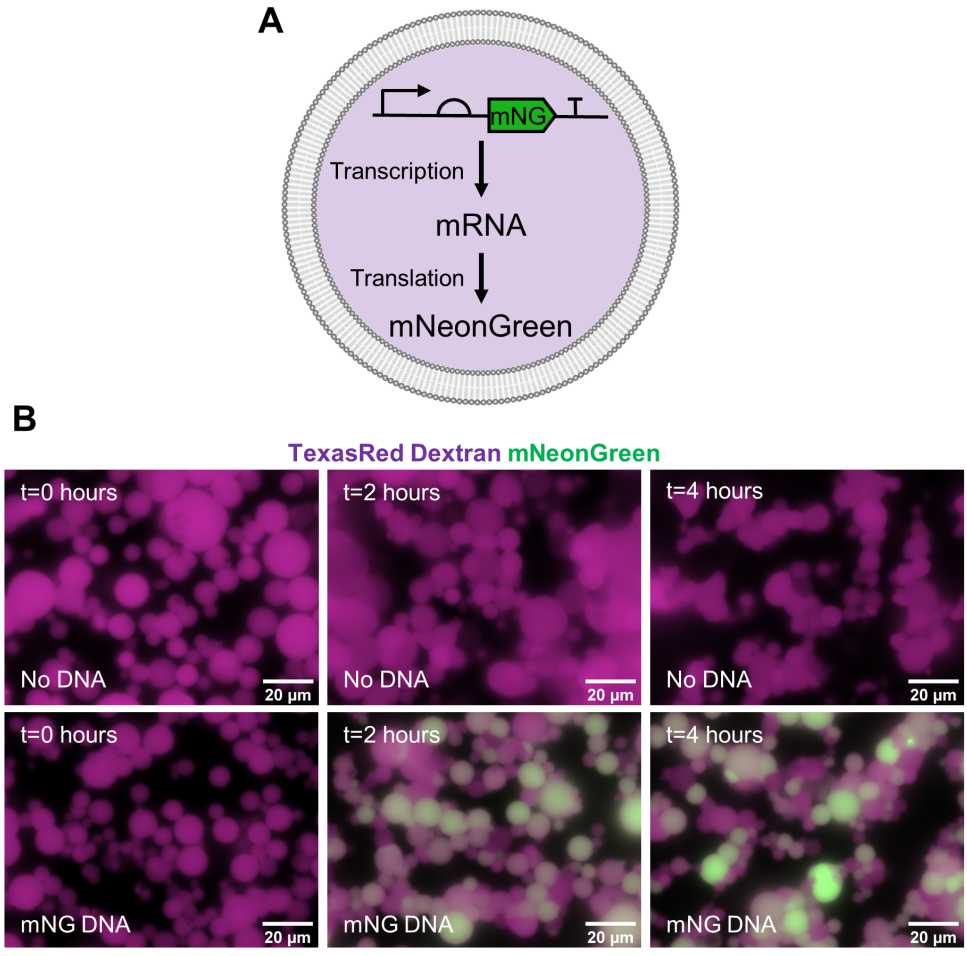


Figure 2.5: *In situ* gene expression inside GUVs
A) Schematic illustrating the *in situ* expression of mNG from linear DNA templates inside GUVs. B) mNG expressing vesicles after 0-4 hours incubation at 37 °C compared to vesicles that contain PURExpress but no DNA template.

From the fluorescence microscopy images in Figure 2.5B, it is clear that the gene-expressing vesicles formed by emulsion droplet transfer were somewhat heterogeneous in size. While this was to be expected since the emulsions were prepared in a non-templated manner, polydispersity is undesirable as it gives rise to compartments with non-uniform behaviours. Indeed, as illustrated by the differences in fluorescence intensity across the individual vesicles, gene expression in these polydisperse vesicles was highly variable and in some instances, no mNG expression was observed at all. To obtain a more meaningful, quantitative description of heterogeneity within the SC population, data extracted at the single vesicle level is required. Since manually analysing the properties of vesicles from fluorescence microscopy images is arduous, time-consuming, and subject to human bias, an automated image processing tool was developed to streamline this process.

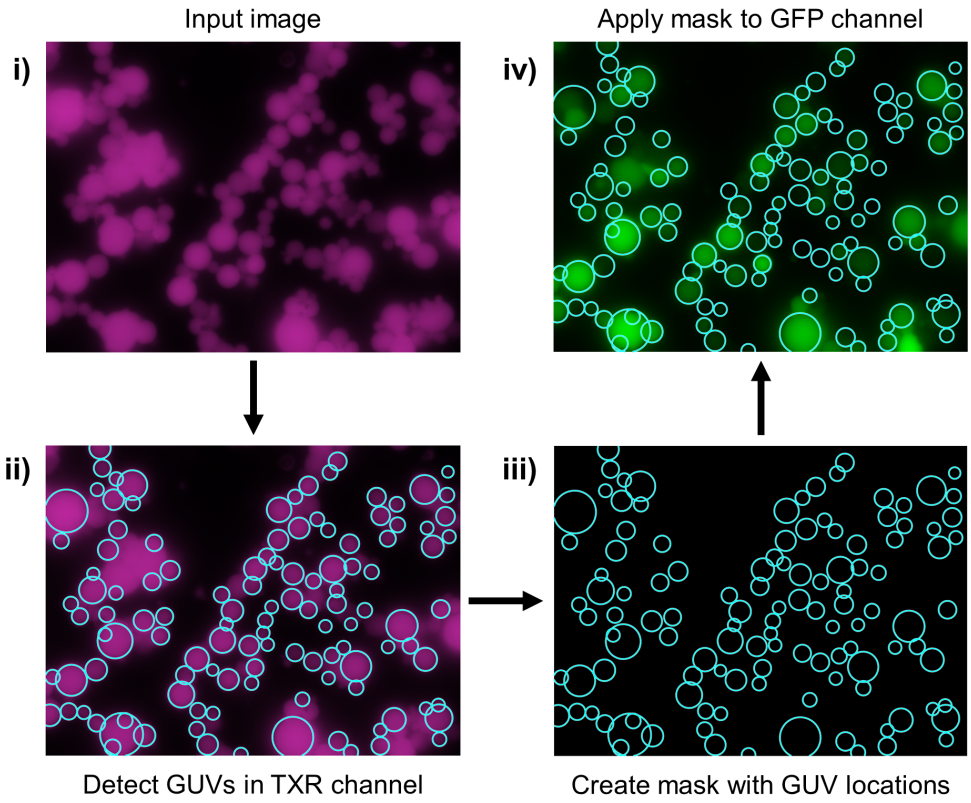


Figure 2.6: Imaging processing workflow to analyse GUVs
TXR channel images showed the locations of TR-containing GUVs (i). A circular hough transform algorithm was used to determine the boundaries between the fluorescent GUVs and dark background, as indicated by the cyan circles (ii). The origin and radii of the circles identified were used to create a map of the GUVs present in the image (iii). The map was used to determine the mNG fluorescence of each vesicle detected (iv).

The analysis pipeline used red (TXR) and green (GFP) channel fluorescence microscopy images to indicate a vesicle's location and mNG expression level, respectively. First, vesicles present in the TXR channel images (Figure 2.6(i)) were identified via a circle-specific edge detection algorithm (Circular Hough transform)(Figure 2.6(ii)), and the space occupied by these vesicles was mapped according to the origins and radii of the circles detected. This information was then used to create masks (Figure 2.6(iii)), which were applied to the GFP channel image to measure the mNG fluorescence of the corresponding vesicles (Figure 2.6(iv)). mNG fluorescence intensity of the vesicles was represented as the mean pixel intensity measured inside the circles. By iterating through this process for each circle within the map, individual vesicles' diameters and fluorescence intensities were obtained.

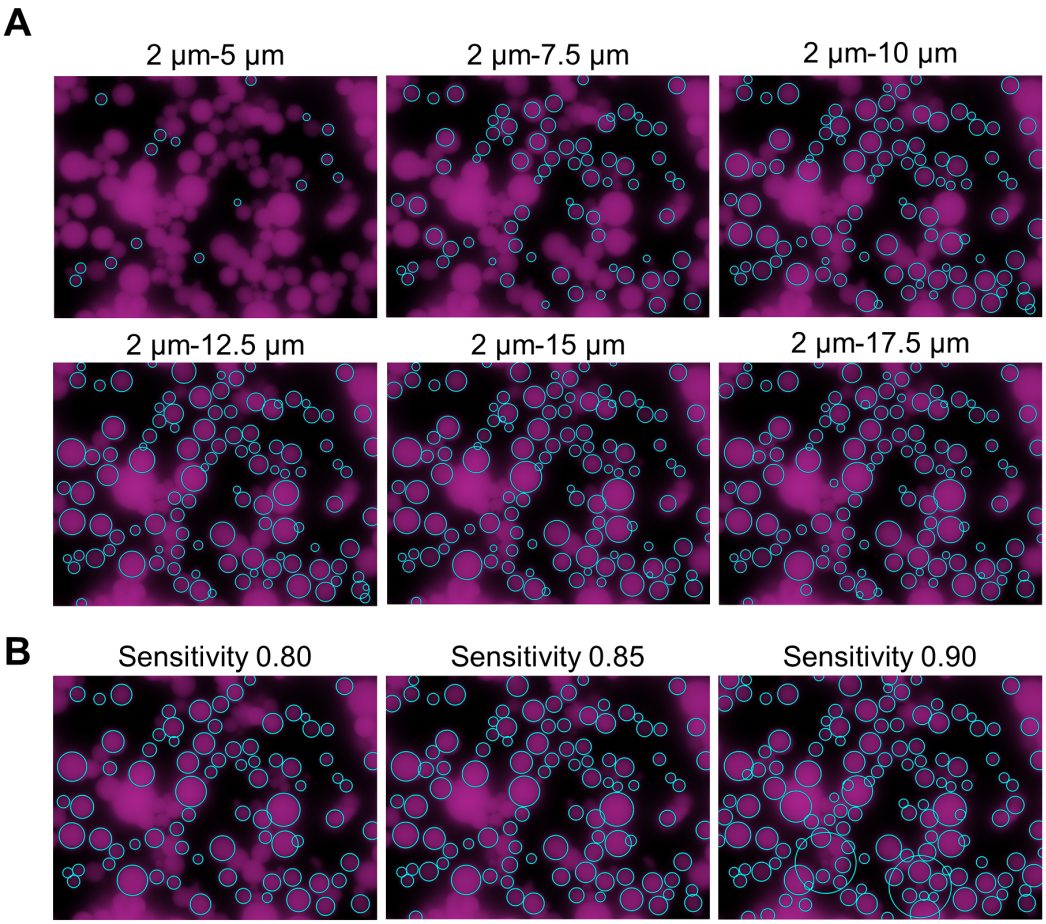


Figure 2.7: Tuning vesicle detection parameters
Vesicles detected after varying the 'radii' (A) and 'sensitivity' parameters (B). These parameters helped avoid clustered vesicles being detected as a single large compartment.

To prevent non-vesicle objects or clusters of vesicles from being detected as single vesicles, the stringency of vesicle detection was tuned with the 'radii' (Figure 2.7A) or 'sensitivity' parameters (Figure 2.7B) to remove structures above a certain size threshold or structures with poor circularity. In this way, some vesicles may be removed from the dataset, however, vesicle clusters are not treated as single compartments.

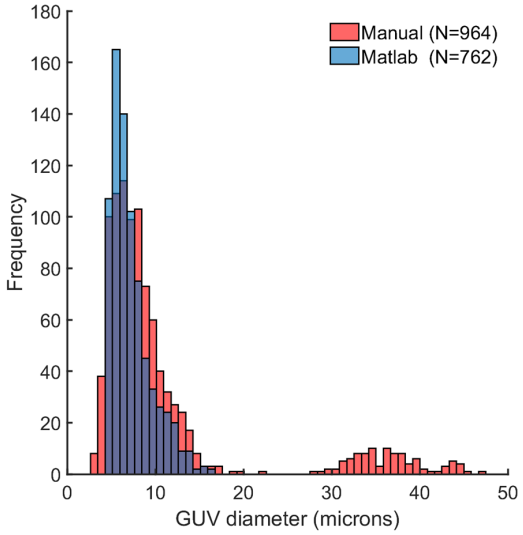


Figure 2.8: Size distribution and mNG expression of GUVs
Vesicle diameters were generally consistent between the manual and automated methods of vesicle analyses. The automated matlab represented the trends from the data in the microscopy images. Vesicles below 3 μm and above 25 μm were not included in the matlab analysis to prevent the detection of artefacts or vesicle aggregates.

The performance of this workflow was tested by comparing the vesicle diameters measured with the Matlab script to values derived manually. In both the Matlab (Sensitivity = 0.84; radii = 3-20 μm;) and manual analyses, vesicles varied greatly in size, mostly ranging from 5-20 μm; $\text{Median}_{\text{Matlab}}$ = 6.49 μm, $\text{Mean}_{\text{Matlab}}$ = 7.14 μm, $\text{Mode}_{\text{Matlab}}$ = 4.43 μm, $\text{Median}_{\text{Manual}}$ = 7.33 μm, $\text{Mean}_{\text{Manual}}$ = 7.79 μm, $\text{Mode}_{\text{Manual}}$ = 4.70 μm (Values excluding vesicles above 20 μm). There was general agreement in the size distribution of the vesicles detected; however, the Matlab script measured slightly inside the outermost edge of the vesicles (outermost edge used for manual measurements), and so the dimensions are slightly lower less than those measured manually (Figure 2.8).

Using this masking approach, the diameters and mean fluorescence intensities of individual SC were extracted from sets of 10 images taken after t=0/2/4/6/8 hours of incubation at 37 °C. As depicted in the microscopy images, mNG expression proceeded rapidly between 0-2 hours, then more gradually between 2-8 hours (Figure 2.9A). In this regard, the kinetics of mNG expression inside the vesicles aligned with mNG expression in bulk; CFPS occurred rapidly when there was an excess of ATP and charged tRNAs available, then proceeded more slowly as the ATP and creatine phosphate for ATP regeneration were consumed, and the amino acids were incorporated into polypeptides.

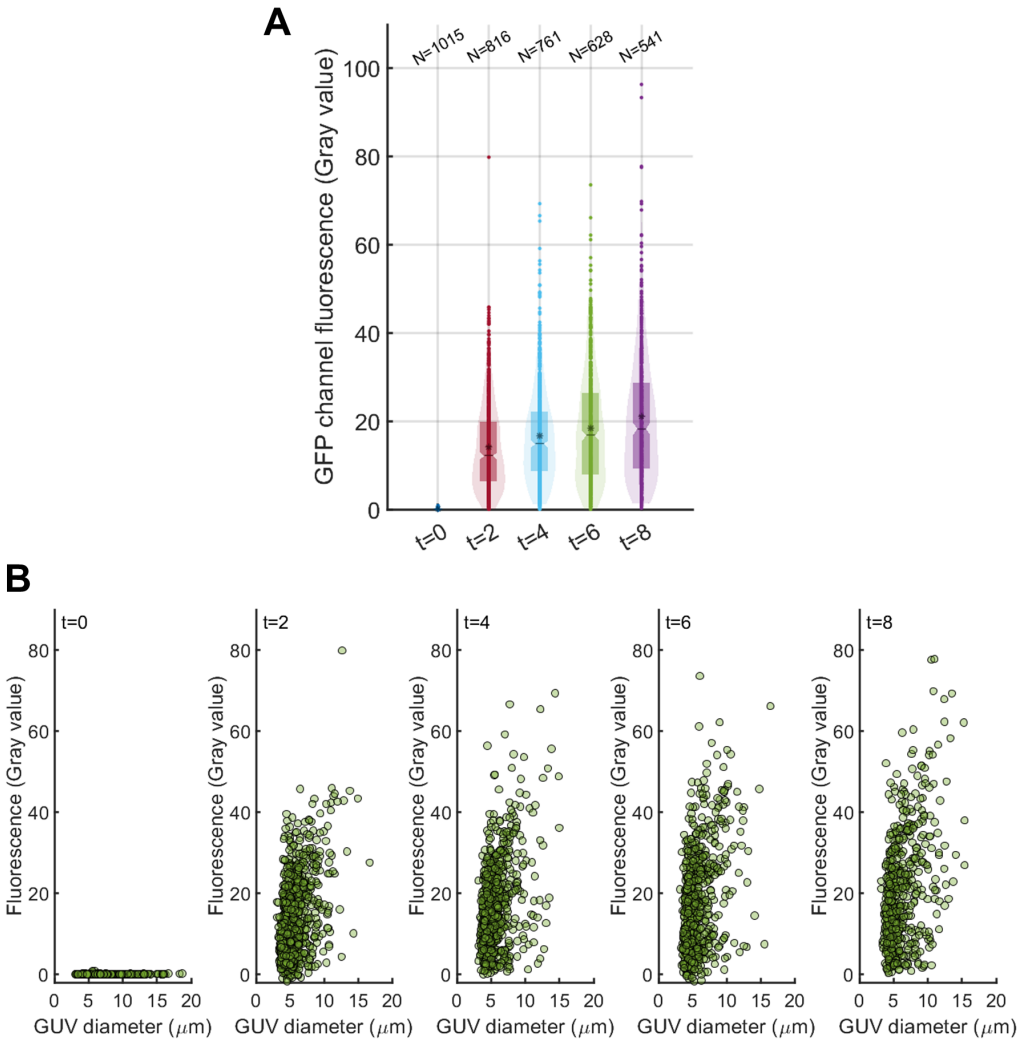


Figure 2.9: mNG expression in the SC population from single vesicle data
A) At t=0, GUV fluorescence was at background level. mNG was expressed and GUV fluorescence increased when GUVs were incubated at 37°C for up to 8 hours. B) There was weak, but observable correlation between GUV diameter and fluorescence intensity. Larger vesicles tended to express more mNG than smaller vesicles, but gene expression was also more variable.

From this single vesicle data, it is clear that mNG expression was remarkably heterogeneous across the SC population. To establish whether this related to the heterogeneity in compartment size, GUV diameter vs mNG fluorescence was plotted for each individual SC. Representing the data in this way indicated that fluorescence intensity was generally proportionally to compartment diameter (Figure 2.9B), but the correlation was not as striking as reported previously [172]. Smaller vesicles (∼3-10 μm) tended to express less mNG and had a functional expression window of around 2 hours, after which their fluorescence intensity remained relatively unchanged. Larger vesicles (>10 μm), on the other hand, generally expressed more mNG and had a more prolonged expression window as their fluorescence intensity continued to increase for up to 8 hours. While differences in the vesicle's dimensions accounted for some of the variability in gene expression, fluorescence intensity was still incredibly variable even across vesicles with the same dimensions. Thus, the heterogeneity was most likely the sum of several different factors.

First, SCs of the same size and prepared from the same bulk inner solution have different compositions [173, 174]. When an inner solution is emulsified in a lipid-containing oil, the individual components of the CFPS system, i.e. the DNA templates and some 36 different proteins, ribosomes, tRNAs and small molecules that makeup PURExpress, are stochastically partitioned into the water-in-oil droplets. Although the overall concentration of each solute is fixed in the bulk solution, different absolute numbers of each solute are segregated into the individual compartments after emulsification. While the effects of stochastic solute partitioning are negligible in large compartments (>20 μm) or when the species is present at high concentrations (>1 mM), it can have a drastic effect on CFPS in smaller sub-micron sized compartments or when a particular component is present at low concentrations (<10 nM), as is the case for the DNA templates. In this experiment, the DNA template was added to the inner solution at a final concentration of 5 ng/μL

(8.1 nM). Given a starting DNA concentration, C, and a SC population with a uniform internal volume, V, the average number of copies of DNA in each vesicle, n, is given by eq 1, whereby N refers to Avogadro's number [174].

$$n = NCV \tag{1}$$

Assuming the DNA template was homogeneously mixed in the inner solution and was encapsulated into a uniform population of vesicles with a diameter equal to $\text{Median}_{\text{Manual}}$ (7.33 μm; 205 fL) according to a Poisson distribution and independently of other solutes, the average number of DNA templates per vesicle was 999 $\pm$ 31. The average copy number is, however, much lower amongst the smallest vesicle diameters measured in the microscopy images; for SCs with a 3 μm diameter, n= 68 $\pm$ 8. Therefore, it seems the variability in mNG expression within the smaller SCs can largely be ascribed to the variable encapsulation of DNA present at low concentrations.

Second, inner solution-membrane interactions occur to different extents in vesicles of different sizes [174]. When encapsulated inside lipid compartments, the various poly-electrolytes that reside in the PURExpress system can interact with lipids in the inner leaflet of the GUV membrane via electrostatic interactions. Even in the presence of neutrally charged membranes, DNA templates and/or mRNA can adsorb to the lipid surface. When bound at the membrane, the nucleic acids become less accessible to the machinery required for transcription and translation, respectively, and protein synthesis is perturbed. This phenomenon, termed surface-induced repression, correlates with the inner leaflet area:volume ratio [174]. Thus, under otherwise highly controlled conditions, gene expression tends to be positively correlated with compartment size.

Finally, macromolecular crowding increases the intrinsic noise of CFPS [173]. In

a well-mixed, non-crowded compartments, macromolecules in the CFPS system diffuse freely and transcription and translation can be assumed to occur throughout the vesicle. However, in the presence of a crowding agent, such as the sucrose added to the inner solution, the diffusion of macromolecule is restricted. This causes random localised hot spots of expression to arise, which, when averaged out, manifests as noisier gene expression within the vesicle population than observed in non-crowded systems [173].

In addition to extracting fluorescence metrics from the individual SCs, the analysis script could also be used to infer how stable the vesicles were over time. As the same SC samples were imaged at each time point, and equal numbers of images were used to create the datasets, the number of vesicles detected could theoretically be used as a proxy for vesicle stability over time. During the experiment, the number of detected vesicles decreased by almost 50%. However, this was primarily due to the vesicles clustering together and failing to be detected by the script rather than the loss of vesicles. Therefore, the SC samples either need to be more dilute or spatially segregated to reduce clustering and gauge vesicle stability using this imaging-based approach. As it wasn't possible to decouple the loss of vesicles from vesicle clustering with the current experimental set-up, vesicle stability could not be quantified.

3

Light-activated gene expression in GUVs

3.1 Introduction

3.1.1 Maximising gene expression in cell-free systems

DNA templates designed for CFPS use strong promoters and RBSs to maximise the rate of transcription and translation initiation, but these sequences are not the only determinants of protein synthesis efficiency. For example, sequences within the 5' UTR of mRNA

transcripts may perturb translation if they sequester the RBS. Regardless of how strong the RBS is, i.e. how closely the Shine Dalgarno sequence complements the anti-Shine Dalgarno sequence, if a ribosome cannot access the RBS it cannot translate the downstream mRNA. In addition to removing potentially problematic sequences and secondary structures, motifs that promote transcription and/or translation can also be introduced into 5' UTRs. Thus, in addition to promoter and RBS strength, the sequence of the 5' UTR should be considered when designing DNA templates in order to truly maximise gene expression.

To increase the transcription initiation rate, bases immediately downstream of the T7 promoter can be manipulated to facilitate the formation of a transcription initiation bubble and promoter escape. It is well known that 3 contiguous guanines at positions +1 to +3 are necessary for efficient transcription [175]. Expanding on this, recent data also suggests that the identity of the bases at positions +4 to +8, those melted to form the initiation bubble, are also important for transcription initiation. By enriching this region with A/T bases, mRNA transcript yields can be increased up to 5-fold due to the lower energetic cost of unwinding A-T base pairs compared to G-C base pairs [175]. Although, simply having fewer hydrogen bonds present does not account for the different responses observed with different permutations of the A/T bases, highlighting a possible sequence preference for transcription bubble formation. Based on these findings, 5' UTRs downstream of T7 promoters should begin with 3 contiguous guanines followed by a combination of 4 A/T bases to maximise transcription initiation.

In conjunction with this, the translation rate can also be improved by removing unfavourable secondary structures that occlude the RBS or start codon, or introducing auxiliary ribosome recognition sequences into the 5' UTR of DNA templates. Such sequences were originally identified within the 5' UTRs of naturally abundant proteins, an

example of which is the so-called T7 g10 leader located upstream of the T7 bacteriophage major capsid protein, which is preferentially expressed in host cells after phage infection. Specifically, this leader contains a potent translation enhancer sequence termed Epsilon (5'-UUAACUUUA-3'), which is thought to interact either with the 16s rRNA [176] or with the S1 protein located within 30s ribosomal subunit [177] like other pyrimidine rich sequences shown to enhancer heterologous gene expression [178, 179]. The additional RNA-protein interaction between the mRNA and ribosome has a negative allosteric effect on the Shine Dalgarno-anti Shine Dalgarno interaction and assists the transition from translation initiation to translation elongation [177]. Consequently, enhancer sequences such as Epsilon can be included in 5' UTRs, or even downstream of the RBS, to enhance dissociation of the ribosome from the RBS after translation initiation.

3.1.2 Chapter overview

In this chapter, light-activated DNA templates were assembled by photocaging the T7 promoter, and utilised in CFPS reactions to repress gene expression until the samples were irradiated with UV light. Subsequently, the 5' UTRs and N-terminal leader sequences of these light-activated DNA templates were modified to improve mNG titres, and the optimised templates were introduced into SCs to regulate *In situ* gene expression. Finally, light-activated SCs were immobilised inside an agarose hydrogel, and activated in a spatiotemporally controlled manner with patterned UV light.

3.2 Preparing and testing light-activated DNA

Linear DNA templates containing a T7 promoter constitutively expressed mNG in bulk CFPS reactions (section 2.3) and inside GUVs (section 2.5), representing a route to as-

sembling minimal, DNA-programmable SCs. However, unregulated gene expression would make it hard to deploy SCs in meaningful ways as we cannot control when and where they are active. To regulate gene expression and the function of the resulting SCs in a user-defined manner, the linear DNA templates were substituted for light-activated DNA (LA-DNA) templates that contained a photocaged T7 promoter. LA-DNA was constructed as shown in Figure 3.1. First, seven thymine bases within the T7 For primer were replaced with amino C-6 thymine bases to introduce amine groups throughout the T7 promoter sequence. Next, photocleavable biotin (PCB) groups were conjugated to these amines via an N-Hydroxysuccinimide (NHS) ester reaction. High-performance liquid chromatography (HPLC) indicated that multiple products were formed, each with a different number of PCB groups attached at different positions. The majority of the material existed within a single, broad peak, which was considered to be the DNA strand with a PCB group conjugated at each of the seven amine-containing bases (Figure 3.2A). Fractions containing the suspected fully modified oligo were isolated (Figure 3.2B), then lyophilised twice to remove volatile ammonium acetate and washed in a 3 kDa Amicon filter using Milli-Q H_2O at least four times as PCR was highly sensitive to any residue remaining from HPLC. Next, the modified oligonucleotide (denoted T7 for PCB) was used as a forward primer in a PCR to amplify DNA templates with seven PCB groups installed within the T7 promoter sequence (denoted PCB-DNA). The modified primer was added at 1.3x molar excess to the reverse primer (Rev CT2), and DreamTaq polymerase was used as opposed to the higher fidelity Phusion DNA polymerase as these measures improved DNA yields. Finally, monovalent streptavidin (mSA), straptavidin with only one functional binding site, was added to the PCB-DNA to bind at each biotin group and photocage the T7 promoter. PCB-DNA with mSA bound at each biotin group is considered the fully assembled LA-DNA.

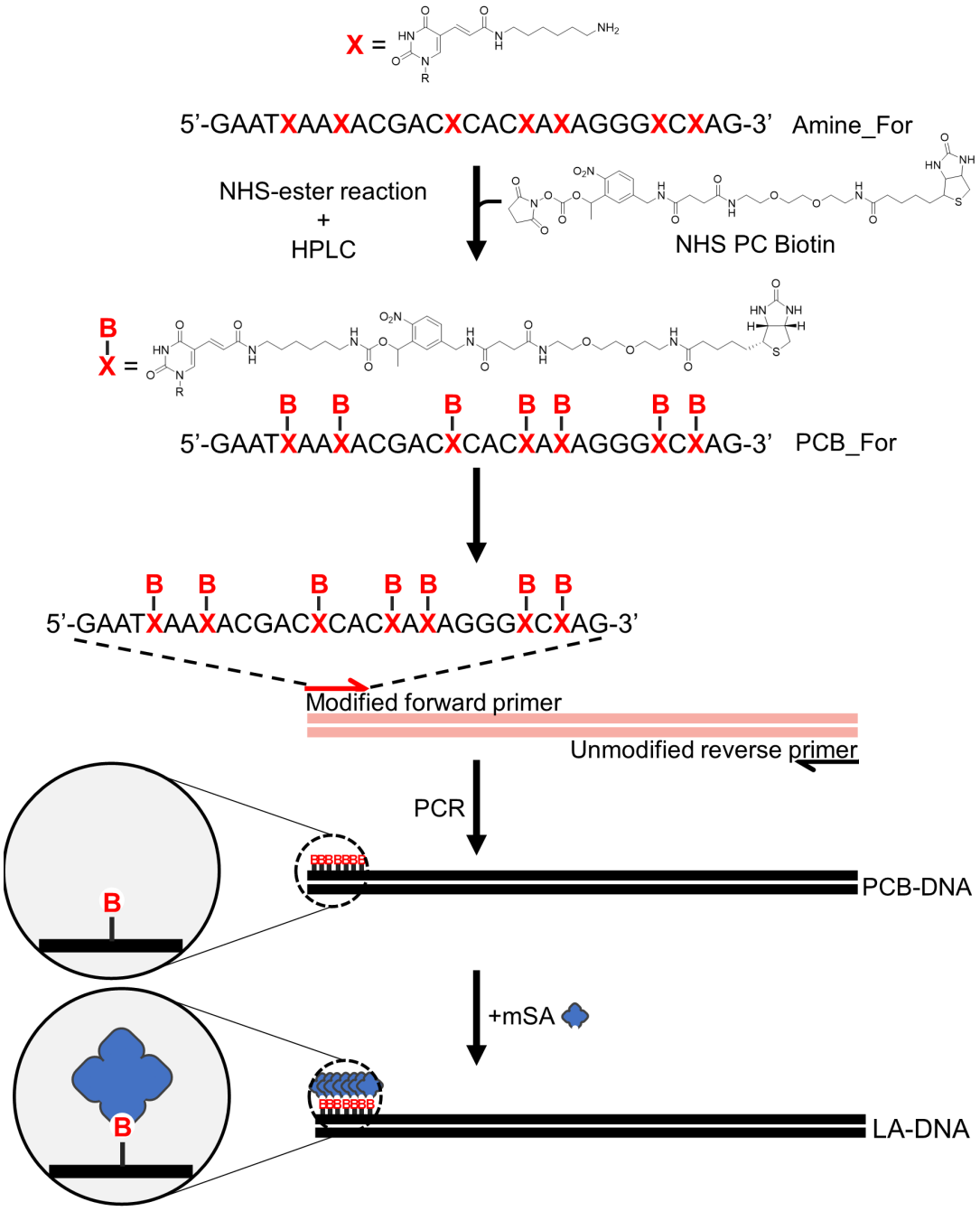


Figure 3.1: Assembly of light-activated DNA
Sequence of the T7 For oligonucleotide with the positions of the amine-modified thymine bases (shown above) labelled as X. An NHS-PCB molecule was reacted with amine groups within the DNA and oligos with all seven amines modified were separated and purified from the partially modified oligos by HPLC. The fully modified oligo (T7 For PCB) was used as a forward primer in PCR to create linear DNA templates with PCB groups positions in the T7 promoter sequence. mSA was bound to the PCB in the resulting DNA to form LA-DNA containing the photocaged T7 promoter.

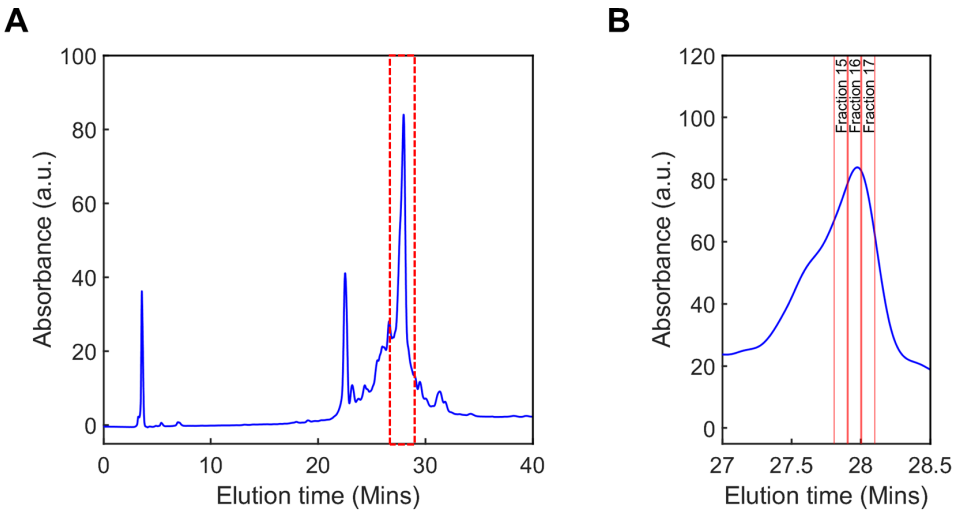


Figure 3.2: HPLC of PCB containing oligo
A) The presence of multiple peaks is consistent with modification of the amine-containing oligo with an increasing number of NHS-PCB groups. B) Main peak indicating the fractions (15 to 17) that were pooled and worked up.

Assembly of LA-DNA templates encoding mNG was validated by gel electrophoresis. mSA was successfully bound to PCB-DNA and caused a DNA band shift, but DNA templates with unmodified T7 promoters or T7 promoters containing only the amino-C6-thymine bases did not bind to mSA, and no band shift occurred (Figure 3.3). Under UV light (365 nm), the 2-nitrobenzyl groups within the steric blockade were photocleaved, and mSA was liberated from the T7 promoter of LA-DNA, restoring its electrophoretic mobility. As before, no band shift was observed for the unmodified or amine-modified DNA templates in response to UV light. The formation of the photocleaved product was proportional to the UV exposure time. After 5 mins of UV irradiation, multiple bands of decreasing size emerged, indicating that only a subset of the 7 blocking groups were removed from the T7 promoter. After 15 mins UV irradiation LA-DNA was almost fully uncaged, and the DNA band returned to its original position on the gel. Convinced that the LA-DNA templates formed and photocleaved as expected, LA-DNA templates were subsequently tested for their ability to control the cell-free expression of mNG.

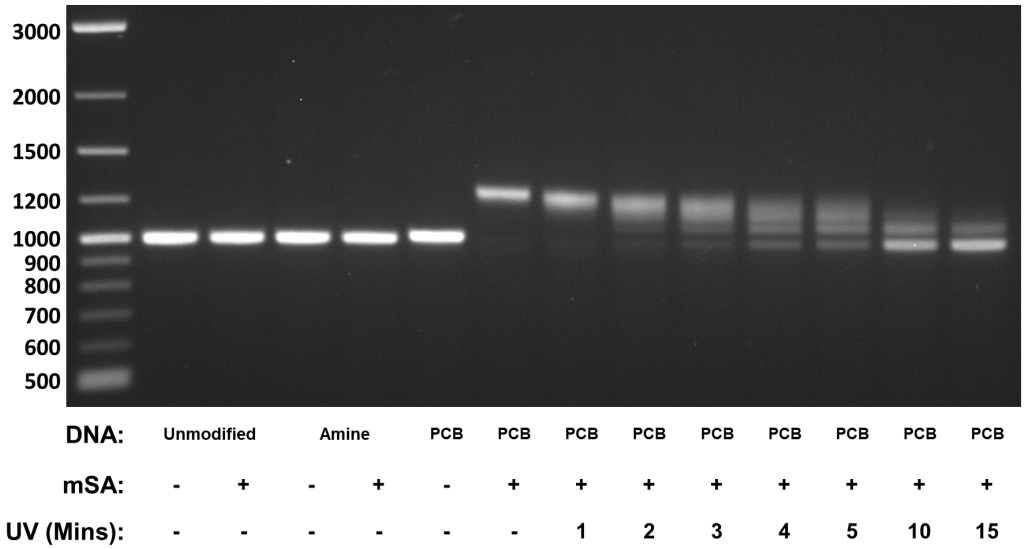


Figure 3.3: Assembly and photocleavage of light-activated DNA
DNA templates with no base modifications, only amine modifications, or PCB modifications in their T7 promoter region all had comparable electrophoretic mobilities on an agarose gel; note a slight band shift due to the presence of the PCB groups. Upon addition of mSA, the band position for PCB-DNA shifted and a single band was present, indicating the binding of mSA to all seven C6-amino thymine bases. Irradiation of LA-DNA with UV light triggered photocleavage of the 2-nitrobenzyl group and removed mSA from the T7 promoter. The ladder-like bands indicate incomplete removal of the blocking groups from the T7 promoter.

mNG expression from LA-DNA templates was confirmed in small scale CFPS reactions. In the absence of light, T7 RNAP was sterically hindered from binding to the T7 promoter by mSAs that occupied the major groove, and mNG expression decreased by 98% compared to the unmodified or amine-DNA templates (Figure 3.4). After irradiating the CFPS reactions containing the LA-DNA with UV light, the steric blockades were removed from the T7 promoter and gene expression was restored. mNG fluorescence reached up to 71% of the amine-DNA control after 3 minutes irradiation (up to 80% when like conditions were compared, i.e amine DNA (4 minutes UV) vs LA-DNA (4 minutes UV)) (Figure 3.4), however, overall expression decreased when reactions were irradiated with UV light for >3 mins, despite further uncaging of the T7 promoter (Figure 3.3). This inverse relationship between UV light exposure time and mNG expression was also observed from amine-DNA templates (Figure 3.4). Thus, low doses of UV light appeared

to deprotect the T7 promoter enough to promote sand/or the LA-DNA templates and perturbed the yield of protein synthesised (Figure 3.4).

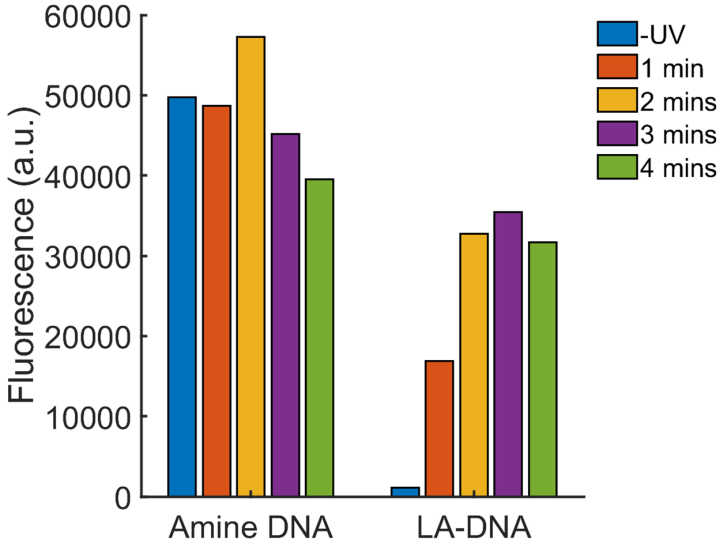


Figure 3.4: Light-controlled CFPS using LA-DNA templates
PURExpress reactions were prepared with 5 ng/μL of amine-modified or LA-DNA templates encoding mNG and irradiated with 0.75 mW UV light for 0-4 minutes. mNG expression was tightly repressed in DNA templates that contained the photocaged T7 promoter in the absence of UV light, but then restored by uncaging the T7 promoter with UV light.

3.3 Maximising protein synthesis with LA-DNA templates

To mitigate against the diminishing expression yields observed after exposing CFPS reactions to UV light, the 5' UTRs of the existing linear DNA templates were refactored to improve transcription and translation. Three templates with transcription-enhancing elements in the 5' UTR were constructed. These had an idealised sequence containing 3 contiguous guanines followed by an A/T-rich string of bases at positions +4 to +8 (GGGAAATA, GGGAATAT and GGGATAAT) and were predicted to generate 'high' mRNA transcript yields. Two other templates with contiguous guanines followed by either 40% or 60% GC content (GGGTGGAA and GGGTTCCC) were also constructed to represent 'medium' or 'low' mRNA transcript yielding controls [175] (Figure 3.5A). The

existing template already had 3 guanines at positions +1 to +3, and had 40% GC bases in positions +4 to +8 (GGGTCTAG), so it was expected to produce similar amounts of mNG to the 'medium' mRNA transcript yielding template.

The existing DNA template already contained an epsilon translation enhancer sequence upstream of the RBS. Consequently, the bases surrounding the enhancer were altered to elucidate whether changing the positional or sequence context of the epsilon motif could enhance translation. DNA templates were constructed with either 10 or 20 adenine bases separating the enhancer and RBS [177] or with the native T7 g10 leader sequence followed by its native amino acid sequence - the first 9 amino acids of the T7 bacteriophage major capsid protein [98] (Figure 3.5B). As before, mNG expression was tested in 3 μL PURExpress reactions with 5 ng/μL of the respective linear DNA templates.

DNA templates with transcription-enhancing 5' UTR sequences performed as expected; the 'high' mRNA-yielding templates with A/T bases at positions +4 to +8 expressed up to 36% more mNG that the 'low' mRNA-yielding DNA template and up to 41% more than the existing template (Figure 3.5C). This suggests that the increased mRNA concentration translated into improved protein yields. A comparable increase was also observed for the 'medium level' mRNA-yielding DNA template, thus above a certain transcript concentration threshold, protein yields were insensitive to further increases in mRNA and limited by other factors, e.g. ribosome or substrate concentration. Of the three DNA templates that contained different translation-enhancer permutations, only the construct with the T7 g10 leader followed by its native amino acid sequence [98] (denoted T7g10*) significantly improved the fluorescence output, increasing mNG expression by $\sim$ 90% (Figure 3.5C).

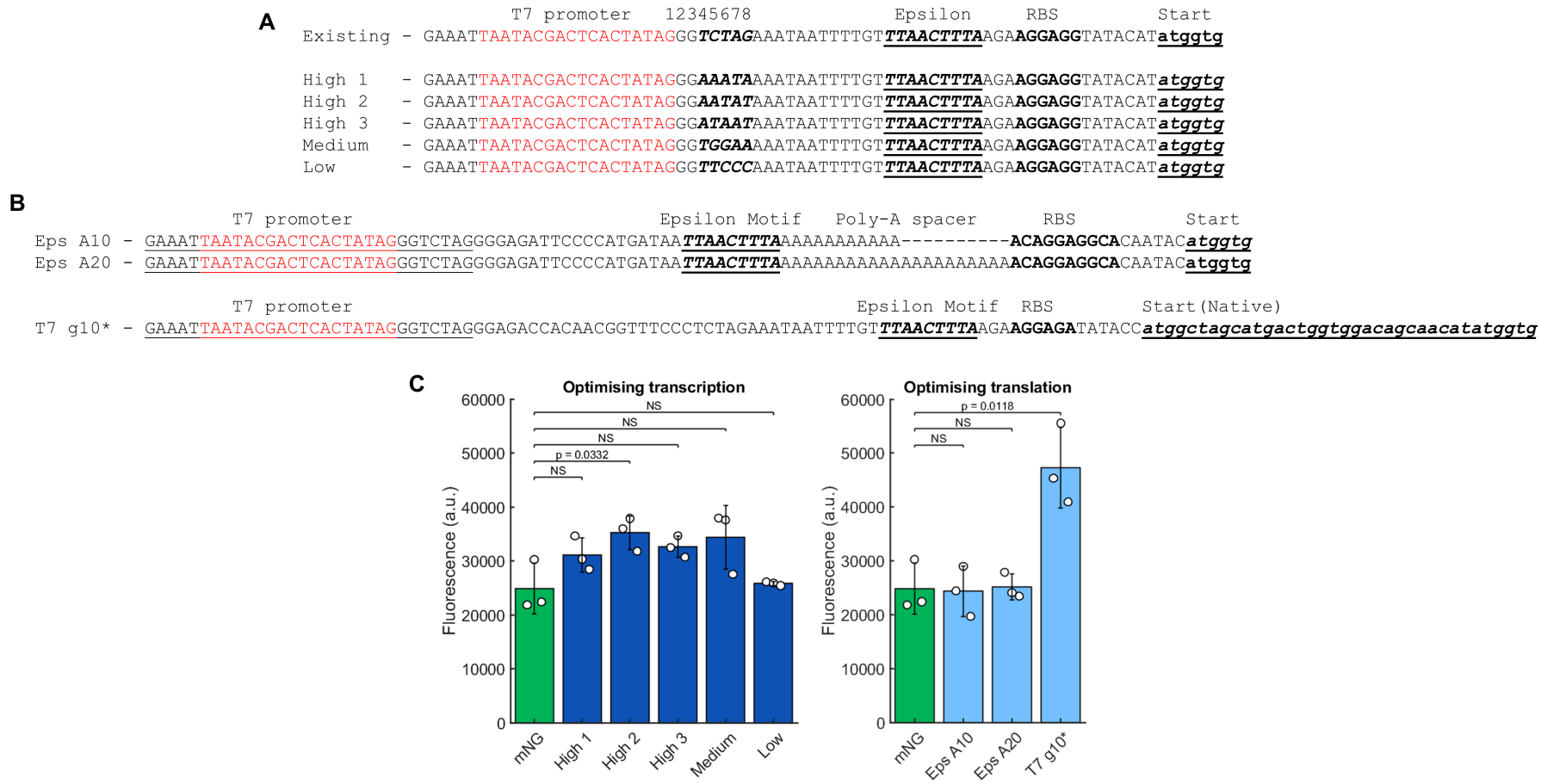


Figure 3.5: Maximising CFPS with transcription and translation enhancers
A) The existing 5' UTR sequence compared to the 5' UTRs with different bases at positions +4 to +8. B) 5' UTRs containing the epsilon motif separated from the RBS by with polyA, and in the context of native T7 g10 leader sequence with the native downstream coding sequence. C) Templates optimised for increased mRNA yields had a modest effect on the mNG yield; a 41% increase was observed for 'High 2'. Introducing the native T7 g10 leader sequence increase fluorescence ~2-fold. Statistical test was Student's t test (unpaired, two-tailed) Error bars, s.d. of three independent experiments ($n = 3$).

The existing DNA template, the templates with poly-A spacers, and the T7 g10* template, all had the same sequence in positions +1 to +10. Thus, there should be no significant differences in transcription initiation rate or transcript concentration, and an increased translation rate was most likely responsible for the improved mNG expression level. Two possible mechanisms for this were considered: 1) Surrounding the epsilon motif and RBS with the native T7 g10 leader sequence minimized the formation of secondary structures in the 5' UTR, making the enhancer and RBS more accessible. 2) The transition from translation initiation to elongation, or the early translation elongation rate itself, was higher because the leader sequence's translation was more favourable than the existing sequence. This could be due to a number of factors, including the utilisation of more abundant codons and/or amino acids.

Predictions of the minimal free energy structure for each of the 5' UTR sequences plus the first 50 nt of the ORF did not indicate any obvious improvements in RBS accessibility for T7g10* vs the other constructs. Consequently, to establish whether enhanced translation was an intrinsic property of the translated N-terminal leader, this sequence was introduced at the N-terminus of mNG encoded on the existing linear DNA template. Indeed, mNG expression increased to a similar extent as T7 g10*, indicating that the 10 amino acid leader alone was able to improve mNG expression (Figure 3.6A).

To establish whether these improvements were limited to the expression of mNG, the T7 g10* sequence was cloned upstream of genes encoding for mVenus. mVenus fluorescence increased 7-fold with the translation enhancing leader sequence (Figure 3.6B). Consequently, inserting this leader sequence could be a generalisable tool for maximising CFPS, assuming the amino acids introduced at the N-terminus of the protein do not disrupt its function.

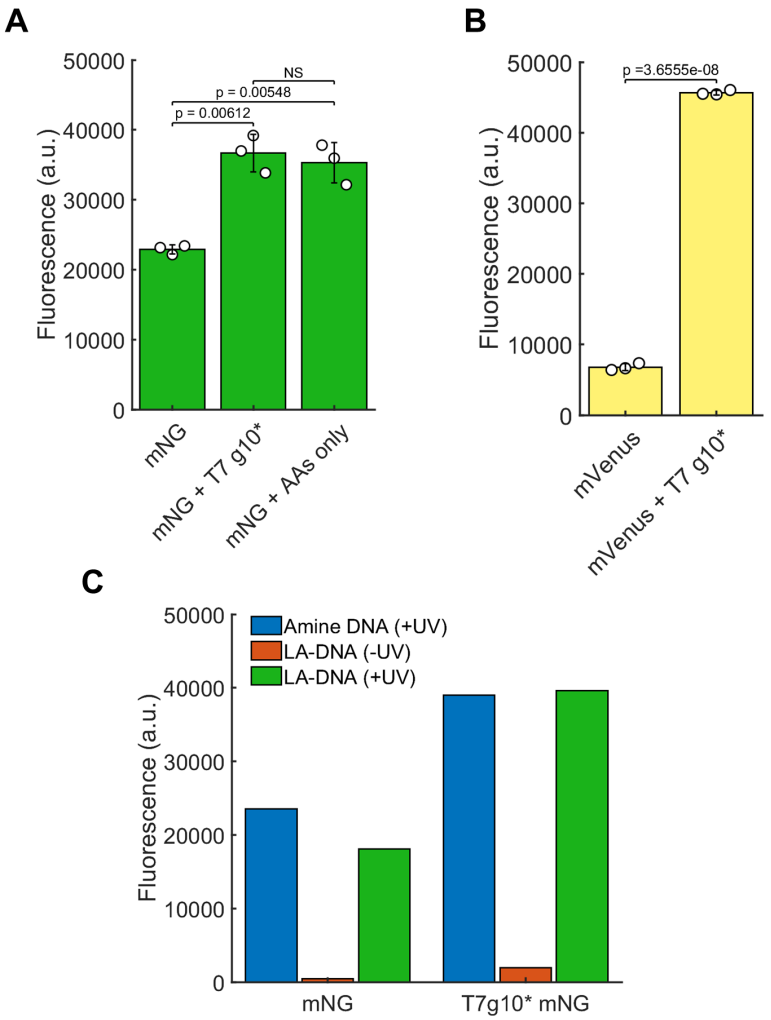


Figure 3.6: Improving CFPS with an translation enhancing leader
A) There was no significant difference between mNG expression when either the T7 g10* or the N-terminal coding leader alone were place upstream of mNG B) mVenus expression increased 7-fold when placed downstream of the T7 g10* leader. C) LA-mNG DNA* expressed 2-fold more mNG after UV irradiation compared to the existing DNA, but this came with a 2-fold increase in the off-state. Statistical test was Student's t test (unpaired, two-tailed) Error bars, s.d. of three independent experiments ($n = 3$).

Only the T7 g10* leader was carried forward for testing in LA-DNA templates. LA-DNA templates that contained the T7 g10* leader, denoted LA-mNG* DNA, produced a 2.2-fold higher fluorescence output than the existing LA-mNG DNA templates and achieved 100% of the potential ON-state. However, this came at the cost of a higher off-state; mNG expression was only repressed 95% in the absence of UV light (98% repression for previous template) (Figure 3.6C).

3.4 Light-activated gene expression inside GUVs

In section 2.5, the PURExpress system and linear DNA templates were encapsulated inside GUVs to create SCs. By substituting linear DNA templates for LA-DNA templates, *in situ* gene expression could be controlled with UV light, and SCs activated in a spatiotemporally controlled manner. In preliminary experiments, GUVs containing 5 ng/μL LA-mNG* DNA were irradiated with the optimal conditions found for bulk CFPS reactions (3 mins, 0.75 mW power). Like mNG expression in bulk CFPS reactions, LA-SCs had a tight off-state, and no mNG was expressed in the absence of UV light. However, mNG expression was minimal, even after 5 minutes irradiation. Consequently, UV light exposure time and DNA concentration were re-optimised to maximise both the number of mNG expressing LA-SCs and the mNG expression level within those compartments. The proportion of mNG expressing vesicles and expression intensity were determined using the imaging processing workflow established in section 2.5.

Varying UV light exposure time from 0-10 mins caused both the proportion of mNG-expressing vesicles and the mNG expression level to increase in a UV dose dependent manner (Figure 3.7). mNG expression then decreased with further UV light exposure mirroring the result of the bulk CFPS reactions; excessive UV light perturbs CFPS despite further uncaging. The requirement for more prolonged UV exposure in SCs compared to in bulk can be accounted for an multiple fronts. Principally, the LA-DNA did not receive 100% of the UV light available; some light was reflected off of the coverslip and the light which did reach the LA-DNA had some of the harmful UV light filtered out - glass transmits light with wavelengths <365 nm less than those at 365 nm. It may also be the case that SC containing fewer copies of LA-DNA must be uncaged more before a measurable fluorescent signal is produced, due to the lack of accessible T7 promoters.

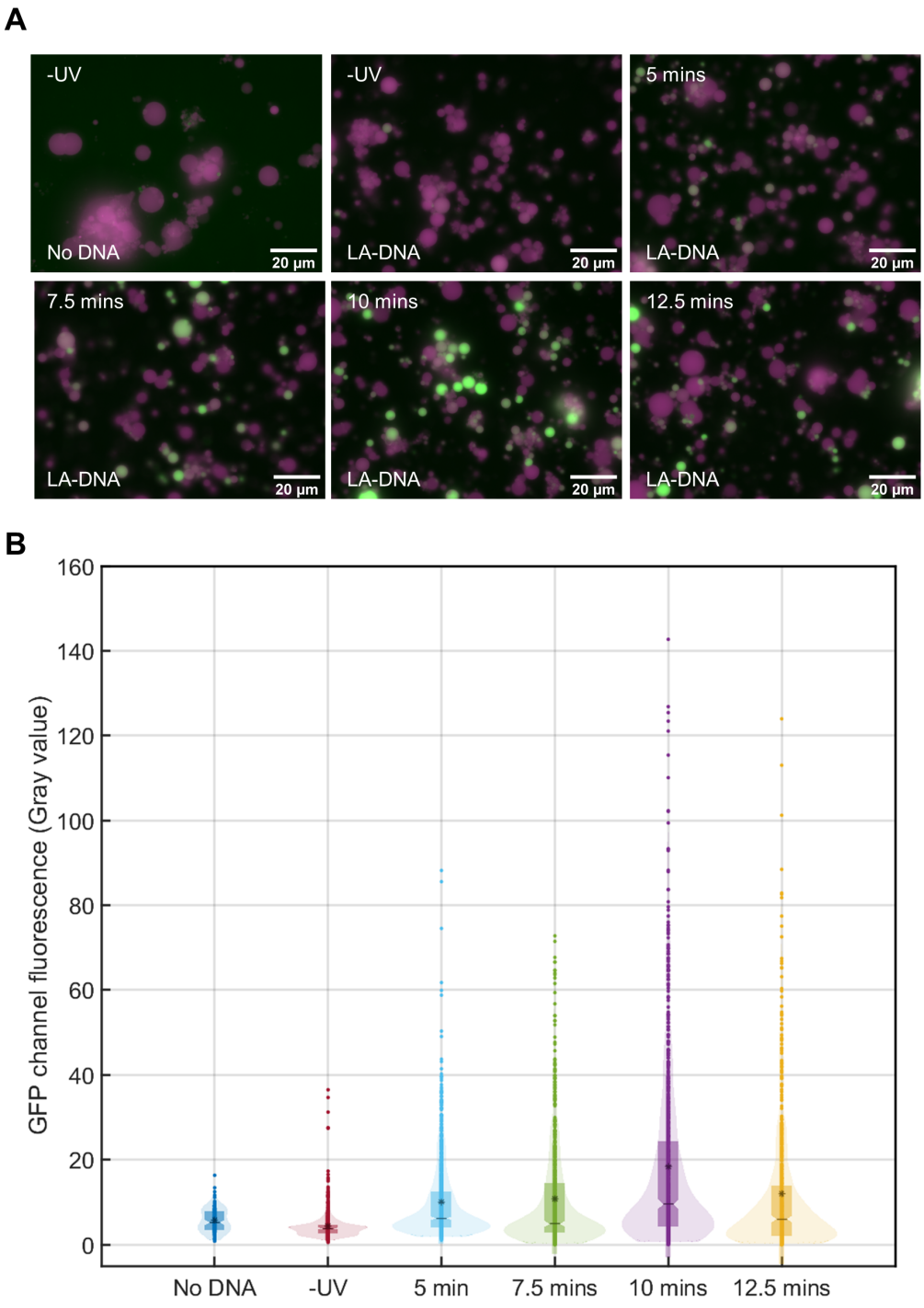


Figure 3.7: Light-activated synthetic cells vs UV light exposure time A) The number of mNG-expressing vesicles observed, and the fluorescence intensity of those mNG-expressing vesicles increased with as UV light exposure time increased, peaking at 10 mins. Further UV light exposure decreased these metrics due to the UV damage of the components inside the vesicles. B) Image quantification of LA-SCs with increasing UV light exposure time

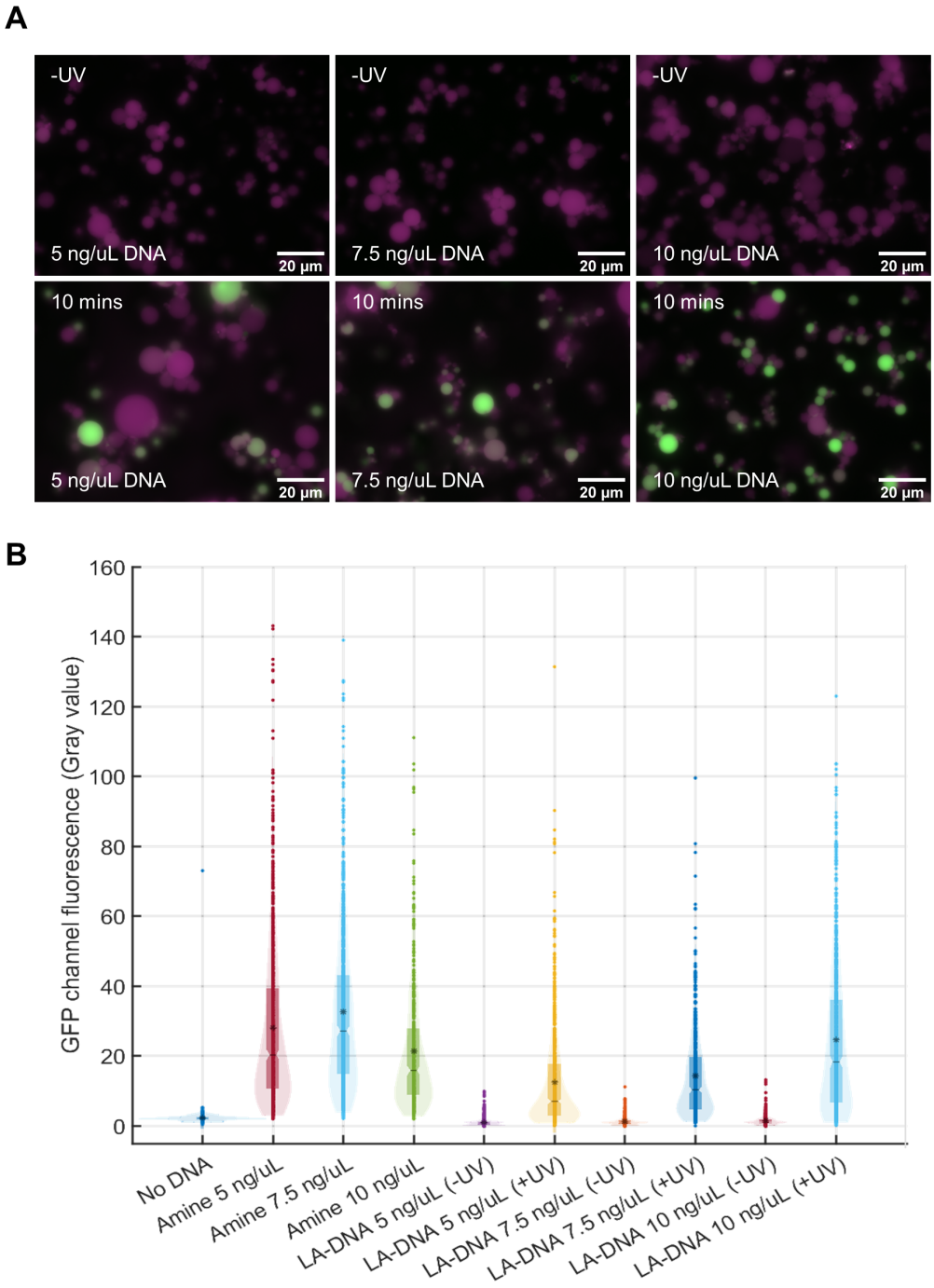


Figure 3.8: Light-activated synthetic cells vs DNA template concentration A) The number of mNG-expressing vesicles, and the fluorescence intensity of those mNG-expressing vesicles increased as LA-DNA concentration increased. At 10 ng/μL LA-DNA, the distribution of mNG expressing vesicles resembled that of the vesicles prepared with amine-containing DNA. Many of the vesicles prepared with 10 ng/uL amine had wetted onto the glass coverslips during the course of the experiment. Therefore, the mNG was artificially decreased compared to the other samples. B) Image quantification of LA-SCs with increasing UV light exposure time.

Next, LA-DNA concentration was varied between 5 ng/μL and 10 ng/μL. 10 ng/μL was the upper DNA concentration limit tested as, beyond that, the PURExpress inner solution became diluted below its 1X working concentration. Again, both the proportion of mNG-expressing vesicles and the mNG fluorescence intensity increased with increasing LA-DNA concentration (Figure 3.8). Interestingly, off-state mNG expression remained generally unchanged despite the increase in LA-DNA concentration, contradicting the equivalent reactions performed in bulk CFPS reactions. Overall, 10 mins UV irradiation at 0.75 mW and 10 ng/μL LA-mNG* DNA concentration represented the optimal conditions of those tested. LA-SCs prepared with 10 ng/μL LA-mNG* DNA had a tight off state in the absence of UV light and expressed he highest amounts of mNG, equivalent to that of amine DNA containing GUVs, in the presence of UV light (Figure 3.9). These conditions were used in all subsequent experiments, unless stated otherwise.

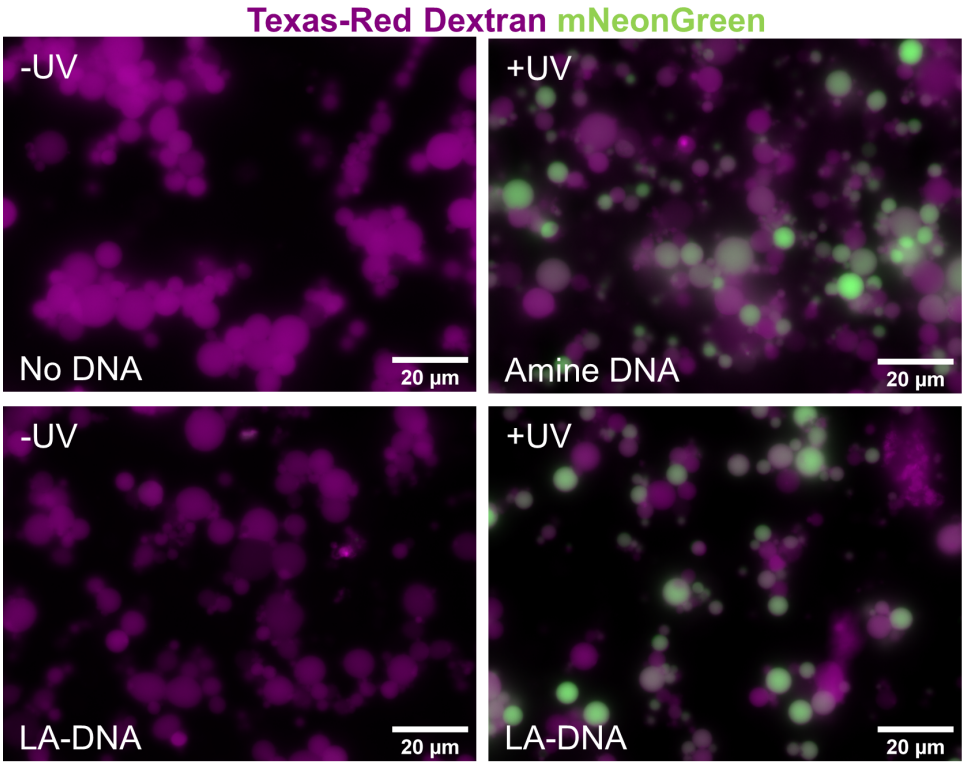


Figure 3.9: Light-activated synthetic cells
Preparing synthetic cells with 10 ng/μL LA-DNA, and irradiating them at 0.75 mW for 10 mins produced many fluorescent compartments. This result was representative of the synthetic cell populations prepared with amine DNA.

3.5 Spatial control of light-activated synthetic cells

In contrast to adding small molecules into a bulk aqueous solution, light can be spatially controlled by patterning the arrangement of the light source or passing a collimated beam of light through photomasks. Consequently, LA-SCs might also be spatially controlled by shaping the light to which they are exposed. In these experiments, the light was patterned by contact photolithography, i.e. placing a film photomask with the desired pattern directly on top of a coverslip, between the light source and sample (Figure 3.10A). Photomasks with 100 μm to 900 μm features were designed to create patterned structures with both simple and complex designs. The chosen patterns were selected to test the

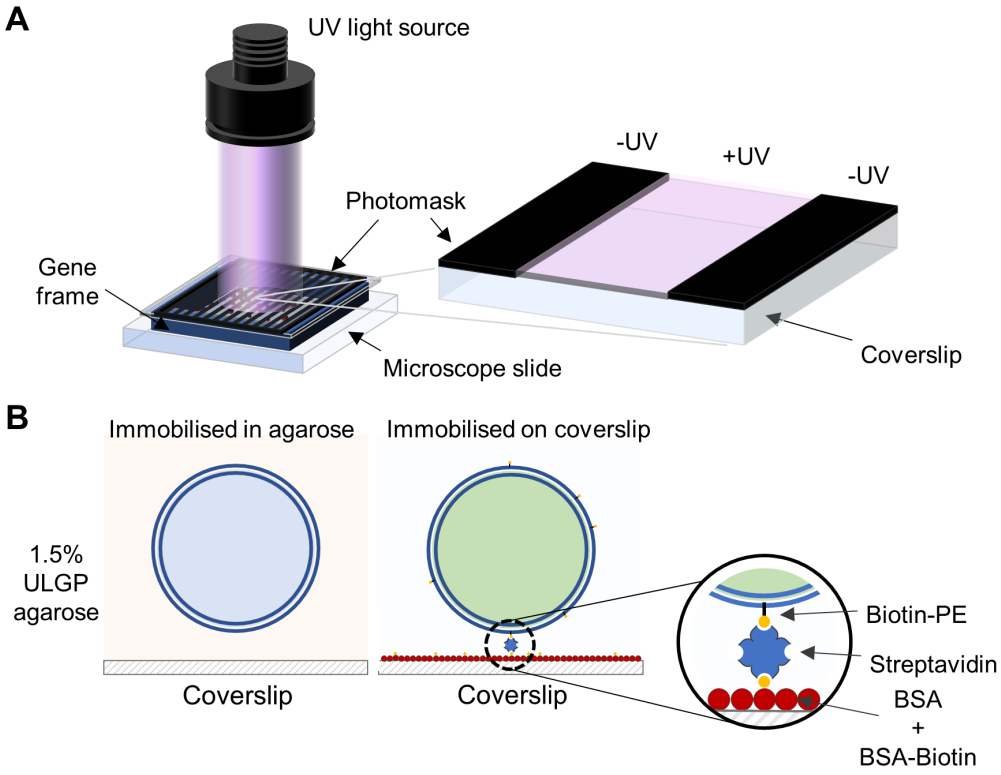


Figure 3.10: Patterning synthetic cell activation
A) Collimated UV light was passed through a photomask to create patterned UV light. B) Left - Pelleted vesicles were resuspended in 1.5% molten ultra-low gelling point agarose, then transferred inside gene frames, attached to a glass slide, and sealed with a coverslip. Vesicles were immobilised in suspension on gelation of the agarose. Right - Vesicles with 0.1% Biotin-PE in their outer leaflet were immobilised on coverslips coated with biotin+biotin-BSA and streptavidin.

resolution limit for patterning LA-SCs, and fill the entire field of view when using the 10X objective lens. To stop the SCs moving after patterned UV irradiation, they were either immobilised inside an agarose hydrogel (Figure 3.10B - Left) or onto coverslips via the interaction between biotinylated lipids in the outer leaflet with BSA-biotin + streptavidin-coated coverslips (Figure 3.10B - Right).

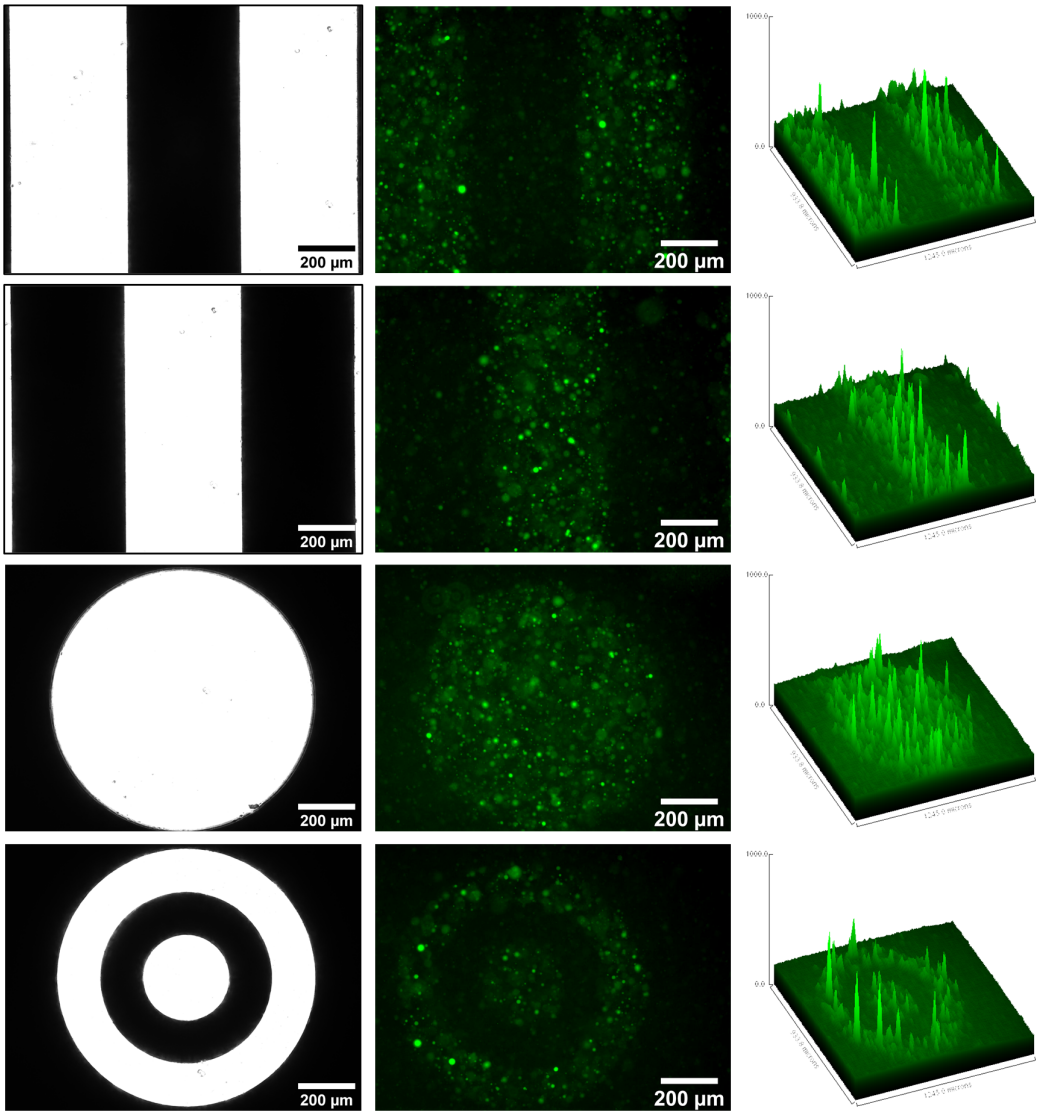


Figure 3.11: Patterned activation of synthetic cells with simple photomasks Light-activated synthetic cells were immobilised in agarose and irradiated with UV light through film photomasks. mNG expression was activated only inside SCs which were exposed to UV light (light regions). No mNG was expressed in SCs protected from the UV light (dark regions). Photomasks had designs containing either 400 μm wide stripes, a 900 μm circle, or a concentric circle pattern containing a 300 μm circle surrounded by a ring of width 150 μm. Left to right; Photomasks, patterned vesicles, surface plots of the patterned vesicles.

Populations of LA-SCs were successfully activated in a spatiotemporally controlled manner. LA-SCs immobilised in agarose demonstrated high patterning fidelity with both the simple (Figure 3.11) and more complex photomask designs (Figure 3.12). mNG-expressing vesicles were restricted to regions exposed to UV light, clearly contrasting the regions protected from the UV light, which were devoid of mNG-expressing vesicles.

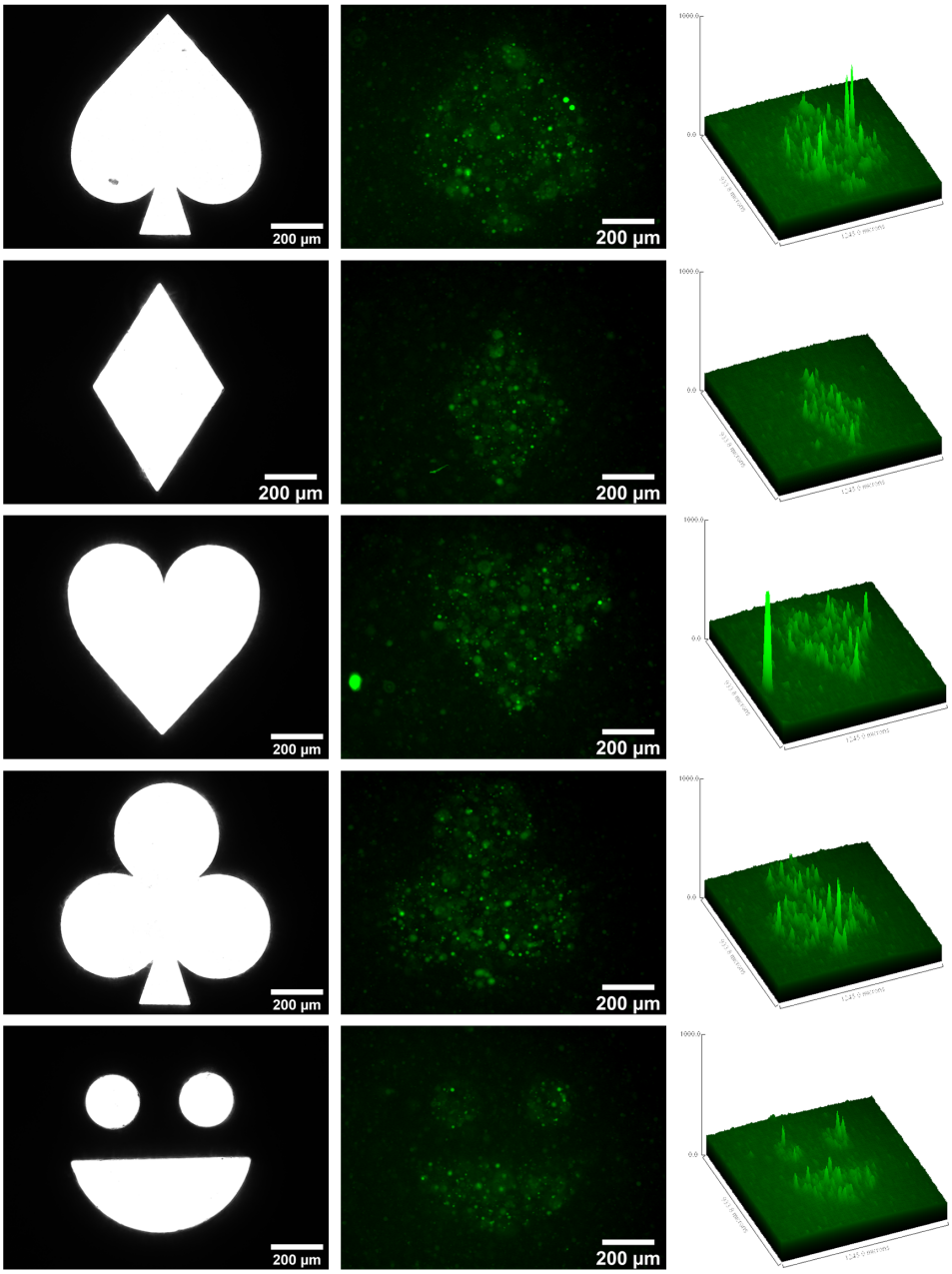


Figure 3.12: Patterned activation of synthetic cells with complex photomasks Light-activated synthetic cells were immobilised in agarose and patterned with UV light using irregular photomasks containing features of varying dimensions. Left to right; Photomasks, patterned vesicles, surface plots of the patterned vesicles.

Guided by the dimensions of the photomasks, microscopy images containing the circle and concentric circle patterns were split into the respective patterned regions, and fluorescence intensity of the vesicles in each area was measured using the imaging processing tool (section 2.5). Vesicles that were protected from the UV light had a fluorescence profile consistent with the no DNA control sample, therefore, no UV light passed through the dark emulsion gel on the photomasks, and no mNG occurred (Figure 3.13A). However, in the case of the concentric circle, vesicles in the inner ring were protected from the UV light had a slightly elevated fluorescence value. This could be an artefact introduced when selecting the region of interest, but more likely, this was due to the UV irradiation on either side of the 150 μm ring, which could easily cross into the inner ring region by reflecting off the foil placed underneath the sample, or refraction on passing through the glass slide and partially uncage the LA-T7 promoter. Vesicles within the irradiated regions of the patterns clearly expressed mNG, however, more mNG-expressing vesicles and greater fluorescence intensities were observed for the larger circle pattern (Figure 3.13A) compared to the inner circle or outer ring of the concentric circle pattern (Figure 3.13A). During these experiments, the SCs were held inside the gelled agarose hydrogel for at least 7 hours (1 hour at 4°C/ and 6 hours at 37°C). Although the primary objective was to immobilise the vesicles for patterning purposes, fixing the vesicles inside hydrogel also kept the vesicles from clustering or fusing; vesicles that make contact with the glass coverslip or slide usually rupture or wet onto the surface. Therefore, immobilisation of SCs in hydrogels could be a potential route to prolonging their lifetime.

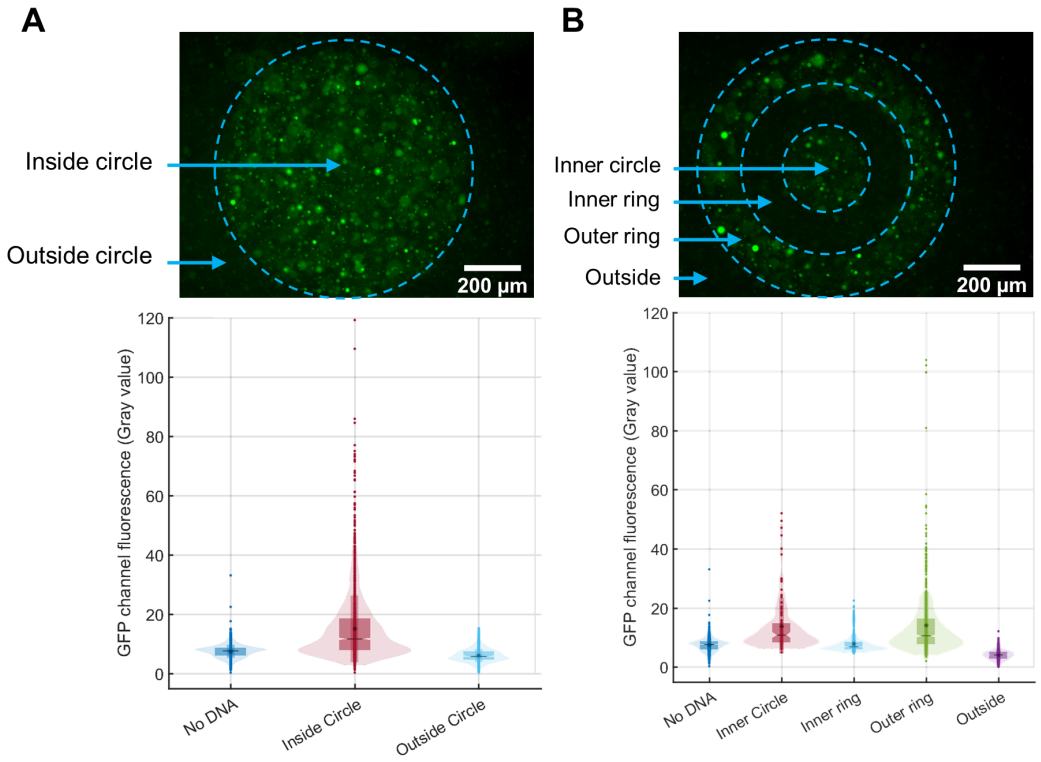


Figure 3.13: Quantification of patterned LA-SCs
A) Synthetic cells inside the patterned 900 μm circle region expressed mNG in response to UV light. Synthetic cells outside of the irradiated pattern did not express mNG and were consistent with the no DNA control. B) Synthetic cells within the inner circle and outer ring. Synthetic cells outside of the patterned region had a fluorescence value equivalent to the no DNA control, however, those located between the inner circle and outer ring had an elevated mNG fluorescence value.

LA-SCs immobilised onto coverslips via biotin-streptavidin tethers showed lower fidelity patterning than those immobilised in agarose (Figure 3.14). Although the desired shapes were still discernible and each SC had better contrast than the SCs held in agarose, since the vesicles held at the coverslip are all at the same Z-position, the edges of the patterns were poorly defined. This is most likely due to the incomplete immobilisation of vesicles that moved freely after the patterns had been irradiated and could be rectified by washing the unbound vesicles before irradiating those still bound to the coverslip with UV light.

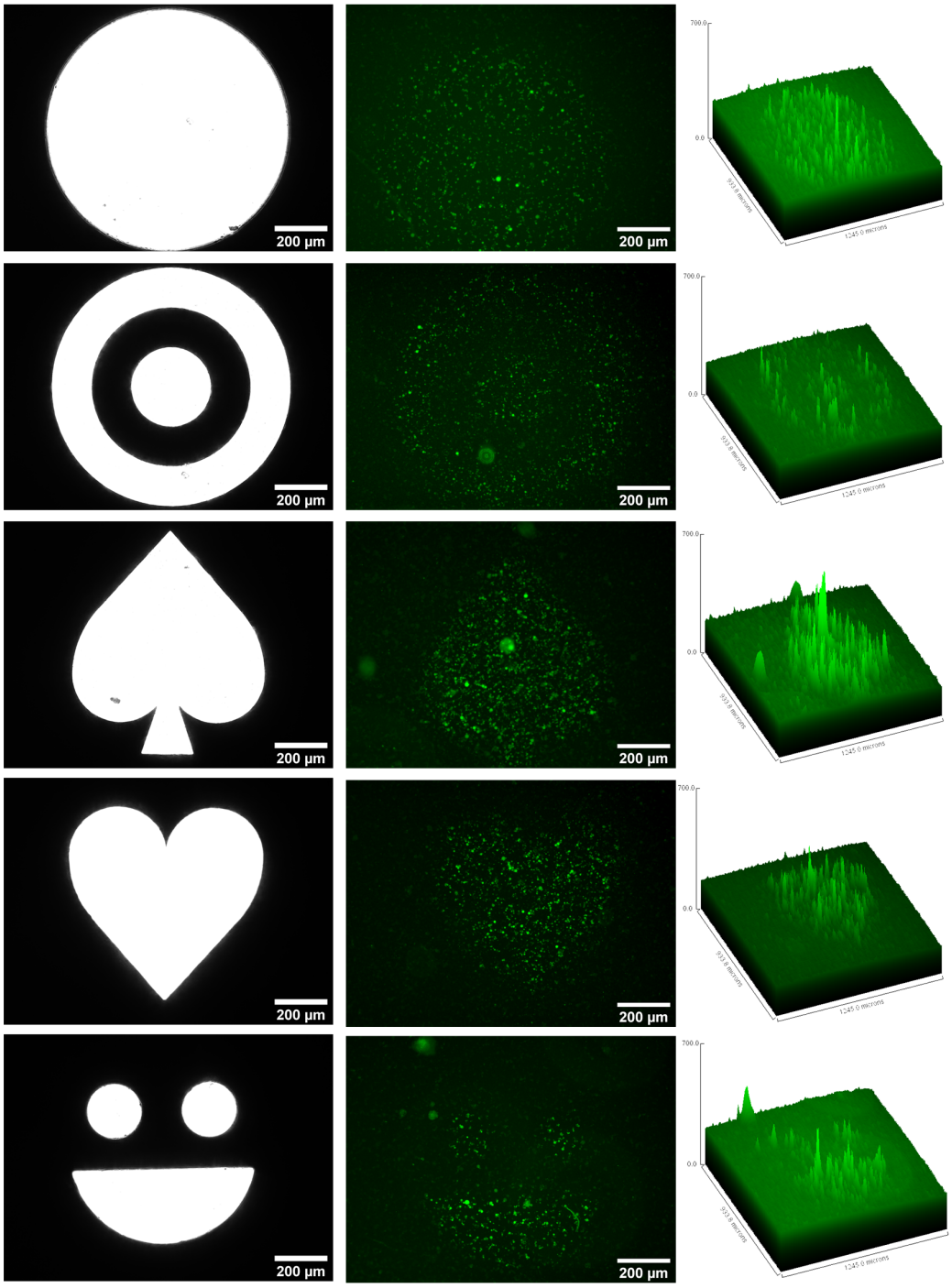


Figure 3.14: Patterning of vesicles immobilised on coverslips
Vesicles immobilised on BSA-biotin + streptavidin coated coverslips were held at the same Z-position, but this did not improve the contrast of the patterned structures. Patterning fidelity was lower than vesicles held in agarose as unbound vesicles were not removed prior to irradiation.

4

Communication between synthetic cells and bacteria

4.1 Introduction

4.1.1 Quorum sensing for synthetic cell communication

SC communication is a vibrant area of research that promises to interface non-living systems with living systems and create interconnected networks of communicating compartments - a prerequisite to constructing SC communities that execute functions at a

population level. To achieve this, infrastructures are required to enable SCs to produce and/or recognise specific cues, which subsequently trigger a predetermined downstream response in a second SC or living cell. QS systems from bacteria are among the most simple yet versatile modes of communication and involve as few as two proteins to function; one to produce the signalling molecule and another to detect it. Hence, QS systems have been reconstituted in SCs to establish SC to SC [72], and SC to living cell communication [57, 180].

An ideal QS-based SC communication system should satisfy the following criteria: 1) The enzyme responsible for acyl homoserine lactone (AHSL) biosynthesis should express well *in vitro*, inside vesicles. 2) This enzyme should synthesise membrane-permeable signalling molecules from membrane-impermeable substrates without the need for other proteins. 3) The signal-responsive gene circuit in the receiver cell/SC should exhibit minimal reporter gene expression in the absence of its cognate signal but high reporter gene expression in the presence of the AHSL. 4) The signalling molecule should be distinguishable from other, structurally similar molecules to eliminate crosstalk between separate communication systems.

Existing QS-based SC communication systems fulfil many of these criteria, but they are not without their caveats and limitations. For example, LuxI and RhlI enzymes have both been expressed inside vesicles and successfully synthesised AHSLs from SAM and acetyl-CoA [57] or butyryl-CoA [102] respectively. However, neither acetyl-CoA nor butyryl-CoA are natural substrates for LuxI [181] and RhlI. In the case of LuxI, acetyl-CoA first had to be loaded onto acyl carrier proteins (ACPs) via fatty acyl synthases present in the S30 lysate to generate the substrates for AHSL biosynthesis. Also, since LuxR is a promiscuous transcription factor, it was unknown which acyl-ACP was assembled and which AHSL was synthesised to activate LuxR [57]. Meanwhile, even though RhlI can

utilise butyryl-CoA as a substrate for C4-HSL biosynthesis, yields are much lower than with the natural substrate, butyryl-ACP [182]. This is problematic in SC communication since the RhlR receiver protein requires micromolar concentrations of C4-HSL to activate gene expression [183, 184] and therefore demands more from the AHSL-producing SCs. Issues also exist in the receiver proteins used to detect these AHSLs; both EsaR and LuxR receiver proteins 3OC6-HSL [57, 72, 74] so these systems could not be used simultaneously within the same SC community. Consequently, there is a need for other QS systems that better meet the desired criteria to diversify the SC communicate toolbox.

The BjaI/R system governing *Bradyrhizobium japonicum* communication could be a promising candidate for SCs communication. In this simple system, an acyl-CoA dependent AHSL synthetase, BjaI, synthesises N-isovaleryl-L-homoserine lactone (IV-HSL) from membrane-impermeable substrates, S-adenosyl methionine (SAM) and isovaleryl CoA (IV-CoA) [121, 182]. IV-HSL diffuses out of the cell and accumulates in the environment. Inside the neighbouring cell, changes in IV-HSL are recognised by an IV-HSL-responsive transcription factor, BjaR. In the absence of IV-HSL, BjaR is inactive; then, upon binding to IV-HSL, BjaR interacts with a consensus DNA sequence found immediately upstream of a Lux-type promoter. This helps to recruit RNA polymerase to the adjacent promoter and activates expression of the downstream gene cluster [121] (Figure 4.1).

The benefits of this system for SC communication are multi-fold. Firstly, as both SAM and IV-CoA are commercially available, no additional enzymes are required to assemble the substrates for IV-HSL biosynthesis. Having these natural substrates readily available also eliminates the need to use substrate homologues and should translate into high IV-HSL titres [182, 185]. Second, as IV-HSL is a branched AHSL that differs more significantly from linear AHSLs, BjaR works orthogonally to many of the other commonly used QS systems [186]. Finally, BjaR is exquisitely sensitive and responds to picomolar

concentrations of IV-HSL under its natural context [121] - this would help reduce the demands on the AHSL-producing SCs.

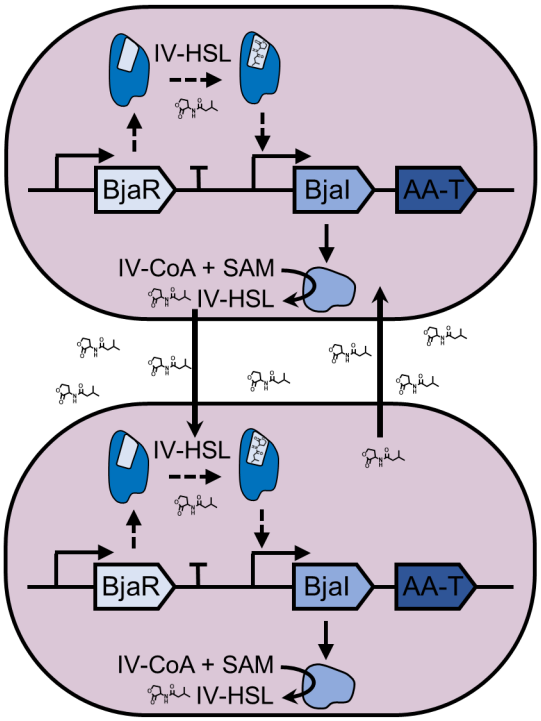


Figure 4.1: BjaI/BjaR QS system
Under basal conditions, *B. japonicum* cells produce low amounts of IV-HSL from SAM and IV-CoA. IV-HSL is membrane permeable and is released from the cell into the environment. Neighbouring cells detect the presence of IV-HSL using a transcription factor, BjaR, which subsequently activates the expression of an operon of genes, including bjaI. BjaI is an acyl homoserine lactone synthetase that synthesises IV-HSL. By detecting IV-HSL and producing IV-HSL in response, cells determine the number of clonemates in their environment by the environmental IV-HSL concentration and synchronise their gene expression.

4.1.2 Directed evolution

Guided by natural selection, proteins and enzymes have gradually evolved into highly processive machines optimised towards a specific function. Evolution manifests as the emergence of random mutations within a gene sequence, which gives rise to proteins with slightly different amino acid sequences and, hence, slightly different properties. Mutations that benefit the protein (and host) are retained and become the dominant protein variant within the population, while those that impair the protein's function (and the host's

fitness) are discarded. Thus, over many cycles of mutagenesis and natural selection, these small changes accumulate and proteins (and cells) iteratively become better adapted to fulfilling their intended purpose. However, if these proteins are then taken out of their native host, they often perform poorly in their new environment, especially if repurposed for a completely different task. By exploiting the basic principles of evolution and natural selection, these proteins can be re-optimised for their new host, and even towards entirely novel functions, through the process of directed evolution.

In its most basic form, directed evolution encompasses iterative rounds of mutagenesis, followed by a screening or selection process to recover the genes that encode proteins with more desirable properties than the starting protein (Figure 4.2). During this process, random mutations are introduced into a gene sequence to create a diverse library spanning a large sequence space. Various techniques can be used to introduce random mutations into genes. Among these, the most popular method is termed error-prone PCR (epPCR) [187]. epPCR uses a low-fidelity DNA polymerase, such as Taq polymerase, instead of the conventional high-fidelity polymerases, such as Q5 DNA polymerase, to amplify a gene of interest. Taq polymerase has an intrinsically high error rate and adds one mismatch every 18,000 bases. In contrast, Q5 DNA polymerase adds one mismatch every 53,000,000 bases [188]. Therefore, low fidelity polymerases enable mutations to be introduced into a gene of interest in line with the natural error rate of the enzyme. However, low-fidelity enzymes alone are typically not enough to generate sufficient sequence diversity within the gene pool, and further modifications to PCRs are required to increase the error rate. These include spiking the PCR mix with manganese, reducing the magnesium concentration, varying the ratios of dNTPs, or adding base analogues to reduce base-pairing fidelity [189].

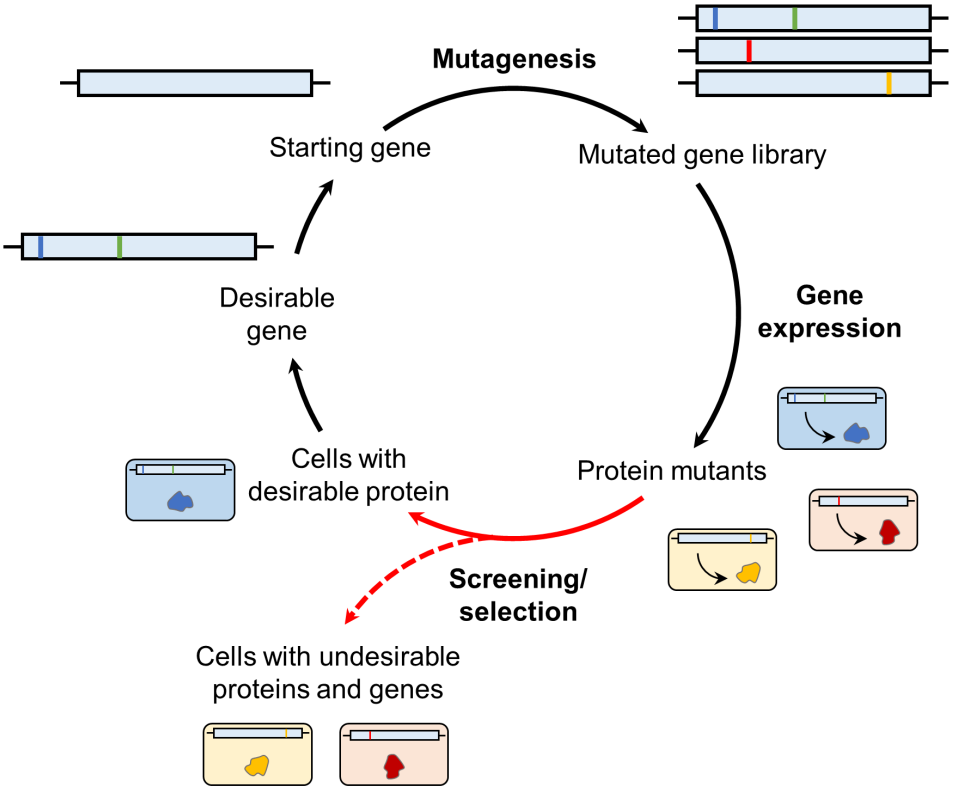


Figure 4.2: Directed evolution cycle Genes are randomly mutated, cloned into plasmids and transformed into cells. Mutant genes are transcribed and translated into mutant proteins, the function of which is assayed against the desired response through a screening or selection process. Cells containing undesirable proteins and genes are removed from the library, while cells containing desirable proteins and genes are retained. Plasmids containing the genes encoding the desirable mutant protein are extracted from the cells and used as the new starting gene for the next round of evolution.

As mutagenesis is random, the identity of the introduced mutations and their impact on the protein's function are unknown. The mutations can either be neutral and have no impact on protein function, beneficial and shift the protein's function towards the desired traits, or deleterious and shift the protein's function further from the desired traits. Thus, after mutagenesis, gene libraries must undergo a screening or selection process to discern the desirable mutants from the undesirable mutants.

Screening involves testing cells containing mutant proteins or the mutant proteins extracted from these cells in function-specific assays to assess whether the mutant proteins possess the desired traits. The assay itself could either be the end goal experiment, for

example, testing the ability of an enzyme to catalyse the biosynthesis of a drug candidate, however, this can often be unfeasible when the substrates are expensive or when the assays are analysed by low-throughput processes such as HPLC. Therefore, simple, robust assays that match the requirements of the enzymes, e.g. amide bond formation, but use cheaper substrates that produce a colourimetric or fluorescent readout are often used to accelerate the screening process. Individual mutants with desirable traits identified in the activity screen are then used as the starting point for the next round of evolution [189].

Selection differs somewhat from screening and enables mutant proteins to be recovered and enriched within a gene library without the need to examine each cell or protein variant individually. This is achieved by coupling the protein function with the fitness of its host while growing under a selection pressure [189]. ON-selection is used to direct mutant proteins towards a particular trait, for example, selecting transcription factors that more strongly activate gene expression in the presence of a cognate ligand. This involves growing cells under a condition whereby cells containing desirable mutants become enriched within the population, while cells harbouring less desirable or non-functional mutants become less represented or removed from the population entirely. Alternatively, off-selection is used to direct mutant proteins away from an undesirable trait. For example, the activation of gene expression with non-cognate ligands. This involves placing cells under a condition where the desirable mutants are retained but not actively enriched within the population, while those with undesirable traits are actively removed from the library. Unlike screening, the selection process is unbiased. Every gene recovered post-selection can be used as the starting point in the next round of evolution, rather than just those that were successfully identified in the screening process. Hence, selection is beneficial for exploring the large sequence space and avoiding optimisation towards local optimisation maxima.

While epPCR is typically used to introduce mutations into a gene during the first

round of directed evolution, complementary techniques are often exploited in subsequent rounds. After the first round of mutagenesis and screening or selection, genes typically contain various individual mutations that confer slight improvements towards the desired protein. These individual mutations can be combined into a single gene construct by DNA shuffling [190–193] or by modifying the PCR cycles [194]. During DNA shuffling, genes are cleaved into short oligonucleotides by DNaseI and then reassembled by recombining the constituent oligonucleotides by overlap extension PCR [190], or ligation and polymerase treatment [192]. In doing so, these mutations can be randomly distributed between the gene pool, forming genes with new permutations of the existing mutations that may have an additive effect on protein function. After multiple rounds of mutagenesis and/or shuffling, followed by screening or selection, proteins iteratively accumulate more beneficial mutations and yield a mutant that is more closely aligned with the desired characteristics.

4.1.3 Directed evolution of transcription factors involved in quorum sensing

Directed evolution has been used to introduce new functionalities into QS transcription factors or to improve their existing activities. Wild-type LuxR responds to 3OC6-HSL as well as similar AHSLs with longer acyl chains (3OC8-HSL and 3OC12-HSL) [184, 195], or chains without carbonyl groups (C6-HSL)[196], and activates the expression of genes downstream of a pLux promoter. Through directed evolution, LuxR mutants with even broader substrate specificities have been identified. By introducing random mutations through epPCR and DNA shuffling and then screening mutant proteins for GFP expression on agar plates containing non-cognate AHSLs, Francis Arnold and colleagues were able to identify mutant LuxR proteins that also responded to octanoyl-homoserine lactone (C8-HSL) [197] or butanoyl-homoserine lactone (C4-HSL) [198] in addition to the existing

substrates. Subsequently, by taking this further and alternating between cycles of ON-state and OFF-state selection, LuxR mutants that responded to decanoyl homoserine lactone (C10-HSL) but not 3OC6-HSL [196], and N-3-oxo-octanoyl homoserine lactone (3OC8-HSL) but not 3OC6-HSL [196] have also been identified.

As well as these LuxR mutants with different substrate specificities, mutants with improved ligand sensitivities [199–201] or tighter OFF-states [202], i.e. variants that resulted in lower gene expression from a pLux promoter in the absence of 3OC6-HSL than the parental variant, have also been identified using directed evolution. epPCR and DNA suffling followed by ON/OFF-selection was utilised to obtain more sensitive EsaR[200] and XylS [199] mutants, while a much simpler approach of just epPCR followed by ON-state selection was used to obtain LuxR mutants that more tightly controlled GFP expression at a pLux promoter [202]. Unlike the previous work whereby specific rare mutations were necessary to evolve the desired proteins, this approach recovered many different mutants containing a variety of mutations across the entire length of the gene. These were denoted 'ligand-addicted' mutants, as they required the presence of the cognate ligand to stabilise the folded structure before the mutant LuxR could regulate the pLux promoter, rather than mutants with specific mutations necessary for a tight OFF-state.

4.1.4 Chapter overview

The aim of this chapter was to establish a small molecule-mediated communication system between LA-SCs and living cells that could be spatiotemporally controlled with light. The communication system used was based on the BjaI/BjaR QS from *B. japonicum*, and involved the production of IV-HSL by SCs, and the detection of IV-HSL by engineered *E. coli* cells.

IV-HSL responsive *E. coli* cells were prepared using an existing BjaR-containing reporter plasmid with GFP placed downstream of a modified pLux promoter. The ability of BjaR to regulate the pLux promoter was determined by measuring GFP expression in response to IV-HSL. To improve the performance of the receiver cells, BjaR underwent 4 rounds of directed evolution with ON-selection to obtain cells with low OFF-state GFP expression in the absence of IV-HSL. The resulting receiver cells were characterised to determine the biological significance of the mutations introduced.

IV-HSL producing SCs were created by expressing BjaI inside GUVs containing SAM and IV-CoA. The bjaI gene was synthesised by polymerase chain assembly, and CFPS confirmed its expression. BjaI expressed in bulk, and inside GUVs synthesised enough IV-HSL to fully activate GFP expression in BjaR receiver cells. Using UV light to activate BjaI expression in SCs held inside thin agarose pads, IV-HSL production was remotely controlled and used to activate GFP expression in BjaR-expressing receiver cells located on top of the agarose pads.

4.2 Charactering BjaR receiver cells

Receiver cells that recognised and responded to IV-HSL were established by transforming *E. coli* XL10-Gold cells with the pSB1A3 BjaR GFP reporter plasmid [186]. In this gene circuit, BjaR was expressed from a constitutively active *E. coli* promoter, while the reporter protein, GFP, was expressed from a BjaR-regulated promoter, pBjaR (Figure 4.3A). pBjaR denotes a hybrid promoter constructed by replacing the LuxR binding site of the pLux promoter with the BjaR binding site, as opposed to the native pBjaR promoter from *B. japonicum*. In the presence of IV-HSL, BjaR was expected to bind its consensus sequence immediately upstream of the pBjaR promoter and activate GFP

expression (Figure 4.3 Left), while in the absence of IV-HSL, BjaR should not bind to its consensus sequence, and no GFP expression should not be observed (Figure 4.3 Right).

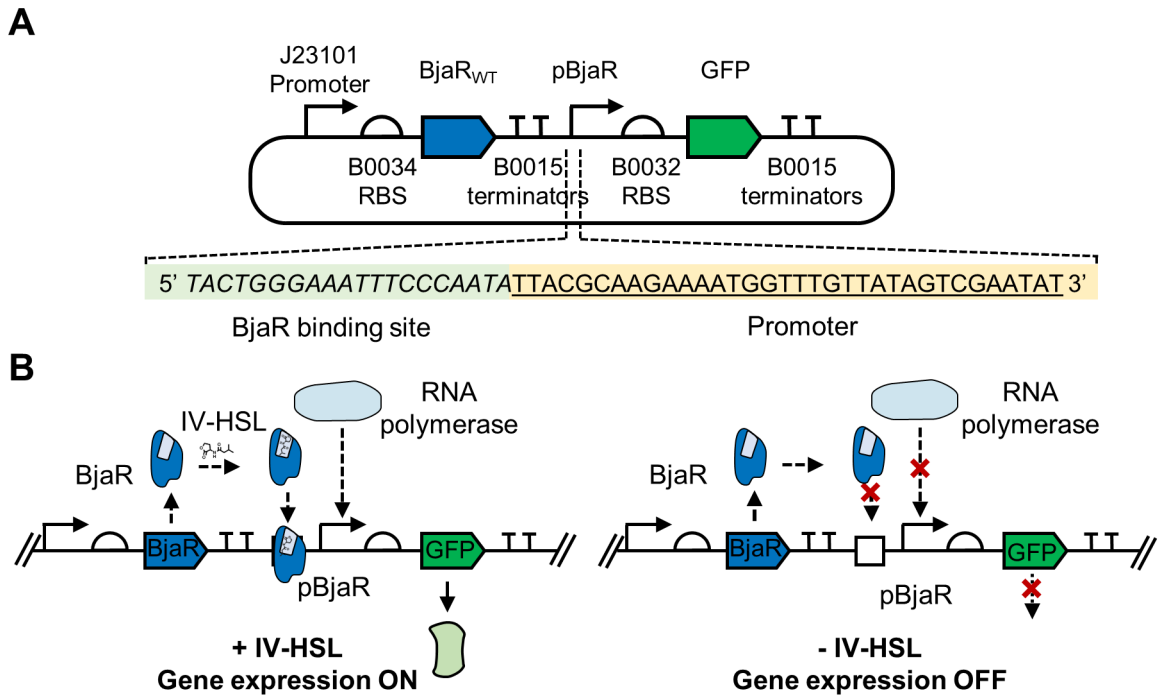


Figure 4.3: pSB1A3 BjaR GFP plasmid schematic
A) BjaR was expressed from a constitutively active *E. coli* promoter (J23101) and from strong RBS (B0034). GFP was expressed from a pBjaR promoter, created by placing the BjaR binding sequence downstream of a Lux-type promoter and a medium strength RBS (B0032). B) Upon binding IV-HSL, BjaR interacts with its consensus binding site upstream of the promoter recruits an *E. coli* RNA polymerase and activates gene expression (Left). In the absence of IV-HSL, BjaR does not interact with the consensus binding site, RNA polymerase alone cannot bind the promoter, and no gene expression occurs (Right).

This reporter plasmid was used in a previous study and achieved ∼5-fold activation of GFP expression upon addition of 10 μM of C4-HSL [186], but the cognate AHSL for BjaR, IV-HSL, was not tested [121]. IV-HSL should theoretically produce a much greater signal at lower AHSL concentrations. The ability of the receiver cells to detect IV-HSL and activate GFP expression was tested by growing the cells to an OD_{600} of 0.05 in M9 minimal media, seeding a 96-well plate containing serially diluted IV-HSL and measuring the fluorescence of cells after 4 hours.

Receiver cell GFP expression increased 3.4-fold between the OFF-state (absence of

IV-HSL) and the ON-state (presence of IV-HSL), with full GFP expression observed with μ10 nM IV-HSL (Figure 4.4). Hence, the BjaR reporter plasmid alone was sufficient to create a highly sensitive IV-HSL receiver cell (EC_{50} = 1.00 ± 0.11 nM), although the high background fluorescence and poor activation range of the receiver cells would be problematic, especially when comparing on and off states in microscopy images of SC to *E. coli* communication. To determine the source of the high basal GFP expression, a $BjaR_{KO}$ version of the reporter plasmid was prepared by truncating the BjaR protein ($BjaR_{1\text{-}12}$). Knocking out BjaR activity completely ablated GFP expression both in the absence and presence of IV-HSL (Figure 4.4A), and massively increased the growth rate of the bacteria due to the reduced cellular burden associated with BjaR and GFP expression (Figure 4.4B). Thus, the high basal GFP expression was due to leaky regulation of the pBjaR promoter by BjaR rather than the off-target activity of host transcription factors or recruitment of RNAP to the pBjaR promoter without transcription factors. To develop an efficient communication system using BjaR, receiver cells with a tighter OFF-state and/or higher ON-state GFP expression were required. To achieve this, BjaR was subjected to directed evolution.

4.3 Directed evolution of BjaR

The stringency of transcription factors involved in quorum sensing has previously been refined by directed evolution (subsection 4.1.3). Here, we adopted the approach described by Kimura and Umena *et al.* and utilised epPCR followed by ON-selection in the presence of IV-HSL and kanamycin, then outgrowth in the absence of IV-HSL and kanamycin to obtain BjaR mutants with a tighter OFF-state [202].

Random mutations were introduced across the entire length of the bjaR gene by

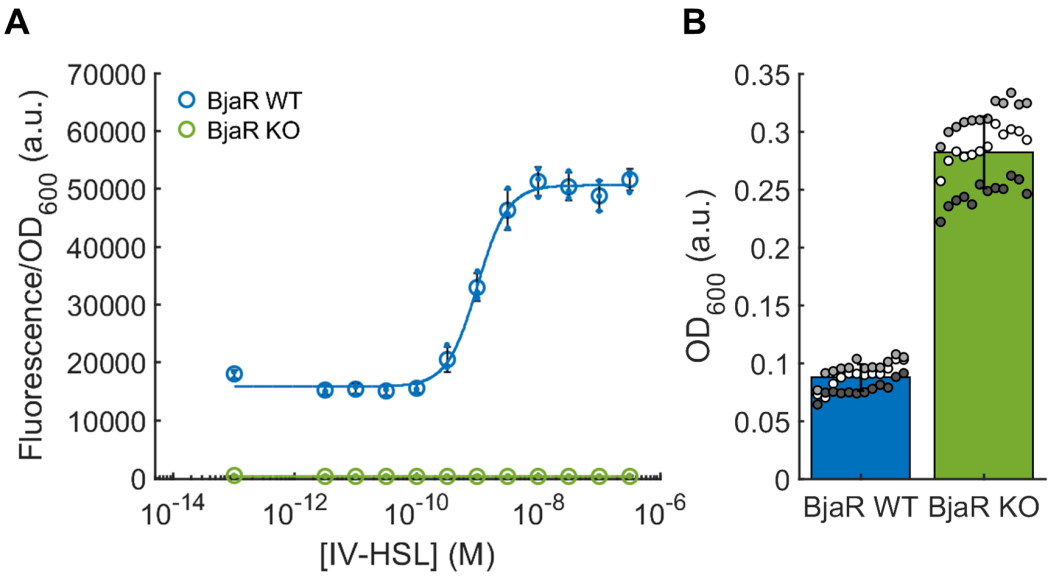


Figure 4.4: GFP expression vs IV-HSL concentration for $\mathbf{BjaR_{WT}}$ and $\mathbf{BjaR_{KO}}$ circuits
A) $BjaR_{WT}$ enabled up to 3.4-fold activation of GFP expression in response to synthetic IV-HSL. 10 nM IV-HSL was required for full GFP expression. (EC_{50} = 1 nM). By truncating BjaR and removing its transcription factor activity, no GFP was expression in the presence and absence of IV-HSL. B) $BjaR_{KO}$ receiver cells grew better than $BjaR_{WT}$ receiver cells due to the reduced cellular burden. Error bars, s.d. of three independent experiments ($n = 3$). Scatter plots represent individual cultures in a 96-well plate across the 3 experiments.

$MnCl_2$ spiked PCR using a Taq DNA polymerase. $MnCl_2$ and cycle number were capped at 100 μM and 30 cycles respectively to introduce ~1-2 mutations into each gene during each round of epPCR [202]. BjaR mutants obtained from epPCR were gel extracted and cloned into a modified BjaR reporter plasmid that contained both GFP and kanamycin resistance genes (KanR) downstream of the pBjaR promoter (Figure 4.5A).

GFP expression was used to score ON-state and OFF-state gene expression, while KanR was used for selection. ON-selection was performed in the presence of low concentrations of IV-HSL, which was decreased during each round of directed evolution (1 nM/0.8 nM/0.6 nM/0.4 nM for rounds 1-4 respectively), as well as a high concentration of kanamycin (200 μg/mL) to recover mutants that expressed significant amounts of GFP and kanamycin even at low IV-HSL concentrations. During ON-selection, cells that harboured non-functional BjaR mutants that had accumulated sufficient mutations to de-

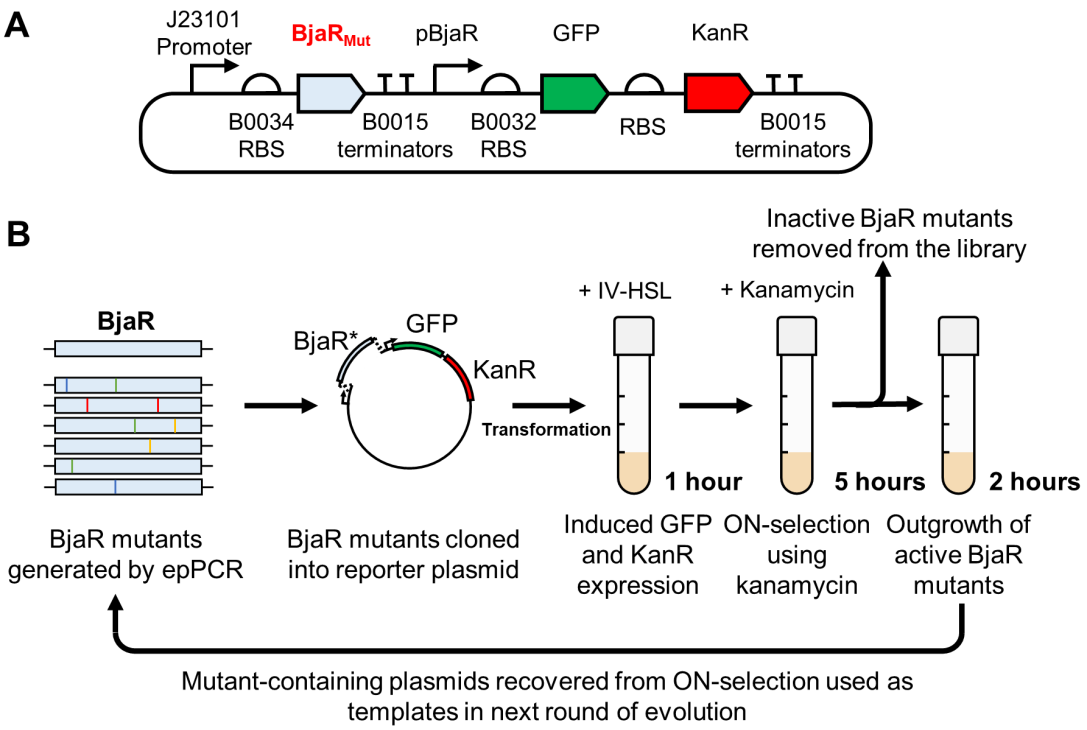


Figure 4.5: Directed evolution workflow
A) Plasmid used in directed evolution. Both GFP and KanR were placed downstream of pBjaR and transcribed as a bicistronic mRNA. B) The workflow used to direct the evolution of BjaR. Random mutations were introduced into the bjaR gene by epPCR. The bjaR gene library was cloned into a reporter plasmid containing both GFP and KanR downstream of the pBjaR promoter. Transformants were grown in liquid culture overnight, then used to seed new cultures. IV-HSL was added to induce GFP and KanR expression, then KanR expressing cells (those with functional BjaR) were recovered after ON-selection in kanamycin. After 5 hours, cells were washed and allowed to grow for 2 hours. Plasmids were extracted from the cells that remained and used as the DNA template for the next round of epPCR.

stroy its activity were removed from the library, while those that maintained the ability to regulate the pBjaR promoter and express sufficient KanR were recovered. Mutants recovered after ON-selection were grown in fresh media without IV-HSL and kanamycin to enrich the library with fast-growing cells with a lower cellular burden and, therefore, more tightly regulated pBjaR promoters. Plasmids from these cells were carried forward into the subsequent round of epPCR and ON-selection (Figure 4.5B). After 4 rounds of epPCR and ON-selection, 45 colonies from the BjaR mutant library were analysed by measuring GFP expression in the absence and presence of 1 nM IV-HSL. 40 mutants had an improved GFP expression activation range compared to BjaR$_{WT}$, with 14 of those

exhibiting an >25-fold activation range (Figure 4.6). The three best-performing mutants, #11, #28, and #36, were carried forward for further characterisation.

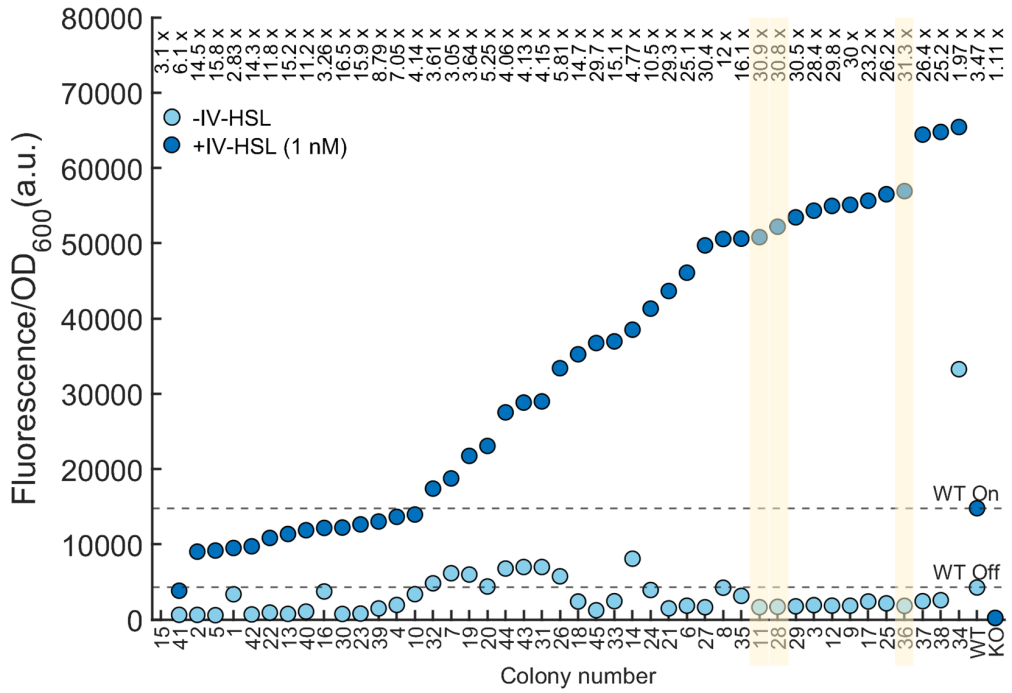


Figure 4.6: Screening BjaR mutants for improved performance
OFF-state vs ON-state GFP expression of 45 BjaR mutants recovered after 4 rounds of directed evolution, compared to $BjaR_{WT}$ and $BjaR_{KO}$ values. GFP expression was induced with 1 nM IV-HSL.

Sanger sequencing revealed all three top-performing mutants contained missense mutations at Met1 (ATG -> CTG; M1L) and Ser107 (AGC -> CGC; S107R) located at the translation start site and within the ligand-binding domain, respectively. After cloning $BjaR_{M1L\ S107R}$ back into the reporter plasmid backbone without KanR (Figure 4.7A), the resulting receiver cells demonstrated 89-fold activation of GFP expression granted by a 7.2-fold decrease in the OFF-state and a 3.6-fold increase in the ON-state. Receiver cells containing the mutant BjaR circuit were also more sensitive to IV-HSL than receiver cells using $BjaR_{WT}$ (EC_{50} $BjaR_{WT}$ = 1.00 ± 0.11 nM vs EC_{50} $BjaR_{M1L\ S107R}$ = 0.44 ± 0.04 nM) (Figure 4.7B).

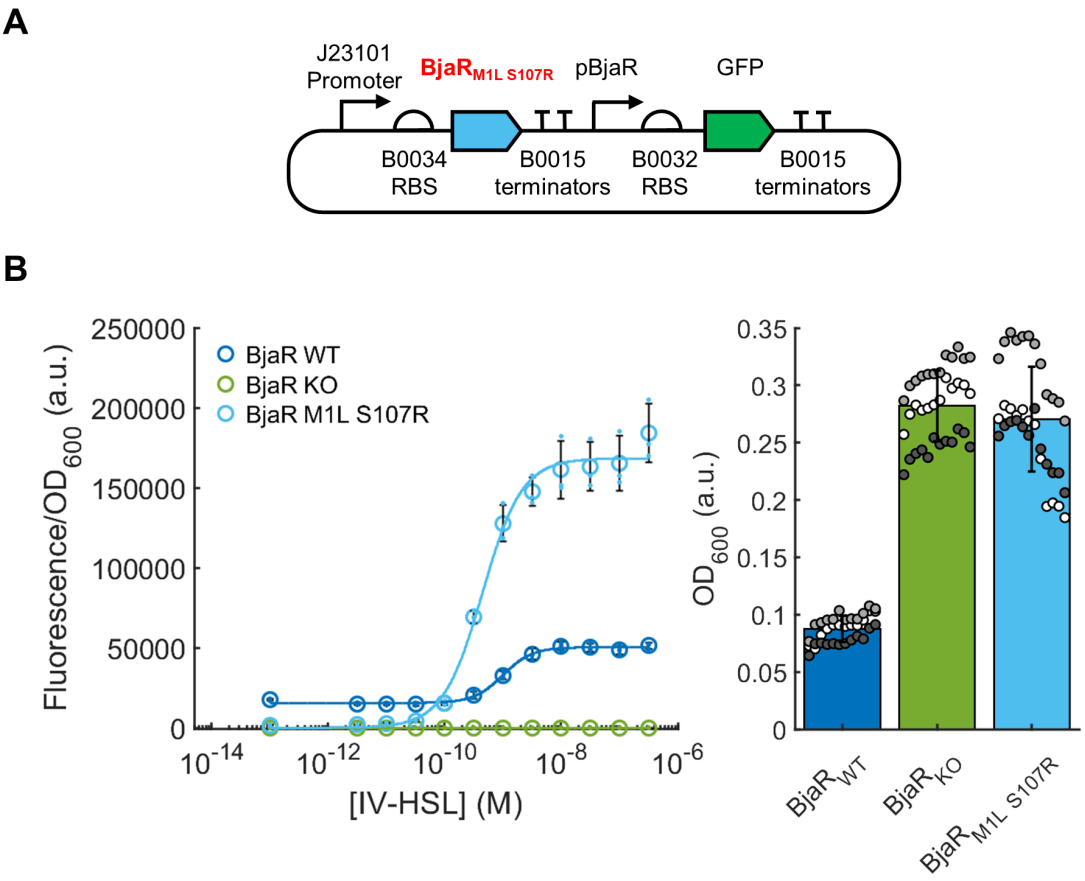


Figure 4.7: Characterisation of BjaR mutant
A) $BjaR_{M1L\ S107R}$ was cloned back into the reporter plasmid with only GFP downstream of the pBjaR promoter B) Dose-response curves of receiver cells containing $BjaR_{WT}$, $BjaR_{1\text{-}12}$, and $BjaR_{M1L\ S107R}$ expressing reporter plasmids. $BjaR_{M1L\ S107R}$ had a better ON-state, OFF-state, and sensitivity than the $BjaR_{WT}$ containing receiver cells. $BjaR_{M1L\ S107R}$ cells grew to a higher OD than BjaR $BjaR_{WT\ cells}$ indicating a lower cellular burden. Error bars, s.d. of three independent experiments ($n = 3$).

4.4 BjaR mutant characterisation

As the best performing mutants identified in the activity screen converged to the same combination of mutations, the decreased OFF-state GFP expression was unlikely due to the low activity of a destabilised, ligand-addicted BjaR variant. If this were the case, one would expect more mutations and greater diversity in the mutations present since perturbations in protein folding can be achieved with many different combinations of mutations [202]. Thus, the M1L and S107R mutations most likely improved the performance of the

BjaR gene circuit by other means. To understand the influence of each mutation, they were decoupled and studied separately.

In nature, ATG codons ubiquitously define the start of an open reading frame; the 30s ribosomal subunit and initiation factor 2 scan the mRNA sequence and place the AUG codon within the P site of the ribosome. AUG bases on the sense strand form complementary base pairs with a UAC anticodon present on a formylmethionine tRNA, and formylmethionine is introduced into the peptidyltransferase site of the 50s ribosomal subunit [48]. Translation initiation occurs in this manner for almost all *E. coli* genes, however, nature is not perfect, and there are instances in which naturally occurring genes use non-AUG start codons to initiate translation; for example, the gene encoding LacI begins with a GUG codon encoding valine [203]. The influence that alternative start codons have on protein translation has been studied in engineered systems by Marc Salit and colleagues, who mutated the initiation methionine codon of lacZ (AUG) to each of the other 64 possible codons and measured the effect this had on protein translation [204]. Unsurprisingly, the AUG methionine codon promoted the highest level of protein expression, an order magnitude higher than the next best start codon tested. The remaining 63 codons were still able to support lacZ expression, albeit at a much lower level. Interestingly, the level of lacZ expression observed from initiation codons identified in the BjaR mutants, the CUG codon encoding leucine, and ACG codon encoding threonine (AUG -> ACG was identified during preliminary experiments) ranked highly amongst the 64 codons in this study, but reduced lacZ expression 100-fold and 1000-fold respectively. Therefore, M1L was predicted to decrease the translation initiation rate of the BjaR protein.

To confirm this, BjaR expression level was decoupled from the identity of the initiation codon using RBSs with decreasing strengths (Figure 4.8A). The weakest RBS (B0033 – Relative strength 0.01) decreased the OFF-state and increased the ON-state GFP ex-

pression to a similar level observed with the BjaR$_{M1L}$ mutant, clearly indicating that the M1L mutation was responsible for decreasing protein expression, and the identity of the amino acid used merely dictated the translation initiation rate (Figure 4.8B). Placing the ACG start codon (M1T mutation) in the bjaR gene created receiver cells with an even better OFF-state (309-fold ON/OFF range) than with the B0033 RBS or ACG start codon, indicating that even lower BjaR expression can further improve the stringency of the pBjaR regulation. However, this came at the expense of reduced sensitivity (EC$_{50}$ BjaR$_{WT}$ = 3.9 ± 0.38 nM; EC$_{50}$ BjaR$_{M1L}$ (B0034) = 2.7 ± 0.57 nM; EC$_{50}$ BjaR$_{M1T}$ (B0034) = 22.3 ± 2.60 nM)(Figure 4.8B).

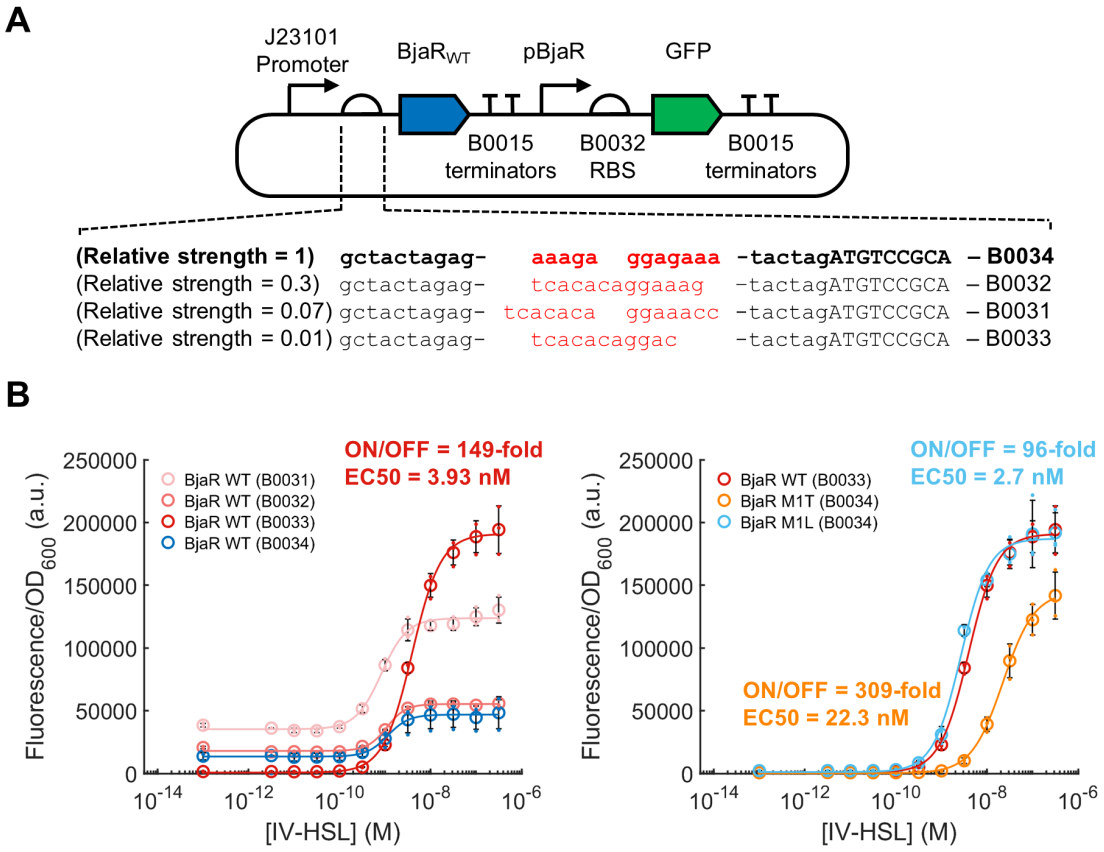


Figure 4.8: Lower BjaR expression improves gene circuit performance
A) Weak RBSs were introduced upstream of BjaR$_{WT}$ in place of the existing RBS (B0034). B) Varying the RBS strength influenced the dynamics of the BjaR gene circuit, and the weakest RBS (B0033) produced an identical response to the BjaR M1L construct. Cells with the BjaR M1T mutant plasmids had an even better ON/OFF ratio of GFP expression but were less sensitive to IV-HSL. Error bars, s.d. of three independent experiments (n = 3).

Next, the influence of the S107R mutation was elucidated by introducing this mutation back into the $BjaR_{WT}$ (B0033) plasmid by site-directed mutagenesis. The resulting reporter plasmid had a lower ON/OFF ratio compared to $BjaR_{WT}$ (B0033) (135-fold vs 149-fold) but was more sensitive to IV-HSL (EC_{50} $BjaR_{WT}$ (B0033) = 3.9 ± 0.38 nM vs EC_{50} $BjaR_{S107R}$ (B0033) = 0.63 ± 0.10 nM). Therefore, the S107R mutation improved the sensitivity of the reporter plasmid, but was unlikely to have dictated the changes in the ON or OFF states. As there is no experimentally obtained crystal structure available for BjaR, it is difficult to rationalise the mechanism of the S107R mutation, although based on its homology with lasR from *P. aeruginosa*, the Ser107 residue is believed to reside within the ligand-binding domain [118]. By substituting serine for arginine, a longer, charged side chain occupies the periphery of the substrate binding pocket and may form additional electrostatic with the lactone ring of IV-HSL.

The $BjaR_{S107R}$ mutant with the low strength B0033 RBS was equally as sensitive as the best performing mutant identified in the BjaR mutant library screen, $BjaR_{M1L\ S107R}$, (EC_{50} $BjaR_{S107R}$ (B0033) = 0.63 ± 0.10 nM vs EC_{50} $BjaR_{M1L\ S107R}$ (B0034) = 0.44 ± 0.04 nM) but had a 1.33-fold lower OFF-state and 1.15-fold higher ON-state, granting a 1.53-fold improvement in the activation range (134-fold ON/OFF ratio). Unless stated otherwise, the $BjaR_{S107R}$ (B0033) reporter plasmid was used in the subsequent work and will be referred to simply as BjaR*. The BjaR* reporter plasmid granted *E. coli* the ability to sense IV-HSL at picomolar concentrations, which is comparable with the concentrations sensed by the native host organism, *B. japonicum* [121].

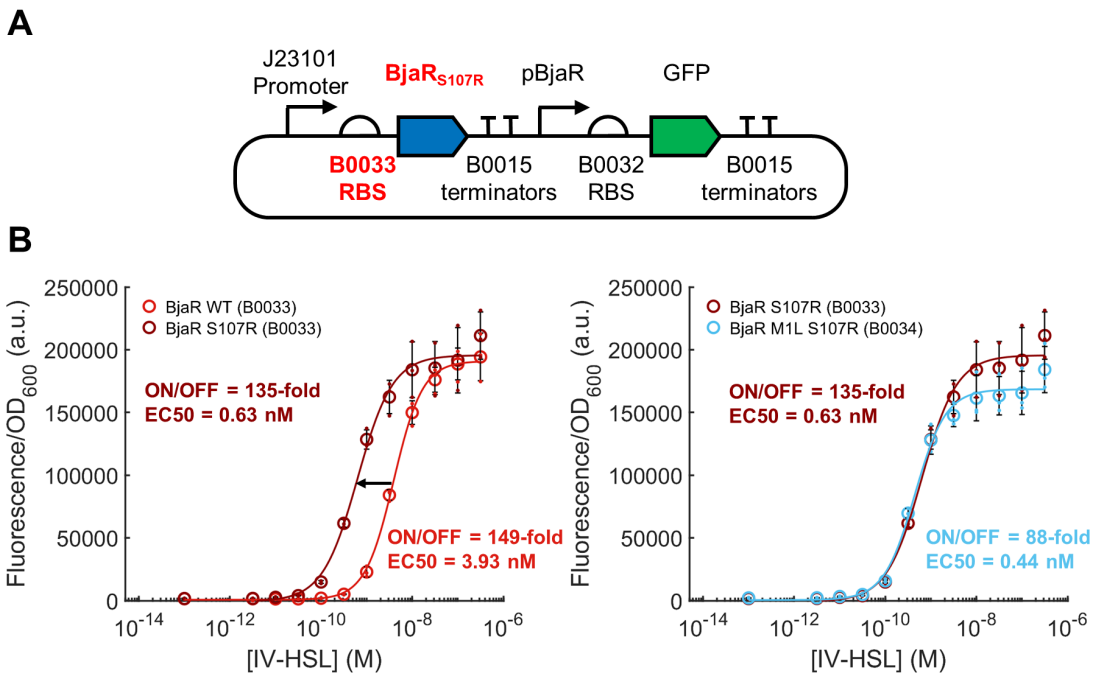


Figure 4.9: S107R mutation improved sensitivity of BjaR for IV-HSL
A) S107R was introduced into the BjaR $_{WT}$ reporter plasmid with the B0033 RBS. B) The S107R mutation massively improved the sensitivity of the BjaR gene circuit to IV-HSL but did not significantly change the ON and OFF state GFP expression levels (Left). The BjaR $_{S107R}$ (B0033) reporter plasmid expressed more GFP in the presence of IV-HSL than the BjaR$_{M1L\ S107R}$ (B0034) mutant (Right). Error bars, s.d. of three independent experiments ($n = 3$).

4.5 Assembly of IV-HSL producing synthetic cells

With a platform to detect IV-HSL in place, attention turned to constructing SCs that could synthesise IV-HSL. In *B. japonicum* QS, IV-HSL is synthesised by BjaI from SAM and IV-CoA (Figure 4.10A). SAM and IV-CoA are relatively large (398.44 g.mol^{-1} and 851.65 g.mol^{-1}), charged molecules that are impermeable to lipid bilayers, while IV-HSL is a smaller (185.22 g.mol^{-1}), more hydrophobic molecule that is membrane-permeable. By reconstituting this reaction *in vitro*, BjaI-expressing SCs containing SAM and IV-CoA should be able to synthesise IV-HSL *in situ* and release IV-HSL across the membrane without the need for a protein pore (Figure 4.10A).

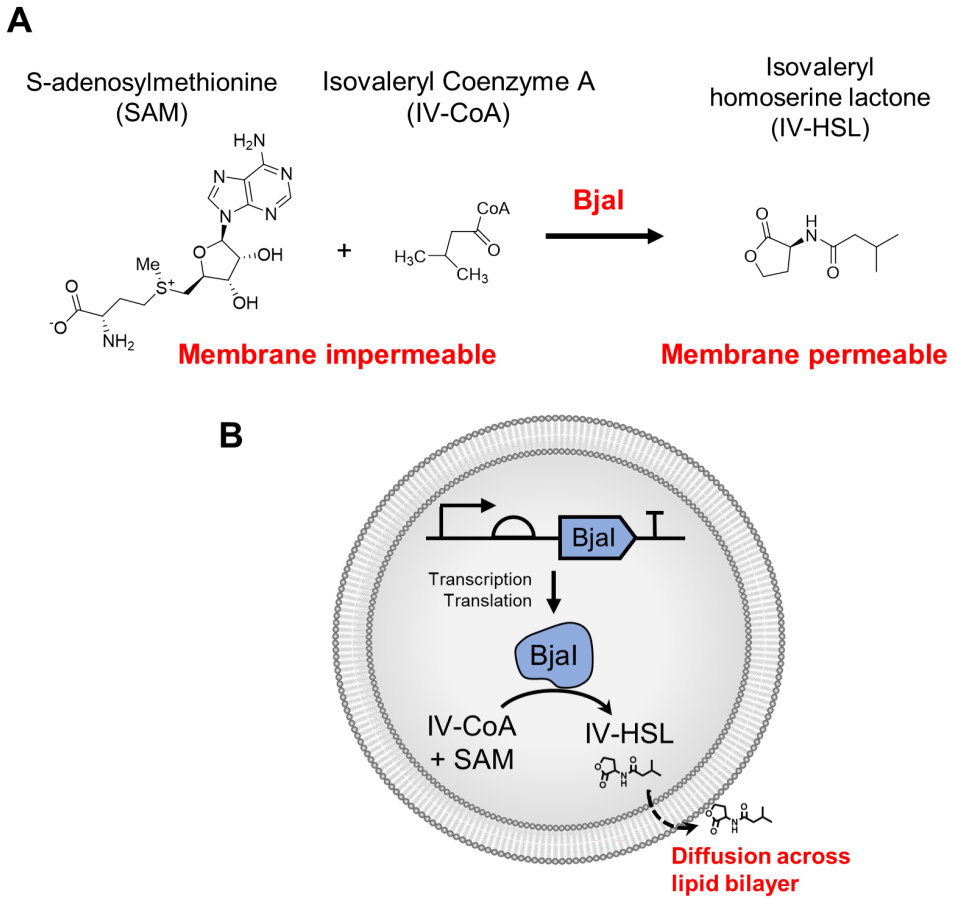


Figure 4.10: IV-HSL synthesis by synthetic cells
A) Biosynthesis of IV-HSL from IV-CoA and SAM. B) BjaI is expressed inside SCs and synthesises IV-HSL from SAM and IV-CoA encapsulated inside the compartment. IV-HSL diffuses across the lipid bilayer into the surrounding environment.

The bjaI gene was synthesised by polymerase chain assembly [205]. During this process, overlapping 60 nt oligonucleotides that collectively encoded the entire bjaI gene were annealed and extended in an untemplated PCR reaction, then the fully assembled gene product was amplified from the pool of extended oligos in a second PCR reaction using amplification primers (Figure 4.11). After inserting bjaI in the PURExpress control template plasmid backbone, downstream of a T7 promoter, linear DNA templates were prepared, and BjaI expression was tested in bulk IVTT reactions with PURExpress containing radiolabelled ^{35}S-methionine.

Autoradiographs of the CFPS reactions confirmed BjaI was successfully expressed from the linear DNA templates, and its expression was not perturbed by SAM and IV-

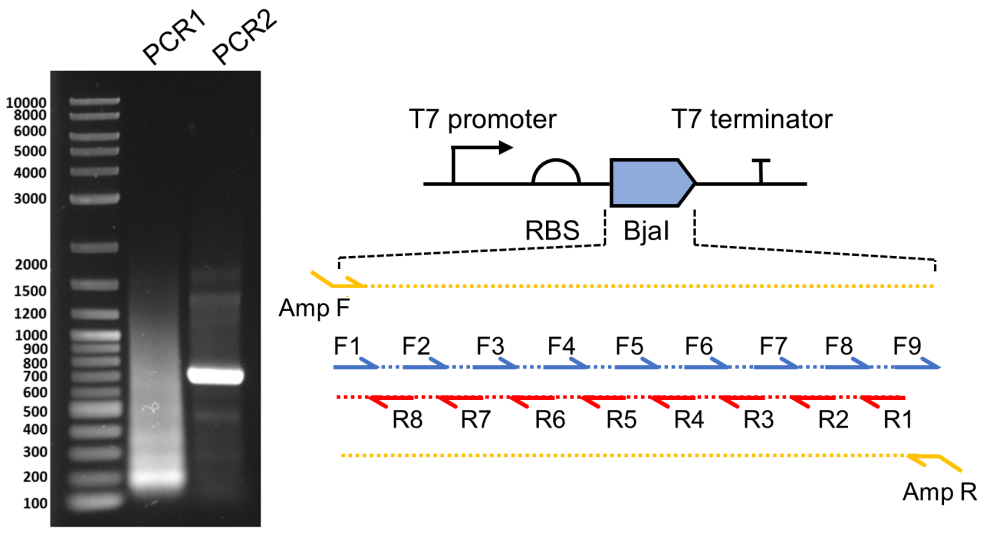


Figure 4.11: bjaI gene synthesis and cell-free expression
During PCR1, oligos encoding bjaI were pooled, annealed, and elongated into products of varying length. The full length bjaI gene was selectively amplified during PCR2 using amplification primers designed at either end of the desired construct.

CoA (Figure 4.12A). To determine whether BjaI expressed *in vitro* was enzymatically active, aliquots of BjaI IVTT reactions performed in the presence of 80 μM IV-CoA and 300 μM SAM were added to BjaR reporter cells ($BjaR_{M1L\ S107R}$) at OD_{600} = 0.05 and incubated for 4 hours. Reactions containing substrates but with no DNA present did not produce IV-HSL, so GFP was not expressed by the receiver cells, whereas reactions with both substrates and bjaI DNA produced sufficient IV-HSL to fully activate GFP expression (BjaR $_{M1L\ S107R}$ cells). The BjaI CFPS reactions were serially diluted until the output was within the linear range of the receiver cell dose-response curve, and the BjaI reactions were estimated to have produced IV-HSL to a final concentration of $\sim$17.8 $\pm$ 2.6 μM (Figure 4.12B).

When this system was transferring inside GUVs, IV-HSL was also successfully produced by the BjaI-expressing SCs. SCs samples were incubated separately from the BjaR recever cells for 5 hours, then combined and incubated for a further 4 hours. The IV-HSL produced was sufficient to fully activated GFP expression, however, the total IV-HSL present was the sum of that passively release across the lipid bilayer, and that released

when the SCs were added to the cell cultures and inevitably ruptured due to the osmotic imbalance between the inner solution and the media. Overall, the SCs sample had a IV-HSL concentration of ∼458.5 ± 119.6 nM (Figure 4.12C).

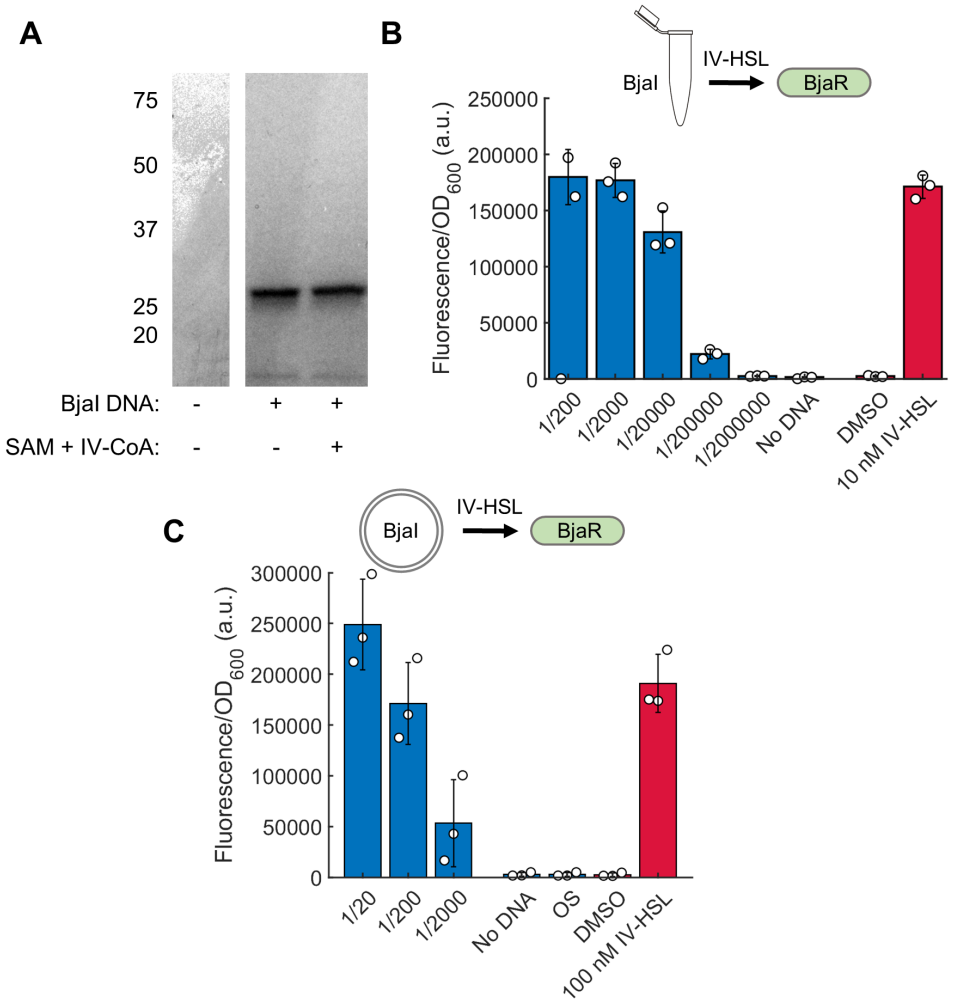


Figure 4.12: Cell-free BjaI expression and IV-HSL biosynthesis
A) Autoradiograph of ^{35}S-Methionine labelled CFPS reactions. Full-length BjaI (25 kDa) was successfully expressed, and expression was not affected by IV-CoA or SAM. B) Cell-free expressed BjaI synthesised IV-HSL that was able to fully activate GFP expression in BjaR receiver cells ($BjaR_{M1L\ S107R}$). ∼18 μM IV-HSL was present in the final CFPS reaction. C) BjaI was expressed inside GUVs containing 300 μM SAM and 80 μM IV-CoA. BjaI-expressing SCs synthesised IV-HSL, and fully activated GFP expression in BjaR receiver cells ($BjaR_{S107R}$ (B0033))although it was not possible to establish whether this had crossed the lipid membrane or been released when the SCs ruptured. ∼460 nM IV-HSL was present in the SC sample. Error bars, s.d. of three independent experiments ($n = 3$).

Up to now, SCs have been incubated in an isotonic outer solution containing just HEPES, potassium glutamate, and glucose. However, SCs must be transferred into a

more physiologically relevant environment if they are to be interfaced with living cells. The main barrier to accomplishing this is the significant difference in osmolarity between the SC inner solution and the media used to grow cells. The osmolarity of the inner solution necessary for BjaI expression and IV-HSL biosynthesis (∼1100 mOsm) far exceeded the osmolarity of the M9 minimal media (∼300 mOsm). Hence, if SCs with this composition were to be placed in M9 media, the massive influx of water would rupture the membrane. To resolve this, the osmolarity of the inner solution needed to be decreased in line with the cell media. One strategy that was considered involved preparing a homemade CFPS system with lower osmolarity buffers by assembling the One-Pot PURE system [61].

Ribosomes were successfully isolated from *E. coli* A19 cells, and an energy solution containing the small molecule components for CFPS was assembled. Both of these worked in the context of an otherwise complete PURE system, i.e. mNG was synthesised when the homemade energy solution was combined with the PURExpress ribosome and protein mix (SolB), and when homemade ribosomes were combined with the PURExpress energy solution and protein mix (SolB Δribosomes) (Figure 4.13A). However, the homemade Onepot PURE protein mix did not support protein synthesis when combined with the PURExpress energy solution and PURExpress ribosomes (Figure 4.13A right), since proteins were noticeably absent (Figure 4.13B). The proteins in question, including the phenylalanine tRNA synthetase and release factor 3, were encoded on pQE expression plasmids and held in M15 cells, whereas the proteins that successfully expressed tended to be encoded on pET21a vectors and held in BL21 DE3 cells. It may be the case that regulatory regions within these plasmids, e.g. promoter regions, were mutated to reduce the burden on cells.

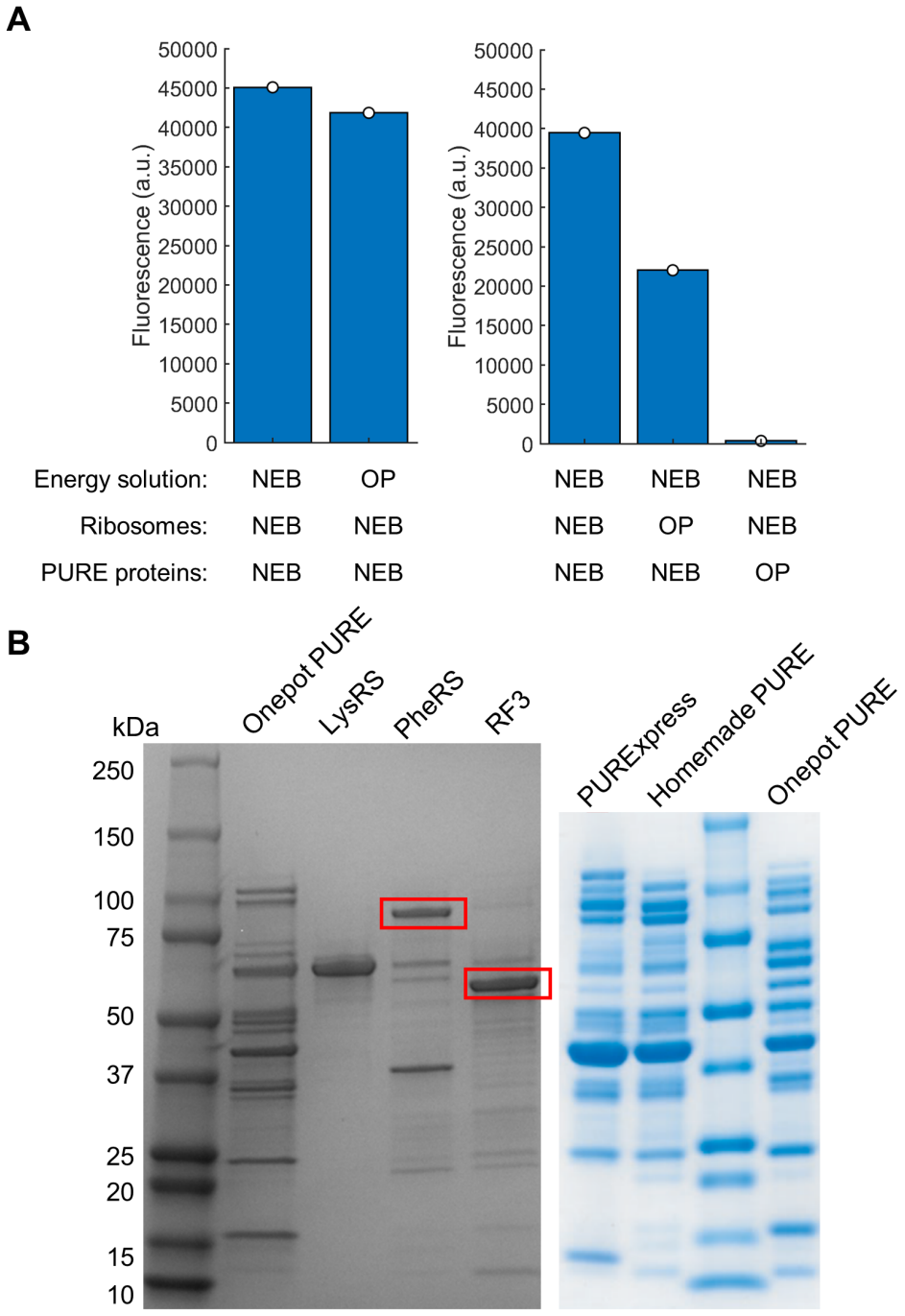


Figure 4.13: Assembling the One-Pot PURE system
A) The homemade energy solution and isolated ribosomes were able to support CFPS in conjunction with the commercial PURExpress kit, but the homemade PURE proteins did not. B) Multiple proteins, such as the phenylalanine tRNA synthetase and release factor 3 (Red boxes), were absent from the PURE protein mix prepared via the one-pot purification step. These proteins were obtained at low yields and were relatively impure even when expressed and purified individually. NEB = PURExpress kit component; OP = Onepot PURE system component.

Consequently, attention instead turned to reducing the osmolarity of the commercial PURExpress system. Murine RNAse inhibitor was omitted from the inner solution due to high amount glycerol in the storage buffer, sucrose concentration was reduced from 200 mM to 50 mM, TR dextran was removed (unless required for imaging experiments), and the PURExpress solution was diluted using 10 mM HEPES pH 7.6. According to the manufacturer, PURExpress can tolerate dilution of up to 20% with only a slight reduction in the protein synthesis yields. Since BjaI is an enzyme and works catalytically, IV-HSL could still be synthesised even if minimal amounts of enzyme were expressed. The ability of diluted PURExpress to express BjaI and synthesise IV-HSL was determined via the GFP expression of $BjaR_{M1L\ S107R}$ reporter cells. Bulk CFPS reactions diluted down to 40% their normal working concentration, and SCs containing 50% PURExpress still expressed BjaI and IV-HSL yields were only slightly impacted (Figure 4.14).

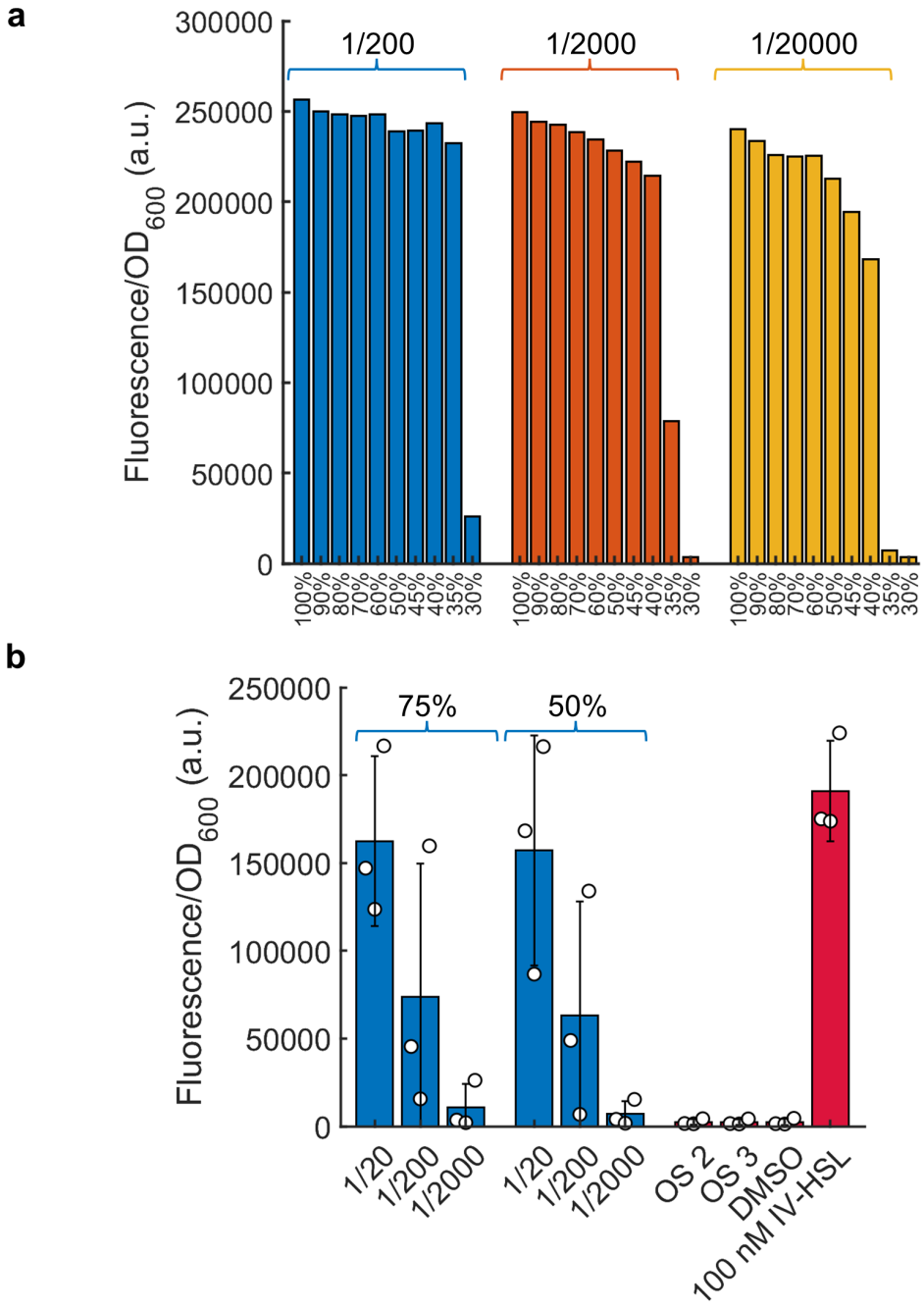


Figure 4.14: IV-HSL biosynthesis by BjaI expressed in diluted PURExpress
A) BjaI was expressed using PURExpress at 100% working concentration to 30% working concentration, then diluted to 1/200 to 1/20000 in BjaR* cells. IV-HSL biosynthesis was only slightly perturbed when PURExpress was diluted down to 35% of its normal working concentration. B) BjaI was expressed inside GUVs containing 75% or 50%, and synthesised IV-HSL to ~32.5 ± 13.6 nM. Error bars, s.d. of three independent experiments ($n = 3$).

4.6 Synthetic cell to living cell communication

As the end goal of this work was to pattern communication between LA-SCs and *E. coli*, the sender SCs and receiver bacteria both needed to be immobilised to detect the resulting patterns. We envisioned that this could be achieved by embedding BjaI-expressing SCs inside agarose containing M9 minimal media and then placing BjaR-expressing receiver cells inside or on top of agarose pads. In this way, cells would be near the SCs, light could easily penetrate the agarose pads, and spatially patterned SC activation should directly relate to spatially patterned SC to living cell communication.

Agarose pads were prepared as illustrated in figure 4.15A. ULGP agarose was dissolved in M9 minimal media to 1.5% (w/v) and then maintained at 25 °C to keep it molten yet slightly viscous. Molten agarose was then added inside a gene frame attached to a clean microscope slide as another clean microscope slide was slid on top (the protective film was still attached to the gene frame at this point). The microscope slides were then left in the fridge for 1 hour to gel the agarose. After 1 hour, the non-adhered microscope slide was carefully slid from the top of the gene frame to reveal the 250 μm thin agarose pad. SCs or synthetic IV-HSL were included at the molten agarose step where necessary.

SCs prepared with 50% PURExpress, 50 mM sucrose, and labelled with 25 μM TR-Dextran were introduced into M9 agarose pads and incubated for at least 16 hours at 37 °C . There was no observable decrease in the number of vesicles present and no increase in background fluorescence due to the rupture of the vesicles and release of TR-Dextran, indicating the SCs were remarkably stable inside M9 agarose pads despite the difference in osmolarity (Figure 4.15B).

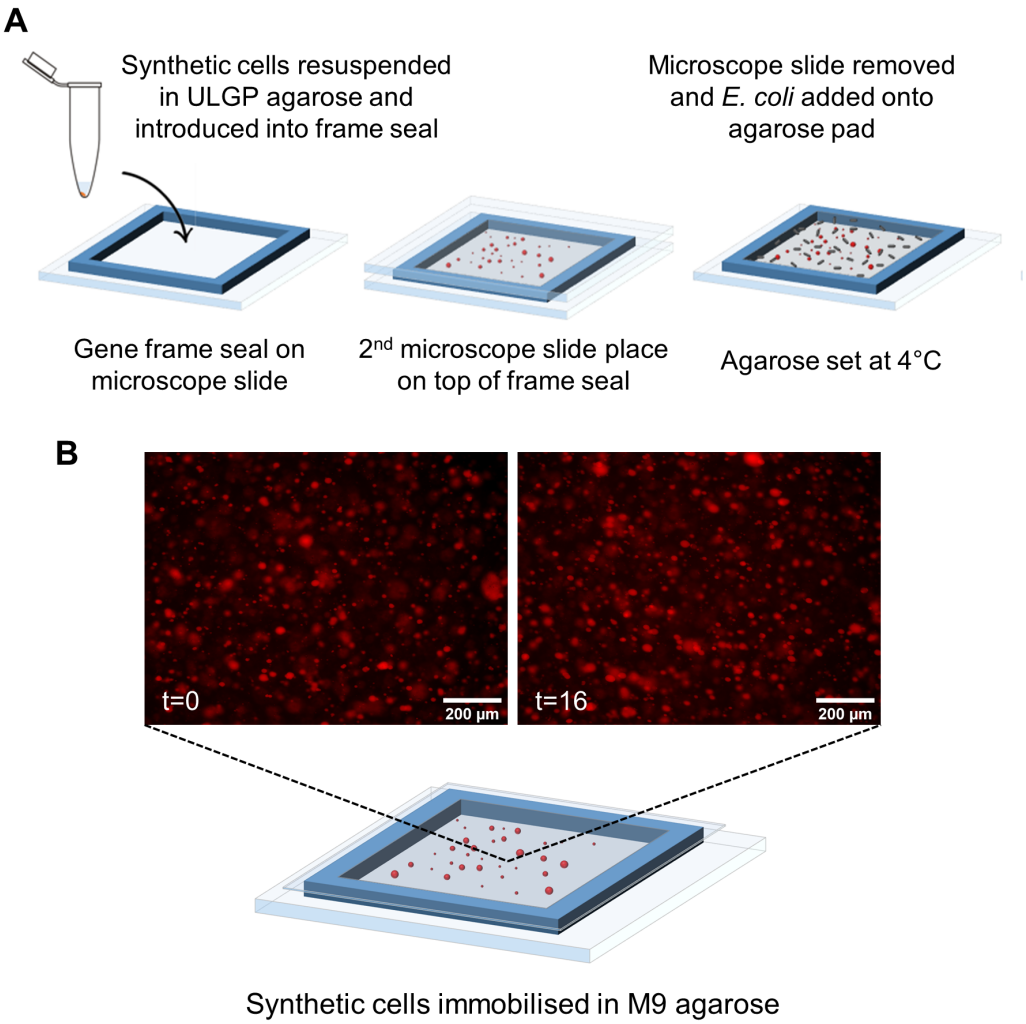


Figure 4.15: Synthetic cell laden agarose pads
A) SCs were resuspended in ULGP agarose containing M9 media and gelled between 2 microscope slides separated by a 250 μm spacer. The agarose pads had dimensions 1 cm x 1 cm x 250 μm. B) SCs were stable in M9 agarose after 16 hours at 37 °C

Subsequently, BjaR* receiver cells were grown on top of BjaI-expressing SC-laden M9 agarose to determine if IV-HSL was produced and released across the membranes. If SC to *E. coli* communication was successful, the microcolonies on top of the agarose should express GFP. Indeed, similar levels of GFP fluorescent BjaR* cells were observed when the cells were grown on M9 agarose containing 10 nM IV-HSL and BjaI-expressing SCs. No GFP expressing cells were observed in the absence of synthetic IV-HSL, or when the SCs contained no DNA (Figure 4.16). This confirmed that IV-HSL produced inside the SCs diffused across the membrane, and SCs communicated with the *E. coli* cells.

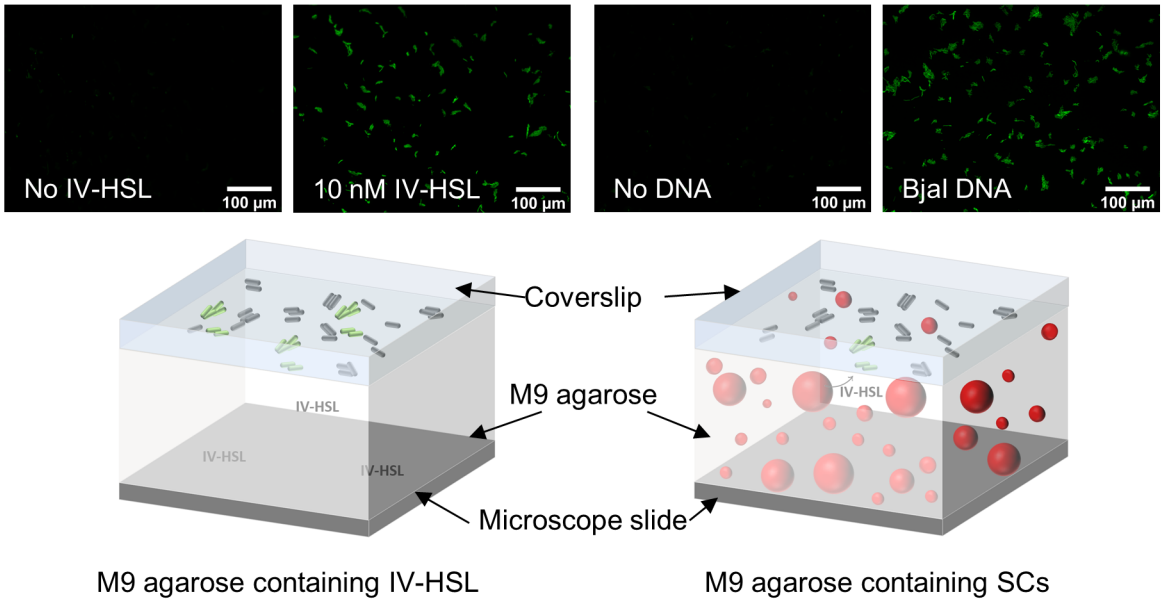


Figure 4.16: Synthetic cell to living cell communication
GFP expression was observed in BjaR* cells grown on M9 agarose pads containing 10 nM IV-HSL and BjaI-expressing SCs, but not M9 agarose with no IV-HSL or SCs containing no DNA template

Finally, LA-SCs expressing BjaI were entrapped within the M9 agarose pads to control where IV-HSL synthesis occurred. In the absence of UV light, or the absence of DNA there were no fluorescent colonies observed on the agarose pad. Conversely, fluorescent *E. coli* cells were observed when LA-SC laden agarose pads were irradiated with UV light. Patterned communication was attempted using the patterned structures indicated in section 3.5, and more gross structures whereby half of the sample was irradiated and half protected from the light. However, the membrane-permeable nature of IV-HSL meant it not only freely diffused out of the SCs but also passed into and out of the *E. coli* cells (Figure 4.17).

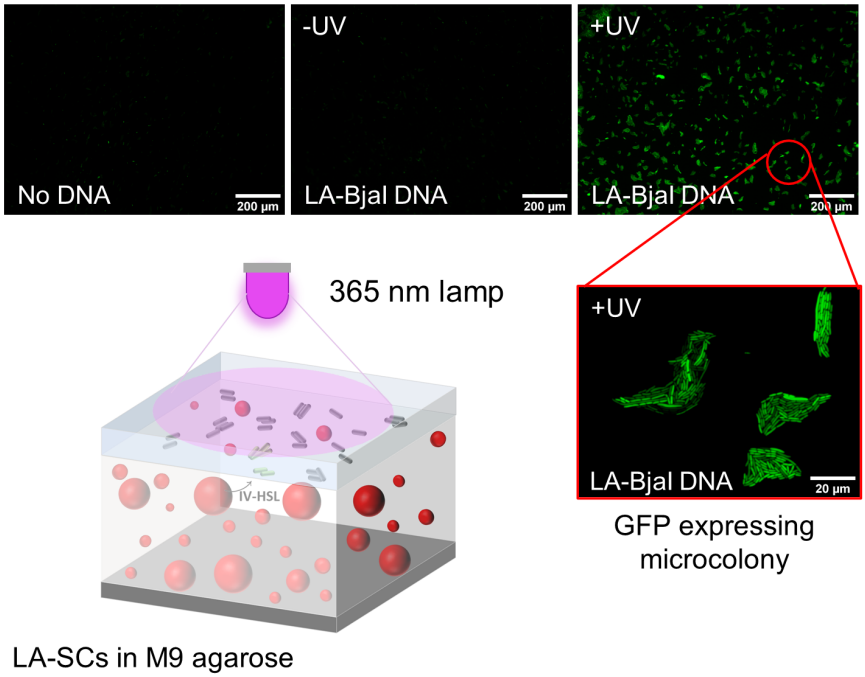


Figure 4.17: Light-activated synthetic cell communication
UV light activated BjaI expression and IV-HSL synthesis. IV-HSL diffused out of the intact SCs and into the M9 agarose, triggering GFP expression in the receiver cells grown on top of the agarose pad. In the absence of UV light or BjaI DNA template, no IV-HSL was synthesised and the receiver *E. coli cells* did not express GFP.

.

5

Dual input activation of synthetic cells

5.1 Introduction

5.1.1 Riboswitches in synthetic cells

Riboswitches are cis-acting regulatory RNA motifs that can be found in the 5' UTRs of certain genes to regulate their expression [206]. They're comprised of an aptamer, a secondary structure RNA that recognises a specific ligand, and a downstream segment of

RNA termed the expression platform, which contains either a transcription terminator or RBS and initiator AUG codon depending on whether the riboswitch regulates transcription or translation, respectively. In transcriptional riboswitches, bases that form part of the terminator helix are sequestered within an RNA hairpin adjacent to the aptamer. Binding of the ligand to the aptamer is coupled with a reconfiguration of the riboswitch and the formation of new WCF base pairs with the RNA sequence previously held within the hairpin. Consequently, the bases required for terminator formation are exposed, the terminator forms, and transcription elongation is halted. Translational riboswitches, on the other hand, achieve the inverse role. In the absence of ligand, an RBS and AUG codon are sequestered within a stem-hairpin loop, which prevents a ribosome from initiating translation. When a ligand binds at the aptamer site, the hairpin structure is again reconfigured, an RBS and AUG codon is released, and translation initiation ensues.

Transcriptional and translational riboswitches are both ancient mechanisms of directly regulating gene expression according to the concentrations of important cellular metabolites, such as SAM, lysine, and adenine [207]. While these riboswitches were identified in bacteria, *in vitro* evolution and selection of novel aptamers has also enabled synthetic riboswitches to be constructed against specific targets for which there are no known naturally occurring riboswitches. In this way, translational riboswitches that recognise theophylline and histamine have been created, but the theoretical pool of potential riboswitches is incredibly diverse and limited only by our ability to evolve functional aptamers [77, 78].

Since theophylline and histamine are both membrane-permeable small molecules and riboswitches are easily incorporated into DNA templates, they offer a simple control mechanism for SCs; the molecules traverse the lipid bilayer, reconfigure the riboswitch, and activate CFPS in the lumen of vesicles. However, their performance in CFPS has varied

greatly. Despite its popularity [66, 67, 208] the theophylline riboswitch (Variant 12.1) [75] has only shown up to ∼8-fold activation of cell-free mYPet expression [208], and a 2.8-ON/OFF ratio for the release of small molecules from vesicles via *in situ* αHL expression, even though the same switch achieved 95-fold activation of lacZ expression in *E. coli* [75]. Conversely, the histamine-responsive H2 riboswitch has demonstrated up to 30.9-fold activation of mCherry expression and up to ∼8-fold ON/OFF ratio for dye release via αHL expression in the presence of 5 mM histamine [79].

5.1.2 Chapter overview

This chapter explores how CFPS can be controlled with multiple inputs by introducing separate modes of regulating transcription and translation into a single DNA template. By placing a GOI downstream of an LA-T7 promoter and an H2 riboswitch, transcription was activated in response to light, and translation was activated in response to histamine. This represents an exciting route towards creating externally controlled SCs that can also sense environmental cues.

5.2 Controlling CFPS with translational riboswitches

Riboswitches that respond to theophylline and histamine have successfully been used to control CFPS in SCs [66, 67, 79]. However, theophylline lacks physiological relevance and theophylline riboswitches used *in vitro* were leaky ,and achieved only slight increases in cell-free gene expression. Consequently, the H2 histamine riboswitch was selected to control the translation of a downstream GOI.

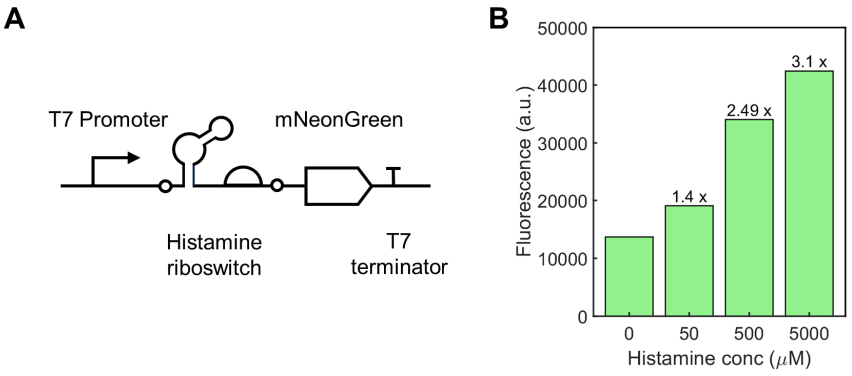
The histamine riboswitch sequence was placed within the 5' UTR of mNG encoding DNA templates, immediately downstream of the bases required to form the LA-T7 pro-

moter (Figure 5.1A). mNG expression from these linear DNA templates was tested in the absence and presence of increasing concentrations of histamine dichloride. mNG was expressed in a dose-dependent manner, and fluorescence output increased 1.4/2.49/3.1-fold in the presence of 50 μM, 500 μM, and 5 mM histamine, respectively (Figure 5.1B). This was much lower than the 30.9-fold range in mCherry expression that was reported in the literature, primarily due to the high level of background mNG expression in the absence of histamine [79]. There are several reasons why this could be the case.

First, differences between the CFPS used (PURExpress in this work vs PUREfrex 3.0 in the literature) such a buffer composition, pH, and ribosome concentration can affect base pairing within the riboswitch and the rate of translation initiation. This was the case when an S30 lysate was used instead of PUREfrex; the activation range for mCherry expression decreased from a 30.9-fold to 10.8-fold [79]. In addition to this, the presence of cryptic RBSs within the gene sequence could give rise to truncated (but still fluorescent) proteins that contribute to the high background. Expression of these ORFs would be insensitive to histamine. Alternatively, the mNG gene sequence itself could perturb proper riboswitch folding and RBS sequestration if the sequence of the early ORF is complementary to the aptamer or leader sequences.

To determine the cause of the high background fluorescence, the mNG gene sequence was first inspected for cryptic RBSs. There were 12 in-frame methionine residues within the mNG protein (including the initiation methionine in the riboswitch leader sequence) from which translation could initiate, but only 4 existed before the GYG tri-peptide that forms the chromophore and could initiate translation of a fluorescent protein. As indicated in section 4.4, other amino acids could be used to initiate translation, at least *in vitro*, although these were not considered as the background signal would be much lower than that observed in Figure 5.1B. The sequences of the 20 bases immediately upstream of each

methionine were compared against the anti-Shine Dalgarno (anti-SD) sequence within the 16s rRNA to determine the extent of base complementarity. Of the 3 alternative methionine candidates located at amino acid positions 10, 19, and 41, complementary bases pairs could form between each of the upstream sequences and the anti-SD sequence. The highest complementarity occurred between the bases upstream of Met 19; 6 base pairs could form in total, 4 of which were contiguous and located 5 nt upstream of the AUG codon (Figure 5.1C). The number of complementary WCF base pairs and their distance from the AUG start codon should be sufficient to constitute a weak RBS (RBSs B0032 (Relative strength 0.3) from section 4.4 also had 4 bp complementarity with the anti-SD and was located 7 bp from the AUG). Therefore, a truncated but still fluorescent mNG product could be translated at low levels from an RBS other than that sequester by the riboswitch [209, 210]. This is consistent with Figure 3.6C; multiple proteins around the correct MW were produced in mNG CFPS reactions.



C

	Base pairing with anti-SD
Met1 (Riboswitch leader)	5′-UCGAAU**UAAGGAGGU**AAAAA**AUG**-3′ 3′-AUUCCUCCACUAG-5′
Met10	5′-UCGACCUGCUGGAUCCAAAC**AUG**-3′ 3′-AUUCCUCCACUAG-5′
Met19	5′-GCAAAGGCGAAGAGGAUAAU**AUG**-3′ 3′-AUUCCUCCACUAG-5′
Met41	5′-UUAACGGCGUGGAUUUUGAU**AUG**-3′ 3′-AUUCCUCCACUAG-5′

Figure 5.1: Histamine-responsive expression of mNeonGreen
A) DNA templates used to regulate gene expression with histamine. B) mNG expression was activated with as little at 50 μM histamine, but fluorescence output was highest with 5 mM histamine. C) WCF base pairs that could form between the anti-SD sequence and bases immediately upstream of various mNG methionine codons.

Consequently, genes encoding different fluorescent proteins, sfGFP, mYPet, mVenus, and mCherry, were cloned downstream of the riboswitch to identify a reporter construct with lower background fluorescence. Templates encoding mVenus, mYPet, and sfGFP all had a lower off-state expression than mNG. When the reporter protein fluorescence was measured using their optimal literature excitation and emission wavelengths (see methods), DNA encoding mYPet had the lowest off-state relative to its on-state and achieved a 12.8-fold increase in fluorescence output in the presence of 5 mM histamine compared to in the absence of histamine (Figure 5.2A). When fluorescence output from each protein was measured using conditions that represented the fluorescence microscope GFP channel (Ex: 470 nm; Em: 525 nm, Bandwidth: 20 nm), mVenus had the lowest absolute off-state fluorescence, but also had a poor on-state. mYPet still had a good off-state and the highest on/off ratio (10.6-fold) (Figure 5.2B). mCherry expression observed in these experiments was very different from that reported in the literature (3.88-fold range vs 30.9-fold range (PUREfrex) or 10.8-fold range (S30 lysate)), however, the mCherry gene sequences were drastically different and very low mCherry yields were achieved even in the presence of 5 mM histamine, indicating general issues in its expression.

Next, histamine-responsive mYPet expression was tested inside GUVs. The GUVs used here had a different membrane composition to the previous chapters to match the composition used in the literature - POPC:Cholesterol (1:2) [79]. The method described in section 2.4 was amended slightly to account for the different lipid composition, namely, formation of w/o droplets of the desired size required more forceful emulsification, and centrifugation speeds were reduced as this was found to improve yields of recovered vesicles.

mYPet expression was analysed in the absence of histamine (-/-), with histamine present in the outer solution only (-/+), and with histamine present in both the inner

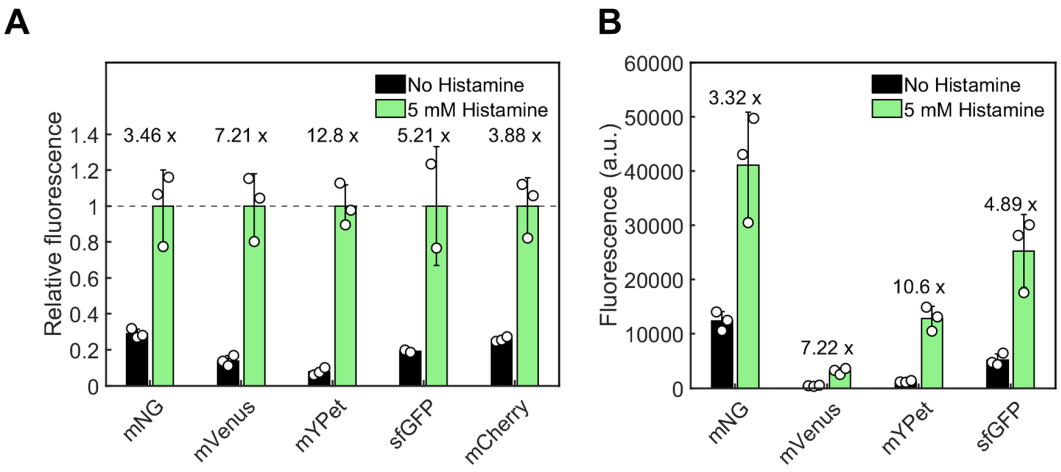


Figure 5.2: Histamine-responsive expression of fluorescent proteins
Placing different genes downstream of the riboswitch resulted in different fold changes in gene expression. mYPet expression was upregulated by histamine the most when fluorescence was measured with optimal Ex/Em wavelengths (A) (12.6-fold increase), and fluorescence microscope wavelengths (B) (10.8-fold increase). Error bars, s.d. of three independent experiments ($n = 3$).

solution and outer solution (+/+). Unsurprisingly, mYPet expression was highest when histamine was provided both internally and externally as this bypassed the need for histamine to cross the membrane, and higher internal histamine concentrations could be achieved. mYPet expression was, however, observed when histamine was provided in the external solution only and was higher than observed in vesicles that were not exposed to histamine; these samples reflected the no DNA control sample (Figure 5.3A, Figure 5.3B). mYPet was not expressed in all vesicles. The highest yields were observed inside the larger vesicles that formed (Figure 5.3C). Overall, this confirmed that histamine could enter SCs by diffusing across the lipid bilayer, and the internal concentrations were sufficient to trigger measurable mYPet expression.

5.3 Controlling CFPS with light and histamine

To regulate the expression of mYPet with both light and histamine, a LA-T7 promoter was installed into the pPURE-histribo-mYPet templates as described in 3.1. In these

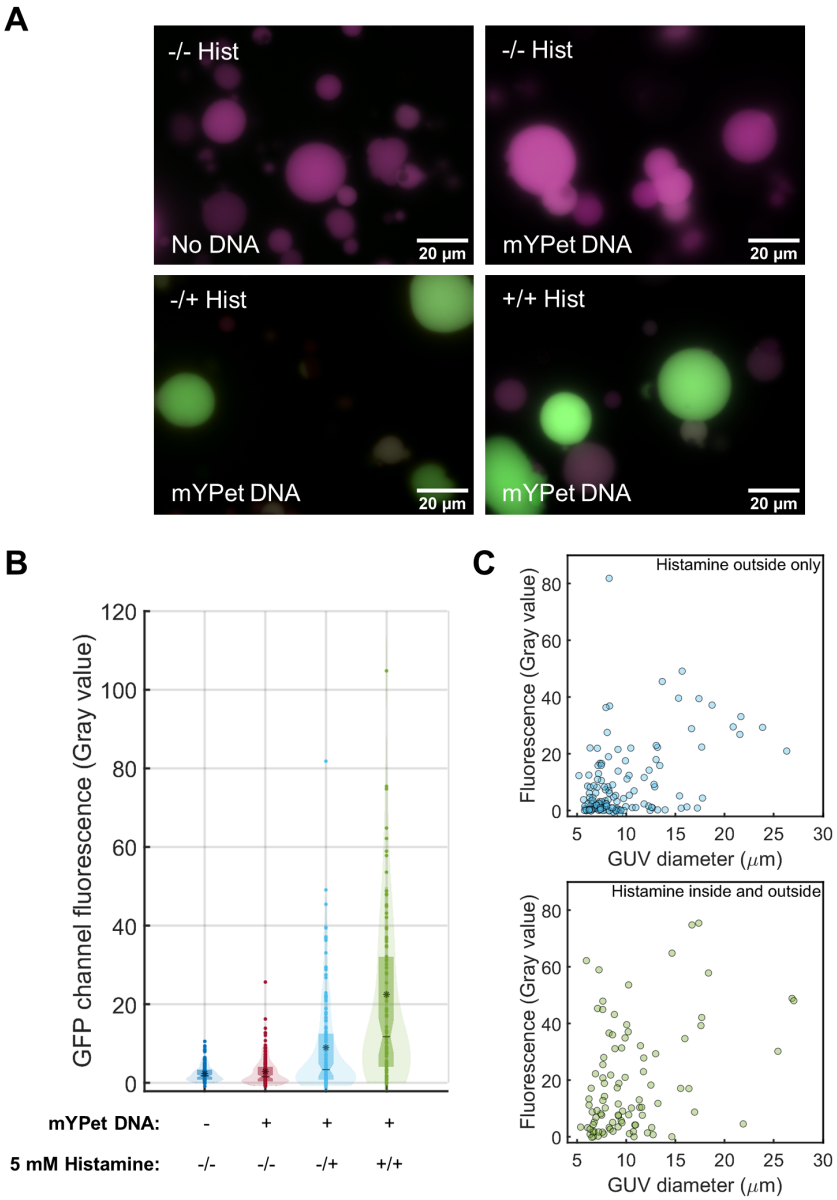


Figure 5.3: Histamine-responsive mYPet expression in GUVs
A) mYPet expression was observed inside GUVs when histamine was added to the outside of vesicles (-/+) or provided both inner and outer solutions (+/+), but not in the absence of histamine (-/-), or a DNA template. B) Image analysis of mYPet expression in vesicles across the different conditions. C) When histamine was only provided in the outer solution, mYPet expression was greatest in the larger vesicles. mYPet expression was but more evenly distributed across vesicles of all sizes when histamine was provided both inside and outside of the vesicles.

dual input DNA templates, light acted as a master regulator, and histamine tuned the expression level. A Boolean 'AND' gate was demonstrated using LA-mYPet-hist ribo linear DNA templates. In the absence of light and histamine, transcription was tightly repressed and any mRNA that was produced was translated at a low level since the RBS

was sequestered by the riboswitch. In the presence of 5 mM histamine and absence of light, mYPet expression remained low as the T7 promoter was still tightly repressed by the photocleavable blockade and minimal mRNA was transcribed. After irradiating the reactions with UV light for 3 minutes, but still in the absence of histamine, mYPet mRNA was transcribed, but the RBS was sequestered within the riboswitch and little mNG was translated. Finally, when both light and histamine were provided, mYPet was expressed at a much higher level from the exposed RBS (376-fold activation compared to samples that were exposed to neither stimulus) (Figure 5.4).

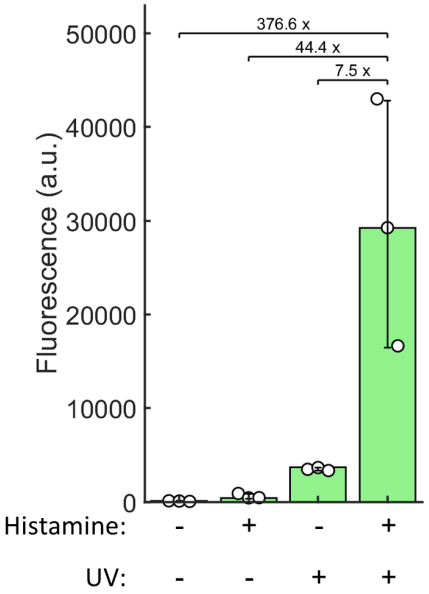


Figure 5.4: Dual input activation of mYPet expression
mYPet expression was tightly repressed in the absence of UV light. Expression increased slghtly after UV light was applied, but full expression was only restored when histamine was also present. The large error bar for the +/+ condition is due to combine variability of LA-T7 promoter uncaging and histamine riboswitch dynamics. Error bars, s.d. of three independent experiments ($n = 3$).

6

Conclusion and future directions

Gene-expressing synthetic cells (SCs) are an incredibly inspired technology that has the potential to disrupt multiple fields, such as diagnostics and drug delivery, and also represents a strong foundation in the pursuit of creating life from scratch. However, SCs are still very much in their infancy. To date, SCs researchers have recycled the same parts to perform simple functions in a highly-controlled lab environment. As soon as SCs are introduced into the body or held under physiologically relevant conditions, many of these functions become redundant, and many additional problems begin to emerge. These include, but are by no means limited to, the drastic difference in osmolarity between the inside of a SC and the outside environment, and the exertion of mechanical forces on the

membranes within the crowded *in vivo* environment; both of these cases could lead to ruptured membranes. Hence, much progress is needed until the true promise of SCs is realised. The work presented here intended to make strides in this direction and build towards SCs that can be used outside a test tube and controlled in a user-defined way.

In this thesis, SCs were assembled by encapsulating a cell-free protein synthesis system (CFPS) inside GUVs, and programmed according to encapsulated DNA templates. Initially, SCs were designed to constitutively express a fluorescent protein, mNeonGreen (mNG), from simple, linear DNA templates (chapter 2). chapter 3 expanded on this platform, and introduced chemically modified light-activated DNA (LA-DNA) templates into the SCs to regulate *in situ* gene expression with UV light. Targeted irradiation with UV light enabled gene expression inside subsets of the LA-SCs to be activated in a spatially controlled manner, demonstrating precise and user-defined control over when and where the SCs were activated. While these proof of concept experiments were limited to mNG expression, more complex, physiologically relevant functions were also demonstrated. In chapter 4, SCs were interfaced with living cells using a quorum sensing system. An AHSL synthetase, BjaI, was expressed inside GUVs to synthesise N-isovaleryl-L-homoserine lactone (IV-HSL) from simple precursors, which was subsequently released and activated reporter gene expression in *E. coli* receiver cells. Furthermore, in chapter 5, SCs were instilled with the ability to sense histamine by including a histamine-sensitive riboswitch into the DNA templates. Light and histamine-responsive gene expression was subsequently demonstrated, highlighting the possibility of creating remotely-activated SCs that vary their behaviours according to their environmental context. Beyond the milestones highlighted in this work, LA-SCs still require further development to become versatile and useful tools. A few easily achievable improvements, plus the future applications of this technology are suggested below.

The LA-DNA presented here contained UV-sensitive 2-nitrobenzyl moieties in their photocleavable biotin (PCB) groups. UV light is cytotoxic and can trigger dimerisation of adjacent pyrimidines within a DNA strand, which introduce mutations into the genome during DNA replication if left undetected. To avoid this, mild doses of UV irradiation (365 nm at 0.75 mW for 3 (Bulk) or 10 minutes (Vesicles)) were used to stimulate photocleavage of the LA-DNA. This seemed to be tolerated by the *E. coli* cells and was sufficient to recover the expression of mNG or BjaI; however, the UV light did perturb CFPS at low DNA concentrations (5 ng/μL). Owing to the modular nature of the photocleavable biotin (PCB) group, LA-DNA constructs could be activated by red-shifted wavelengths of light by simply replacing the light-sensitive group. For example, if the 2-nitrobenzyl group was replaced with a coumarin-based group, LA-DNA might be activated more biocompatible blue or green light [83]. Moreover, the generation of a diverse library of LA-DNAs that are photocleaved with distinct wavelengths of light would also open up avenues to multiplexing optogenetic gene control; a single gene could be placed under the control of two separate wavelengths of light, or different genes could be placed under the control of different wavelengths of light.

While attempting to create the Onepot PURE system in chapter 4, it became apparent that diluted PURExpress could be used to form GUVs that were stable in M9 media and still synthesised IV-HSL. This work-around was sufficient to satisfy our overall end goal, SC to living cell communication, however, the BjaR* cells engaging in this communication were incredibly sensitive to IV-HSL. If this same strategy were applied to the expression of other proteins, the SCs might fall short of their intended function. Consequently, the second immediately serviceable improvement required for this work is the generation of CFPS systems that are osmotically balanced with various physiological buffers/growth media but still achieve high expression yields. This has been eluded to

previously [74], and allowed SCs to exert greater influence over the biological system of interest.

Should both of these advances be achieved, SCs could immediately be deployed in more complex scenarios to manipulate biological systems in meaningful ways. For example, we foresee that LA-SCs could be used to control the delivery of therapeutically active biomolecules. *In vitro*, this might find use in creating user-controlled morphogen gradients for tissue engineering effort; light would control both the location and concentration of the small molecule produced. Meanwhile, LA-SCs applied *in vivo* could deliver drugs, proteins, or signalling molecules to specific targets within the body. Specifically, in the context of the work discussed in chapter 5, we see dual input SCs as ideal platforms for drug delivery. Light-activated expression of a pore protein might enable bioactive small molecules to be released, and the extent of the release could be tuned according to its environment and proximity to the target site via second level of transcription or translation regulation (Figure 6.1A). Taking this a step further, the expression of an enzyme tasked with synthesizing the molecule, or protein toxin, could be placed under the control of light, but this would only be released when a second criterion is met, which triggers pore expression or breakdown of the SC membrane.

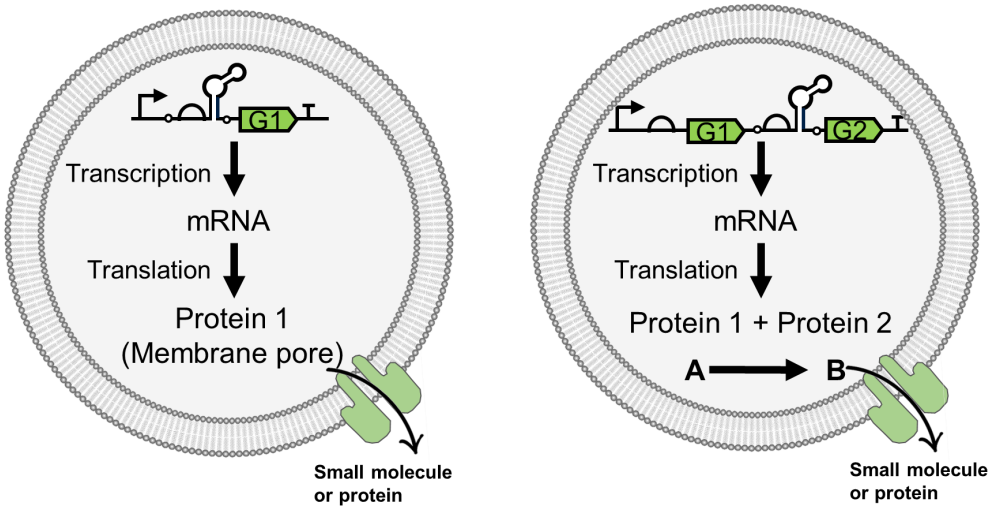


Figure 6.1: Small molecule delivery with synthetic cells
Targeted release (Left) or targeted production and release (Right) of small molecules from synthetic cells might find application in drug delivery or manipulating cell behaviours.

.

7

Methods

7.1 Materials

All solvents and reagents were purchased from Sigma/Merck unless stated otherwise. NHS-PCB-Biotin was purchased from Ambergen and stored in dry DMF. PURExpress was purchased from New England Biolabs NEB. All enzymes were purchased from New England Biolabs, unless stated otherwise. Standard DNA oligonucleotides were synthesized by Integrated DNA Technologies. Amine-modified DNA oligonucleotides were synthesized by ATD-Bio. Egg PC and POPC were purchased from Avanti Polar Lipids. Geneframes were

purchased from Thermofisher. The 1 mm diamond drill bit was purchased from Eternal tools. DNA encoding the histamine H2 riboswitch and mYPet gene were synthesized by IDT as gBlocks. pMAT-mNeonGreen was synthesised by GeneArt. Monovalent streptavidin was a gift from Prof Mark Howarth (University of Oxford). pSB1A3 BjaR-GFP was a gift from Prof. Karmella Haynes (Arizona State University). pGRG25-Pmax-sfGFP was a gift from Prof Kevin Foster (University of Oxford). OnePot PURE plasmids were a gift from Prof. Florian Hollfelder (University of Cambridge).

7.2 General methods

The following methods were used consistently throughout each of the chapters. They are written in full here and then referred in each respective chapter when used.

7.2.1 Homologous recombination

50 ng of vector DNA was mixed with insert DNA at a 1:3 mol/mol ratio and added to 10 μL *E. coli* XL10-Gold cells in a 14 mL RB Falcon tube. Cells were incubated on ice for 20 minutes, heated to 42 °C for 30 seconds, then placed back on ice for 1 minute. 500 μL SOC media was added to each tube and incubated at 37 °C, 225 rpm for 45 mins. 200 μL of cells were spread onto LB + Ampicillin (100 μg/mL) agar plates with glass beads and the plates were incubated at 37 °C for ∼14 hours. Transformants were picked with pipette tips and used to inoculate 5 mL LB media + (100 μg/mL) ampicillin in 50 mL falcon tubes; lids were loosely applied. Cells were incubated at 37 °C, 225 rpm for ∼16 hours. 3 mL of overnight culture was centrifuged at 14,000 x g for 1 minute and plasmids were extracted from the cell pellets using a PUREyield mini prep kit. Plasmid sequences were verified by Sanger sequencing.

7.2.2 Preparation of linear DNA templates

Linear DNA templates were obtained by PCR of pPURE-based plasmids encoding the desired GOI. PCRs were performed with Phusion DNA polymerase mastermix using 1 ng plasmid and 500 nM T7 e.long/Rev CT 2 primers. Reactions were cycled according to the following programme: 98 °C 30s, 35 cycles of [98 °C 10 s, 54 °C for 20 s and 72 °C for 30 s], 72 °C 5 minutes, 4 °C HOLD. PCR products were purified using QIAquick PCR purification kits – 2 x 50 μL of elution buffer were used to recover as much DNA as possible from the spin columns. Linear DNA templates were then ethanol precipitated and resuspended in TE buffer or Milli-Q H_2O to 75 ng/μL.

7.2.3 Ethanol precipitation

DNA samples were mixed with 1/10 volumes of 3 M Ammonium acetate (pH 5.2) in a 1.5 mL centrifuge tube and vortexed until well mixed. 3 volumes of ice cold 99% ethanol were added, and the samples were vortexed again. Samples were incubated at -80 °C for >1 hour, or at -20 °C overnight. Tubes were centrifuged at 16,000 x g, 4 °C for 30 minutes to pellet the precipitated DNA and the ethanol was carefully removed as to not disturb the DNA pellet. 500 μL of ice cold 70% ethanol was added to the DNA pellet and tubes were centrifuged at 16,000 x g, 4 °C for another 15 minutes. All the ethanol was carefully removed, and tubes containing the DNA pellet were centrifuged under vacuum for 10 minutes using a speed vac to remove residual ethanol. Dry DNA pellets were were resuspended in Milli-Q H_2O to a final concentration of 75 ng/μL.

7.2.4 DNA quantification

dsDNA concentrations were determined with the dsDNA setting on a Nanophotometer (Implen). PCB-modified oligonucleotide concentrations were determined using the beer-lambert law via its A260 (measured on a Nanophotometer) and its extinction coefficient (371900 $L.mol^{-1}.cm^{-1}$).

7.3 Chapter 2 methods

7.3.1 Plasmid construction

pPURE-mNG was prepared by introducing the mNG gene into the PURExpress control template plasmid, downstream of the T7 promoter, by restriction digest/ligation cloning. The mNG gene was amplified by PCR using Phusion DNA polymerase mastermix containing 1 ng pMAT mNeongreen plasmid and 500 nM T7 e.long/Rev CT 2 primers. Reactions were cycled with the following programme: 98 °C 30 s, 35 cycles of [98 °C 10 s, 59 °C for 20 s and 72 °C for 45 s], 72 °C 10 minutes, 4 °C HOLD. 1 μg of PCR product and PURExpress control template plasmid were digested with XbaI/BamHI-HF for 1 hour at 37 °C and then electrophoresed on a 1.2% TAE agarose gel prestained with 3% GelRed at 100 V for 1 hour. Bands for the double digested DNA were cut from the gel with a scalpel and purified from the gel using QIAquick gel extraction purification kit. The mNG gene insert was ligated into the plasmid backbone using T4 DNA ligase (3:1 insert:vector ratio) and 2 μL of ligation was transformed into 10 μL XL10 Gold *E. coli* cells by heat shock. Cells were incubated in 500 μL SOC media for 45 minutes, then 100 μL was plated onto LB agar containing 100 μg/mL ampicillin. Plates were incubated at 37 °C for ∼14 hours. Colonies were picked with pipette tips and grown as 5 mL liquid cultures in LB +

ampicillin (100 ug/mL) at 37 °C, 225 rpm, overnight. Plasmids were harvested from 3 mL overnight culture using a QIAprep spin mini-prep kit and verified by Sanger sequencing with primers T7 e.long and Rev CT2.

7.3.2 Linear DNA templates

Linear DNA templates of pPURE-mNG were prepared as described in subsection 7.2.2.

7.3.3 Cell-free protein synthesis

3 μL IVTT reactions were prepared with 1X PURExpress and supplemented with 0.8 U/μL Murine RNase inhibitor. Final linear DNA template concentration was 5 ng/μL. Sucrose and TexasRed-Dextran were added to reactions at 200 mM and 25 μM where indicated. Reactions were incubated in a thermal cycler at 37 °C for 4 hours, then held at 4 °C for at least 15 minutes. Reactions were worked up with 47 μL PBS and transferred to 384-well black, flat bottom, optiplates and fluorescence was measured using a Tecan Infinite M1000 fluorescence plate reader. Plates were shaken at 306 rpm for 10 seconds to ensure the samples reached the bottom of the well and measured with the following settings: Ex = 506 nm; Em = 517 nm; Bandwidth = 5 nm; Z-position = 23179 μm; Gain = 130.

7.3.4 Formation of GUVs

Glass vials were cleaned with isopropanol and then held under vacuum for > 1 hour. Egg PC dissolved in chloroform (50 mg/mL) was transferred to a 2 mL glass vial (Supelco), then chloroform was added up to ∼200 μL. Chloroform was evaporate under gentle N_2 flow while the vials were held at 45°and rotated gently to distribute lipids evenly up the

walls of the vial, but below the height corresponding with the volume of oil to be added. Vials containing lipid films were held under vacuum in a desiccator for >2 hours to remove residual chloroform. Mineral oil (filtered through 0.22 μm PES membrane) was added to Egg PC films, by mass, to a final concentration of 2 mg/mL Egg PC. Vials were vortexed for 1 minute, then incubated in a heat block at 80 °C for 10 minutes with the lids removed. Lids were reapplied to vials and sealed tightly using Teflon tape and parafilm, then the vials were sonicated in a sonication bath heated to 50 °C for 1 hour. Lipid containing oil was stored at room temperature overnight and sonicated for 10 mins at room temperature immediately before use.

250 μL of 2 mg/mL Egg PC in mineral oil was transferred to 1.5 mL centrifuge tubes and placed on ice. 3 μL inner solution (PURExpress containing 10 mM 5,6-Carboxyfluorescein and 200 mM sucrose, or PURExpress containing 5 ng/μL linear mNG DNA template, 0.8 U/μL Murine, 25 μM TR-Dextran and 200 mM sucrose) was added into the chilled lipid-containing oil ensuring the tip was constantly moved through the lipid-containing oil to disperse the inner solution. Tubes were passed across a centrifuge rack 3-5 times using light pressure to form cloudy W/O emulsions that were place on ice for ∼5 minutes. Meanwhile, 100 μL of lipid-containing-oil was layered on top of 250 μL of chilled outer solution (50 mM HEPES, 400 mM potassium glutamate, 200 mM glucose (pH 7.6)) and place at room temperature. W/O emulsions were then added on top of this oil phase, and this tube was placed on ice for ∼5 minutes. Centrifuge tubes containing the W/O emulsion above outer solution were centrifuged at 16,000 x g, 4 °C, for 30 minutes.

After centrifugation the oil phase should be clear, although white sediment will exist at the interface, and a hazy pellet should be present at the bottom of the tube. The oil phase and ∼200 μL of outer solution was removed from the tube and discarded. By gently ejecting ∼10 μL of the outer solution against the wall of the tube, the intact GUV pellet

was displaced, aspirated into the pipette tip, and transferred to a new tube containing 250 μL outer solution. Any remaining vesicles from the tube were recovered by pipetting up and down and transferring around $\sim$30 μL of the remaining outer solution to the new tube. The pellet was broken down by gently pipetting up and down using a fresh 200 μL pipette tip. Vesicles were centrifuged at 10,000 x g, 4 °C for 10 minutes. All outer solution was removed and the pellets were gently resuspended in 25 μL of fresh outer solution. Care was taken to avoid adding buffer to oil deposits on the walls of the tube. Resuspended vesicles were loaded into imaging chambers and incubated in a 37 °C oven for 2-8 hours, coverslip side down.

7.3.5 Imaging chambers

1 mm holes were drilled through 25 mm x 75 mm microscope slides using a 1 mm diamond toolbit and Dremel 3000 rotary tool to correspond with diagonal corners of 25 μL gene frames (Figure 2.4). All slides and coverslips (22 mm x 22 mm) were cleaned with 2% decon, isopronaol and Milli-Q H_2O, then sonicated in Milli-Q H_2O for at least 10 minutes and dried under N_2 flow before use. Coverslips were O_2 plasma treated for 5 minutes, before 25 μL gene frames were attached. 0.1% BSA in PBS was added inside the gene frames and incubated at room temperature for 15 minutes. BSA was removed and coverslips were washed with outer solution, twice. Outer solution was removed and gene frames were applied to the drilled microscope slides. 25 μL of samples were introduced through the drilled holes and then the holes were sealed with double sided tape. Samples were incubated coverslip side down.

7.3.6 Epifluorescence microscopy

Samples held inside imaging chambers were imaged with a Lecia DMi8 e inverted epifluorescence microscope using an 100x oil immersion objective lens. GUVs were imaged using the brightfield, TXR, and GFP filter settings.

7.3.7 Image processing

TXR and GFP channel brightness was normalised across all images within a single experiment, then the separate channels were saved as individual .PNG files. All images corresponding to a single sample were stored within the same directory. 'Background' images were created by manually selecting vesicle-free regions of microscopy images (1 from each sample within the experiment) and measuring the mean pixel intensity. PNG files were input into the vesicle_analysis script (see appendix for scripts).

Manual analysis of GUVs was performed in ImageJ by creating a region of interest corresponding with the area of an individual vesicle using the circle tool and measuring the diameter and mean pixel intensity within this ROI for both the TXR channel and GFP channel images. Values were exported into excel file and plotted using matlab.

7.4 Chapter 3 methods

7.4.1 Plasmid construction

Variants of the pPURE-mNG plasmid containing different 5' UTRs, and pPURE-mVenus and pPURE-DHFR plasmids were prepared by homologous recombination [211]. PCR products were amplified according to tables 1.1 and 1.2 with Phusion DNA polymerase

(2X), 500 nM primers, 1 ng DNA template with the following thermal cycler programme: 98 °C 30s, 35 cycles of [98 °C 10 s, Tm for 20 s and 72 °C for Ex time], 72 °C 10 mins, 4 °C. Amplification of a single band PCR product was confirm by running 2 μL of the PCRs on a prestained 1.2% TAE agarose gel containing 3% GelRed at 100 V for 45 mins. Meanwhile, 1 U of DpnI was added to each reaction that used a plasmid-based template and incubated at 37 °C for 1 hour, followed by 20 mins at 80 °C. PCR products were purified from the reaction mixture using a QIAquick spin PCR purification kit. Homologous recombination was performed using the DNA combinations shown in table 1.3 according to the steps described in subsection 7.2.1).

PCR	DNA template	For primer	Rev primer
mNG high 1 insert	pPURE-mNG	T7 high1 for	AAS rev3
mNG high 2 insert	pPURE-mNG	T7 high2 for	AAS rev3
mNG high 3 insert	pPURE-mNG	T7 high3 for	AAS rev3
mNG medium insert	pPURE-mNG	T7 medium for	AAS rev3
mNG low insert	pPURE-mNG	T7 low for	AAS rev3
pPURE BB 1	pPURE-mNG	AAS for3	T7 rev
mNG EpsA10 PCR1	pPURE-mNG	Eps A10 for 1	Eps A10 rev 1
mNG EpsA10 BB	mNG EpsA10 PCR1	Eps A10 for 2	Eps A10 rev 2
mNG EpsA20 PCR 1	pPURE-mNG	EpsA10 for 1	AAs rev 3
mNG EpsA20 insert	mNG EpsA20 PCR 1	EpsA20 for	AAS rev 3
mNG EpsA20 BB	pPURE-mNG	AAS for 3	EpsA20 rev
mNG T7g10* PCR 1	pPURE-mNG	T7g10* for 1	T7g10* rev 1
mNG T7g10* BB	mNG T7g10* PCR 1	T7g10* for 2	T7g10* rev 2
mNG g10(1-10) insert	pPURE-mNG T7g10*	g10 for	AAsRev3
mNG g10(1-10) BB	pPURE-mNG	g10 rev	AASfor3
mVenus T7g10* insert	pPURE-mVenus	mV T7g10* for	AAS Rev 3
DHFR T7g10* insert	PURExpress VT	DHFR T7g10* for	AAS rev 3
mNG T7g10* BB	pPURE-mNG	T7g10* for 3	AAS for 3

Table 1.1: Chapter 3 PCR reaction compositions

PCR	Tm	Ex time
mNG high 1 insert	63 °C	30 s
mNG high 2 insert	63 °C	30 s
mNG high 3 insert	63 °C	30 s
mNG medium insert	63 °C	30 s
mNG low insert	63 °C	30 s
pPURE BB 1	66 °C	1 min 30 s
mNG EpsA10 PCR 1	66 °C	1 min 30 s
mNG EpsA10 BB	66 °C	1 min 30 s
mNG EpsA20 PCR 1	66 °C	30 s
mNG EpsA20 insert	61 °C	30 s
pPURE EpsA20 BB	67 °C	1 min 30 s
mNG T7g10* PCR 1	63 °C	1 min 30 s
mNG T7g10* BB	63 °C	1 min 30 s

Table 1.2: Chapter 3 PCR reaction conditions

Plasmid	Insert	Vector
pPURE-High1-mNG	mNG high1 insert	pPURE BB 1
pPURE-High2-mNG	mNG high2 insert	pPURE BB 1
pPURE-High3-mNG	mNG high3 insert	pPURE BB 1
pPURE-Medium-mNG	mNG medium insert	pPURE BB 1
pPURE-low-mNG	mNG low insert	pPURE BB 1
pPURE-EpsA10-mNG	-	mNG EpsA10 BB
pPURE-EpsA20-mNG	mNG Eps20 insert	pPURE EpsA20 BB
pPURE-T7g10*-mNG	-	mNG T7g10* BB
pPURE-T7g10*-mVenus	mVenus T7g10* insert	pPURE T7g10* BB
pPURE-T7g10*-DHFR	DHFR T7g10* insert	pPURE T7g10* BB
pPURE-g10(1-9)-mNG	mNG g10(1-9) insert	pPURE g10(1-9) BB

Table 1.3: Chapter 3 homologous recombination reactions

7.4.2 Linear DNA templates

Linear DNA templates encoding the various mNG UTR variants were prepared as described in subsection 7.2.2.

7.4.3 Modification of amine DNA

10μM T7 For Amine was combined with PCB-NHS (Final conc = 5 mM), Sodium bicarbonate (Final conc 100 mM) and DMF (Final conc 50% v/v) to a final volume of 50 μL in 500 μL protein-lo bind tubes and incubated in the dark for 3 hours with gentle shaking. 5 μL 1 M Tris pH 8.0 followed by 445 μL Milli-Q H_2O were added to the tube, and then transferred to a 3 kDa Amicon column. Samples were centrifuged at 14,000 x g for 15

mins at RT 3 times.

7.4.4 HPLC

100 μL sample was injected onto a Discovery C-18 column pre-equilibrated with 5% ACN 95%buffer A (10 mM ammonium acetate). 5-35% buffer A:ACN gradient over 40 mins was used to separate oligos with different modifications. Fractions spanning the entire major peak were collected and those corresponding with the peak maxima were pooled and lyophilised until just dry. 500 μL Milli-Q H_2O added and samples were lyophilised again. Lyophilised oligos were made up in 500 μL Milli-Q H_2O, transferred to a 3 kDa Amicon column and centrifuged at 14,000 x g. Flow through was discarded and 420 μL Milli-Q H_2O added to the column. This was process was repeated 4 times, until A260/A230 >1.6 but ¡2.0.

7.4.5 Formation of light-activated DNA

PCB-DNA templates encoding mNG were prepared by PCR with DreamTaq DNA polymerase master mix (Thermofisher) and 325 nM T7 For PCB/250 nM Rev CT 2 primers from pPURE-mNG or pPURE-T7g10*-mNG plasmids with the following programme: 95 °C for 2 mins, 35 cycles of [95 °C for 30 s, 49 °C for 30 s, 72 °C for 1 min)], 72 °C for 5 mins, 4 °C HOLD. PCR products were purified using the QIAquick PCR purification kit, ethanol precipitated and resuspended in Milli-Q H_2O. 1 μg of linear PCB-DNA was added to a 50x molar excess of monovalent streptavidin and made up to 50 ng/μL with 10 mM tris pH 8.0. Samples were incubated at 24 °C, 600 rpm for 3 hours in the dark and vortex around every hour. Samples were stored at 4 °C for at least 12 hours before use. Samples were kept at 4 °C when used regularly, or at 20 °C for long term storage.

7.4.6 UV lamp irradiation

A M365L2-C5 lamp attached to a clamp stand was held 28.5 cm above the foiled wrapped stand base. The beam was collimated to a diameter of ∼2.2 cm to ensure uniform 365 nm irradiation across the beam area. Driver current was set to 1 mA and power adjusted until power was 0.75 mW, as measured with a light meter. Samples were irradiated one at a time. PCR tubes were irradiated in a PCR tube rack for 1-15 mins (DNA gel), 1-5 mins (CFPS reactions), and 5-15 mins (LA-SCs).

7.4.7 Gel electrophoresis

50 ng of DNA was combined with 6X loading dye and added to wells of a 1.5% TAE agarose gel. Gels were run in 1X TAE buffer at 100 V for 1 hour 15 mins, then stained in 3X GelRed for up to 1 hour. Gels were imaged using a BioRad Geldoc XR+ gel imager.

7.4.8 Cell-free protein synthesis

3 μL IVTT reactions were prepared with 1X PURExpress and supplemented with 0.8 U/μL Murine RNase inhibitor. Final linear DNA template concentration was 5 ng/μL. Sucrose and TexasRed-Dextran were added to reactions at 170 mM and 25 μM where indicated. Reactions were incubated in a thermal cycler at 37 °C for 4 hours, then held at 4 °C for at least 15 minutes. Reactions were worked up with 47 μL PBS and transferred to 384-well black, flat bottom, optiplates and fluorescence was measured using a Tecan Infinite M1000 fluorescence plate reader. Plates were shaken at 306 rpm for 10 seconds to ensure the samples reached the bottom of the well and measured with the following settings: Ex = 506 nm; Em = 517 nm; Bandwidth = 5 nm; Z-position = 23179 μm; Gain = 130.

7.4.9 Assembling LA-SCs

SCs were prepared as described in subsection 7.3.4 except linear DNA templates were replaced by LA-DNA templates. GUVs with biotinylated lipid in their outer leaflet were prepared using 2 lipid containing oils. 2 mg/mL Egg PC was used to for emulsions, while 2 mg/mL Egg PC + 0.1% PE-Biotin was used to create the oil/water phase columns. LA-SCs were irradiated for 10 mins at 0.75 mW using the set up described subsection 7.4.6. Patterned LA-SCs activation was performed by placing film photomasks containing various repeating designs directly on the microscope slide/coverslip and irradiating samples with the UV lamp through the masks. When LA-SCs were immobilised inside agarose, they were resuspended in 1.5% ULGP agarose prepared using outer solution and then gelled inside sealed gene frame at 4 °C for ∼30 minutes. When LA-SCs were immobilised on coverslips, the coverslips were incubated with 1:1 1 mg/mL BSA:BSA-Biotin for 15 mins, then washed with PBS and incubated with 1 mg/mL streptavidin (NEB) for another 15 mins. Coverslips were washed twice with outer solution before forming the imaging chamber sand loading vesicles.

7.5 Chapter 4 methods

7.5.1 Media

Supplemented M9 minimal media (1X M9 salts, 0.34 mg/mL thiamine hydrochloride, 0.2% Cas amino acids, 2 mM $MgSO_4$, 100 μM $CaCl_2$, 0.4% (w/v) glucose) [212] was prepared fresh for every experiment. Buffer was sterilised by passing it through a 0.22 μm PES syringe filter.

7.5.2 BjaI gene synthesis

The BjaI gene sequence was obtained from the European Nucleotide Archive database (Sequence BA000040.2)[121]. Short ∼60 nt oligonucleotides with ∼20 nt terminal overhangs were designed to collectively encode the full BjaI gene sequence (Figure 4.11). Oligos BjaI For 1-9 and BjaI Rev 1-8 were pooled to a final concentration of ∼5 μM, then annealed and elongated via polymerase chain assembly (100 nM oligo mix, 1X Phusion DNA polymerase mastermix, 3% DMSO) with the following thermal cycler programme (98 °C 2 mins, 30 cycles of [98 °C 10 s, 60 °C for 20 s and 72 °C for 15 s], 72 °C 5 mins, 4 °C). The complete BjaI gene was amplified from the pool of assembled oligos via a second PCR step with amplification primers. BjaI PCR product and CT plasmid were double digested with XbaI/BamHI-HF and NdeI/EcoRI-HF and electrophoresed on a 1.2% TAE agarose gel. Digested DNA was cut out from the agarose gel and purified using the Monarch gel extraction purification kit. The BjaI gene was ligated into digested CT using T4 DNA ligase and the ligation was transformed into XL10-Gold *E. coli* cells by heat shock. Transformants were grown on LB agar containing 100 μg/mL ampicillin and then grown as liquid cultures overnight. Plasmids were harvested from overnight cultures using a Pure Yield mini-prep kit and verified by Sanger sequencing.

7.5.3 Plasmid construction

The pSB1A3-BjaR$_{KO}$-GFP plasmid was prepared by truncating the BjaR gene (1-12) by introducing a stop codon followed by a randomly generated sequence via homologous recombination at the ends of a linear dsDNA. pSB1A3 BjaR-GFP-KanR and pSB1A3 BjaR$_{KO}$-GFP-KanR were prepared by inserting an RBS and KanR gene between the GFP and its stop codon via 2-fragment homologous recombination. pSB1A3

$BjaR_{M1LS107R}$pSB1A3 $BjaR_{M1T}$-GFP were prepared by amplifying mutant genes obtained by directed evolution from the pSB1A3 $BjaR_{Mutant}$ GFP-KanR plasmids and introducing them into the pSB1A3 GFP backbone by 2-fragment homologous recombination. pSB1A3 BjaR(B0030/31/32/33)-GFP plasmids were prepared by replacing the B0034 RBS upstream of BjaR with the other RBS variants via 2-fragment homologous recombination. The S107R mutation was introduced into the pSB1A3 BjaR(B0031)-GFP plasmid by site-directed mutagenesis.

Insert and vector fragments were amplified by PCR using Phusion DNA mastermix, 1 ng DNA template, and 500 nM primers according to tables tables 2.1 and 2.2. Reactions were cycled with the following programme: 98 °C for 30 s, 35 cycles of [98 °C for 10 s, Tm for 20 s, 72 °C for 30 s (Insert) or 2 mins (Vector)], 72 °C for 5 mins, 4 °C HOLD. Amplification of a single band PCR product was confirm by running 2 μL of the PCRs on a prestained 1.2% TAE agarose gel containing 3% GelRed at 100 V for 45 mins. Meanwhile, 1 U of DpnI was added to each reaction that used a plasmid-based template and incubated at 37 °C for 1 hour, followed by 20 mins at 80 °C. PCR products were purified from the reaction mixture using a QIAquick spin PCR purification kit. Insert DNA was integrated into the vector DNA by homologous recombination (subsection 7.2.1).

PCR	**DNA template**	**For primer**	**Rev primer**
pSB1A3 BjaR$_{KO}$-GFP PCR	pSB1A3 BjaR-GFP (NcoI)	BjaR KO for	BjaR KO rev
KanR PCR1	pET24a	KanR for 1	KanR rev
KanR insert	KanR PCR1	KanR for 2	KanR rev
pSB1A3 BjaR-GFP BB 1	pSB1A3 BjaR-GFP	Vector for	Vector rev
pSB1A3 BjaR$_{KO}$-GFP BB 1	pSB1A3 BjaR$_{KO}$-GFP	Vector for	Vector rev
BjaR$_{M1L\ S107R}$ insert	pSB1A3 BjaR$_{M1L\ S107R}$-GFP-KanR	pSB1A3 for 1	pSB1A3 rev 1
BjaR$_{M1T}$ insert	pSB1A3 BjaR$_{M1T}$-GFP-KanR	pSB1A3 for 1	pSB1A3 rev 1
pSB1A3 BjaR-GFP BB 2	pSB1A3 BjaR-GFP	pSB1A3 for 2	pSB1A3 rev 2
BjaR(B0030) insert	pSB1A3 BjaR-GFP	B0030 for 1	pSB1A3 rev 1
BjaR(B0030) BB	pSB1A3 BjaR-GFP	pSB1A3 for 1	B0030 rev
BjaR(B0031) insert	pSB1A3 BjaR-GFP	B0031 for	pSB1A3 rev 1
BjaR(B0031) BB	pSB1A3 BjaR-GFP	pSB1A3 for 1	B0031 rev
BjaR(B0032) insert	pSB1A3 BjaR-GFP	B0032 for	pSB1A3 rev 1

BjaR(B0032) BB	pSB1A3 BjaR-GFP	pSB1A3 for 1	B0032 rev
BjaR(B0033) insert	pSB1A3 BjaR-GFP	B0033 for	pSB1A3 rev 1
BjaR(B0033) BB	pSB1A3 BjaR-GFP	pSB1A3 for 1	B0033 rev 1
$BjaR_{S107R}$ insert	pSB1A3 BjaR(B0033)-GFP	S107R for	pSB1A3 rev 1
$BjaR_{S107R}$ BB	pSB1A3 BjaR(B0033)-GFP	pSB1A3 for 2	S107R rev

Table 2.1: Chapter 4 PCR reaction compositions

PCR	Tm	Ex time
pSB1A3 $BjaR_{KO}$-GFP PCR	65	1 min
KanR PCR1	66 °C	30 s
KanR insert	65 °C	30 s
pSB1A3 BjaR-GFP BB 1	63 °C	2 mins
pSB1A3 $BjaR_{KO}$-GFP BB 1	65 °C	1 min
$BjaR_{M1L\ S107R}$ insert	63 °C	30 s
$BjaR_{M1T}$ insert	63 °C	30 s
pSB1A3 BjaR-GFP BB 2	63 °C	2 mins
BjaR(B0030) insert	66 °C	30 s
BjaR(B0030) BB	66 °C	1 min 15 s
BjaR(B0031) insert	66 °C	30 s
BjaR(B0031) BB	66 °C	1 min 15 s
BjaR(B0032) insert	66 °C	30 s
BjaR(B0032) BB	66 °C	1 min 15 s
BjaR(B0033) insert	66 °C	30 s
BjaR(B0033) BB	66 °C	1 min 15 s
$BjaR_{S107R}$ insert	63 °C	15 s
$BjaR_{S107R}$ BB	63 °C	1 min 30 s

Table 2.2: Chapter 4 PCR reaction conditions

Plasmid	Insert	Vector
pSB1A3 BjaR$_{KO}$-GFP	-	pSB1A3 BjaR$_{KO}$-GFP PCR
pSB1A3 BjaR-GFP-KanR	KanR insert	pSB1A3 BjaR-GFP BB 1
pSB1A3 BjaR$_{KO}$-GFP-KanR	KanR insert	pSB1A3 BjaR$_{KO}$-GFP BB1
pSB1A3 BjaR$_{M1L\ S107R}$-GFP	BjaR$_{M1L\ S107R}$ insert	pSB1A3 BjaR-GFP BB 2
pSB1A3 BjaR$_{M1T}$-GFP	BjaR$_{M1T}$ insert	pSB1A3 BjaR-GFP BB 2
pSB1A3 BjaR(B0030)-GFP	BjaR(B0030) insert	BjaR(B0030) BB
pSB1A3 BjaR(B0031)-GFP	BjaR(B0031) insert	BjaR(B0031) BB
pSB1A3 BjaR(B0032)-GFP	BjaR(B0032) insert	BjaR(B0032) BB
pSB1A3 BjaR(B0033)-GFP	BjaR(B0033) insert	BjaR(B0033) BB
pSB1A3 BjaR$_{S107R}$(B0031)-GFP	BjaR$_{S107R}$ insert	BjaR$_{S107R}$ BB

Table 2.3: Chapter 4 homologous recombination reactions

7.5.4 Directed evolution

BjaR underwent 4 rounds of directed evolution based on a previously published protocol [202]. Briefly, epPCR of the BjaR gene was performed in the presence of 100μM $MnCl_2$ using Taq DNA polymerase and 500 nM pSB1A3 for 1 and pSB1A3 rev 1 primers. Reactions were cycled using the following programme: 95 °C for 30 s, 30 cycles of [95 °C for 15 s, 51 °C for 30 s, 68 °C for 1 min], 68 °C for 5 mins, 4 °C HOLD. PCR products were electrophoresed on a 1.2% TAE agarose gel and gel extracted using a Monarch Gel extraction kit. Gel extracted BjaR DNA was cloned into the pSB1A3 GFP-KanR BB using a home-made Gibson's assembly master mix [1] and transformed into XL10-Gold *E. coli*. Cells were incubated in 500 μL SOC media for 1 hour at 37 °C, 225 rpm, then 4.5 mL LB + amp (100 μg/mL final) was added, and cells were incubated overnight at 37 °C, 225

rpm. 1 x 10^7 cells from overnight culture were transferred into 1 mL M9 minimal + Amp in the presence of decreasing IV-HSL (1 nM/0.8 nM/0.6 nM/0.4 nM) and incubated for 1 hour 37 °C. After 1 hour, kanamycin was added to a final concentration of 200 μg/mL and incubated for a further 5 hours. Cells were centrifuged at 8,000 x g for 3 mins and washed in LB, then resuspended in 2 mL LB + amp and incubated for 2 hours. Cells were pelleted and plasmids extracted using a PUREyield mini prep kit. Plasmids from rounds 1/2/3 were used as DNA templates for epPCR in rounds 2/3/4 respectively.

7.5.5 Measuring BjaR reporter performance

BjaR receiver cells were incubated in 5 mL LB + Amp media overnight. Overnight cultures were diluted 1/250 or 1/500 in 5 mL M9 minimal media + Amp and incubated at 37 °C, 225 rpm for 3 hours 45 mins (until $OD_{600} \sim 0.075$). Cultures were diluted down to OD600 = 0.05 with M9 minimal media + Amp and 200 μL was added to wells of a 96-well plate containing 1 μL IV-HSL dissolved in DMSO or 1 μL BjaI CFPS reactions (IV-HSL concs obtained from serial dilution from 63.2 μM to 632 pM; final DMSO conc = 0.5%). Cells were incubated at 37 °C, 800 rpm in a thermomixer with a heated lid for 4 hours. Fluorescence and OD_{600} were measured in a Tecan M1000 infinite plate reader (Ex: 488 nm, Em: 510 nm, BW: 5 nm Gain: 101, Z-position: 21311 um).

7.5.6 Preparation of linear DNA templates

Linear DNA templates encoding BjaI were amplified from the pPURE-BjaI plasmids as described in subsection 7.2.2.

7.5.7 Preparing LA-BjaI DNA templates

LA-BjaI DNA templates were prepared from pPURE-BjaI as described in subsection 7.4.5.

7.5.8 CFPS of BjaI

3 μL CFPS reactions were prepared using PURExpress with 0.8 U/μL Murine RNase inhibitor and 5 ng/μL linear BjaI DNA. IVTT reactions were supplemented with ^{35}S-Methionine, 300 μM SAM and 80 μM IV-CoA where indicated. Reactions were incubated for 3 hours at 37 °C in a water bath (Radioactive) or for 5 hours at 37 °C in a thermal cycler (Non-radioactive). Radioactive reactions were run on a precast 10% mini protean TGX gel at 200V for 30 mins, then dried onto filter papers using a Biorad Model583 gel dryer and exposed to Kodak Biomax MS film overnight. Films were developed with an XRay film processor.

7.5.9 Preparing a OnePot PURE system

PURE proteins, ribosomes and energy solution were all prepared as described in [61].

7.5.10 Preparation of synthetic cells

SCs were prepared as described in subsection 7.3.4 with exceptions. When SCs were incubated separately from *E. coli*, the inner solution comprised of PURExpress (1X), 0.8 U/μL Murine RNase inhibitor, 300 μM SAM, 80 μM IV-CoA and 170 mM sucrose. When SCs were co-cultured with *E. coli* in M9 agarose, the inner solution comprised of PURExpress (0.5X), 300 μM SAM, 80 μM IV-CoA and 50 mM sucrose. The outer solution in this case was 50 mM HEPES (pH 7.6), 200 mM potassium glutamate, 50 mM

glucose. GUV pellets were resuspended in 25 μL of outer solution and incubated at 37 °C , 300 rpm for 5 hours. 10 μL was transferred to 190 μL BjaR* or $BjaR_{M1LS107R}$ to measure IV-HSL production. This was performed as described in subsection 7.5.5.

7.5.11 Preparing agarose pads

Microcope slides were first cleaned with Milli-Q H_2O and isopropanol. 2 x 25 μL gene frames were attached to a single microscope slide with the open side still covered with the transparent film. Molten 1.5% ultra-low gelling point agarose was mixed with SCs or IV-HSL as required and added inside the gene frames. A second microscope slides was carefully slid on top of the gene frames to distribute the molten agarose throughout the frame. Microscope slides sandwiching the gene frame were transferred to the fridge for 1 hour, then the top slide was carefully removed by moving it off of the gene frame horizontally. 3 μL BjaR* cells at OD_{600} = 0.1 were added on top of the gelled agarose pads and the excess liquid was allowed to evaporate. The transparent film was removed from the gene frame and a clean coverslip was placed on top of the agarose pad to seal it.

7.6 Chapter 5 methods

7.6.1 Plasmid construction

The pPURE-H2-mNG plasmid was prepared by replacing the 5' UTR of the pPURE-mNG plasmid with the H2 histamine riboswitch via 2-fragment homologous recombination. pPURE-H2-mNG was then used as the plasmid backbone and mCherry, mVenus, mYPet, and sfGFP genes were placed downstream of the H2 riboswitch, again via 2-fragment homologous recombination.

Insert and vector fragments were amplified by PCR using Phusion DNA mastermix, 1 ng DNA template, and 500 nM primers according to tables 3.1 and 3.2 Reactions were cycled with the following programme: 98 °C for 30 s, 35 cycles of [98 °C for 10 s, Tm for 20 s, 72 °C for Ex time], 72 °C for 5 mins, 4 °C HOLD. Amplification of a single band PCR product was confirm by running 2 μL of the PCRs on a prestained 1.2% TAE agarose gel containing 3% GelRed at 100 V for 45 mins. Meanwhile, 1 U of DpnI was added to each reaction that used a plasmid-based template and incubated at 37 °C for 1 hour, followed by 20 mins at 80 °C. PCR products were purified from the reaction mixture using a QIAquick spin PCR purification kit. Insert DNA was integrated into the vector DNA by homologous recombination (subsection 7.2.1) according to table 3.3.

PCR	**DNA template**	**For primer**	**Rev primer**
H2 insert	H2 riboswitch gBlock	His insert for	His insert rev
mVenus insert	pPURE-mVenus	mVenus his for	AAS342
mCherry insert	pPURE-mCherry	mCherry his for	mYPet his rev
mYPet insert	mYPet gBlock	mYPet his for	mYPet his rev
sfGFP insert	pGRG25-Pmax-sfGFP	sfGFP his for	sfGFP his rev
pPURE-mNG BB	pPURE-mNG	His vector for 1	His vector rev 1
pPURE-H2 BB	pPURE-H2-mNG	His vector for 2	His vector rev 2

Table 3.1: Chapter 5 PCR reaction compositions

PCR	Tm	Ex time
H2 insert	66 °C	30 s
mVenus insert	66 °C	30 s
mCherry insert	63 °C	30 s
mYPet insert	67 °C	30 s
sfGFP insert	66 °C	30 s
pPURE-mNG BB	66 °C	1 min 30 s
pPURE-H2 BB	66 °C	1 min

Table 3.2: Chapter 5 PCR reaction conditions

Plasmid	Insert	Vector
pPURE-H2-mNG	H2 insert	pPURE-mNG BB
pPURE-H2-mVenus	mVenus insert	pPURE-H2 BB
pPURE-H2-mYPet	mYPet insert	pPURE-H2 BB
pPURE-H2-sfGFP	sfGFP insert	pPURE-H2 BB
pPURE-H2-mCherry	mCherry insert	pPURE-H2 BB

Table 3.3: Chapter 5 homologous recombination reactions

7.6.2 Preparation of linear DNA templates

Linear DNA templates were obtained from pPURE-H2-mNG/mVenus/mCherry/mYPet/sfGFP plasmids as described in subsection 7.2.2

7.6.3 Preparation of LA-DNA templates

LA-DNA templates of the histribo mYPet construct were constructed as described in subsection 7.4.5.

7.6.4 Cell-free protein synthesis

3 μL CFPS reactions were prepared with 1X PURExpress and supplemented with 0.8 U/μL Murine RNase inhibitor. Linear DNA templates were added at to a final concentration of 5 ng/μL. Histamine was added to a final concentration of 5 mM, unless stated otherwise. Reactions were irradiated with UV light for 3 minutes where indicated. Reactions were incubated in a thermal cycler at 37 °C for 4 hours. Reactions were worked up with 47 μL PBS and transferred to 384-well black, flat bottom, optiplates and fluorescence was measured using a Tecan Infinite M1000 fluorescence plate reader.

Protein	**Ex (nm)**	**Em (nm)**	**Bandwidth (nm)**
mNG	506	517	5
mVenus	515	528	5
mYPet	517	530	5
sfGFP	485	510	5
mCherry	587	610	5
Microscope	470	525	20

7.6.5 GUV assembly

GUVs were formed as described in subsection 7.3.4, with exceptions. The lipid in oil was prepared with 5 mg/mL POPC + cholesterol (1:2). Vesicles were formed by centrifugation

at 4,000 x g for 30 minutes and repelleted by centrifugation at 1,000 x g for 10 mins. Care was taken when resuspending the vesicle pellets, as GUVs with this composition were often larger and less stable than GUVs prepared with Egg PC.

7.7 Primer sequences

Name	**Sequence (5'-3')**	**Chapter**
T7 e.long	GAAATTAATACGACTCACTATAGGGTCTAG	2, 3, 4, 5
Rev CT 2	GATATAGTTCCTCCTTTCAG	2, 3, 4, 5
AAS324 Rev3	GCCTCCTGCAGGTTAACCTTAC	3,5
g10 leader for	ATGGCTAGCATGACTGGTGGAC	3
BjaI For 1	GAAGGAGGTATACATATGATTCACGCAATTT CCGCGGTCAATCGCCACTTATACGAGGAC	4
BjaI For 2	GCGTCATGACATCTTTGTCGAGGAGCGGCA CTGGGAGACGCTGCGCAGGCCGGATGGCCG	4
BjaI For 3	GAGGATACCGTCTATCTGCTTGCGCTGGAG GGACGGCGCGTCGTCGGCGGCCACCGGCTC	4
BjaI For 4	CTCGATGATGAGCGAGGTCTTCCCGCATCT GGCGGCGGTTCGCGGCTGCCCCTCGGATC	4
BjaI For 5	CTACTTCGTCGTCCGCGATCGCCGCGACGG CGCGCTCAACCTGCAACTGATGGCGGCG	4
BjaI For 6	GAATCGCGCAGGTCAGCGCGATCATGGAAA CCTGGTGGTTGCCGCGCTTCCACGAGGCCG	4
BjaI For 7	CTGCCGGCTCTGGTCGAGAACGCCTGGACC ATGGCGGCCACCGTCGACATTCGTCGCCAG	4

BjaI For 8	GATCGCATCGGCATGCCTTCCATCGTGCAAC AGGACGGCCCGCGTCTGGACGCCGTCGC	4
BjaI For 9	GCCGCGCAACGAAAGAGCGCCTGATGAAAT GGATCCCGGGAATTCTCGA	4
BjaI Rev 1	GCTCTTTCGTTGCGCGGCAGCGAGGCCGCA AAGGTTGGCACGGGCGACGGCGTCCAGACG	4
BjaI Rev 2	GAAGGCATGCCGATGCGATCATGCAGGACA TCGAGCGTCTGGCGACGAATGTCGACG	4
BjaI Rev 3	CTCGACCAGAGCCGGCAGGCCGAGCGGCGT CACGACGAAGCCGGCCTCGTGGAAGCGCG	4
BjaI Rev 4	GCTGACCTGCGCGATTCCCTGGTCGAGGCA GAACTCCTGCACCGCCGCCATCAGTTGCAG	4
BjaI Rev 5	GATCGCGGACGACGAAGTAGCGCGACCATT CCCAGATCAGCGGATCCGAGGGGCAGCCGC	4
BjaI Rev 6	GACCTCGCTCATCATCGAGGGCTTGGTCGT GGGGTAGAGCCGGTGGCCGCCGAC	4
BjaI Rev 7	GCAGATAGACGGTATCCTCGTCGTCATAGGA ATCGACCTCGCGGCCATCCGGCCTGCGC	4
BjaI Rev 8	GACAAAGATGTCATGACGCAGCCGGAAATG CTGCTCGAGTACGTCCTCGTATAAGTGGCG	4
BjaI For Amp	GAAGGAGGTATACATATGATTCACGC	4
BjaI Rev Amp	CGAGAATTCCCGGGATCCATTTC	4
BjaR KO For	TGACATTCTCTCAAAGTATTATGCAGGGCCA TCCGTCACAAAATTATCAAC	4

BjaR KO Rev	CCTGCATAATACTTTGAGAGAATGTCACAGG GCTTCACGCCCATAATCTAC	4
KanR for 1	AGTAAATCTAAGCAGGTCCGCATGAGCCATA TTCAACGGGAAAC	4
KanR for 2	CATGGCATGGATGAACTATACAAATAATAAA GTAAATCTAAGCAGGTCCGC	4
KanR rev	CTGACCGATAAGCCGGCTCTAGTATTATTAG AAAAACTCATCGAGCATC	4
Vector for	TACTAGAGCCGGCTTATCGGTCAG	4
Vector rev	TTATTATTTGTATAGTTCATCCATGCCATG	4
pSB1A3 for 1	GCTACTAGAGAAAGAGGAGAAATACTAG	4
pSB1A3 for 2	TACTAGAGCCAGGCATCAAATAAAACG	4
pSB1A3 rev 1	CGTTTTATTTGATGCCTGGCTCTAGTA	4
pSB1A3 rev 2	CTAGTATTTCTCCTCTTTCTCTAGTAGC	4
B0030 for	CTAGAGATTAAAGAGGAGAAATACTAGATGT CCGCAGTAGATTATGGGC	4
B0030 rev	GTATTTCTCCTCTTTAATCTCTAGTAGCTAG CACTGTACCTAGGAC	4
B0031 for	CTAGAGTCACACAGGAAACCTACTAGATGTC CGCAGTAGATTATGGGC	4
B0031 rev	GTAGGTTTCCTGTGTGACTCTAGTAGCTAGC ACTGTACCTAGGAC	4
B0032 for	CTAGAGTCACACAGGAAAGTACTAGATGTCC GCAGTAGATTATGGGC	4

B0032 rev	CTAGTACTTTCCTGTGTGACTCTAGTAGCTA GCACTGTACCTAGGAC	4
B0033 for	CTACTAGAGTCACACAGGACTACTAGATGTC CGCAGTAGATTATGGGC	4
B0033 rev	GTAGTCCTGTGTGACTCTAGTAGCTAGCACT GTACCTAGGAC	4
S107R for	GAATTAGAACCACGCGCCGC	4
S107R rev	GCGGCGCGTGGTTCTAATTC	4
His insert for	GCATTTATCAGGGTTATTGTCTC	5
His insert rev	GCGGAACCAGAATCCACG	5
His vector for 1	GCAGTTTAGCCCGTGGATTCTG	5
His vector rev 1	CCGCTCATGAGACAATAACCCTG	5
His vector for 2	GAATTCTCGAGTAAGGTTAACCTGCAG	5
His vector rev 2	CATGTTTGGATCCAGCAGGTCGAC	5
mVenus his for	CAAGTCGACCTGCTGGATCCAAACATGGTG AGCAAGGGCGAGGAGC	5
mCherry his for	CAAGTCGACCTGCTGGATCCAAACATGGTG AGCAAGGGCGAGGAG	5
mYPet his for	CAAGTCGACCTGCTGGATCCAAACATGGTG TCCAAAGGCGAAGAACTG	5
mYPet his rev	TACTCGAGAATTCCCGGGATCCTCATTATT TATACAGTTCGTTCATACCCTCCG	5
sfGFP his for	CAAGTCGACCTGCTGGATCCAAACATGCGT AAAGGCGAAGAGCTG	5

sfGFP his rev	TACTCGAGAATTCCCGGGATCCTCATTATT TGTACAGTTCATCCATACCATGCG	5

Table 7.3: Primer sequences
Underlined bases indicate overhangs used for homologous recombination

Bibliography

[1] D. G. Gibson et al. "Enzymatic assembly of DNA molecules up to several hundred kilobases". In: *Nat Methods* 6.5 (2009), pp. 343–5. ISSN: 1548-7105 (Electronic) 1548-7091 (Linking). DOI: 10.1038/nmeth.1318. URL: https://www.ncbi.nlm.nih.gov/pubmed/19363495.

[2] E. Weber et al. "A modular cloning system for standardized assembly of multigene constructs". In: *PLoS One* 6.2 (2011), e16765. ISSN: 1932-6203 (Electronic) 1932-6203 (Linking). DOI: 10.1371/journal.pone.0016765. URL: https://www.ncbi.nlm.nih.gov/pubmed/21364738.

[3] J. K. Joung and J. D. Sander. "TALENs: a widely applicable technology for targeted genome editing". In: *Nat Rev Mol Cell Biol* 14.1 (2013), pp. 49–55. ISSN: 1471-0080 (Electronic) 1471-0072 (Linking). DOI: 10.1038/nrm3486. URL: https://www.ncbi.nlm.nih.gov/pubmed/23169466.

[4] J. A. Doudna and E. Charpentier. "Genome editing. The new frontier of genome engineering with CRISPR-Cas9". In: *Science* 346.6213 (2014), p. 1258096. ISSN: 1095-9203 (Electronic) 0036-8075 (Linking). DOI: 10.1126/science.1258096. URL: https://www.ncbi.nlm.nih.gov/pubmed/25430774.

[5] A. A. Nielsen et al. “Genetic circuit design automation”. In: *Science* 352.6281 (2016), aac7341. ISSN: 1095-9203 (Electronic) 0036-8075 (Linking). DOI: 10.1126/science.aac7341. URL: https://www.ncbi.nlm.nih.gov/pubmed/27034378.

[6] R. Kwok. “Five hard truths for synthetic biology”. In: *Nature* 463.7279 (2010), pp. 288–90. ISSN: 1476-4687 (Electronic) 0028-0836 (Linking). DOI: 10.1038/463288a. URL: https://www.ncbi.nlm.nih.gov/pubmed/20090726.

[7] D. G. Gibson et al. “Complete chemical synthesis, assembly, and cloning of a Mycoplasma genitalium genome”. In: *Science* 319.5867 (2008), pp. 1215–20. ISSN: 1095-9203 (Electronic) 0036-8075 (Linking). DOI: 10.1126/science.1151721. URL: https://www.ncbi.nlm.nih.gov/pubmed/18218864.

[8] D. G. Gibson et al. “Creation of a bacterial cell controlled by a chemically synthesized genome”. In: *Science* 329.5987 (2010), pp. 52–6. ISSN: 1095-9203 (Electronic) 0036-8075 (Linking). DOI: 10.1126/science.1190719. URL: https://www.ncbi.nlm.nih.gov/pubmed/20488990.

[9] 3rd Hutchison C. A. et al. “Design and synthesis of a minimal bacterial genome”. In: *Science* 351.6280 (2016), aad6253. ISSN: 1095-9203 (Electronic) 0036-8075 (Linking). DOI: 10.1126/science.aad6253. URL: https://www.ncbi.nlm.nih.gov/pubmed/27013737.

[10] J. F. Pelletier et al. “Genetic requirements for cell division in a genomically minimal cell”. In: *Cell* 184.9 (2021), 2430–2440 e16. ISSN: 1097-4172 (Electronic) 0092-8674 (Linking). DOI: 10.1016/j.cell.2021.03.008. URL: https://www.ncbi.nlm.nih.gov/pubmed/33784496.

[11] S. M. Richardson et al. “Design of a synthetic yeast genome”. In: *Science* 355.6329 (2017), pp. 1040–1044. ISSN: 1095-9203 (Electronic) 0036-8075 (Linking). DOI: 10.

1126/science.aaf4557. URL: https://www.ncbi.nlm.nih.gov/pubmed/28280199.

[12] F. J. Isaacs et al. "Precise manipulation of chromosomes in vivo enables genome-wide codon replacement". In: *Science* 333.6040 (2011), pp. 348–53. ISSN: 1095-9203 (Electronic) 0036-8075 (Linking). DOI: 10.1126/science.1205822. URL: https://www.ncbi.nlm.nih.gov/pubmed/21764749.

[13] H. S. Park et al. "Expanding the genetic code of Escherichia coli with phosphoserine". In: *Science* 333.6046 (2011), pp. 1151–4. ISSN: 1095-9203 (Electronic) 0036-8075 (Linking). DOI: 10.1126/science.1207203. URL: https://www.ncbi.nlm.nih.gov/pubmed/21868676.

[14] D. Cervettini et al. "Rapid discovery and evolution of orthogonal aminoacyl-tRNA synthetase-tRNA pairs". In: *Nat Biotechnol* 38.8 (2020), pp. 989–999. ISSN: 1546-1696 (Electronic) 1087-0156 (Linking). DOI: 10.1038/s41587-020-0479-2. URL: https://www.ncbi.nlm.nih.gov/pubmed/32284585.

[15] J. S. Dymond et al. "Synthetic chromosome arms function in yeast and generate phenotypic diversity by design". In: *Nature* 477.7365 (2011), pp. 471–6. ISSN: 1476-4687 (Electronic) 0028-0836 (Linking). DOI: 10.1038/nature10403. URL: https://www.ncbi.nlm.nih.gov/pubmed/21918511.

[16] B. A. Blount et al. "Rapid host strain improvement by in vivo rearrangement of a synthetic yeast chromosome". In: *Nat Commun* 9.1 (2018), p. 1932. ISSN: 2041-1723 (Electronic) 2041-1723 (Linking). DOI: 10.1038/s41467-018-03143-w. URL: https://www.ncbi.nlm.nih.gov/pubmed/29789540.

[17] Z. Hu et al. "The MinC component of the division site selection system in Escherichia coli interacts with FtsZ to prevent polymerization". In: *Proc Natl Acad Sci U S A* 96.26 (1999), pp. 14819–24. ISSN: 0027-8424 (Print) 0027-8424 (Link-

ing). DOI: 10.1073/pnas.96.26.14819. URL: https://www.ncbi.nlm.nih.gov/pubmed/10611296.

[18] C. P. N. Rampley et al. "Development of SimCells as a novel chassis for functional biosensors". In: *Sci Rep* 7.1 (2017), p. 7261. ISSN: 2045-2322 (Electronic) 2045-2322 (Linking). DOI: 10.1038/s41598-017-07391-6. URL: https://www.ncbi.nlm.nih.gov/pubmed/28775370.

[19] C. Fan et al. "Chromosome-free bacterial cells are safe and programmable platforms for synthetic biology". In: *Proc Natl Acad Sci U S A* 117.12 (2020), pp. 6752–6761. ISSN: 1091-6490 (Electronic) 0027-8424 (Linking). DOI: 10.1073/pnas.1918859117. URL: https://www.ncbi.nlm.nih.gov/pubmed/32144140.

[20] X. J. Chen et al. "Rational Design and Characterization of Nitric Oxide Biosensors in E. coli Nissle 1917 and Mini SimCells". In: *ACS Synth Biol* 10.10 (2021), pp. 2566–2578. ISSN: 2161-5063 (Electronic) 2161-5063 (Linking). DOI: 10.1021/acssynbio.1c00223. URL: https://www.ncbi.nlm.nih.gov/pubmed/34551261.

[21] Konstantinos Vavitsas. "Could cells without genomes become the new synthetic biology chassis?" In: *Synthetic Biology* 5.1 (2020), ysaa003. ISSN: 2397-7000. DOI: 10.1093/synbio/ysaa003. URL: https://doi.org/10.1093/synbio/ysaa003.

[22] E. Rideau et al. "Liposomes and polymersomes: a comparative review towards cell mimicking". In: *Chem Soc Rev* 47.23 (2018), pp. 8572–8610. ISSN: 1460-4744 (Electronic) 0306-0012 (Linking). DOI: 10.1039/c8cs00162f. URL: https://www.ncbi.nlm.nih.gov/pubmed/30177983.

[23] M. Li et al. "Electrostatically gated membrane permeability in inorganic protocells". In: *Nat Chem* 5.6 (2013), pp. 529–36. ISSN: 1755-4349 (Electronic) 1755-4330 (Linking). DOI: 10.1038/nchem.1644. URL: https://www.ncbi.nlm.nih.gov/pubmed/23695636.

[24] X. Huang et al. “Interfacial assembly of protein-polymer nano-conjugates into stimulus-responsive biomimetic protocells”. In: *Nat Commun* 4 (2013), p. 2239. ISSN: 2041-1723 (Electronic) 2041-1723 (Linking). DOI: 10.1038/ncomms3239. URL: https://www.ncbi.nlm.nih.gov/pubmed/23896993.

[25] S. S. Yadavalli et al. “Bioactive cell-like hybrids from dendrimersomes with a human cell membrane and its components”. In: *Proc Natl Acad Sci U S A* 116.3 (2019), pp. 744–752. ISSN: 1091-6490 (Electronic) 0027-8424 (Linking). DOI: 10.1073/pnas.1811307116. URL: https://www.ncbi.nlm.nih.gov/pubmed/30591566.

[26] K. Vogele et al. “Towards synthetic cells using peptide-based reaction compartments”. In: *Nat Commun* 9.1 (2018), p. 3862. ISSN: 2041-1723 (Electronic) 2041-1723 (Linking). DOI: 10.1038/s41467-018-06379-8. URL: https://www.ncbi.nlm.nih.gov/pubmed/30242152.

[27] A. F. Mason and J. C. M. van Hest. “Multifaceted cell mimicry in coacervate-based synthetic cells”. In: *Emerg Top Life Sci* 3.5 (2019), pp. 567–571. ISSN: 2397-8554 (Print) 2397-8554 (Linking). DOI: 10.1042/ETLS20190094. URL: https://www.ncbi.nlm.nih.gov/pubmed/33523170.

[28] J. de Gier, J. G. Mandersloot, and L. L. van Deenen. “Lipid composition and permeability of liposomes”. In: *Biochim Biophys Acta* 150.4 (1968), pp. 666–75. ISSN: 0006-3002 (Print) 0006-3002 (Linking). DOI: 10.1016/0005-2736(68)90056-4. URL: https://www.ncbi.nlm.nih.gov/pubmed/5690752.

[29] V. Noireaux and A. Libchaber. “A vesicle bioreactor as a step toward an artificial cell assembly”. In: *Proc Natl Acad Sci U S A* 101.51 (2004), pp. 17669–74. ISSN: 0027-8424 (Print) 0027-8424 (Linking). DOI: 10.1073/pnas.0408236101. URL: https://www.ncbi.nlm.nih.gov/pubmed/15591347.

[30] T. Oberholzer, K. H. Nierhaus, and P. L. Luisi. "Protein expression in liposomes". In: *Biochem Biophys Res Commun* 261.2 (1999), pp. 238–41. ISSN: 0006-291X (Print) 0006-291X (Linking). DOI: 10.1006/bbrc.1999.0404. URL: https://www.ncbi.nlm.nih.gov/pubmed/10425171.

[31] W. Yu et al. "Synthesis of functional protein in liposome". In: *J Biosci Bioeng* 92.6 (2001), pp. 590–3. ISSN: 1389-1723 (Print) 1347-4421 (Linking). DOI: 10.1263/jbb.92.590. URL: https://www.ncbi.nlm.nih.gov/pubmed/16233152.

[32] T. Pols et al. "A synthetic metabolic network for physicochemical homeostasis". In: *Nat Commun* 10.1 (2019), p. 4239. ISSN: 2041-1723 (Electronic) 2041-1723 (Linking). DOI: 10.1038/s41467-019-12287-2. URL: https://www.ncbi.nlm.nih.gov/pubmed/31534136.

[33] M. Osawa and H. P. Erickson. "Liposome division by a simple bacterial division machinery". In: *Proc Natl Acad Sci U S A* 110.27 (2013), pp. 11000–4. ISSN: 1091-6490 (Electronic) 0027-8424 (Linking). DOI: 10.1073/pnas.1222254110. URL: https://www.ncbi.nlm.nih.gov/pubmed/23776220.

[34] S. Kretschmer et al. "Synthetic cell division via membrane-transforming molecular assemblies". In: *BMC Biol* 17.1 (2019), p. 43. ISSN: 1741-7007 (Electronic) 1741-7007 (Linking). DOI: 10.1186/s12915-019-0665-1. URL: https://www.ncbi.nlm.nih.gov/pubmed/31126285.

[35] E. Godino et al. "Cell-free biogenesis of bacterial division proto-rings that can constrict liposomes". In: *Commun Biol* 3.1 (2020), p. 539. ISSN: 2399-3642 (Electronic) 2399-3642 (Linking). DOI: 10.1038/s42003-020-01258-9. URL: https://www.ncbi.nlm.nih.gov/pubmed/32999429.

[36] J. P. Frohnmayer et al. "Minimal synthetic cells to study integrin-mediated adhesion". In: *Angew Chem Int Ed Engl* 54.42 (2015), pp. 12472–8. ISSN: 1521-3773

(Electronic) 1433-7851 (Linking). DOI: 10.1002/anie.201503184. URL: https://www.ncbi.nlm.nih.gov/pubmed/26257266.

[37] P. M. Gardner, K. Winzer, and B. G. Davis. "Sugar synthesis in a protocellular model leads to a cell signalling response in bacteria". In: *Nat Chem* 1.5 (2009), pp. 377–83. ISSN: 1755-4349 (Electronic) 1755-4330 (Linking). DOI: 10.1038/nchem.296. URL: https://www.ncbi.nlm.nih.gov/pubmed/21378891.

[38] C. Tanford. "The hydrophobic effect and the organization of living matter". In: *Science* 200.4345 (1978), pp. 1012–8. ISSN: 0036-8075 (Print) 0036-8075 (Linking). DOI: 10.1126/science.653353. URL: https://www.ncbi.nlm.nih.gov/pubmed/653353.

[39] D. E. Discher and F. Ahmed. "Polymersomes". In: *Annu Rev Biomed Eng* 8 (2006), pp. 323–41. ISSN: 1523-9829 (Print) 1523-9829 (Linking). DOI: 10.1146/annurev.bioeng.8.061505.095838. URL: https://www.ncbi.nlm.nih.gov/pubmed/16834559.

[40] B. M. Discher et al. "Polymersomes: tough vesicles made from diblock copolymers". In: *Science* 284.5417 (1999), pp. 1143–6. ISSN: 0036-8075 (Print) 0036-8075 (Linking). DOI: 10.1126/science.284.5417.1143. URL: https://www.ncbi.nlm.nih.gov/pubmed/10325219.

[41] M. Garni et al. "Biopores/membrane proteins in synthetic polymer membranes". In: *Biochim Biophys Acta Biomembr* 1859.4 (2017), pp. 619–638. ISSN: 0005-2736 (Print) 0005-2736 (Linking). DOI: 10.1016/j.bbamem.2016.10.015. URL: https://www.ncbi.nlm.nih.gov/pubmed/27984019.

[42] C. Martino et al. "Protein expression, aggregation, and triggered release from polymersomes as artificial cell-like structures". In: *Angew Chem Int Ed Engl* 51.26 (2012), pp. 6416–20. ISSN: 1521-3773 (Electronic) 1433-7851 (Linking). DOI: 10.

1002/anie.201201443. URL: https://www.ncbi.nlm.nih.gov/pubmed/22644870.

[43] A. Joesaar et al. "DNA-based communication in populations of synthetic protocells". In: *Nat Nanotechnol* 14.4 (2019), pp. 369–378. ISSN: 1748-3395 (Electronic) 1748-3387 (Linking). DOI: 10.1038/s41565-019-0399-9. URL: https://www.ncbi.nlm.nih.gov/pubmed/30833694.

[44] J. F. Milligan et al. "Oligoribonucleotide synthesis using T7 RNA polymerase and synthetic DNA templates". In: *Nucleic Acids Res* 15.21 (1987), pp. 8783–98. ISSN: 0305-1048 (Print) 0305-1048 (Linking). DOI: 10.1093/nar/15.21.8783. URL: https://www.ncbi.nlm.nih.gov/pubmed/3684574.

[45] D. F. Browning and S. J. Busby. "The regulation of bacterial transcription initiation". In: *Nat Rev Microbiol* 2.1 (2004), pp. 57–65. ISSN: 1740-1526 (Print) 1740-1526 (Linking). DOI: 10.1038/nrmicro787. URL: https://www.ncbi.nlm.nih.gov/pubmed/15035009.

[46] R. G. Roeder. "The role of general initiation factors in transcription by RNA polymerase II". In: *Trends Biochem Sci* 21.9 (1996), pp. 327–35. ISSN: 0968-0004 (Print) 0968-0004 (Linking). URL: https://www.ncbi.nlm.nih.gov/pubmed/8870495.

[47] V. M. Weake and J. L. Workman. "Inducible gene expression: diverse regulatory mechanisms". In: *Nat Rev Genet* 11.6 (2010), pp. 426–37. ISSN: 1471-0064 (Electronic) 1471-0056 (Linking). DOI: 10.1038/nrg2781. URL: https://www.ncbi.nlm.nih.gov/pubmed/20421872.

[48] M. V. Rodnina. "Translation in Prokaryotes". In: *Cold Spring Harb Perspect Biol* 10.9 (2018). ISSN: 1943-0264 (Electronic) 1943-0264 (Linking). DOI: 10.1101/

cshperspect . a032664. URL: https : / / www . ncbi . nlm . nih . gov / pubmed / 29661790.

[49] A. D. Silverman, A. S. Karim, and M. C. Jewett. "Cell-free gene expression: an expanded repertoire of applications". In: *Nat Rev Genet* 21.3 (2020), pp. 151–170. ISSN: 1471-0064 (Electronic) 1471-0056 (Linking). DOI: 10.1038/s41576-019-0186-3. URL: https://www.ncbi.nlm.nih.gov/pubmed/31780816.

[50] J. Garamella et al. "The All E. coli TX-TL Toolbox 2.0: A Platform for Cell-Free Synthetic Biology". In: *ACS Synth Biol* 5.4 (2016), pp. 344–55. ISSN: 2161-5063 (Electronic) 2161-5063 (Linking). DOI: 10.1021/acssynbio.5b00296. URL: https://www.ncbi.nlm.nih.gov/pubmed/26818434.

[51] David Garenne et al. "The all-E. coliTXTL toolbox 3.0: new capabilities of a cell-free synthetic biology platform". In: *Synthetic Biology* (2021). ISSN: 2397-7000. DOI: 10.1093/synbio/ysab017. URL: https://doi.org/10.1093/synbio/ysab017.

[52] Y. Shimizu et al. "Cell-free translation reconstituted with purified components". In: *Nat Biotechnol* 19.8 (2001), pp. 751–5. ISSN: 1087-0156 (Print) 1087-0156 (Linking). DOI: 10.1038/90802. URL: https://www.ncbi.nlm.nih.gov/pubmed/11479568.

[53] M. W. Nirenberg and J. H. Matthaei. "The dependence of cell-free protein synthesis in E. coli upon naturally occurring or synthetic polyribonucleotides". In: *Proc Natl Acad Sci U S A* 47 (1961), pp. 1588–602. ISSN: 0027-8424 (Print) 0027-8424 (Linking). DOI: 10.1073/pnas.47.10.1588. URL: https://www.ncbi.nlm.nih.gov/pubmed/14479932.

[54] T. W. Kim et al. "Simple procedures for the construction of a robust and cost-effective cell-free protein synthesis system". In: *J Biotechnol* 126.4 (2006), pp. 554–61. ISSN: 0168-1656 (Print) 0168-1656 (Linking). DOI: 10.1016/j.jbiotec.2006.05.014. URL: https://www.ncbi.nlm.nih.gov/pubmed/16797767.

[55] N. E. Gregorio, M. Z. Levine, and J. P. Oza. "A User's Guide to Cell-Free Protein Synthesis". In: *Methods Protoc* 2.1 (2019). ISSN: 2409-9279 (Electronic) 2409-9279 (Linking). DOI: 10.3390/mps2010024. URL: https://www.ncbi.nlm.nih.gov/pubmed/31164605.

[56] Q. M. Dudley, A. S. Karim, and M. C. Jewett. "Cell-free metabolic engineering: biomanufacturing beyond the cell". In: *Biotechnol J* 10.1 (2015), pp. 69–82. ISSN: 1860-7314 (Electronic) 1860-6768 (Linking). DOI: 10.1002/biot.201400330. URL: https://www.ncbi.nlm.nih.gov/pubmed/25319678.

[57] R. Lentini et al. "Two-Way Chemical Communication between Artificial and Natural Cells". In: *ACS Cent Sci* 3.2 (2017), pp. 117–123. ISSN: 2374-7943 (Print) 2374-7943 (Linking). DOI: 10.1021/acscentsci.6b00330. URL: https://www.ncbi.nlm.nih.gov/pubmed/28280778.

[58] H. H. Wang et al. "Multiplexed in vivo His-tagging of enzyme pathways for in vitro single-pot multienzyme catalysis". In: *ACS Synth Biol* 1.2 (2012), pp. 43–52. ISSN: 2161-5063 (Electronic) 2161-5063 (Linking). DOI: 10.1021/sb3000029. URL: https://www.ncbi.nlm.nih.gov/pubmed/22737598.

[59] T. R. Shepherd et al. "De novo design and synthesis of a 30-cistron translation-factor module". In: *Nucleic Acids Res* 45.18 (2017), pp. 10895–10905. ISSN: 1362-4962 (Electronic) 0305-1048 (Linking). DOI: 10.1093/nar/gkx753. URL: https://www.ncbi.nlm.nih.gov/pubmed/28977654.

[60] F. Villarreal et al. "Synthetic microbial consortia enable rapid assembly of pure translation machinery". In: *Nat Chem Biol* 14.1 (2018), pp. 29–35. ISSN: 1552-4469 (Electronic) 1552-4450 (Linking). DOI: 10.1038/nchembio.2514. URL: https://www.ncbi.nlm.nih.gov/pubmed/29131146.

[61] B. Lavickova and S. J. Maerkl. "A Simple, Robust, and Low-Cost Method To Produce the PURE Cell-Free System". In: *ACS Synth Biol* 8.2 (2019), pp. 455–462. ISSN: 2161-5063 (Electronic) 2161-5063 (Linking). DOI: 10.1021/acssynbio.8b00427. URL: https://www.ncbi.nlm.nih.gov/pubmed/30632751.

[62] C. Tuckey et al. "Protein synthesis using a reconstituted cell-free system". In: *Curr Protoc Mol Biol* 108 (2014), pp. 16 31 1–22. ISSN: 1934-3647 (Electronic) 1934-3647 (Linking). DOI: 10.1002/0471142727.mb1631s108. URL: https://www.ncbi.nlm.nih.gov/pubmed/25271715.

[63] M. Lewis. "The lac repressor". In: *C R Biol* 328.6 (2005), pp. 521–48. ISSN: 1631-0691 (Print) 1631-0691 (Linking). DOI: 10.1016/j.crvi.2005.04.004. URL: https://www.ncbi.nlm.nih.gov/pubmed/15950160.

[64] R. Schleif. "AraC protein, regulation of the l-arabinose operon in Escherichia coli, and the light switch mechanism of AraC action". In: *FEMS Microbiol Rev* 34.5 (2010), pp. 779–96. ISSN: 1574-6976 (Electronic) 0168-6445 (Linking). DOI: 10.1111/j.1574-6976.2010.00226.x. URL: https://www.ncbi.nlm.nih.gov/pubmed/20491933.

[65] R. Bertram and W. Hillen. "The application of Tet repressor in prokaryotic gene regulation and expression". In: *Microb Biotechnol* 1.1 (2008), pp. 2–16. ISSN: 1751-7915 (Electronic) 1751-7915 (Linking). DOI: 10.1111/j.1751-7915.2007.00001.x. URL: https://www.ncbi.nlm.nih.gov/pubmed/21261817.

[66] K. P. Adamala et al. "Engineering genetic circuit interactions within and between synthetic minimal cells". In: *Nat Chem* 9.5 (2017), pp. 431–439. ISSN: 1755-4349. DOI: 10.1038/nchem.2644. URL: https://www.ncbi.nlm.nih.gov/pubmed/28430194.

[67] R. Lentini et al. “Integrating artificial with natural cells to translate chemical messages that direct E. coli behaviour”. In: *Nat Commun* 5 (2014), p. 4012. ISSN: 2041-1723 (Electronic) 2041-1723 (Linking). DOI: 10.1038/ncomms5012. URL: https://www.ncbi.nlm.nih.gov/pubmed/24874202.

[68] J. Garamella et al. “An Adaptive Synthetic Cell Based on Mechanosensing, Biosensing, and Inducible Gene Circuits”. In: *ACS Synth Biol* 8.8 (2019), pp. 1913–1920. ISSN: 2161-5063 (Electronic) 2161-5063 (Linking). DOI: 10.1021/acssynbio.9b00204. URL: https://www.ncbi.nlm.nih.gov/pubmed/31310519.

[69] J. Engebrecht and M. Silverman. “Identification of genes and gene products necessary for bacterial bioluminescence”. In: *Proc Natl Acad Sci U S A* 81.13 (1984), pp. 4154–8. ISSN: 0027-8424 (Print) 0027-8424 (Linking). DOI: 10.1073/pnas.81.13.4154. URL: https://www.ncbi.nlm.nih.gov/pubmed/6377310.

[70] T. Miyashiro and E. G. Ruby. “Shedding light on bioluminescence regulation in Vibrio fischeri”. In: *Mol Microbiol* 84.5 (2012), pp. 795–806. ISSN: 1365-2958 (Electronic) 0950-382X (Linking). DOI: 10.1111/j.1365-2958.2012.08065.x. URL: https://www.ncbi.nlm.nih.gov/pubmed/22500943.

[71] T. D. Minogue et al. “The autoregulatory role of EsaR, a quorum-sensing regulator in Pantoea stewartii ssp. stewartii: evidence for a repressor function”. In: *Mol Microbiol* 44.6 (2002), pp. 1625–35. ISSN: 0950-382X (Print) 0950-382X (Linking). DOI: 10.1046/j.1365-2958.2002.02987.x. URL: https://www.ncbi.nlm.nih.gov/pubmed/12067349.

[72] Y. Ding et al. “Minimizing Context Dependency of Gene Networks Using Artificial Cells”. In: *ACS Appl Mater Interfaces* 10.36 (2018), pp. 30137–30146. ISSN: 1944-8252 (Electronic) 1944-8244 (Linking). DOI: 10.1021/acsami.8b10029. URL: https://www.ncbi.nlm.nih.gov/pubmed/30113814.

[73] T. D. Tang et al. “Gene-Mediated Chemical Communication in Synthetic Protocell Communities”. In: *ACS Synth Biol* 7.2 (2018), pp. 339–346. ISSN: 2161-5063 (Electronic) 2161-5063 (Linking). DOI: 10.1021/acssynbio.7b00306. URL: https://www.ncbi.nlm.nih.gov/pubmed/29091420.

[74] O. D. Toparlak et al. “Artificial cells drive neural differentiation”. In: *Sci Adv* 6.38 (2020). ISSN: 2375-2548 (Electronic) 2375-2548 (Linking). DOI: 10.1126/sciadv.abb4920. URL: https://www.ncbi.nlm.nih.gov/pubmed/32948587.

[75] S. A. Lynch and J. P. Gallivan. “A flow cytometry-based screen for synthetic riboswitches”. In: *Nucleic Acids Res* 37.1 (2009), pp. 184–92. ISSN: 1362-4962 (Electronic) 0305-1048 (Linking). DOI: 10.1093/nar/gkn924. URL: https://www.ncbi.nlm.nih.gov/pubmed/19033367.

[76] A. Espah Borujeni et al. “Automated physics-based design of synthetic riboswitches from diverse RNA aptamers”. In: *Nucleic Acids Res* 44.1 (2016), pp. 1–13. ISSN: 1362-4962 (Electronic) 0305-1048 (Linking). DOI: 10.1093/nar/gkv1289. URL: https://www.ncbi.nlm.nih.gov/pubmed/26621913.

[77] C. Tuerk and L. Gold. “Systematic evolution of ligands by exponential enrichment: RNA ligands to bacteriophage T4 DNA polymerase”. In: *Science* 249.4968 (1990), pp. 505–10. ISSN: 0036-8075 (Print) 0036-8075 (Linking). DOI: 10.1126/science.2200121. URL: https://www.ncbi.nlm.nih.gov/pubmed/2200121.

[78] A. D. Ellington and J. W. Szostak. “In vitro selection of RNA molecules that bind specific ligands”. In: *Nature* 346.6287 (1990), pp. 818–22. ISSN: 0028-0836 (Print) 0028-0836 (Linking). DOI: 10.1038/346818a0. URL: https://www.ncbi.nlm.nih.gov/pubmed/1697402.

[79] M. Dwidar et al. “Programmable Artificial Cells Using Histamine-Responsive Synthetic Riboswitch”. In: *J Am Chem Soc* 141.28 (2019), pp. 11103–11114. ISSN:

1520-5126 (Electronic) 0002-7863 (Linking). DOI: 10.1021/jacs.9b03300. URL: https://www.ncbi.nlm.nih.gov/pubmed/31241330.

[80] A. A. Green et al. "Toehold switches: de-novo-designed regulators of gene expression". In: *Cell* 159.4 (2014), pp. 925–39. ISSN: 1097-4172 (Electronic) 0092-8674 (Linking). DOI: 10.1016/j.cell.2014.10.002. URL: https://www.ncbi.nlm.nih.gov/pubmed/25417166.

[81] P. Q. Nguyen et al. "Wearable materials with embedded synthetic biology sensors for biomolecule detection". In: *Nat Biotechnol* 39.11 (2021), pp. 1366–1374. ISSN: 1546-1696 (Electronic) 1087-0156 (Linking). DOI: 10.1038/s41587-021-00950-3. URL: https://www.ncbi.nlm.nih.gov/pubmed/34183860.

[82] M. Nallani et al. "A nanophosphor-based method for selective DNA recovery in Synthosomes". In: *Biotechnol J* 1.7-8 (2006), pp. 828–34. ISSN: 1860-7314 (Electronic) 1860-6768 (Linking). DOI: 10.1002/biot.200600042. URL: https://www.ncbi.nlm.nih.gov/pubmed/16927281.

[83] D. Hartmann et al. "Controlling gene expression with light: a multidisciplinary endeavour". In: *Biochem Soc Trans* 48.4 (2020), pp. 1645–1659. ISSN: 1470-8752 (Electronic) 0300-5127 (Linking). DOI: 10.1042/BST20200014. URL: https://www.ncbi.nlm.nih.gov/pubmed/32657338.

[84] P. Jayaraman et al. "Cell-Free Optogenetic Gene Expression System". In: *ACS Synth Biol* 7.4 (2018), pp. 986–994. ISSN: 2161-5063 (Electronic) 2161-5063 (Linking). DOI: 10.1021/acssynbio.7b00422. URL: https://www.ncbi.nlm.nih.gov/pubmed/29596741.

[85] P. Zhang et al. "Bringing Light into Cell-Free Expression". In: *ACS Synth Biol* 9.8 (2020), pp. 2144–2153. ISSN: 2161-5063 (Electronic) 2161-5063 (Linking). DOI:

10.1021/acssynbio.0c00211. URL: https://www.ncbi.nlm.nih.gov/pubmed/32603590.

[86] A. Moglich, R. A. Ayers, and K. Moffat. "Design and signaling mechanism of light-regulated histidine kinases". In: *J Mol Biol* 385.5 (2009), pp. 1433–44. ISSN: 1089-8638 (Electronic) 0022-2836 (Linking). DOI: 10.1016/j.jmb.2008.12.017. URL: https://www.ncbi.nlm.nih.gov/pubmed/19109976.

[87] R. Ohlendorf et al. "From dusk till dawn: one-plasmid systems for light-regulated gene expression". In: *J Mol Biol* 416.4 (2012), pp. 534–42. ISSN: 1089-8638 (Electronic) 0022-2836 (Linking). DOI: 10.1016/j.jmb.2012.01.001. URL: https://www.ncbi.nlm.nih.gov/pubmed/22245580.

[88] A. I. Nash et al. "Structural basis of photosensitivity in a bacterial light-oxygen-voltage/helix-turn-helix (LOV-HTH) DNA-binding protein". In: *Proc Natl Acad Sci U S A* 108.23 (2011), pp. 9449–54. ISSN: 1091-6490 (Electronic) 0027-8424 (Linking). DOI: 10.1073/pnas.1100262108. URL: https://www.ncbi.nlm.nih.gov/pubmed/21606338.

[89] G. Rivera-Cancel, L. B. Motta-Mena, and K. H. Gardner. "Identification of natural and artificial DNA substrates for light-activated LOV-HTH transcription factor EL222". In: *Biochemistry* 51.50 (2012), pp. 10024–34. ISSN: 1520-4995 (Electronic) 0006-2960 (Linking). DOI: 10.1021/bi301306t. URL: https://www.ncbi.nlm.nih.gov/pubmed/23205774.

[90] P. Jayaraman et al. "Blue light-mediated transcriptional activation and repression of gene expression in bacteria". In: *Nucleic Acids Res* 44.14 (2016), pp. 6994–7005. ISSN: 1362-4962 (Electronic) 0305-1048 (Linking). DOI: 10.1093/nar/gkw548. URL: https://www.ncbi.nlm.nih.gov/pubmed/27353329.

[91] W. T. Monroe et al. “Targeting expression with light using caged DNA”. In: *J Biol Chem* 274.30 (1999), pp. 20895–900. ISSN: 0021-9258 (Print) 0021-9258 (Linking). DOI: 10.1074/jbc.274.30.20895. URL: https://www.ncbi.nlm.nih.gov/pubmed/10409633.

[92] A. Schroeder et al. “Remotely activated protein-producing nanoparticles”. In: *Nano Lett* 12.6 (2012), pp. 2685–9. ISSN: 1530-6992 (Electronic) 1530-6984 (Linking). DOI: 10.1021/nl2036047. URL: https://www.ncbi.nlm.nih.gov/pubmed/22432731.

[93] V. Chan et al. “Controlled Transcription of Exogenous mRNA in Platelets Using Protocells”. In: *Angew Chem Int Ed Engl* 54.46 (2015), pp. 13590–3. ISSN: 1521-3773 (Electronic) 1433-7851 (Linking). DOI: 10.1002/anie.201506500. URL: https://www.ncbi.nlm.nih.gov/pubmed/26368852.

[94] M. J. Booth et al. “Light-activated communication in synthetic tissues”. In: *Sci Adv* 2.4 (2016), e1600056. ISSN: 2375-2548 (Electronic) 2375-2548 (Linking). DOI: 10.1126/sciadv.1600056. URL: https://www.ncbi.nlm.nih.gov/pubmed/27051884.

[95] M. J. Booth et al. “Functional aqueous droplet networks”. In: *Mol Biosyst* 13.9 (2017), pp. 1658–1691. ISSN: 1742-2051 (Electronic) 1742-2051 (Linking). DOI: 10.1039/c7mb00192d. URL: https://www.ncbi.nlm.nih.gov/pubmed/28766622.

[96] Y. Kamiya et al. “Synthetic gene involving azobenzene-tethered T7 promoter for the photocontrol of gene expression by visible light”. In: *ACS Synth Biol* 4.4 (2015), pp. 365–70. ISSN: 2161-5063 (Electronic) 2161-5063 (Linking). DOI: 10.1021/sb5001092. URL: https://www.ncbi.nlm.nih.gov/pubmed/25144622.

[97] A. Estevez-Torres et al. “Sequence-independent and reversible photocontrol of transcription/expression systems using a photosensitive nucleic acid binder”. In: *Proc Natl Acad Sci U S A* 106.30 (2009), pp. 12219–23. ISSN: 1091-6490 (Electronic)

0027-8424 (Linking). DOI: 10.1073/pnas.0904382106. URL: https://www.ncbi.nlm.nih.gov/pubmed/19617550.

[98] A. Venancio-Marques et al. "Modification-free photocontrol of beta-lactam conversion with spatiotemporal resolution". In: *ACS Synth Biol* 1.11 (2012), pp. 526–31. ISSN: 2161-5063 (Electronic) 2161-5063 (Linking). DOI: 10.1021/sb300010a. URL: https://www.ncbi.nlm.nih.gov/pubmed/23656229.

[99] A. Diguet et al. "UV-induced bursting of cell-sized multicomponent lipid vesicles in a photosensitive surfactant solution". In: *J Am Chem Soc* 134.10 (2012), pp. 4898–904. ISSN: 1520-5126 (Electronic) 0002-7863 (Linking). DOI: 10.1021/ja211664f. URL: https://www.ncbi.nlm.nih.gov/pubmed/22316240.

[100] S. Zhang et al. "Engineering motile aqueous phase-separated droplets via liposome stabilisation". In: *Nat Commun* 12.1 (2021), p. 1673. ISSN: 2041-1723 (Electronic) 2041-1723 (Linking). DOI: 10.1038/s41467-021-21832-x. URL: https://www.ncbi.nlm.nih.gov/pubmed/33723263.

[101] B. C. Buddingh, J. Elzinga, and J. C. M. van Hest. "Intercellular communication between artificial cells by allosteric amplification of a molecular signal". In: *Nat Commun* 11.1 (2020), p. 1652. ISSN: 2041-1723 (Electronic) 2041-1723 (Linking). DOI: 10.1038/s41467-020-15482-8. URL: https://www.ncbi.nlm.nih.gov/pubmed/32246068.

[102] G. Rampioni et al. "Synthetic cells produce a quorum sensing chemical signal perceived by Pseudomonas aeruginosa". In: *Chem Commun (Camb)* 54.17 (2018), pp. 2090–2093. ISSN: 1364-548X (Electronic) 1359-7345 (Linking). DOI: 10.1039/c7cc09678j. URL: https://www.ncbi.nlm.nih.gov/pubmed/29334092.

[103] Bruce Alberts. *Molecular biology of the cell*. 5th. New York: Garland Science, 2008. ISBN: 9780815341055.

[104] P. R. Baraniak and T. C. McDevitt. "Stem cell paracrine actions and tissue regeneration". In: *Regen Med* 5.1 (2010), pp. 121–43. ISSN: 1746-076X (Electronic) 1746-0751 (Linking). DOI: 10.2217/rme.09.74. URL: https://www.ncbi.nlm.nih.gov/pubmed/20017699.

[105] S. T. Rutherford and B. L. Bassler. "Bacterial quorum sensing: its role in virulence and possibilities for its control". In: *Cold Spring Harb Perspect Med* 2.11 (2012). ISSN: 2157-1422 (Electronic) 2157-1422 (Linking). DOI: 10.1101/cshperspect.a012427. URL: https://www.ncbi.nlm.nih.gov/pubmed/23125205.

[106] N. A. Whitehead et al. "Quorum-sensing in Gram-negative bacteria". In: *FEMS Microbiol Rev* 25.4 (2001), pp. 365–404. ISSN: 0168-6445 (Print) 0168-6445 (Linking). DOI: 10.1111/j.1574-6976.2001.tb00583.x. URL: https://www.ncbi.nlm.nih.gov/pubmed/11524130.

[107] Scott F. Gilbert. *Developmental biology.* 6th. Sunderland, Mass.: Sinauer Associates, 2000, xviii, 749 p. ISBN: 0878932437 (cloth).

[108] S. J. Bray. "Notch signalling: a simple pathway becomes complex". In: *Nat Rev Mol Cell Biol* 7.9 (2006), pp. 678–89. ISSN: 1471-0072 (Print) 1471-0072 (Linking). DOI: 10.1038/nrm2009. URL: https://www.ncbi.nlm.nih.gov/pubmed/16921404.

[109] N. J. Severs. "The Cardiac Gap Junction and Intercalated Disk". In: *International Journal of Cardiology* 26.2 (1990), pp. 137–173. ISSN: 0167-5273. DOI: Doi10.1016/0167-5273(90)90030-9. URL: %3CGo%20to%20ISI%3E://WOS:A1990CM85400002.

[110] L. C. Antunes et al. "Transcriptome analysis of the Vibrio fischeri LuxR-LuxI regulon". In: *J Bacteriol* 189.22 (2007), pp. 8387–91. ISSN: 1098-5530 (Electronic) 0021-9193 (Linking). DOI: 10.1128/JB.00736-07. URL: https://www.ncbi.nlm.nih.gov/pubmed/17827287.

[111] W. C. Fuqua, S. C. Winans, and E. P. Greenberg. "Quorum sensing in bacteria: the LuxR-LuxI family of cell density-responsive transcriptional regulators". In: *J Bacteriol* 176.2 (1994), pp. 269–75. ISSN: 0021-9193 (Print) 0021-9193 (Linking). DOI: 10.1128/jb.176.2.269-275.1994. URL: https://www.ncbi.nlm.nih.gov/pubmed/8288518.

[112] M. J. Gambello and B. H. Iglewski. "Cloning and characterization of the Pseudomonas aeruginosa lasR gene, a transcriptional activator of elastase expression". In: *J Bacteriol* 173.9 (1991), pp. 3000–9. ISSN: 0021-9193 (Print) 0021-9193 (Linking). DOI: 10.1128/jb.173.9.3000-3009.1991. URL: https://www.ncbi.nlm.nih.gov/pubmed/1902216.

[113] J. P. Pearson et al. "Structure of the autoinducer required for expression of Pseudomonas aeruginosa virulence genes". In: *Proc Natl Acad Sci U S A* 91.1 (1994), pp. 197–201. ISSN: 0027-8424 (Print) 0027-8424 (Linking). DOI: 10.1073/pnas.91.1.197. URL: https://www.ncbi.nlm.nih.gov/pubmed/8278364.

[114] U. A. Ochsner et al. "Isolation and characterization of a regulatory gene affecting rhamnolipid biosurfactant synthesis in Pseudomonas aeruginosa". In: *J Bacteriol* 176.7 (1994), pp. 2044–54. ISSN: 0021-9193 (Print) 0021-9193 (Linking). DOI: 10.1128/jb.176.7.2044-2054.1994. URL: https://www.ncbi.nlm.nih.gov/pubmed/8144472.

[115] J. P. Pearson et al. "A second N-acylhomoserine lactone signal produced by Pseudomonas aeruginosa". In: *Proc Natl Acad Sci U S A* 92.5 (1995), pp. 1490–4. ISSN: 0027-8424 (Print) 0027-8424 (Linking). DOI: 10.1073/pnas.92.5.1490. URL: https://www.ncbi.nlm.nih.gov/pubmed/7878006.

[116] L. Zhang et al. "Agrobacterium conjugation and gene regulation by N-acyl-L-homoserine lactones". In: *Nature* 362.6419 (1993), pp. 446–8. ISSN: 0028-0836 (Print)

0028-0836 (Linking). DOI: 10.1038/362446a0. URL: https://www.ncbi.nlm.nih.gov/pubmed/8464475.

[117] W. C. Fuqua and S. C. Winans. "A LuxR-LuxI type regulatory system activates Agrobacterium Ti plasmid conjugal transfer in the presence of a plant tumor metabolite". In: *J Bacteriol* 176.10 (1994), pp. 2796–806. ISSN: 0021-9193 (Print) 0021-9193 (Linking). DOI: 10.1128/jb.176.10.2796-2806.1994. URL: https://www.ncbi.nlm.nih.gov/pubmed/8188582.

[118] René Michele Davis, Ryan Yue Muller, and Karmella Ann Haynes. "Can the Natural Diversity of Quorum-Sensing Advance Synthetic Biology?" In: *Frontiers in Bioengineering and Biotechnology* 3 (2015), p. 30. ISSN: 2296-4185. URL: https://www.frontiersin.org/article/10.3389/fbioe.2015.00030.

[119] A. L. Schaefer et al. "A new class of homoserine lactone quorum-sensing signals". In: *Nature* 454.7204 (2008), pp. 595–9. ISSN: 1476-4687 (Electronic) 0028-0836 (Linking). DOI: 10.1038/nature07088. URL: https://www.ncbi.nlm.nih.gov/pubmed/18563084.

[120] N. A. Ahlgren et al. "Aryl-homoserine lactone quorum sensing in stem-nodulating photosynthetic bradyrhizobia". In: *Proc Natl Acad Sci U S A* 108.17 (2011), pp. 7183–8. ISSN: 1091-6490 (Electronic) 0027-8424 (Linking). DOI: 10.1073/pnas.1103821108. URL: https://www.ncbi.nlm.nih.gov/pubmed/21471459.

[121] A. Lindemann et al. "Isovaleryl-homoserine lactone, an unusual branched-chain quorum-sensing signal from the soybean symbiont Bradyrhizobium japonicum". In: *Proc Natl Acad Sci U S A* 108.40 (2011), pp. 16765–70. ISSN: 1091-6490 (Electronic) 0027-8424 (Linking). DOI: 10.1073/pnas.1114125108. URL: https://www.ncbi.nlm.nih.gov/pubmed/21949379.

[122] T. Chakraborty and S. V. Wegner. "Cell to Cell Signaling through Light in Artificial Cell Communities: Glowing Predator Lures Prey". In: *ACS Nano* 15.6 (2021), pp. 9434–9444. ISSN: 1936-086X (Electronic) 1936-0851 (Linking). DOI: 10.1021/acsnano.1c01600. URL: https://www.ncbi.nlm.nih.gov/pubmed/34152740.

[123] Y. Elani, R. V. Law, and O. Ces. "Vesicle-based artificial cells as chemical microreactors with spatially segregated reaction pathways". In: *Nature Communications* 5 (2014). ISSN: 2041-1723. DOI: ARTN530510.1038/ncomms6305. URL: %3CGo%20to%20ISI%3E://WOS:000344061500004.

[124] B. B. Johnson and A. P. Heuck. "Perfringolysin O structure and mechanism of pore formation as a paradigm for cholesterol-dependent cytolysins". In: *Subcell Biochem* 80 (2014), pp. 63–81. ISSN: 0306-0225 (Print) 0306-0225 (Linking). DOI: 10.1007/978-94-017-8881-6_5. URL: https://www.ncbi.nlm.nih.gov/pubmed/24798008.

[125] K. Y. Wen et al. "A Cell-Free Biosensor for Detecting Quorum Sensing Molecules in P. aeruginosa-Infected Respiratory Samples". In: *ACS Synth Biol* 6.12 (2017), pp. 2293–2301. ISSN: 2161-5063 (Electronic) 2161-5063 (Linking). DOI: 10.1021/acssynbio.7b00219. URL: https://www.ncbi.nlm.nih.gov/pubmed/28981256.

[126] K. Adamala and J. W. Szostak. "Nonenzymatic Template-Directed RNA Synthesis Inside Model Protocells". In: *Science* 342.6162 (2013), pp. 1098–1100. ISSN: 0036-8075. DOI: 10.1126/science.1241888. URL: %3CGo%20to%20ISI%3E://WOS:000327518600058.

[127] E. Beltran-Gracia et al. "Nanomedicine review: clinical developments in liposomal applications". In: *Cancer Nanotechnology* 10.1 (2019). ISSN: 1868-6958. DOI: ARTN1110.1186/s12645-019-0055-y. URL: %3CGo%20to%20ISI%3E://WOS:000504928200002.

[128] K. Miller et al. “HERMIONE: a randomized Phase 2 trial of MM-302 plus trastuzumab versus chemotherapy of physician’s choice plus trastuzumab in patients with previously treated, anthracycline-naive, HER2-positive, locally advanced/metastatic breast cancer”. In: *BMC Cancer* 16 (2016), p. 352. ISSN: 1471-2407 (Electronic) 1471-2407 (Linking). DOI: 10.1186/s12885-016-2385-z. URL: https://www.ncbi.nlm.nih.gov/pubmed/27259714.

[129] P. C. Lyon et al. “Clinical trial protocol for TARDOX: a phase I study to investigate the feasibility of targeted release of lyso-thermosensitive liposomal doxorubicin (ThermoDox (R)) using focused ultrasound in patients with liver tumours”. In: *Journal of Therapeutic Ultrasound* 5 (2017). ISSN: 2050-5736. DOI: ARTN2810.1186/s40349-017-0104-0. URL: %3CGo%20to%20ISI%3E://WOS:000414177100001.

[130] M. H. M. E. van Stevendaal, J. C. M. van Hest, and A. F. Mason. “Functional Interactions Between Bottom-Up Synthetic Cells and Living Matter for Biomedical Applications”. In: *Chemsystemschem* 3.5 (2021). DOI: 10.1002/syst.202100009. URL: %3CGo%20to%20ISI%3E://WOS:000657819400001.

[131] M. Amidi et al. “Antigen-expressing immunostimulatory liposomes as a genetically programmable synthetic vaccine”. In: *Syst Synth Biol* 5.1-2 (2011), pp. 21–31. ISSN: 1872-5333 (Electronic) 1872-5325 (Linking). DOI: 10.1007/s11693-010-9066-z. URL: https://www.ncbi.nlm.nih.gov/pubmed/21949673.

[132] N. Krinsky et al. “Synthetic Cells Synthesize Therapeutic Proteins inside Tumors”. In: *Adv Healthc Mater* 7.9 (2018), e1701163. ISSN: 2192-2659 (Electronic) 2192-2640 (Linking). DOI: 10.1002/adhm.201701163. URL: https://www.ncbi.nlm.nih.gov/pubmed/29283226.

[133] Z. Chen et al. “Synthetic beta cells for fusion-mediated dynamic insulin secretion”. In: *Nat Chem Biol* 14.1 (2018), pp. 86–93. ISSN: 1552-4469 (Electronic) 1552-4450

(Linking). DOI: 10.1038/nchembio.2511. URL: https://www.ncbi.nlm.nih.gov/pubmed/29083418.

[134] Leticia Hosta-Rigau et al. "Extracellular Microreactor for the Depletion of Phenylalanine Toward Phenylketonuria Treatment". In: *Advanced Functional Materials* 25.25 (2015), pp. 3860–3869. ISSN: 1616-301X. DOI: https://doi.org/10.1002/adfm.201404180. URL: https://doi.org/10.1002/adfm.201404180.

[135] M. K. Rhoads et al. "Incorporating LsrK AI-2 quorum quenching capability in a functionalized biopolymer capsule". In: *Biotechnol Bioeng* 115.2 (2018), pp. 278–289. ISSN: 1097-0290 (Electronic) 0006-3592 (Linking). DOI: 10.1002/bit.26397. URL: https://www.ncbi.nlm.nih.gov/pubmed/28782813.

[136] S. Liu et al. "Enzyme-mediated nitric oxide production in vasoactive erythrocyte membrane-enclosed coacervate protocells". In: *Nat Chem* 12.12 (2020), pp. 1165–1173. ISSN: 1755-4349 (Electronic) 1755-4330 (Linking). DOI: 10.1038/s41557-020-00585-y. URL: https://www.ncbi.nlm.nih.gov/pubmed/33219364.

[137] M. Amidi et al. "Induction of humoral and cellular immune responses by antigen-expressing immunostimulatory liposomes". In: *J Control Release* 164.3 (2012), pp. 323–30. ISSN: 1873-4995 (Electronic) 0168-3659 (Linking). DOI: 10.1016/j.jconrel.2012.08.016. URL: https://www.ncbi.nlm.nih.gov/pubmed/22940204.

[138] A. Lanzi et al. "Effects of antigen-expressing immunostimulatory liposomes on chemotaxis and maturation of dendritic cells in vitro and in human skin explants". In: *Pharm Res* 31.2 (2014), pp. 516–26. ISSN: 1573-904X (Electronic) 0724-8741 (Linking). DOI: 10.1007/s11095-013-1179-0. URL: https://www.ncbi.nlm.nih.gov/pubmed/24072262.

[139] A. D. Bangham and R. W. Horne. "Negative Staining of Phospholipids + Their Structural Modification by-Surface Active Agents as Observed in Electron Microscope". In: *Journal of Molecular Biology* 8.5 (1964), 660–. ISSN: 0022-2836. DOI: Doi10.1016/S0022-2836(64)80115-7. URL: %3CGo%20to%20ISI%3E://WOS:A19645823B00001.

[140] Rumiana Dimova and Carlos Marques. *The giant vesicle book*. Boca Raton, FL: CRC Press, Taylor Francis Group, 2019.

[141] H. Stein et al. "Production of Isolated Giant Unilamellar Vesicles under High Salt Concentrations". In: *Front Physiol* 8 (2017), p. 63. ISSN: 1664-042X (Print) 1664-042X (Linking). DOI: 10.3389/fphys.2017.00063. URL: https://www.ncbi.nlm.nih.gov/pubmed/28243205.

[142] K. Tsumoto et al. "Efficient formation of giant liposomes through the gentle hydration of phosphatidylcholine films doped with sugar". In: *Colloids Surf B Biointerfaces* 68.1 (2009), pp. 98–105. ISSN: 1873-4367 (Electronic) 0927-7765 (Linking). DOI: 10.1016/j.colsurfb.2008.09.023. URL: https://www.ncbi.nlm.nih.gov/pubmed/18993037.

[143] K. Akashi et al. "Preparation of giant liposomes in physiological conditions and their characterization under an optical microscope". In: *Biophys J* 71.6 (1996), pp. 3242–50. ISSN: 0006-3495 (Print) 0006-3495 (Linking). DOI: 10.1016/S0006-3495(96)79517-6. URL: https://www.ncbi.nlm.nih.gov/pubmed/8968594.

[144] K. S. Horger et al. "Films of agarose enable rapid formation of giant liposomes in solutions of physiologic ionic strength". In: *J Am Chem Soc* 131.5 (2009), pp. 1810–9. ISSN: 1520-5126 (Electronic) 0002-7863 (Linking). DOI: 10.1021/ja805625u. URL: https://www.ncbi.nlm.nih.gov/pubmed/19154115.

[145] A. Weinberger et al. “Gel-assisted formation of giant unilamellar vesicles”. In: *Biophys J* 105.1 (2013), pp. 154–64. ISSN: 1542-0086 (Electronic) 0006-3495 (Linking). DOI: 10.1016/j.bpj.2013.05.024. URL: https://www.ncbi.nlm.nih.gov/pubmed/23823234.

[146] N. Lopez Mora et al. “Preparation of size tunable giant vesicles from cross-linked dextran(ethylene glycol) hydrogels”. In: *Chem Commun (Camb)* 50.16 (2014), pp. 1953–5. ISSN: 1364-548X (Electronic) 1359-7345 (Linking). DOI: 10.1039/c3cc49144g. URL: https://www.ncbi.nlm.nih.gov/pubmed/24407820.

[147] F. Szoka et al. “Preparation of unilamellar liposomes of intermediate size (0.1-0.2 mumol) by a combination of reverse phase evaporation and extrusion through polycarbonate membranes”. In: *Biochim Biophys Acta* 601.3 (1980), pp. 559–71. ISSN: 0006-3002 (Print) 0006-3002 (Linking). DOI: 10.1016/0005-2736(80)90558-1. URL: https://www.ncbi.nlm.nih.gov/pubmed/6251878.

[148] Z. Nourian, W. Roelofsen, and C. Danelon. “Triggered gene expression in fed-vesicle microreactors with a multifunctional membrane”. In: *Angew Chem Int Ed Engl* 51.13 (2012), pp. 3114–8. ISSN: 1521-3773 (Electronic) 1433-7851 (Linking). DOI: 10.1002/anie.201107123. URL: https://www.ncbi.nlm.nih.gov/pubmed/22246637.

[149] J. A. Peruzzi et al. “Barcoding Biological Reactions with DNA-Functionalized Vesicles”. In: *Angew Chem Int Ed Engl* 58.51 (2019), pp. 18683–18690. ISSN: 1521-3773 (Electronic) 1433-7851 (Linking). DOI: 10.1002/anie.201911544. URL: https://www.ncbi.nlm.nih.gov/pubmed/31596992.

[150] Miglena I. Angelova and Dimiter S. Dimitrov. “Liposome electroformation”. In: *Faraday Discussions of the Chemical Society* 81.0 (1986), pp. 303–311. ISSN: 0301-

7249. DOI: 10.1039/DC9868100303. URL: http://dx.doi.org/10.1039/DC9868100303.

[151] M. C. Blosser, B. G. Horst, and S. L. Keller. "cDICE method produces giant lipid vesicles under physiological conditions of charged lipids and ionic solutions". In: *Soft Matter* 12.35 (2016), pp. 7364–71. ISSN: 1744-6848 (Electronic) 1744-683X (Linking). DOI: 10.1039/c6sm00868b. URL: https://www.ncbi.nlm.nih.gov/pubmed/27510092.

[152] A. C. Spencer, P. Torre, and S. S. Mansy. "The encapsulation of cell-free transcription and translation machinery in vesicles for the construction of cellular mimics". In: *J Vis Exp* 80 (2013), e51304. ISSN: 1940-087X (Electronic) 1940-087X (Linking). DOI: 10.3791/51304. URL: https://www.ncbi.nlm.nih.gov/pubmed/24192867.

[153] S. Pautot, B. J. Frisken, and D. A. Weitz. "Production of unilamellar vesicles using an inverted emulsion". In: *Langmuir* 19.7 (2003), pp. 2870–2879. ISSN: 0743-7463. DOI: 10.1021/la026100v. URL: %3CGo%20to%20ISI%3E://WOS:000181980900049.

[154] M. Chiba, M. Miyazaki, and S. Ishiwata. "Quantitative Analysis of the Lamellarity of Giant Liposomes Prepared by the Inverted Emulsion Method". In: *Biophysical Journal* 107.2 (2014), pp. 346–354. ISSN: 0006-3495. DOI: 10.1016/j.bpj.2014.05.039. URL: %3CGo%20to%20ISI%3E://WOS:000339148500010.

[155] S. Fujii et al. "Liposome display for in vitro selection and evolution of membrane proteins". In: *Nat Protoc* 9.7 (2014), pp. 1578–91. ISSN: 1750-2799 (Electronic) 1750-2799 (Linking). DOI: 10.1038/nprot.2014.107. URL: https://www.ncbi.nlm.nih.gov/pubmed/24901741.

[156] K. Nishimura et al. "Size control of giant unilamellar vesicles prepared from inverted emulsion droplets". In: *Journal of Colloid and Interface Science* 376 (2012),

pp. 119–125. ISSN: 0021-9797. DOI: 10.1016/j.jcis.2012.02.029. URL: %3CGo%20to%20ISI%3E://WOS:000303422800017.

[157] P. C. Hu and N. Malmstadt. "Microfluidic Fabrication of Asymmetric Giant Lipid Vesicles". In: *Biophysical Journal* 100.3 (2011), pp. 169–169. ISSN: 0006-3495. URL: %3CGo%20to%20ISI%3E://WOS:000306288601313.

[158] M. Abkarian, E. Loiseau, and G. Massiera. "Continuous droplet interface crossing encapsulation (cDICE) for high throughput monodisperse vesicle design". In: *Soft Matter* 7.10 (2011), pp. 4610–4614. ISSN: 1744-683x. DOI: 10.1039/c1sm05239j. URL: %3CGo%20to%20ISI%3E://WOS:000290227400006.

[159] L. Van de Cauter et al. "Optimized cDICE for Efficient Reconstitution of Biological Systems in Giant Unilamellar Vesicles". In: *Acs Synthetic Biology* 10.7 (2021), pp. 1690–1702. ISSN: 2161-5063. DOI: 10.1021/acssynbio.1c00068. URL: %3CGo%20to%20ISI%3E://WOS:000674933400012.

[160] N. N. Deng, M. Yelleswarapu, and W. T. S. Huck. "Monodisperse Uni- and Multicompartment Liposomes". In: *Journal of the American Chemical Society* 138.24 (2016), pp. 7584–7591. ISSN: 0002-7863. DOI: 10.1021/jacs.6b02107. URL: %3CGo%20to%20ISI%3E://WOS:000378584600030.

[161] S. Deshpande et al. "Octanol-assisted liposome assembly on chip". In: *Nature Communications* 7 (2016). ISSN: 2041-1723. DOI: ARTN1044710.1038/ncomms10447. URL: %3CGo%20to%20ISI%3E://WOS:000369023100002.

[162] M. Weiss et al. "Sequential bottom-up assembly of mechanically stabilized synthetic cells by microfluidics". In: *Nature Materials* 17.1 (2018), pp. 89–+. ISSN: 1476-1122. DOI: 10.1038/Nmat5005. URL: %3CGo%20to%20ISI%3E://WOS:000422790000020.

[163] N. Yandrapalli et al. "Surfactant-free production of biomimetic giant unilamellar vesicles using PDMS-based microfluidics". In: *Communications Chemistry* 4.1

(2021). ISSN: 2399-3669. DOI: ARTN10010 . 1038 / s42004 - 021 - 00530 - 1. URL: %3CGo%20to%20ISI%3E://WOS:000671141300001.

[164] T. Trantidou et al. "Droplet microfluidics for the construction of compartmentalised model membranes". In: *Lab on a Chip* 18.17 (2018), pp. 2488–2509. ISSN: 1473-0197. DOI: 10 . 1039 / c8lc00028j. URL: %3CGo%20to%20ISI%3E : / / WOS : 000443279400001.

[165] S. Matosevic and B. M. Paegel. "Stepwise Synthesis of Giant Unilamellar Vesicles on a Microfluidic Assembly Line". In: *Journal of the American Chemical Society* 133.9 (2011), pp. 2798–2800. ISSN: 0002-7863. DOI: 10 . 1021 / ja109137s. URL: %3CGo%20to%20ISI%3E://WOS:000289455200002.

[166] K. Karamdad et al. "Preparation and mechanical characterisation of giant unilamellar vesicles by a microfluidic method". In: *Lab on a Chip* 15.2 (2015), pp. 557–562. ISSN: 1473-0197. DOI: 10.1039/c4lc01277a. URL: %3CGo%20to%20ISI%3E://WOS:000346477500021.

[167] X. Ge, D. Luo, and J. Xu. "Cell-free protein expression under macromolecular crowding conditions". In: *PLoS One* 6.12 (2011), e28707. ISSN: 1932-6203 (Electronic) 1932-6203 (Linking). DOI: 10.1371/journal.pone.0028707. URL: https://www.ncbi.nlm.nih.gov/pubmed/22174874.

[168] G. Bolognesi et al. "Sculpting and fusing biomimetic vesicle networks using optical tweezers". In: *Nat Commun* 9.1 (2018), p. 1882. ISSN: 2041-1723 (Electronic) 2041-1723 (Linking). DOI: 10.1038/s41467-018-04282-w. URL: https://www.ncbi.nlm.nih.gov/pubmed/29760422.

[169] Daniela Azucena Garcia Soriano. "Towards Bottom-up Reconstitution of a Minimal Division Machinery: Characterization of FtsZ chimera protein in different membrane systems". Thesis. 2018.

[170] Hang Zhao. “Synthetic membranes in microfluidic interfaces”. Thesis. 2017.

[171] A. Moga et al. “Optimization of the Inverted Emulsion Method for High-Yield Production of Biomimetic Giant Unilamellar Vesicles”. In: *Chembiochem* 20.20 (2019), pp. 2674–2682. ISSN: 1439-7633 (Electronic) 1439-4227 (Linking). DOI: 10.1002/cbic.201900529. URL: https://www.ncbi.nlm.nih.gov/pubmed/31529570.

[172] R. Sakamoto, V. Noireaux, and Y. T. Maeda. “Anomalous Scaling of Gene Expression in Confined Cell-Free Reactions”. In: *Sci Rep* 8.1 (2018), p. 7364. ISSN: 2045-2322 (Electronic) 2045-2322 (Linking). DOI: 10.1038/s41598-018-25532-3. URL: https://www.ncbi.nlm.nih.gov/pubmed/29743508.

[173] M. M. Hansen et al. “Macromolecular crowding creates heterogeneous environments of gene expression in picolitre droplets”. In: *Nat Nanotechnol* 11.2 (2016), pp. 191–7. ISSN: 1748-3395 (Electronic) 1748-3387 (Linking). DOI: 10.1038/nnano.2015.243. URL: https://www.ncbi.nlm.nih.gov/pubmed/26501750.

[174] E. Altamura et al. “Extrinsic stochastic factors (solute partition) in gene expression inside lipid vesicles and lipid-stabilized water-in-oil droplets: a review”. In: *Synth Biol (Oxf)* 3.1 (2018), ysy011. ISSN: 2397-7000 (Electronic) 2397-7000 (Linking). DOI: 10.1093/synbio/ysy011. URL: https://www.ncbi.nlm.nih.gov/pubmed/32995519.

[175] T. Conrad et al. “Maximizing transcription of nucleic acids with efficient T7 promoters”. In: *Commun Biol* 3.1 (2020), p. 439. ISSN: 2399-3642 (Electronic) 2399-3642 (Linking). DOI: 10.1038/s42003-020-01167-x. URL: https://www.ncbi.nlm.nih.gov/pubmed/32796901.

[176] P. O. Olins and S. H. Rangwala. “A novel sequence element derived from bacteriophage T7 mRNA acts as an enhancer of translation of the lacZ gene in Escherichia

coli". In: *J Biol Chem* 264.29 (1989), pp. 16973–6. ISSN: 0021-9258 (Print) 0021-9258 (Linking). URL: https://www.ncbi.nlm.nih.gov/pubmed/2676996.

[177] S. Takahashi et al. "Translation enhancer improves the ribosome liberation from translation initiation". In: *J Am Chem Soc* 135.35 (2013), pp. 13096–106. ISSN: 1520-5126 (Electronic) 0002-7863 (Linking). DOI: 10.1021/ja405967h. URL: https://www.ncbi.nlm.nih.gov/pubmed/23927491.

[178] I. V. Boni et al. "Ribosome-messenger recognition: mRNA target sites for ribosomal protein S1". In: *Nucleic Acids Res* 19.1 (1991), pp. 155–62. ISSN: 0305-1048 (Print) 0305-1048 (Linking). DOI: 10.1093/nar/19.1.155. URL: https://www.ncbi.nlm.nih.gov/pubmed/2011495.

[179] D. R. Gallie and C. I. Kado. "A translational enhancer derived from tobacco mosaic virus is functionally equivalent to a Shine-Dalgarno sequence". In: *Proc Natl Acad Sci U S A* 86.1 (1989), pp. 129–32. ISSN: 0027-8424 (Print) 0027-8424 (Linking). DOI: 10.1073/pnas.86.1.129. URL: https://www.ncbi.nlm.nih.gov/pubmed/2643095.

[180] G. Rampioni et al. "Gene-Expressing Liposomes as Synthetic Cells for Molecular Communication Studies". In: *Front Bioeng Biotechnol* 7 (2019), p. 1. ISSN: 2296-4185 (Print) 2296-4185 (Linking). DOI: 10.3389/fbioe.2019.00001. URL: https://www.ncbi.nlm.nih.gov/pubmed/30705882.

[181] A. L. Schaefer et al. "Generation of cell-to-cell signals in quorum sensing: acyl homoserine lactone synthase activity of a purified Vibrio fischeri LuxI protein". In: *Proc Natl Acad Sci U S A* 93.18 (1996), pp. 9505–9. ISSN: 0027-8424 (Print) 0027-8424 (Linking). DOI: 10.1073/pnas.93.18.9505. URL: https://www.ncbi.nlm.nih.gov/pubmed/8790360.

[182] Q. H. Christensen et al. “Evolution of acyl-substrate recognition by a family of acyl-homoserine lactone synthases”. In: *PLoS One* 9.11 (2014), e112464. ISSN: 1932-6203 (Electronic) 1932-6203 (Linking). DOI: 10.1371/journal.pone.0112464. URL: https://www.ncbi.nlm.nih.gov/pubmed/25401334.

[183] M. K. Winson et al. “Multiple N-acyl-L-homoserine lactone signal molecules regulate production of virulence determinants and secondary metabolites in Pseudomonas aeruginosa”. In: *Proc Natl Acad Sci U S A* 92.20 (1995), pp. 9427–31. ISSN: 0027-8424 (Print) 0027-8424 (Linking). DOI: 10.1073/pnas.92.20.9427. URL: https://www.ncbi.nlm.nih.gov/pubmed/7568146.

[184] N. Kylilis et al. “Tools for engineering coordinated system behaviour in synthetic microbial consortia”. In: *Nat Commun* 9.1 (2018), p. 2677. ISSN: 2041-1723 (Electronic) 2041-1723 (Linking). DOI: 10.1038/s41467-018-05046-2. URL: https://www.ncbi.nlm.nih.gov/pubmed/29992956.

[185] S. H. Dong et al. “Molecular basis for the substrate specificity of quorum signal synthases”. In: *Proc Natl Acad Sci U S A* 114.34 (2017), pp. 9092–9097. ISSN: 1091-6490 (Electronic) 0027-8424 (Linking). DOI: 10.1073/pnas.1705400114. URL: https://www.ncbi.nlm.nih.gov/pubmed/28784791.

[186] S. J. Tekel et al. “Engineered Orthogonal Quorum Sensing Systems for Synthetic Gene Regulation in Escherichia coli”. In: *Front Bioeng Biotechnol* 7 (2019), p. 80. ISSN: 2296-4185 (Print) 2296-4185 (Linking). DOI: 10.3389/fbioe.2019.00080. URL: https://www.ncbi.nlm.nih.gov/pubmed/31058147.

[187] D. W. Leung. “A method for random mutagenesis of a defined DNA segment using a modified polymerase chain reaction”. In: *Technique* 1 (1989), pp. 11–15. URL: https://ci.nii.ac.jp/naid/10003752379/en/.

[188] V. Potapov and J. L. Ong. "Examining Sources of Error in PCR by Single-Molecule Sequencing". In: *PLoS One* 12.1 (2017), e0169774. ISSN: 1932-6203 (Electronic) 1932-6203 (Linking). DOI: 10.1371/journal.pone.0169774. URL: https://www.ncbi.nlm.nih.gov/pubmed/28060945.

[189] M. S. Packer and D. R. Liu. "Methods for the directed evolution of proteins". In: *Nat Rev Genet* 16.7 (2015), pp. 379–94. ISSN: 1471-0064 (Electronic) 1471-0056 (Linking). DOI: 10.1038/nrg3927. URL: https://www.ncbi.nlm.nih.gov/pubmed/26055155.

[190] W. P. Stemmer. "DNA shuffling by random fragmentation and reassembly: in vitro recombination for molecular evolution". In: *Proc Natl Acad Sci U S A* 91.22 (1994), pp. 10747–51. ISSN: 0027-8424 (Print) 0027-8424 (Linking). DOI: 10.1073/pnas.91.22.10747. URL: https://www.ncbi.nlm.nih.gov/pubmed/7938023.

[191] W. P. Stemmer. "Rapid evolution of a protein in vitro by DNA shuffling". In: *Nature* 370.6488 (1994), pp. 389–91. ISSN: 0028-0836 (Print) 0028-0836 (Linking). DOI: 10.1038/370389a0. URL: https://www.ncbi.nlm.nih.gov/pubmed/8047147.

[192] W. M. Coco et al. "DNA shuffling method for generating highly recombined genes and evolved enzymes". In: *Nat Biotechnol* 19.4 (2001), pp. 354–9. ISSN: 1087-0156 (Print) 1087-0156 (Linking). DOI: 10.1038/86744. URL: https://www.ncbi.nlm.nih.gov/pubmed/11283594.

[193] K. M. Muller et al. "Nucleotide exchange and excision technology (NExT) DNA shuffling: a robust method for DNA fragmentation and directed evolution". In: *Nucleic Acids Res* 33.13 (2005), e117. ISSN: 1362-4962 (Electronic) 0305-1048 (Linking). DOI: 10.1093/nar/gni116. URL: https://www.ncbi.nlm.nih.gov/pubmed/16061932.

[194] H. Zhao et al. "Molecular evolution by staggered extension process (StEP) in vitro recombination". In: *Nat Biotechnol* 16.3 (1998), pp. 258–61. ISSN: 1087-0156 (Print) 1087-0156 (Linking). DOI: 10.1038/nbt0398-258. URL: https://www.ncbi.nlm.nih.gov/pubmed/9528005.

[195] S. R. Scott and J. Hasty. "Quorum Sensing Communication Modules for Microbial Consortia". In: *ACS Synth Biol* 5.9 (2016), pp. 969–77. ISSN: 2161-5063 (Electronic) 2161-5063 (Linking). DOI: 10.1021/acssynbio.5b00286. URL: https://www.ncbi.nlm.nih.gov/pubmed/27172092.

[196] C. H. Collins, J. R. Leadbetter, and F. H. Arnold. "Dual selection enhances the signaling specificity of a variant of the quorum-sensing transcriptional activator LuxR". In: *Nat Biotechnol* 24.6 (2006), pp. 708–12. ISSN: 1087-0156 (Print) 1087-0156 (Linking). DOI: 10.1038/nbt1209. URL: https://www.ncbi.nlm.nih.gov/pubmed/16715074.

[197] C. H. Collins, F. H. Arnold, and J. R. Leadbetter. "Directed evolution of Vibrio fischeri LuxR for increased sensitivity to a broad spectrum of acyl-homoserine lactones". In: *Mol Microbiol* 55.3 (2005), pp. 712–23. ISSN: 0950-382X (Print) 0950-382X (Linking). DOI: 10.1111/j.1365-2958.2004.04437.x. URL: https://www.ncbi.nlm.nih.gov/pubmed/15660998.

[198] A. C. Hawkins et al. "Directed evolution of Vibrio fischeri LuxR for improved response to butanoyl-homoserine lactone". In: *Appl Environ Microbiol* 73.18 (2007), pp. 5775–81. ISSN: 0099-2240 (Print) 0099-2240 (Linking). DOI: 10.1128/AEM.00060-07. URL: https://www.ncbi.nlm.nih.gov/pubmed/17675429.

[199] T. E. Vee Aune et al. "Directed evolution of the transcription factor XylS for development of improved expression systems". In: *Microb Biotechnol* 3.1 (2010), pp. 38–47. ISSN: 1751-7915 (Electronic) 1751-7915 (Linking). DOI: 10.1111/j.

1751-7915.2009.00126.x. URL: https://www.ncbi.nlm.nih.gov/pubmed/21255304.

[200] J. Shong et al. "Directed evolution of the quorum-sensing regulator EsaR for increased signal sensitivity". In: *ACS Chem Biol* 8.4 (2013), pp. 789–95. ISSN: 1554-8937 (Electronic) 1554-8929 (Linking). DOI: 10.1021/cb3006402. URL: https://www.ncbi.nlm.nih.gov/pubmed/23363022.

[201] Y. Kimura et al. "Directed evolution of Vibrio fischeri LuxR signal sensitivity". In: *J Biosci Bioeng* 122.5 (2016), pp. 533–538. ISSN: 1347-4421 (Electronic) 1347-4421 (Linking). DOI: 10.1016/j.jbiosc.2016.04.010. URL: https://www.ncbi.nlm.nih.gov/pubmed/27222380.

[202] Yuki Kimura et al. "Directed Evolution of the Stringency of the LuxR Vibrio fischeri Quorum Sensor without OFF-State Selection". In: *ACS Synthetic Biology* 9.3 (2020), pp. 567–575. DOI: 10.1021/acssynbio.9b00444. URL: https://doi.org/10.1021/acssynbio.9b00444.

[203] P. J. Farabaugh. "Sequence of the lacI gene". In: *Nature* 274.5673 (1978), pp. 765–9. ISSN: 0028-0836 (Print) 0028-0836 (Linking). DOI: 10.1038/274765a0. URL: https://www.ncbi.nlm.nih.gov/pubmed/355891.

[204] A. Hecht et al. "Measurements of translation initiation from all 64 codons in E. coli". In: *Nucleic Acids Res* 45.7 (2017), pp. 3615–3626. ISSN: 1362-4962 (Electronic) 0305-1048 (Linking). DOI: 10.1093/nar/gkx070. URL: https://www.ncbi.nlm.nih.gov/pubmed/28334756.

[205] W. P. Stemmer et al. "Single-step assembly of a gene and entire plasmid from large numbers of oligodeoxyribonucleotides". In: *Gene* 164.1 (1995), pp. 49–53. ISSN: 0378-1119 (Print) 0378-1119 (Linking). DOI: 10.1016/0378-1119(95)00511-4. URL: https://www.ncbi.nlm.nih.gov/pubmed/7590320.

[206] T. M. Henkin. "Riboswitch RNAs: using RNA to sense cellular metabolism". In: *Genes Dev* 22.24 (2008), pp. 3383–90. ISSN: 0890-9369 (Print) 0890-9369 (Linking). DOI: 10.1101/gad.1747308. URL: https://www.ncbi.nlm.nih.gov/pubmed/19141470.

[207] A. Serganov and E. Nudler. "A decade of riboswitches". In: *Cell* 152.1-2 (2013), pp. 17–24. ISSN: 1097-4172 (Electronic) 0092-8674 (Linking). DOI: 10.1016/j.cell.2012.12.024. URL: https://www.ncbi.nlm.nih.gov/pubmed/23332744.

[208] L. Martini and S. S. Mansy. "Cell-like systems with riboswitch controlled gene expression". In: *Chem Commun (Camb)* 47.38 (2011), pp. 10734–6. ISSN: 1364-548X (Electronic) 1359-7345 (Linking). DOI: 10.1039/c1cc13930d. URL: https://www.ncbi.nlm.nih.gov/pubmed/21869957.

[209] R. Weiss. "Cellular computation and communications using engineered genetic regulatory networks". Thesis. 2000.

[210] R. Lentini et al. "Fluorescent proteins and in vitro genetic organization for cell-free synthetic biology". In: *ACS Synth Biol* 2.9 (2013), pp. 482–9. ISSN: 2161-5063 (Electronic) 2161-5063 (Linking). DOI: 10.1021/sb400003y. URL: https://www.ncbi.nlm.nih.gov/pubmed/23654270.

[211] A. P. Jacobus and J. Gross. "Optimal cloning of PCR fragments by homologous recombination in Escherichia coli". In: *PLoS One* 10.3 (2015), e0119221. ISSN: 1932-6203 (Electronic) 1932-6203 (Linking). DOI: 10.1371/journal.pone.0119221. URL: https://www.ncbi.nlm.nih.gov/pubmed/25774528.

[212] OpenWetWare. *Endy:M9 media/supplemented — OpenWetWare*. [Online; accessed 16-January-2022]. 2007. URL: https://openwetware.org/mediawiki/index.php?title=Endy:M9_media/supplemented&oldid=111004.